



**HAL**  
open science

# Photodégradation de polluants organiques induite par des complexes Fe(III)-carboxylate en solutions aqueuses

Lei Wang

► **To cite this version:**

Lei Wang. Photodégradation de polluants organiques induite par des complexes Fe(III)-carboxylate en solutions aqueuses. Chimie organique. Université Blaise Pascal - Clermont-Ferrand II, 2008. Français. NNT : 2008CLF21833 . tel-00728829

**HAL Id: tel-00728829**

**<https://theses.hal.science/tel-00728829>**

Submitted on 6 Sep 2012

**HAL** is a multi-disciplinary open access archive for the deposit and dissemination of scientific research documents, whether they are published or not. The documents may come from teaching and research institutions in France or abroad, or from public or private research centers.

L'archive ouverte pluridisciplinaire **HAL**, est destinée au dépôt et à la diffusion de documents scientifiques de niveau recherche, publiés ou non, émanant des établissements d'enseignement et de recherche français ou étrangers, des laboratoires publics ou privés.

Numéro d'Ordre: D. U. 1833

**UNIVERSITE BLAISE PASCAL**

U. F. R. Sciences et Technologies

**ECOLE DOCTORALE DES SCIENCES FONDAMENTALES**

N°: 567

**THESE EN COTUTELLE**

Avec l'Université de Wuhan (Chine)

**Présentée pour obtenir le grade de**

**DOCTEUR D'UNIVERSITE**

Spécialité: Chimie Physique et chimie de l'environnement

**Par**

**Lei WANG**

Diplômé de Master

**PHOTODEGRADATION OF ORGANIC POLLUTANTS  
INDUCED BY FE(III)-CARBOXYLATE COMPLEXES IN  
AQUEOUS SOLUTIONS**

Soutenue publiquement à Wuhan le 6 juin 2008, devant la commission d'examen

Président:	Mr. Feng WU
Rapporteurs:	Mrs. Marie-Thérèse MAURETTE Mr. Yuegang Zuo
Examineurs:	Mrs. Michèle BOLTE Mr. Nansheng DENG Mr. Gilles MAILHOT Ms. Hana MESTANKOVA



## **Acknowledgements**

This work was supported by the cooperation program between Wuhan University and Blaise Pascal University. Part of my work was finished in the Laboratory of Environmental Science directed by Pro. Nansheng Deng and he is my supervisor in Wuhan University. Most of my work was finished in Laboratory of Molecular and Macromolecular Photochemistry UMR CNRS 6505 from the University Blaise Pascal led by by Mrs. Claire RICHARD, Director of Research at CNRS. I would sincerely like to thank them for the confidence they placed in me in the laboratory.

I cordially express my thanks to Mr. Feng Wu, who gives me a lot of help during my study in Wuhan University. Thanks a lot for his great support and helpful guide on my thesis. I learn a lot from him.

It is my great pleasure to express my gratitude and appreciation to Mrs. Michèle BOLTE, Director of Research at CNRS and Mr. Gilles MAILHOT, Director of Research at CNRS, and Ms. Hana MESTANKOVA, who provided the scientific responsibility of this thesis. It is a good opportunity and joy for me to prepare my thesis under their direction. Their enthusiasm and availability throughout last year of research, their friendly and everlasting help and attention, their moral support have established an atmosphere conducive to work. I spend a very happy time in France with their company.

I am very grateful to Mrs. Mei Xiao, Mrs. Lin Zhang and Mrs. Chaozhen Hu, who give me a lot of help when I study in Wuhan University.

I want to sincerely thank Mr. Changbo Zhang, Mr. Yanxiang Liu, Mr. Jie Sun Ms. ZhangE Peng, Ms. Jing Li, Ms. Beibei Wang, Mr. Xu zhang, Mr. Li Guo, Mr. Xiaofei Xue, Ms. Liu Yang, who are my colleague and friends in Wuhan University.

I cordially thank Mrs. Bernadette Lavedrine, Mr. Guillaume Voyard and Mr. Jean Philippe for giving me good advice, as well as their availability.

I also wish to express my thanks to all members of the laboratory Madam MAILHOT Benedicte, Mr. Mohamed SARAHA, Mr. Pascal WONG-WAG-CHUNG, Madam Alexandra, Mr. Vincent They, Mr. Lawrence, Mr. Ghislain, Mr. Rodrigue, Mr. Selvain, Ms. Fatima, Mr. Marius, Mr. Christian, Ms. Marie, Ms. Annie Rossi, Mr. Boris, Ms. Delphine, Mr. Andreï, Mr. Michal, Ms. Marie, Ms. Sabrina, Mr. Matthieu, Mr. Sylvain, Ms. Anne-Marie, Ms. Charlene and I apologize to the people that I forgot the name and that I have not mentioned. Thanks for their friendship and help for me when I stay in Blaise Pascal University.

Thanks for the fund support of China Scholarship Council (CSC) affiliated with the Ministry of Education of the P.R.China. Thanks also go to the Education Service of China Embassy in Paris France.

To my parents,

I want to express my gratitude to my dear parents, without your love I can not live happily. No words can express my feelings. I love you very much.

# CATALOGUE

<b>I-INTRODUCTION</b> .....	1
<b>II-BIBLIOGRAPHY STUDY</b> .....	5
<b>A-Iron in the environment and its photochemical properties</b> .....	7
A-1-Iron in the natural environment.....	7
A-2-Transformation of iron in the aqueous solution.....	13
A-3-The species of Fe(III) in the aqueous solution.....	15
A-3-1 Influence of pH.....	17
A-3-2 Influence of iron concentration.....	19
A-4-Characterization of Fe(III) aqueous solution.....	19
<b>B-The Iron-Carboxylate complexes</b> .....	21
B-1-Carboxylic acids in the environment.....	21
B-2-Photochemical property of Fe-Carboxylate complexes.....	22
B-2-1-Fe-Oxalate complexes.....	25
B-2-2-Fe-Citrate complexes.....	29
B-2-3-Fe-Tartrate complexes.....	30
<b>C-Chlorophenols</b> .....	34
C-1-The contamination potential of 2, 4-Dichlorophenol in the environment.....	35
C-2-Degradation of 2,4-DCP.....	36
<b>D-The 2, 4-Dichlorophenoxyacetic acid (2, 4-D)</b> .....	39
D-1-Physicochemical properties of 2, 4-D and contamination potential in the environment.....	39
D-2-Degradation of 2,4-D.....	42
<b>III-EXPERIMENTAL MATERIALS AND METHODS</b> .....	45
<b>A-REAGENTS</b> .....	47
<b>B-PREPARATION OF SOLUTIONS</b> .....	48

B-1-Preparation of stock solution.....	48
B-2-Preparation of reaction solutions.....	50
<b>C-IRRADIATION.....</b>	<b>50</b>
C-1-Ferrioxalate actinometry.....	50
C-2-Irradiation with monochromator.....	52
C-3-Irradiation at 365nm.....	54
C-4-Irradiation with Metal Halide Lamp .....	55
<b>D-ANALYSIS METHODS .....</b>	<b>57</b>
D-1-Spectroscopy methods.....	57
D-2-Chromatography methods.....	58
D-3-Dosage methods.....	59
D-4-Molar ratio method .....	64
<b>IV RESULTS.....</b>	<b>65</b>
<b>IV-A Study of Physicochemical properties of Fe(III)-Carboxylate</b>	<b>67</b>
<b>complexes.....</b>	<b>67</b>
<b>A-1-Properties of the carboxylic acids.....</b>	<b>67</b>
A-1-1-Tartaric acid (Tar).....	68
A-1-2-Pyruvic acid (Pyr).....	70
A-1-3-Citric acid (Cit).....	71
<b>A-2-Study of the stoichiometric composition of Fe(III) in complexes</b>	<b>72</b>
<b>with carboxylic acids.....</b>	<b>72</b>
A-2-1 Stoichiometry of Fe(III) in complex with Tartaric acid.....	72
A-2-1-1 Fe(III)-D-Tar complex.....	73
A-2-1-2 Fe(III)-L-Tar complex.....	74
A-2-2 Stoichiometry of Fe(III) in complex with Pyruvic acid.....	76
<b>A-3-Properties of Fe(III)-Carboxylate complexes.....</b>	<b>77</b>
A-3-1 Stability of Fe(III)-Tar complexes.....	77
A-3-2 pH effect.....	78
A-3-3 Irradiation effect.....	81

<i>Conclusions</i> .....	82
<b>IV-B Determination of hydroxyl radicals from photolysis of Fe(III)-Carboxylate complexes in aqueous solutions</b> .....	83
<b>B-1-Photoproduction of hydroxyl radicals in the aqueous solutions with Fe(III)-Pyr complexes</b> .....	83
B-1-1 Generation of hydroxyl radicals in the irradiated aqueous solution containing Fe(III)-Pyr complexes.....	85
B-1-2 Effect of pH on the generation of hydroxyl radicals in the irradiated aqueous solution containing Fe(III)-Pyr complexes.....	86
B-1-3 Effect of Fe(III) and Pyr concentrations on the photogeneration of hydroxyl radicals in the aqueous solution.....	87
B-1-4 Effect of temperature on the photogeneration of hydroxyl radicals in the aqueous solution.....	89
<b>B-2-Photoproduction of hydroxyl radicals in the aqueous solutions with Fe(III)-Cit complexes</b> .....	89
B-2-1 Generation of hydroxyl radicals in the irradiated aqueous solution containing Fe(III)-Cit complexes.....	90
B-2-2 Effect of pH on the generation of hydroxyl radicals in the irradiated aqueous solution containing Fe(III)-Cit complexes.....	92
B-2-3 Effect of Fe(III) and Cit concentrations on the generation of hydroxyl radicals in the irradiated aqueous solution containing Fe(III)-Cit complexes.....	94
<b>B-3-Photoproduction of hydroxyl radicals in the aqueous solutions with Fe(III)-Tar complexes</b> .....	96
B-3-1 Generation of hydroxyl radicals in the irradiated aqueous solution containing Fe(III)-Tar complexes.....	97
B-3-2 Effect of pH on the generation of hydroxyl radicals in the irradiated aqueous solution containing Fe(III)-Tar complexes.....	98
B-3-3 Effect of Tar concentration on the generation of hydroxyl radicals	100



in the irradiated aqueous solution containing Fe(III)-Tar complexes.....	
B-3-4 Effect of Fe(III) concentration on the generation of hydroxyl radicals in the irradiated aqueous solution containing Fe(III)-Tar complexes.....	101
B-3-5 Effect of temperature on the generation of hydroxyl radicals in the irradiated aqueous solution containing Fe(III)-Tar complexes.....	102
<b>Conclusions</b> .....	104
<b>IV-C Degradation of 2, 4-Dichlorophenol photoinduced by the Fe(III)-Carboxylate complexes</b> .....	106
<b>C-1-Properties of 2,4-Dichlorophenol (2,4-DCP) aqueous solution</b> .....	106
<b>C-2-Photodegradation of 2,4-DCP induced by Fe(OH)<sup>2+</sup></b> .....	109
C-2-1 Properties of Fe(III) solutions.....	109
C-2-2 Properties of Fe(III)/2,4-DCP solutions.....	110
C-2-3 Degradation of 2,4-DCP photoinduced by Fe(III).....	112
C-2-4 Quantum yields of Fe(II) and 2,4-DCP in the Fe(III) solution ( $\lambda_{irr}= 365\text{nm}$ ).....	114
<b>C-3-Degradation of 2,4-DCP induced by the photolysis of Fe(III)-Carboxylate complexes</b> .....	114
<b>C-3-1 Quantum yields of 2, 4-DCP degradation and Fe(II) formation</b> .....	115
C-3-1-1 Influence of the irradiation wavelength on the quantum yields of Fe(II) and 2,4-DCP in different Fe(III)-Carboxylate complexes systems.....	115
C-3-1-2 Effect of oxygen on the quantum yields of Fe(II) and 2,4-DCP in different reaction systems ( $\lambda_{irr}= 365\text{nm}$ ).....	117
C-3-1-3 Effect of pH on the quantum yields of Fe(II) and 2,4-DCP in different reaction systems ( $\lambda_{irr}= 365\text{nm}$ ).....	118
C-3-1-4 Effect of complexes concentration on the quantum yields of Fe(II) and 2,4-DCP in different reaction systems ( $\lambda_{irr}= 365\text{nm}$ ).....	121

C-3-1-5 Effect of 2,4-DCP concentration on the quantum yields of Fe(II) and 2,4-DCP in different reaction systems ( $\lambda_{irr}= 365\text{nm}$ ).....	122
<b>C-3-2 Photodegradation of 2,4-DCP at 365nm in the presence of Fe(III)-Carboxylate complexes.....</b>	<b>123</b>
C-3-2-1 Degradation of 2,4-DCP photoinduced by Fe(III)-Cit complex.....	123
C-3-2-1-1 Effects of Fe(III)-Cit concentration.....	125
C-3-2-1-2 Effect of pH.....	127
C-3-2-1-2 Effect of oxygen.....	128
C-3-2-2 Degradation of 2,4-DCP photoinduced by Fe(III)-D or L-Tar complex.....	130
C-3-2-2-1 Effect of Fe(III)-D or L-Tar concentration.....	130
C-3-2-2-2 Effect of pH.....	134
C-3-2-2-3 Effect of oxygen.....	136
C-3-2-3 Degradation of 2,4-DCP photoinduced by Fe(III)-Pyr complex.....	138
C-3-2-3-1 Effect of Fe(III)-Pyr concentration.....	138
C-3-2-3-2 Effect of pH.....	140
C-3-2-3-3 Effect of oxygen.....	141
C-3-2-4 Comparing of the photodegradation of 2,4-DCP in different systems.....	142
<b>C-3-3 Mineralization analysis by TOC.....</b>	<b>144</b>
<b>Conclusions.....</b>	<b>147</b>
<b>IV-D Degradation of 2,4-Dichlorophenoxyacetic acid (2,4-D) photoinduced by the Fe(III)-Carboxylate complexes.....</b>	<b>149</b>
<b>D-1-Properties of 2,4-D aqueous solution .....</b>	<b>149</b>
<b>D-2-Quantum yields of 2, 4-D degradation and Fe(II) formation.....</b>	<b>151</b>
D-2-1 Influence of the irradiation wavelength on the quantum yields of	151

Fe(II) and 2,4-D in different Fe(III)-Carboxylate complexes systems.....	
D-2-2 Influence of oxygen on the quantum yields of Fe(II) and 2,4-D in different Fe(III)-Carboxylate complexes systems ( $\lambda_{irr}=365\text{nm}$ ).....	152
D-2-3 Influence of pH on the quantum yields of Fe(II) and 2,4-D in different Fe(III)-Carboxylate complexes systems ( $\lambda_{irr}=365\text{nm}$ ).....	153
D-2-4 Influence of 2, 4-D concentration on the quantum yields of Fe(II) and 2,4-D with different Fe(III)-Carboxylate complexes ( $\lambda_{irr}=365\text{nm}$ ).....	155
<b>D-3-Photodegradation of 2,4-D at 365nm in the presence of Fe(III)-Carboxylate complexes.....</b>	<b>157</b>
D-3-1 Degradation of 2,4-D photoinduced by Fe(III)-Cit complex.....	157
D-3-1-1 Effects of Fe(III)-Cit concentration.....	157
D-3-1-2 Effect of oxygen.....	159
D-3-1-3 Effect of pH.....	160
D-3-2 Degradation of 2,4-D photoinduced by Fe(III)-Pyr complex.....	162
D-3-2-1 Effect of Fe(III)-Pyr concentration.....	162
D-3-2-2 Effect of oxygen.....	164
D-3-2-3 Effect of pH.....	165
D-3-3 Degradation of 2,4-D photoinduced by Fe(III)-Tar complex.....	168
D-3-3-1 Effects of Fe(III)-Tar concentration.....	168
D-3-3-2 Effects of pH.....	170
D-3-3 Comparison of the photodegradation of 2,4-D in different systems.....	172

D-3-4 Total organic carbon analysis .....	174
<i>Conclusions</i> .....	176
<b>IV-E-Photodegradation mechanism</b> .....	178
IV-E-1-Study of Fe(III)-Carboxylate complexes by ESR (electron spin resonance) spectroscopy in aqueous solution under irradiation.....	178
IV-E-2-Identification of photoproducts and degradation mechanism.....	183
<b>V-GENERAL CONCLUSIONS</b> .....	194
<b>VI-APPENDIX</b> .....	200
List of tables.....	202
List of figures.....	204
<b>VII-REFERENCES</b> .....	218



# I

## INTRODUCTION



## **I-Introduction**

Iron is considered to be the most abundant transition metal in the environment. Photoreduction product Fe(II) could react with H<sub>2</sub>O<sub>2</sub> through Fenton's mechanism, which represents a significant thermal source of hydroxyl radicals ( $\cdot$ OH). Many references indicated that the production of  $\cdot$ OH radicals in atmospheric water droplets is an important process as they can oxidize a wide variety of natural and anthropogenic organic and inorganic substances.

The photo-oxidation of carboxylic acids has long been known to be sensitized by Fe(III), but only till the 1960s attention has been paid to the coordinate species involved. The carboxylate group [RC(O)O<sup>-</sup>] is one of the most common functional groups of the dissolved organic compounds present in natural waters. Low molecular weight organic acids have been identified and measured in a wide variety of environments, such as marine and continental air, rural and remote atmospheres and tropical and temperate zones. Various organic acids viz. EDTA, acetic, formic, citric, ascorbic, succinic, tartaric and oxalic acids are effective coordination reagents, which play an important role on the metal ions (especially copper and iron) removal. References report the formation of iron-carboxylate complexes, which can undergo rapid photochemical reactions under solar irradiation. The photolysis of Fe(III)-polycarboxylates could represent an important source of H<sub>2</sub>O<sub>2</sub> to some atmospheric and surface waters. Fe(III)-NTA, Fe-EDTA, Fe-Oxalate and Fe(III)-Cit have been used to degrade organic and inorganic pollutants (Cr(VI)). However, there are little published studies on the photochemical reactivity of Fe(III)-Pyr and Fe(III)-Tar complexes.

2,4-dichlorophenoxyacetic acid (2,4-D) was one of the first herbicides to be commercially marketed. It was first introduced in the United States in the late 1940's. 2,4-D made up a major portion (about 50%) of the herbicide known as Agent Orange, which was used during the Vietnam War. However, it is thought that most of the health problems are related to its natural degradation products including



2,4-dichlorophenol (2,4-DCP), 2,4,5-trichlorophenoxyacetic acid (2,4,5-T) and 2,3,7,8-tetrachlorodibenzo-p-dioxin (2,3,7,8-TCDD). While 2,4,5-T was the main culprit and has now been banned. 2,4-DCP has been listed by the US EPA as priority pollutants. Until now, 2,4-D and its related product 2,4-DCP are very popular pollutants in the organochlorine family. Many kinds of methods are used to degrade them. Advanced oxidation technologies is thought to be the preferable means for the degradation of 2,4-D and 2,4-DCP. However, little references reported using iron complexes to degrade them under irradiation.

The objective of this work is to understand the fate of pollutants in the aquatic environment in the presence of light and different organic complexes of Fe(III) naturally present in the aquatic environment.

In the present work, first we studied the physicochemical properties of Fe(III)-Carboxylate complexes, including Fe(III) with citric acid (Cit), tartaric acid (Tar) or pyruvic acid (Pyr) complexes. The stoichiometry of Fe(III) in complex with tartaric acid and pyruvic acid was studied. It should be indicated that until now no published reports about the stoichiometry of Fe(III)-Pyr complex were found.

Second, the photo-generation of  $\cdot\text{OH}$  and peroxy radicals have been determined in the aqueous solutions with different iron-carboxylate complexes.

Third, 2,4-DCP and 2,4-D were used as model compounds to certify the photochemical property of iron-carboxylate complexes. Irradiation experiments were carried out separately under monochromatic irradiation in a short time and irradiation at 365 nm (93% of all the radiation) in a long time. Quantum yields of Fe(II) formation, 2,4-D and 2,4-DCP disappearance were determined in the present study. Parameters affecting the photoreaction, including excitation wavelength, concentrations of iron-carboxylate complexes and pollutants, oxygen and pH were all studied in this work.

## **II**

### **BIBLIOGRAPHY STUDY**



## **II-Bibliography study**

### **A-Iron in the environment and its photochemical properties**

#### **A-1-Iron in the natural environment**

Iron is the most abundant transition metal in the natural environment. Iron widely exists in the soil, fresh waters, ocean and atmosphere. It plays a central role in many biological and chemical processes. Its average concentration in the Earth's crust is about 5.6%. However, like other reactive elements its concentration in seawater remains low, 0.1 nM, in the near surface waters of the Eastern Pacific due to active biological uptake and passive scavenging by particulate material. The low background concentrations of iron, combined with its short residence time in seawater (2-13 years, Landing and Bruland, 1987) means that the distribution of dissolved iron in surface seawater is likely dominated by its input pattern. The distribution of iron, along with those of other reactive elements, can then be particularly useful in identifying the location and magnitude of material exchange between the Earth's crust and the oceans. In addition to its ability to delimit chemical and physical transfer processes, iron is also an essential micronutrient and may limit or co-limit phytoplankton growth in the euphotic zone of surface waters. Martin and co-investigators have proposed that iron may be the limiting nutrient in some remote oceanic regions where the only sources of iron to the surface ocean are from either eolian deposition or from the upwelling of iron-enriched subsurface waters (Martin et al., 1988, 1989, 1990, 1991, 1994).

Dissolved Fe can exist in two different oxidation states in seawater, Fe(III) and Fe(II). Fe(III) is generally believed to be the dominant form of dissolved iron in surface seawater, because the oxidation of Fe(II) by hydrogen peroxide and oxygen is rapid (Moffett and Zika, 1987b; Millero et al., 1987; Millero and Sotolongo, 1989; Byrne et al., 1988). The speciation of Fe(III) in seawater (equivalent to a salinity S =

35) as a function of pH is shown in Figure II-A-1 (Millero et al., 1995).

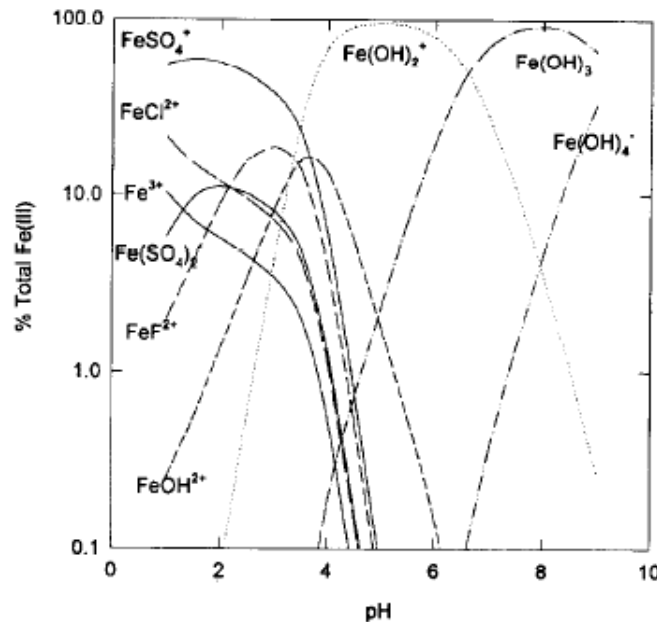


**Figure II-A-1 Speciation of Fe(III) in seawater as a function of pH  
(Millero et al., 1995)**

However, Fe(III) is rapidly removed from the photic zone of the ocean by precipitation and particle scavenging. In contrast, Fe(II) is highly soluble in seawater. A process that converts significant amounts of Fe(III) into Fe(II) may therefore facilitate iron uptake by organisms by creating a reservoir of soluble iron in the photic zone. Therefore, Fe(II) has been detected at concentrations comparable to those of Fe(III) in sunlit seawater (O'Sullivan et al., 1991) and in seawater samples exposed to simulated sunlight in laboratory experiments (Kester, 1994).

Atmospheric iron input is a significant external iron source to many oceanographic regimes, especially to the subtropical and the subarctic Pacific. For example, in the subarctic Pacific, which lies in the path of an extended aerosol plume that originates in China, Martin et al. (1989) estimated that atmospheric deposition accounted for 84-93% of the external iron input to these surface waters. Concentrations of iron in tropospheric aerosols range from 1 to 4000 ng m<sup>-3</sup> in remote areas, from 50 to 15,000 ng m<sup>-3</sup> in rural areas, and from 20 to 30,000 ng m<sup>-3</sup> in urban areas (Schroeder et al., 1987). Desert dust is a chief source of aeolian mineral dust.

Aerosol particles are incorporated into cloud water as condensation nuclei or are captured by cloud water through impaction or differential settling (Siefert et al., 1994). In atmospheric waters, iron undergoes photoredox cycling yielding dissolved Fe(II) (Behra and Sigg, 1990; Zuo and Hoigné, 1992; Sedlak and Hoigné, 1993; Zuo, 2003), one important reaction being photoreductive dissolution of particulate and colloidal iron phases (Faust and Hoffmann, 1986; Zhu et al., 1992; Zhuang et al., 1992a; Pehkonen et al., 1993; Siefert et al., 1994). It has been reported that Fe(II) contributed  $56 \pm 32\%$  of the total iron in marine aerosol samples collected over the central North Pacific and  $49 \pm 15\%$  at Barbados (Zhuang et al., 1992b).

Although the total concentrations of iron in freshwater systems are generally higher than in the oceans, due to larger particulate inputs (Davison, 1993; Sigg et al., 1991), and therefore limitation of phytoplankton growth by this element is not likely, its speciation and biological availability as essential element is an important and puzzling issue. The thermodynamically stable form of iron in oxic natural waters, Fe(III), has an extremely low solubility, while Fe(II) is much more soluble under most natural water conditions. It has been shown that light-induced reduction of Fe(III) is a process of major importance for the formation of dissolved iron in marine surface waters (Wells and Mayer, 1991; King et al., 1993; Voelker and Sedlak, 1995; Voelker et al., 1997; Miller et al., 1995) and in acidic surface waters (Sulzberger et al., 1990; Mcknight et al., 1988). Emmenegger et al., (1998) studied the oxidation of Fe(II) in the euphotic Swiss lake. In oxic environmental systems, the reduced iron species are rapidly oxidized by  $O_2$  at near-neutral pH, yielding Fe(III) and reactive oxygen species.

The inorganic speciation of dissolved Fe(III) and Fe(II) differ considerably. Inorganic species comprising dissolved Fe(III) are dominated by the hydrolysis products,  $Fe(OH)_2^+$ ,  $Fe(OH)_3^0$ , and  $Fe(OH)_4^-$ . The free hydrated  $Fe^{3+}$  ion is not only an extremely rare species, being only  $10^{-10}$  to  $10^{-11}M$  of the summed concentration of the hydrolysis species, it is also the slowest of the inorganic species to react with ligands or surface sites due to its slow water-loss rate constant (Hudson et al., 1992). In marked contrast, inorganic Fe(II) exists primarily as the free  $Fe^{2+}$  ion (Millero et al.,



in the remote marine aerosols, see Figure II-A-2.

**Table II-A-1 Concentrations of the total iron and dissolved iron in the rain, snow, fog or seawater systems in different locations.**

Location	Total Fe ( $\mu\text{mol.L}^{-1}$ )	Dissolved Fe ( $\mu\text{mol.L}^{-1}$ )	Dissolved Fe /Total Fe(%)	Aqueous phase	References
Great Britain (rural)	0.89-1.79			rain	Cawse et al., Peirson, 1972
Great Britain (rural)	3.58			rain	Peirson et al., 1973
Germany (urban)	4.12			rain	Betz, 1976
Northern Nigeria (rural)	23.30			rain	Beavington et al., Cawse, 1979
Germany (urban)	3.80			rain	Gravenhorst et al., 1980
Dakota and Minnesota, United-States	0.68-2.85			rain	Thornton et al., Eisenreich, 1982
Germany	0.27-2.35			rain	Georgii et al., 1983
Germany	1.02			rain	Nürnberg et al., 1983
Delaware (California), United-States (coastal)	0.27			rain	Church et al., 1984
Ontario, Canada (rural)	0.76			rain	Chan et al., 1986
Great Britain	0.36-1.18			rain	Radojevic et al., Clarke, 1987
Great Britain (near the North Sea)	9-670			rain	Balls, 1989
Sweden	0.2-3			rain	Ross, 1990
2 sites	0.03-1.81			rain	
Darmstadt (urban)	0.63	0.41	65	rain	Hofmann et al., 1991
Groß-Rohrheim (rural), Germany	0.43	0.18	41		
Germany	0.39-0.98			rain	Brandt et al., 1994
Poland	0.43			rain	Brandt et al., 1994
Chernogolovska, Russia (urban)		5.9-21.4		rain	Hoffmann et al., 1997
Plynlimon, Mid Wales (rural)		0.0009-6.68		rain	Wilkinson et al., 1997



Tour du Valat, France (coastal)		0.28		rain	Guien et al., 1997
Lamto, Ivory Coast (rural)		< 0.02-0.19			
Kollo, Niger (rural)		< 0.02-3.18		rain	Freydier et al., 1998
Lannemezan, France (rural)		0.03-0.19			
Jaipur, Kota, India (urban)	5.3			rain	Manoj et al., 2000
Riyadh, Saudi Arabia (urban)		0.007-0.40		rain	Alabdula'aly and Khan, 2000
Paradize, New-Zealand (remote)		0.04		rain	Halstead et al., 2000
Raipur, India urban		0.8-4-3		rain	Patel et al., 2001
rural		1.3			
Ajlune, Jordan (rural)		1.64 ± 1.86		rain	Al-Momani, 2003
Germany	0.21-1.95			snow	Brandt et al., 1994
Germany	2.5			snow	Brandt et al., 1994
Norway	3.64			snow	Brandt et al., 1994
Bakersfield (California), United-States	0.02-0.2			fog	Jacob et al., 1984
Suburb of Zürich, Switzerland	0.5-2			fog	Behra and Sigg, 1990
Zindelen (Zürick), Switzerland	0.3-91.4			fog	Joss and Baltensperger, 1991
San Pedro Hill, California, United-States	1-11.3	0.5-11.3			
Henninger Flats, California, United-States	2.2-27	2.3-11.6		fog	Erel et al., 1993
San Pietro (Pô Valley), Italy		1-4.6		fog	Schwanz et al., 1998
San Joaquim, United-states		5.4-9.8		fog	Rao and Collett Jr, 1998
Los Angeles, California, United-States	26			cloud	Waldman et al., 1985
Japan	86.4			cloud	Hosono et al., 1994

Germany	0.5-3.4			cloud	Wobrock et al., 1994
Munich, Germany	0.09-8.3	0.09-2.15		cloud	Sinner et al., 1994
Whiteface mountain, New York, United-States	0.32-0.95			cloud	Khwaja et al., 1995
Whiteface Mountain, United-States		0.08-1.57		cloud	Arakaki and Faust, 1998
Puy de Dôme, France		0.21-3.4		cloud	Marinoni et al., 2003
Massachusetts Bay Boston Harbor, United-States			50-74 25-53 25-74	seawater rain snow	Zhuang et al., 1995
North Pacific	0.01-0.15µg/L	5-135ng/L	11-100	marine aerosols	Zhuang et al., 1993
Equatorial Pacific		0.4 nM/kg		Surface seawater	O'Sullivan et al. 1991
Barbodas	0.6-5µg/L	28-150ng/L	7.5	marine aerosols	Zhu et al., 1993a
Urban Xian China			4-11	aerosol water	Zhuang et al., 1992a
Los Angeles basin Delaware Bay, United-States	300-5000nM		17-55	fog cloud water	Eral et al., 1993
Funka Bay Japan		20-40nM/kg		oxic Seawater	Kuma et al., 1992
Coast of Peru		0-15nM/kg		Seawater	Hong et al., 1986
Narragansett Bay		15nM/kg (unfiltered) 4.2nM/kg (0.45µm filtered)		Surface water	King et al., 1988 King et al., 1991
South Atlantic	0.5-10nM			Surface seawater	Powell et al., 1995

### **A-2-Transformation of iron in the aqueous solution**

The redox cycling of iron has been intensively studied in marine and freshwater (Waite and Morel, 1984; Hong and Kester, 1986; Johnson et al., 1994; Waite et al.,

1995; Gledhill and van den Berg, 1995; Voelker et al., 1997) and in atmospheric water systems (Figure II-A-3) (Behra and Sigg, 1990; Kotronarou and Sigg, 1993; Sedlak and Hoigné, 1993; Zuo et al., 2005). The kinetics of Fe(III) reduction and of Fe(II) oxidation are of crucial importance in determining the speciation and thus the bioavailability of iron, since most photosynthetic aquatic organisms can take up iron only in the dissolved form (Anderson et al., 1982; Sunda et al., 1996).

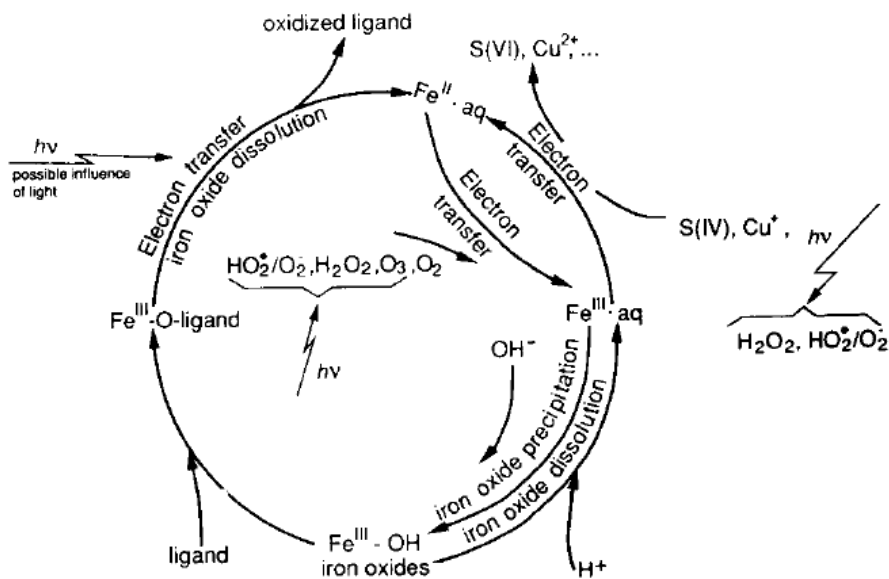


**Figure II-A-3 Scheme of iron recycling in the atmospheric water  
Behra and Sigg (1990)**

Figure II-A-4 presents the scheme of photochemical transformation of iron in aqueous solution in the presence of oxygen. Under irradiation, Fe(III) was effectively reduced into Fe(II) by superoxide radical ( $O_2^{\cdot-}$ ) (Voelker and Sedlak, 1995). At the same time Fe(II) was reoxidized into Fe(III) by reactive species generated in the reaction. Table II-A-2 lists the rate constants about the reactions occur in the seawater.

**Table II-A-2 Reactions and rate constants in (S=35) sea water at 298 k.**

Reaction	$K (M^{-1}s^{-1})$	References
<b>Iron reactions</b>		
$Fe(II) + O_2 \rightarrow Fe(III) + O_2^{\cdot-}$	$\log(k) = -14.06 + 1.87 (pH)$	Millero, 1987
$Fe(II) + O_2^{\cdot-} + 2H^+ \rightarrow Fe(III) + H_2O_2$	$1.0 \times 10^7 M^{-1}s^{-1}$	Rush and Bielski, 1985
$Fe(III) + O_2^{\cdot-} \rightarrow Fe(II) + O_2$	$1.5 \times 10^8 M^{-1}s^{-1}$	Rush and Bielski, 1985
$Fe(II) + H_2O_2 \rightarrow Fe(III) + \cdot OH + OH^-$	$\log(k) = -3.04 + 1.0 (pH)$	Millero and Sotolongo, 1989
$Fe(II) + \cdot OH \rightarrow Fe(III) + OH^-$	$5.0 \times 10^8 M^{-1}s^{-1}$	Farahataziz and Ross, 1977
$Fe(III)-L + hv \rightarrow Fe(II) + L^{\cdot}$	$6.3 \times 10^{-4} s^{-1}$	Miller et al., 1995
<b>Superoxide dismutation</b>		
$O_2^{\cdot-} + O_2^{\cdot-} + 2H^+ \rightarrow H_2O_2 + O_2$	$\log(k) = 12.7 - 1.0 (pH)$	Zafiriou, 1990

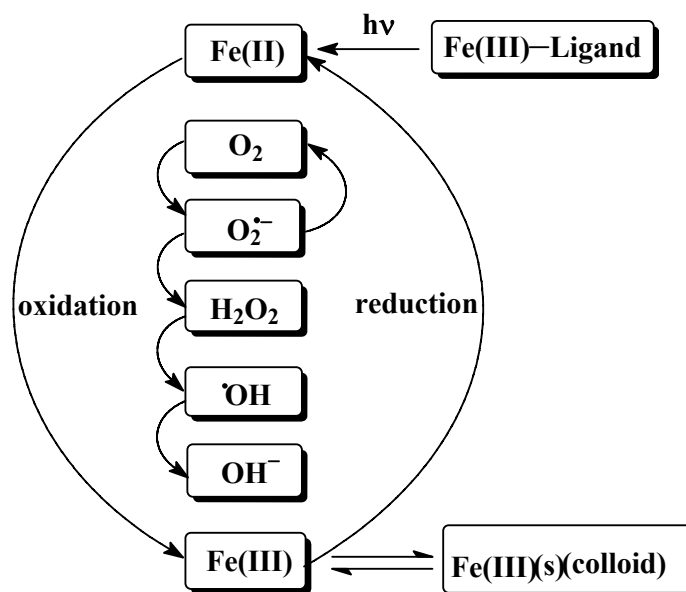


**Figure II-A-4 Photochemical transformation of iron**

### A-3-The species of Fe(III) in the aqueous solution

Fe(III) ions are easily hydrolyzed in the aqueous solutions and usually exist as the hydrolytic low molecular complexes:

- The monomer  $[Fe(H_2O)_6]^{3+}$ , which corresponds to  $Fe^{3+}$  surrounded by six water molecules (Figure II-A-5).

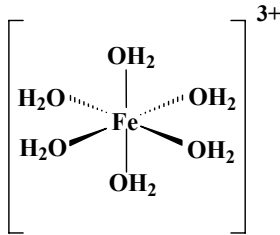


**Figure II-A-5 Structure of octahedral  $[\text{Fe}(\text{H}_2\text{O})_6]^{3+}$**

- The monomer  $[\text{Fe}(\text{H}_2\text{O})_5(\text{OH})]^{2+}$  or  $\text{Fe}(\text{OH})^{2+}$ , in which a water molecule has been replaced by an OH<sup>-</sup> group.
- The monomer species  $[\text{Fe}(\text{H}_2\text{O})_4(\text{OH})_2]^+$  or  $\text{Fe}(\text{OH})_2^+$ , in which two water molecules have been replaced by two hydroxide groups.
- The dimer species  $[\text{Fe}_2(\text{H}_2\text{O})_8(\text{OH})_2]^{4+}$  or  $\text{Fe}_2(\text{OH})_2^{4+}$  composed with two metal ions, the structure of which is described in the following figure:

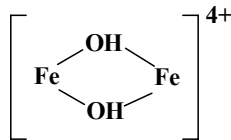


**Figure II-A-6 Proposed structure of dimer species Fe(III)  
by Sommer et Margerum (1970)**

Fe(III) served as donor to form water-soluble polymers:

- The trimer species of Fe(III) seems to exist in two forms,  $[\text{Fe}_3(\text{OH})_3(\text{H}_2\text{O})_{12}]^{6+}$  or  $[\text{Fe}_3(\text{OH})_3]^{6+}$  and  $[\text{Fe}_3(\text{OH})_4(\text{H}_2\text{O})_{14}]^{5+}$  or  $[\text{Fe}_3(\text{OH})_4]^{5+}$ , represented in the following Figure II-A-7.

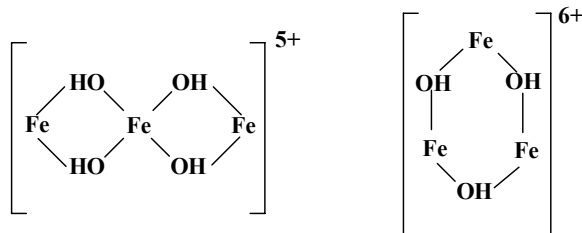


**Figure II-A-7 Proposed structure of trimeric species Fe(III)  
by Sommer et Margerum (1970)**

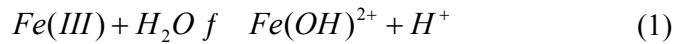
- The oligomers, polymers or aggregates of iron (III) are also present in the solution, but the structure was never clearly identified.

- Finally, oxides of iron (III) are also present in the form of suspended particles such as:  $\alpha$  and  $\gamma$ -FeO(OH) (goethite and lépidocrocite),  $\alpha$  and  $\gamma$ -Fe<sub>2</sub>O<sub>3</sub> (magnetite and hematite) or Fe(OH)<sub>3</sub> (ferrihydrite).

Since Fe(III) is very reactive, usually existing as many different species in the aqueous solutions, especially under irradiation. It is necessary to study the factors influencing the speciation of Fe(III), the pH value and the initial Fe(III) concentration.

### A-3-1 Influence of pH

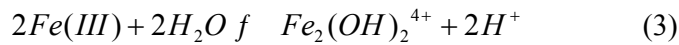
pH is a very important factor on the equilibrium and distribution of different iron species in the aqueous solutions. The main Fe(III)-hydroxy complexes in water are pH dependent. At pH  $\leq 5$ , the dominant species are Fe<sup>3+</sup>, Fe(OH)<sup>2+</sup>, Fe(OH)<sub>2</sub><sup>+</sup> and the dimer Fe<sub>2</sub>(OH)<sub>2</sub><sup>4+</sup>. Calculation of Fe(III)-hydroxy complexes as function of pH is based on the following equilibria:



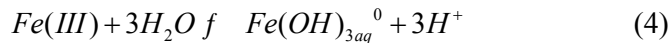
$$K_1 = 2.7 \times 10^{-3} \text{ mol. L}^{-1}$$



$$K_2 = 1.3 \times 10^{-8} (\text{mol. L}^{-1})^2$$



$$K_3 = 6.0 \times 10^{-4} \text{ mol. L}^{-1}$$

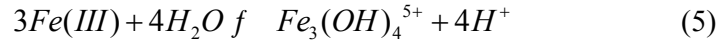


$$K_4 = 1.2 \times 10^{-13} (\text{mol. L}^{-1})^3$$

K<sub>1</sub>, K<sub>2</sub> and K<sub>3</sub> were determined by Faust and Hoigné (1990), at 298k with ionic strength 0.03 mol.L<sup>-1</sup>. K<sub>4</sub> was taken from a value 2.4 × 10<sup>-14</sup> (Byrne and kester, 1976) of in sea water at 36.22% salinity and 298k, with a correction ionic strength effects from 0.7 to 0.03 mol.L<sup>-1</sup>. The proportion of each monomer Fe(III) complexes depends on the pH of the solution.

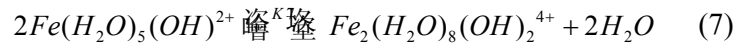
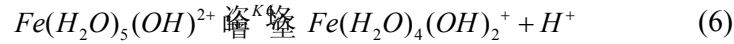
The following reaction is an equilibrium reaction of Fe(III) complex that leads to

trimer Fe(III) species.



$$K_5 = 1.7 \times 10^{-6} \text{ (mol. L}^{-1}\text{)}^2$$

The formation of species monomer  $Fe(OH)_2^+$  and dimer  $Fe_2(OH)_2^{4+}$  has also been reported from the species  $Fe(OH)^{2+}$  (Murray, 1974).



Regarding speeds of balances (1) and (6), Hemmes et al., (1971) showed that the balance (1) was very fast compared to the balance (6). Thus, they proposed the following values  $k_1 > 3 \times 10^7 \text{ s}^{-1}$  and  $k_6 = 6.1 \times 10^4 \text{ s}^{-1}$ . Therefore, it can be concluded that after the dissolution of the crystals of iron (III) in the low-acidity, the complex  $Fe^{3+}$  exist in small quantities and the complex  $Fe(OH)^{2+}$  will be quickly formed.

Figure II-A-8 represents the distribution of the three low molecular weight Fe(III) species as a function of pH. This distribution has been determined from the equilibrium constants cited above.

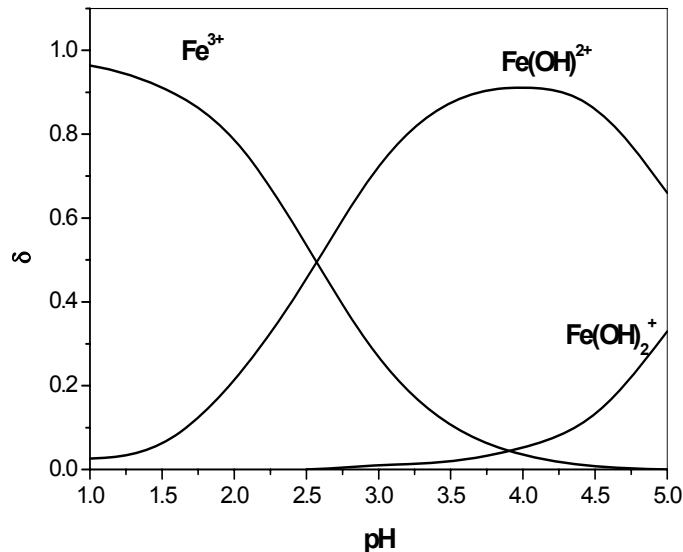
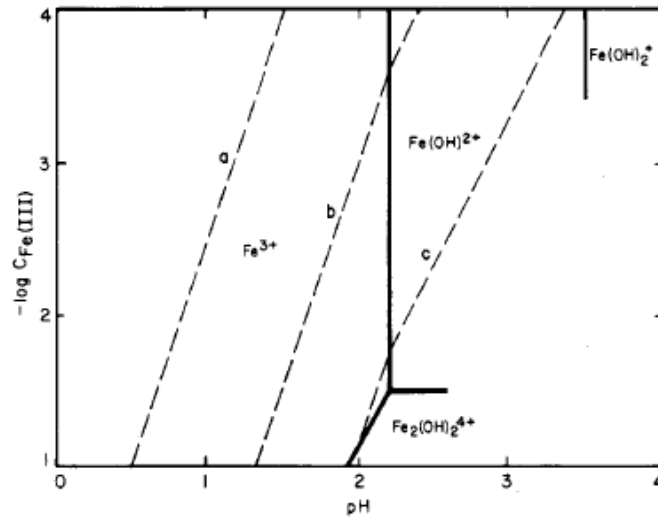


Figure II-A-8 The distribution of Fe(III) complexes as function of pH  
 $[Fe(III)] = 0.03 \text{ mol.L}^{-1}$ ,  $T = 298 \text{ k}$  (Mestankova, 2004)

### A-3-2 Influence of iron concentration

The species of Fe(III) present in the aqueous solutions also depend on the initial concentration of Fe(III). Flynn (1984) has established areas of prevalence of these complexes, depending both of pH and Fe(III) concentration (Figure II-A-9).



**Figure II-A-9** Approximate predominance-area pH vs  $\log C_{\text{Fe(III)}}$  (M) diagram, 25°C, ionic strength 0. The dashed lines labeled a, b, and c are the saturation lines for goethite, aged amorphous hydrous oxide, and fresh amorphous hydrous oxide, respectively.

According to the figure above, the iron complex will be in the form of dimers only in highly concentrated solutions with Fe(III) ( $> 5 \times 10^{-2} \text{ mol.L}^{-1}$ ).

### A-4-Characterization of Fe(III) aqueous solution

In the aqueous solutions, Fe(III) is not stable and normally exists in the form of Fe(III)-hydroxy complexes. Figure II-A-10 shows the different UV-vis spectra of iron complexes present in aqueous solution.



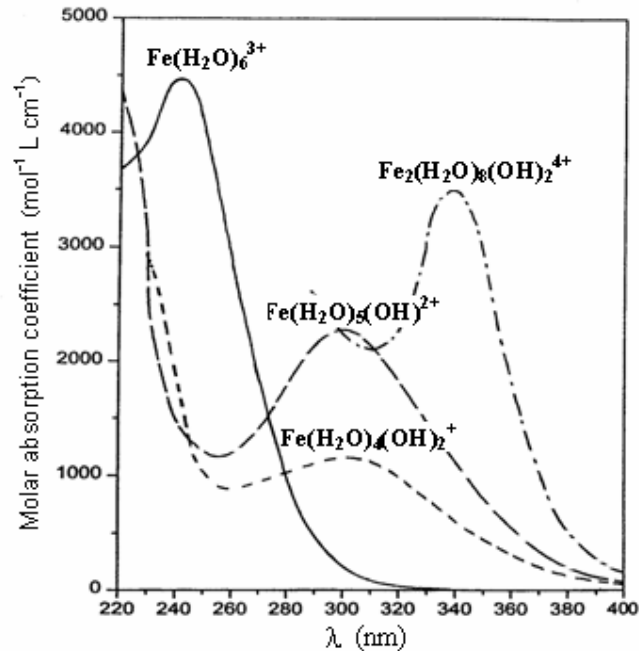


Figure II-A-10 UV-visible spectra of Fe(III) aqueous complexes

- The UV-visible absorption spectra of  $\text{Fe}^{3+}$  complex ( $\text{Fe}(\text{H}_2\text{O})_6^{3+}$ ) presents a maximum absorbance at 240 nm with a molar absorption coefficient of 3850-4500  $\text{L} \cdot \text{mol}^{-1} \cdot \text{cm}^{-1}$  (Langford et al., 1975; Knight et Sylva, 1975; Milburn, 1956).
- The UV-visible spectra of  $\text{Fe}(\text{OH})^{2+}$  complex ( $\text{Fe}(\text{H}_2\text{O})_5(\text{OH})^{2+}$ ) presents a maximum absorbance at 297 nm with a molar absorption coefficient 2000  $\text{L} \cdot \text{mol}^{-1} \cdot \text{cm}^{-1}$  (Weschler et al., 1986; Faust and Hoigné, 1990).
- The UV-visible spectra of  $\text{Fe}(\text{OH})_2^+$  complex ( $\text{Fe}(\text{H}_2\text{O})_4(\text{OH})_2^+$ ) presents a maximum absorbance at 297 nm with a molar absorption coefficient poorly defined, between 1100  $\text{L} \cdot \text{mol}^{-1} \cdot \text{cm}^{-1}$  (Escot, 1973) and 1800  $\text{L} \cdot \text{mol}^{-1} \cdot \text{cm}^{-1}$  (Knight and Sylva, 1975).
- The UV-visible spectra of dimeric  $\text{Fe}_2(\text{OH})_2^+$  complex ( $\text{Fe}_2(\text{H}_2\text{O})_8(\text{OH})_2^{4+}$ ) has a maximum absorbance at 350 nm with a molar absorption coefficient of 3500  $\text{L} \cdot \text{mol}^{-1} \cdot \text{cm}^{-1}$  (Milburn, 1956) or 8300  $\text{L} \cdot \text{mol}^{-1} \cdot \text{cm}^{-1}$  (Knight et Sylva, 1975) according to the authors.
- The Fe(III) aggregates present in aqueous solution has a continuous absorption increasing from 500 to 200 nm.

## **B-Iron-Carboxylate complexes**

### **B-1-Carboxylic acids in the environment**

Carboxylic acids have received considerable attention as one of the most common dissolved organic compounds present in natural environment (Thurman, 1985; Perdue et al., 1990). They are also considered to be one of the dominant classes of organic compounds found in the atmosphere in a variety of phases (Talbot et al., 1995, 1996a, b, 1997a, b, Chebbi and Carlier, 1996). They have been found in rainwater (Kumar et al., 1993; Guiang et al., 1984; Khare, 1997; Sempéré, 1996), snow and ice (Gunz and Hoffmann, 1990), on aerosol particles (Limbeck et al., 1999; Kawamura and Ikushima, 1993; Khwaja, 1995; Grosjean, 1989) and in the gas phase (Kumar et al., 1996; Talbot et al., 1988; Grosjean, 1990; Hartmann et al., 1989). Formic and acetic acids constitute the most abundant carboxylic acids in the global troposphere (Keene and Galloway, 1984; 1986).

Polycarboxylates, including citrate, malonate, and oxalate, are common constituents of precipitation (Likens et al., 1983), fog (Kawamura et al., 1985), urban (Grosjean et al., 1978; Satsumabayashi et al., 1990) and remote (Kawamura and Gagosian, 1990) tropospheric aerosols, surface waters (Thurman, 1985; Lamar and Goerlitz, 1966), and soil solutions (Fox, 1990). Table II-B-1 gives some distribution of carboxylic acids in different sites. The ubiquitous presence of carboxylic acids in the environment is an important aspect to be investigated.

**Table II-B-1 Monocarboxylic and dicarboxylic acids investigated in aerosols at different sites**

<b>Sampling sites</b>	<b>Monocarboxylic acids</b>	<b>Dicarboxylic acids</b>	<b>Polyfunctional compounds</b>	<b>References</b>
Antwerpen (urban)	C12-C29	-	-	Cautreels and Cauwenberghe, 1976
Los Angeles (urban)		C3-C10		Grosjean et al., 1978

Los Angeles (urban)	C9-C30	C3-C9		Rogge et al., 1993b
Hong Kong (urban)	C12-C32			Zheng et al., 1997
Kuala Lumpur (urban)	C12-C32	C9-C29		Radzi B. A. and Simoneit, 1996
Tokyo (urban)	C8-C32			Matsumoto and Hanya, 1980
Tokyo (urban)		C2-C9		Sempéré and Kawamura, 1994
New York (State)	C1, C2	C2,C4	C2,C3	Khwaja, 1995
Antarctica		C2-C11	C2-C9	Kawamura, et al., 1996
Vienna	C12-C18	C2-C8	C2,C3	Limbeck and Puxbaum., 1999
South Africa	C12-C18	C2-C8	C2,C3	Limbeck and Puxbaum., 1999
Soonblick	C12-C18	C2-C8	C2,C3	Limbeck and Puxbaum., 1999

### **B-2-Photochemical property of Fe-Carboxylate complexes**

Many bibliographies indicate that carboxylates can form strong complexes with iron. Inorganic Fe(III) complexes are recognised to be photoreactive (King et al., 1993; Deng et al., 2006), natural organic chromophores greatly enhance the Fe(III) reduction rates under solar radiation conditions (Waite and Morel, 1984a; Wells et al., 1991; Erel et al., 1993).

In systems containing organic ligands which adsorb to Fe(III) oxides, there is generally an increase in the efficiency of iron photodissolution over that observed in inorganic solutions. Carboxylic acids (Waite and Morel, 1984a; Cunningham et al., 1988), thiol containing compounds (Waite and Torikov, 1987), adsorbed alcohols (Cunningham et al., 1985), and freshwater fulvic acids (Waite and Morel, 1984a) have all been shown to significantly enhance photochemical production of Fe(II) from Fe(III) oxides. In all of these cases, the resulting reaction products were Fe<sup>2+</sup> and oxidation products of the adsorbed species. Evidence from studies on the photooxidation of oxalate, sulfite, and iodide by iron oxides suggest that reduction of

Fe(III) proceeds by direct light absorbance at the LMCT (ligand to metal charge transfer) band of the surface bound organic complex (Faust and Hoffmann, 1986; Leland and Bard, 1987; Sulzberger et al., 1989; Waite, 1990). This process provides a simple explanation of experimental observations but does not exclude the alternative mechanisms of electron transfer after light excitation at other chromophoric sites within the ligand or solid (Waite and Morel, 1984b; Cunningham et al., 1988; Waite, 1990).

In the presence of dissolved organic ligands of iron, the photoreactivity of iron is significantly altered (Figure II-B-1). Oxalic, citric, malic, glyceric, salicylic, tartaric, glutaric, gluconic, and p-hydroxybenzoic acids have all been shown to increase photoproduction of Fe(II) in solution (Cunningham et al., 1988; Kuma et al., 1992; Zuo and Zhan, 2005) by as much as three orders of magnitude depending on the nature and concentration of the ligand. Evidence has been presented for the extensive organic complexation of iron in oceanic waters (Gledhill and van den Berg, 1994; Rue and Bruland, 1995-this volume; Wells et al., 1995) which should make homogenous mechanisms for Fe(II) photoproduction (reviewed by Faust, 1994) also relevant to any explanation of observed Fe(II) distributions in natural waters.

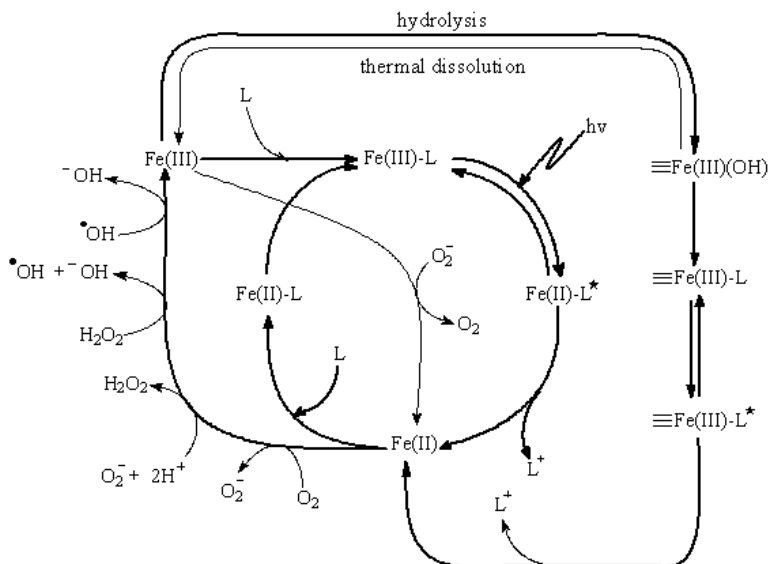


**Figure II-B-1** The mechanism of photochemical redox cycling of iron in the aqueous solution. Fe(II)-L and Fe(III)-L represent Fe(II) and Fe(III) complexed with Ligand. (Abida, 2005)

The half-lives of Fe(III)-polycarboxylate species in sunlight (latitude 34° N, at midday in June) are 0.2 min for Fe(oxalate)<sup>+</sup>/Fe(oxalate)<sub>2</sub><sup>-</sup> (Hoigné, 1990; Zuo and Hoigné, 1992), 5 min for Fe(malonate)<sup>+</sup>/Fe(malonate)<sub>2</sub><sup>-</sup>, and 0.9 min for Fe(OH)(citrate)<sup>-</sup> (Faust and Zepp, 1993). With half-lives on the order of minutes, the photolysis of Fe(III)-polycarboxylates represents a potentially important source of Fe(II) to atmospheric and surface waters and could easily account for much of the Fe(II) formation in many natural waters. Figure II-B-2 presents the reaction scheme for the photolysis of Fe(III) complexes of polycarboxylates (oxalate, malonate, citrate). Under irradiation, many kinds of active radicals (ROO·, ·O<sub>2</sub><sup>-</sup>, HO<sub>2</sub>·, ·OH) are generated in the solution. From the scheme, iron concentration, pH and oxygen are all important parameters

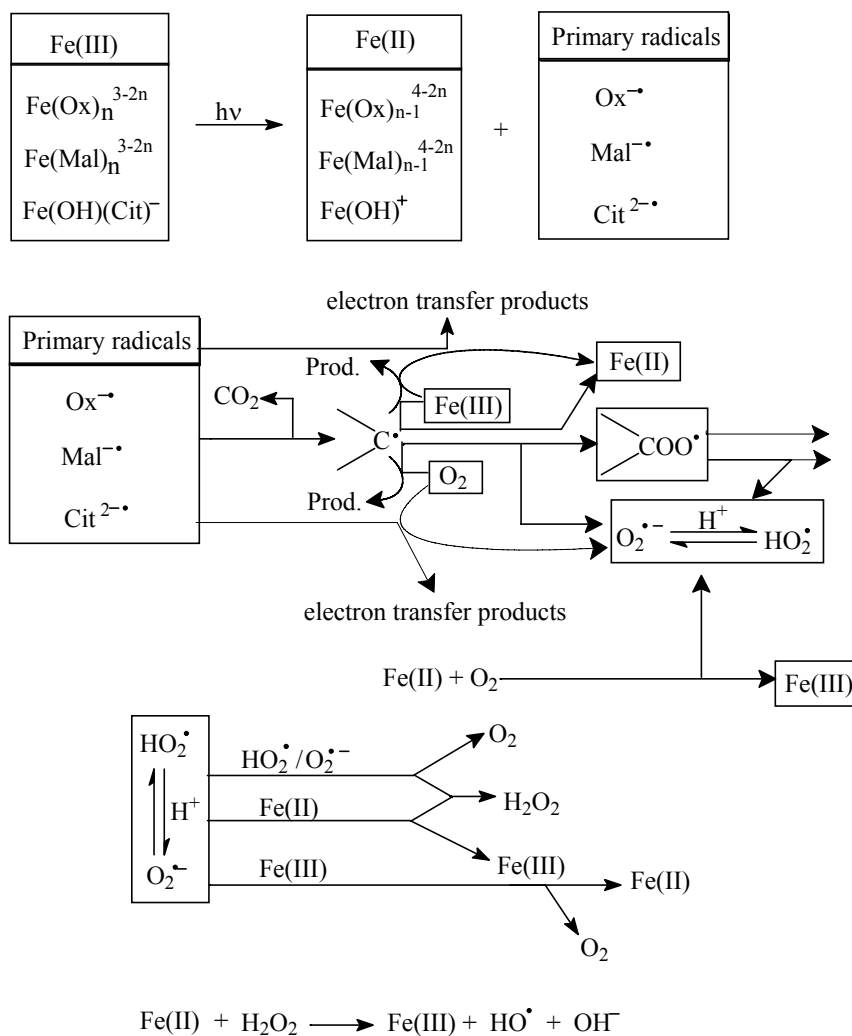


Figure II-B-2 Reaction scheme for the photolysis of Fe(III)-polycarboxylate complexes

The oxidation rate of Fe(II) was apparently affected by the chelators with oxygen ligands in the aqueous solution (Welch et al., 2002). The first order rate constant of Fe(II) oxidation has been listed in Table II-B-2. EDTA, NTA, citric acid, deferoxamine and benzoquinone significantly increased the rate of Fe(II) oxidation, approximately six- to tenfold over the rate of autoxidation in the buffer alone. Conversely, chelators with nitrogen ligands that would stabilize Fe(II), inhibited the rate of oxidation, although not as significantly as the oxygen rich chelators had a stimulating effect. However, pyruvic acid appeared to inhibit the rate of Fe(II) oxidation.

**Table II-B-2 The effect of chelation on the rate of Fe(II) oxidation.**  
**[Fe(II)] = 110  $\mu\text{mol.L}^{-1}$ , [chelator] = 550  $\mu\text{mol.L}^{-1}$ , 50  $\text{mmol.L}^{-1}$  Tris buffer, pH 7.0**

<b>Chelator</b>	<b>k (<math>\text{s}^{-1}</math>)</b>
None	1.2
EDTA	>11.5
NTA	>11.5
Citric acid	7.2
ADP	4.0
Oxalic acid	2.3
Histidine	2.0
Histamine	1.0
Glycine	1.5
Deferoxamine	>11.5
Hydroquinone	1.2
Pyruvic acid	0.8
Benzoquinone	10.7

**Note.** Ultra pure tris(hydroxymethyl) aminomethane hydrochloride (Tris)

### **B-2-1-Fe-Oxalate complexes**

As indicated above, ferrioxalate is a photosensitive complex that is able to expand the usage of solar spectrum range up to 450 nm (18% of solar irradiation) improving the oxidation efficiency of the solar-Fenton process (Nogueira et al., 2000, 2005; Emilio et al., 2002).

There is very little information on the ferrioxalate assisted photo-Fenton systems using ferrous initiated processes. Sulzberger (1995) presented a linear free energy relation between the redox potential of Fe(III)/Fe(II) species and the pseudo first-order rate constant of Fe(II) oxygenation, as shown in Figure II-B-3.

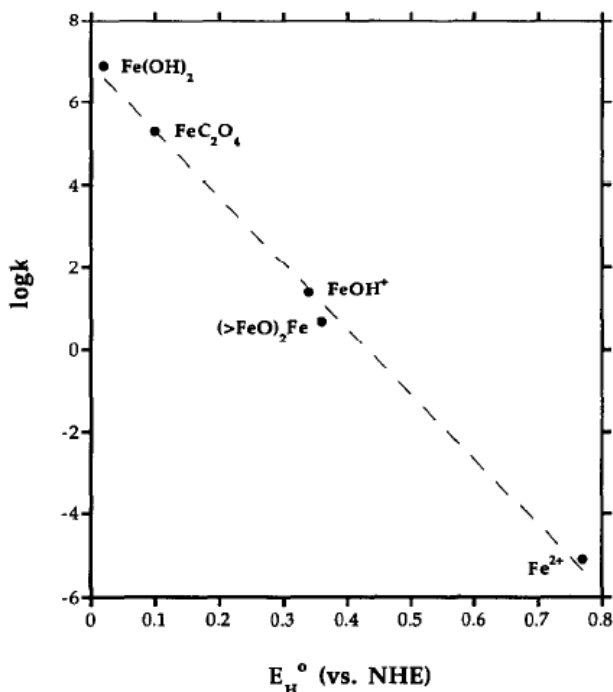
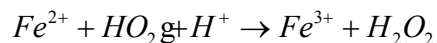


Figure II-B-3 Logarithm of the reaction rate constant ( $\text{mol}^{-1} \cdot \text{L} \cdot \text{s}^{-1}$ ) of oxidation of Fe(II) species by  $\text{O}_2$ , as a function of the redox potential,  $E_H^0$  (vs. NHE), for the corresponding Fe(III)/Fe(II) redox couples (Sulzberger *et al.*, 1995)

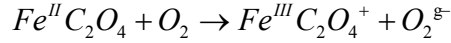
The redox potential of the oxygenation of Fe(II) that is inner-spherically adsorbed on a goethite surface,  $(>\text{FeO})_2\text{Fe}$ , can be estimated from the experimentally determined rate constant (Tamura *et al.*, 1976), and the rate constant of oxygenation of  $\text{Fe}^{\text{II}}\text{C}_2\text{O}_4$  can be estimated from the calculated redox potential. Data for the rate constants of  $\text{Fe}^{2+}$  and  $\text{Fe(OH)}^+$  oxygenation are from Singer and Stumm (1970) and for  $\text{Fe(OH)}_2$  oxygenation from Millero *et al.* (1987) (modified from Wehrli, 1990).

Fe(II) is readily oxidized by  $\text{HO}_2\cdot / \text{O}_2\cdot^-$ , At pH 3.0,  $\text{HO}_2\cdot$  is predominant, since its acidity constant is 4.8 (Bielski *et al.*, 1985):

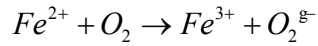


$$\log k = 6.1 \text{ (Rush and Bielski, 1985)}$$

Using the linear free energy relation shown in Fig. 4, the bimolecular rate constant of oxidation of  $Fe^{II}C_2O_4$  (1: 1 stoichiometry) by  $O_2$  may be estimated and compared to that of  $Fe^{2+}$  oxygenation:

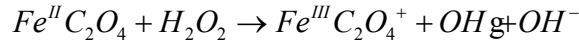


$$\log k = 5.3 \text{ (Sulzberger et al., 1995)}$$

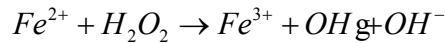


$$\log k = 5.1 \text{ (Singer and Stumm, 1970)}$$

Complexation by oxalate also enhances Fe(II) oxidation by  $H_2O_2$  (Sedlak and Hoigne, 1993):



$$\log k = 4.5 \text{ (Sedlak and Hoigne, 1993)}$$



$$\log k = 1.8 \text{ (Hartwick, 1957)}$$

In recent years, ferrioxalate has been widely used in the photo-Fenton reaction involving ferric compounds.

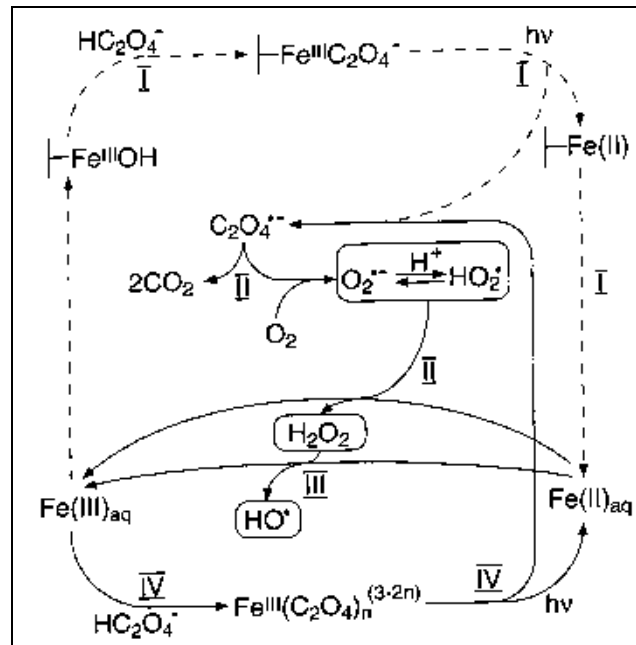
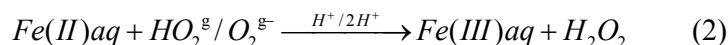
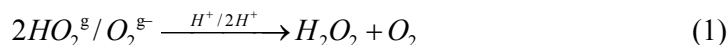


Figure II-B-4. Light-induced iron cycling, and surface (--) and solution (s) reactions in heterogeneous photo-Fenton systems. (Mazellier and Sulzberger, 2001)



Figure II-B-4 presents the various surfaces and solution reactions, the intermediates and products formed in heterogeneous photo-Fenton systems in which Fe(III) oxalate surface and solution complexes are photolyzed. Dissolved Fe(II) [Fe(II)(aq)], the superoxide/hydroperoxyl radicals ( $O_2^{\cdot-}/HO_2^{\cdot}$ ), and hydrogen peroxide ( $H_2O_2$ ) are key intermediates. In systems containing initially a solid Fe(III) (hydr)oxide phase such as goethite (R-FeOOH), Fe(II)(aq) formation proceeds initially via photolysis of Fe(III) oxalate surface complexes (Waite and Morel, 1984; Siffert and Sulzberger, 1991) (reaction sequence I). Thereby, the first essential step consists of the specific adsorption of oxalic acid on the surface of the Fe(III) (hydr)oxide. Photolysis of the Fe(III) surface complex is followed by dissociation of the oxalate radical,  $C_2O_4^{\cdot-}$ , from the surface and detachment of the reduced surface iron center from the crystal lattice and transfer into solution. The oxalate radical reacts with molecular oxygen yielding  $O_2^{\cdot-}$ , where  $O_2^{\cdot-}$  is in equilibrium with  $HO_2^{\cdot}$  ( $pK_a = 4.8$ ; Bielski et al., 1995). The product of  $HO_2^{\cdot}/O_2^{\cdot-}$  dismutation is  $H_2O_2$ , by the following reactions:



Hydrogen peroxide formed from  $HO_2^{\cdot}/O_2^{\cdot-}$  is another significant oxidant of Fe(II)(aq) by the Fenton reaction yielding  $\cdot HO$ ,



The rate constants of Fe(II)(aq) oxidation by  $HO_2^{\cdot}/O_2^{\cdot-}$  and by  $H_2O_2$  depend critically on the Fe(II)(aq) speciation. In the presence of excess oxalate, Fe(III)(aq) is present as dissolved iron(III) oxalate complexes that undergo photolysis (reactions IV in Figure II-B-2) leading ultimately to  $\cdot OH$  production.

Hug et al., (1997) studied the photoreduction of Cr(VI) induced by Fe(III)-Oxalate complexes (Figure II-B-5).

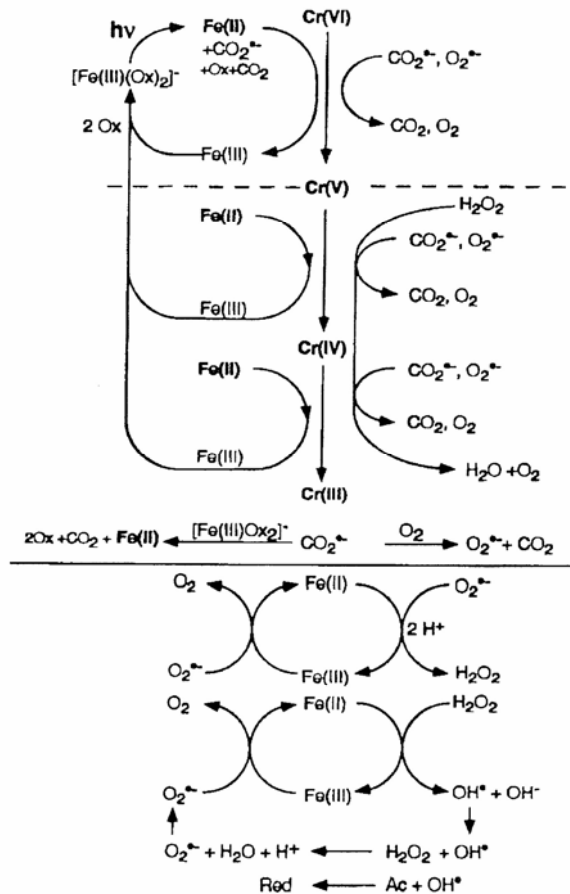
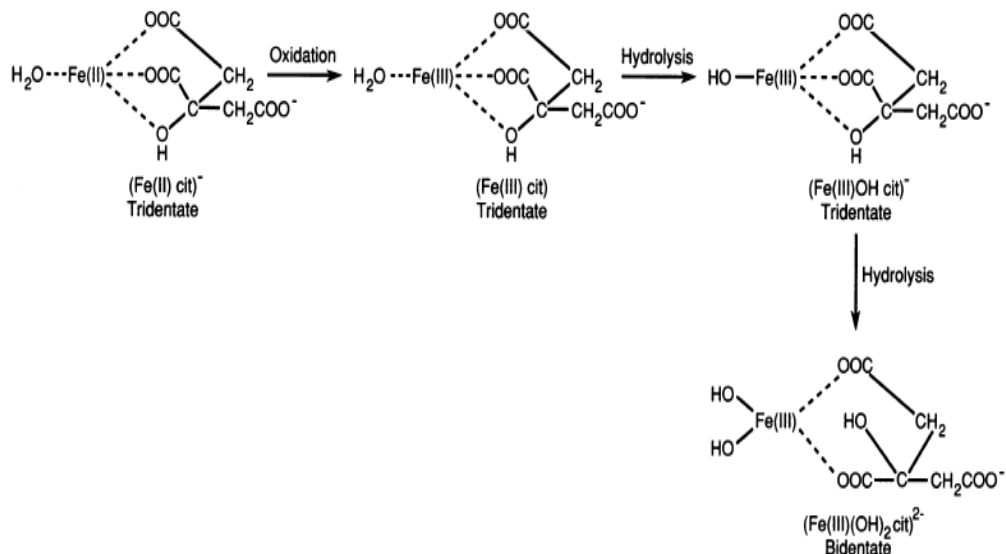


Figure II-B-5 Possible reactions in illuminated solution containing Cr(VI), Oxalate, and Fe(II, III) (Hug et al., 1997).

**B-2-2-Fe-Citrate complexes**

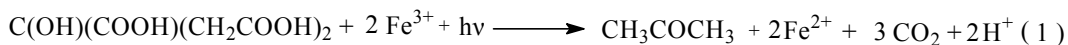
Hamm studied the formation of Fe(III) complexes with Citric acid (Cit) and got the following forms,  $(\text{FeHCit})^+$ ,  $\text{FeCit}$ ,  $(\text{FeOHCit})^-$  and  $(\text{Fe}(\text{OH})_2\text{Cit})^{2-}$  (Hamm et al, 1954). Citric acid forms a mononuclear bidentate complex,  $[\text{Fe}(\text{III})(\text{OH})_2\text{Cit}]^{2-}$ , with ferric iron involving two carboxylic acid groups and a tridentate complex,  $[\text{Fe}(\text{II})\text{Cit}]^-$ , with ferrous iron involving two carboxylic acid groups and the hydroxyl group. But some study also have indicated that a tridentate complex  $[\text{Fe}(\text{III})\text{cit}]$  is formed below pH 3 (Timberlake, 1964), and a bidentate dimer complex formed at neutral pH (Dhar et al., 1969). Nuclear magnetic resonance studies of ferrous-citrate confirmed the formation of a tridentate complex involving the hydroxyl group (Strouse, 1977). In the presence of oxygen, the ferrous-citrate complex undergoes oxidation and

hydrolysis, leading to the formation of ferric iron-citrate complex. The intermediates involved in the conversion of ferrous-citrate to ferric-citrate are presented in Figure II-B-6.



**Figure II-B-6 Oxidation and hydrolysis of tridentate Fe(II)-Citrate complex to bidentate Fe(III)-Citrate complex.**

From the 1910s, numerous investigations have shown that photochemical dissociation of Fe(III)-citrate complexes in aqueous solution involved reduction of Fe(III) to Fe(II) and concomitant oxidation of the carboxylic acid, resulting in the formation of acetone and carbon dioxide as the final products (Abrahamson et al., 1994; Buchanan, 1970; Frahn, 1958). The general reaction can simply be represented as:



The efficiency of the photoreduction reaction in aqueous solutions depends much on two factors; the pH and the initial citrate to metal ratio (Zhang et al., 2006). From above, it is indicated that the photolysis of Fe(III)-citrate complexes cause the formation of some reactive species (e. g.  $\text{H}_2\text{O}_2$  and  $\cdot\text{OH}$ ). Hydroxyl radicals produced in the water containing Fe(III)-citrate complexes can oxidize organic compounds coexisting in the aqueous solutions (Chen et al., 2007).

### B-2-3-Fe-Tartrate complexes

Tartaric acid (Tar) in aqueous solution is of considerable significance in many biochemical and chemical processes. Neutral and acid salts of tartaric acid ( $H_2Tar$ ) are produced in large quantities and used in the food, cosmetic, pharmaceutical and chemical industries. Tartrate ions are ubiquitous in environmental samples and are found in the concentration range from low ppb to ppm. The formation of Fe(III)-Tar complexes has been reported in many bibliographies. Most reports is about the complex stoichiometry in 1:1 or 2:2 (Chevela et al., 1995; Mentasti and Baiocchi, 1980). Kostromina et al. (1987) studied the distribution of complexes in the solution with the concentration of  $Fe(NO_3)_3$ /Tartaric acid in 1:1 (as Figure II-B-7).

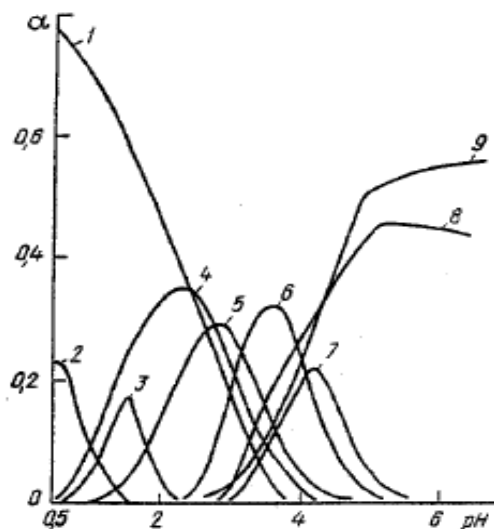


**Figure II-B-7 Diagram of distribution of complexes in the system  $Fe(NO_3)_3$ -Tartaric acid (1:1): 1)  $Feaq$ ; 2)  $FeH_3tar$ ; 3)  $Fe_2-(H_3Tar)(H_2Tar)$ ; 4)  $FeH_2Tar$ ; 5)  $Fe_2(H_2Tar)_2$ ; 6)  $FeHTar$ ; 7)  $Fe_2(HTar)_2$ ; 8)  $FeTar$ ; 9)  $Fe_2(Tar)_2$ .(Kostromina et al., 1988)**

The construction of Stuart-Briegleb three-dimensional models showed that when dimmer complexes are formed (Figure II-B-8), two iron atoms may be bonded to all the donor groups of the tartaric acid anions ( $H_2Tar^{2-}$ ,  $HTar^{3-}$ ,  $Tar^{4-}$ ).

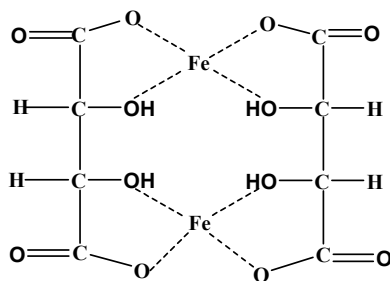


Figure II-B-8 Dimer complexes

In the complex  $\text{Fe}_2(\text{H}_3\text{Tar})(\text{H}_2\text{Tar})$ , either the same mode of coordination with delocalization of a proton is set up, or there is no bond to the COOH group. The structure of the dimer complexes and the changes in the stability constants during deprotonation and dimerization suggest the following most probable modes of coordination for monomer complexes (Kostromina et al., 1988):

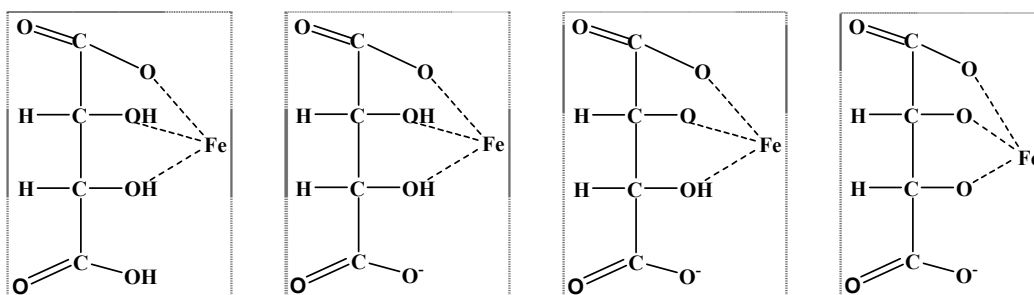
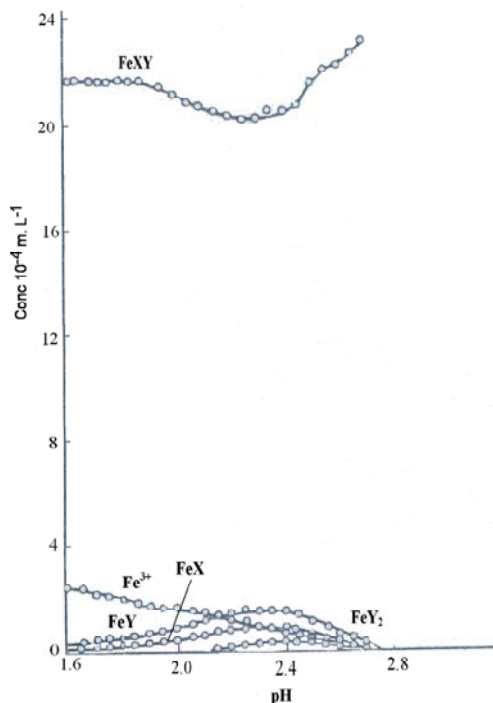


Figure II-B-9 Proposed monomer complexes

Ramamoorthy and Manning (1972) have studied the formation of Fe(III)-Tar complexes in the mixed-ligand system with DL- and meso-Tartaric acid. Titrations were performed for metal/ligand = 1:1 and 1:2 to allow the formation of higher complexes. Results indicated the formation of complexes in 1:1 and 1:2. The value of  $\log K_{\text{ML}2}$  for the Fe(III)-meso-tartrate system is greater than that of the DL-Tartrate.

Figure II-B-10 presents the distribution of Fe(III) into various complex species as well as free Fe(III) ions, as a function of pH. The mixed ligand complex is the predominant species, binding nearly 88% of total free ion around pH 1.6, the free Fe(III) being the other species. The concentration of free Fe(III) and mixed complex

decrease slightly in the pH range 2.0~2.4 with consequent formation of the simple complexes. The concentration of simple complexes reaches a maximum around pH 2.4 and thereafter the concentration of mixed complex starts increasing again.



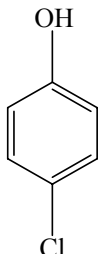
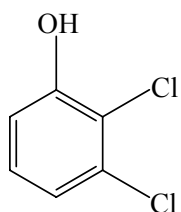
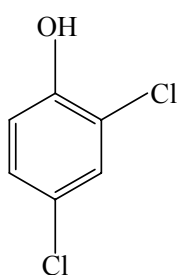
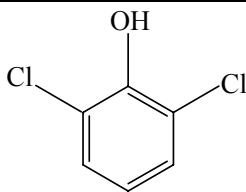
**Figure II-B-10 Distribution of complexes in Fe(III)-meso-dl tartaric acid systems.**  
 $[\text{Fe(III)}]:[\text{meso-Tar}]:[\text{DL-Tar}]=2.458:2.484:2.493 \times 10^{-3} \text{ mol.L}^{-1}$ . X represents DL-Tar and Y represents meso-Tar.

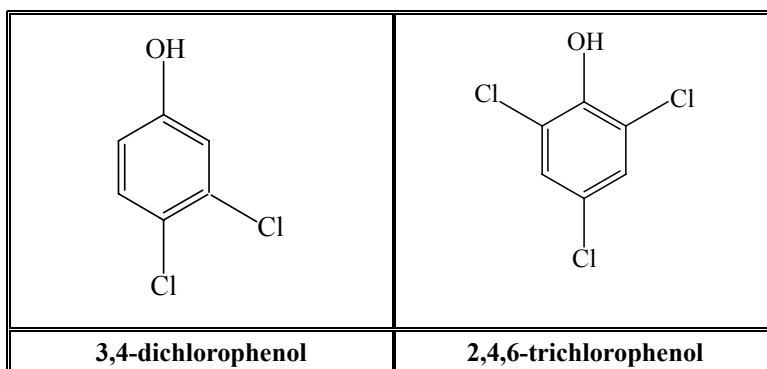
Tartrate as a ligand can form complex with other metal ions, such as Al (Desroches et al., 2000). Gallet and Paris (1968) reported the formation of only 1:1 and 1:2 complexes from thermometric studies of tartrates and citrates of lanthanides. Motekaitis and Martell (1984) calculated constants for the following series of complexes (with M standing for Al(III) and L for dianionic tartrate):  $\text{MLH}_{-1}$ ,  $\text{MLH}_{-2}$ ,  $\text{ML}_2$ ,  $\text{ML}_2\text{H}_{-1}$ ,  $\text{ML}_2\text{H}_{-3}$ ,  $\text{ML}_3\text{H}_{-4}$ ,  $\text{ML}_3\text{H}_{-5}$  and  $\text{ML}_3\text{H}_{-6}$  in  $0.1 \text{ mol.L}^{-1}$  of  $\text{KNO}_3$  and at  $25^\circ\text{C}$ . However, Marklund and Öhman (1990) characterized instead  $\text{ML}$ ,  $\text{M}_2\text{L}_2\text{H}_{-1}$ ,  $\text{M}_2\text{L}_2\text{H}_{-2}$ ,  $\text{M}_2\text{L}_2\text{H}_{-3}$ ,  $\text{M}_2\text{L}_2\text{H}_{-4}$  in  $0.6 \text{ mol.L}^{-1}$  of  $\text{NaCl}$  and at  $25^\circ\text{C}$ .

## C-Chlorophenols

Like many phenolic compounds, chlorophenols are environmental pollutants of great health concern. Among the 19 different chlorophenols, 2-chlorophenol (2-CP), 2,4-dichlorophenol (2,4-DCP), 2,4,6-trichlorophenol (2,4,6-TCP) and pentachlorophenol (PCP) have been listed by the US EPA as priority pollutants (Ormad, et al., 2001). Table II-C-1 lists some common chlorophenols. These compounds have widely been used in the manufacture of pesticides, insecticides, herbicides, fungicides, intermediates of dyes and other industrial chemicals. Chlorination of phenols during the disinfection of waste water also produces chlorophenols. These result in contamination of many lakes and water streams by chlorophenols (Keating et al., 1978; Othmer et al., 1979; Prengle et al., 1976). Due to their toxicity, they are consequently harmful to human, animal, and fish that are exposed to such contaminated environments. Thus, the removal or destruction of these compounds by other chemical or physical means is often required.

**Table II-C-1 Structures of common chlorophenols**

	
<b>4-chlorophenol</b>	<b>2,3-dichlorophenol</b>
	
<b>2,4-dichlorophenol</b>	<b>2,6-dichlorophenol</b>



**C-1-The contamination potential of 2, 4-Dichlorophenol (2,4-DCP) in the environment**

2,4-dichlorophenol (2,4-DCP) as a dichlorophenol, has a wide environmental concern because it is commonly used as mothproofing and miticide. Its molecular structure is shown in Table II-C-1. The largest uses for 2,4-DCP have also been found as an intermediate, especially in the manufacture of the herbicide 2,4-dichlorophenoxyacetic acid (2,4-D) and pesticides. 2,4-DCP is so highly toxic that even a small amount on the skin can be lethal. In October 1998, the U.S. Environmental Protection Agency (EPA) was notified of the death of a worker acutely exposed to 2,4-DCP. Five chemical-plant workers has died from 2,4-DCP exposure in the US from 1980-1998 (US EPA, 2000). Man who is exposed to 2,4-DCP, could through breathing cause risk of cancers, and through the skin developed acne and cause mild injure to his livers (ATSDR, 1999). 2,4-DCP can be present in drinking water when chlorine is used to disinfect it, therefore, the most likely source from which children could be exposed to 2,4-DCP, is water that has been disinfected by chlorine.

Volatilization may be the major dispersal mechanism of DCP into the atmosphere, as a result, it has often been detected in atmospheric emissions from the combustion of municipal solid waste, hazardous waste, coal, wood, and 2,4-DCP-based herbicides (Oberg et al.,1989). It was reported that 2,4-DCP was also found in the leachate from an industrial landfill (Brown et al., 1988). Moreover, some



chlorophenols, such as 2,4,5-trichlorophenoxyacetic acid (2,4,5-T) that is often used as herbicide on food crops, can break down to form 2,4-DCP. Therefore it has often been detected both in surface water and groundwater in addition to various aqueous systems and terrestrial systems.

However, the majority (85%) of known environmental releases of 2,4-DCP were to surface water through effluents discharged from industries that manufacture iron and steel, electrical components, photographic processing, pharmaceuticals, organic chemicals and from paper or pulp mills (US EPA, 1981; Paasivirta et al., 1985). Due to the great solubility and high mobility and wide distribution in the environment, 2,4-DCP has been taken as one of the priority pollutants in effluent by US EPA (1992) that regulates a wastewater discharge limitation  $112 \text{ mg.L}^{-1}$  for one day, and monthly average maximum concentration should not exceed  $39 \text{ mg.L}^{-1}$  under the best available treatment technology while  $0.3 \text{ mg.L}^{-1}$  for the drinking water quality standard and  $3.08 \text{ mg.L}^{-1}$  for both ambient water quality criteria and fishery water. The environmental fate and transport of 2,4-DCP are controlled by its physical and chemical properties and environmental conditions. Volatilization of 2,4-DCP from water is expected to be slow and, therefore, not a major removal process from surface waters. The biological treatment of waste containing 2,4-DCP has showed that none of the chemicals is removed by stripping (Stover and Kincannon, 1983). Volatilization from topsoil is also not expected to be a significant removal process. Thus, the environmental fate and transport of 2,4-DCP has the tendency to partition into sediments and lipids and to bioconcentrate.

### **C-2-Degradation of 2,4-DCP**

In recent years, advanced oxidation processes (AOPs) have been widely used in wastewater treatment (Stafford et al., 1994; Lunar et al., 2000; Kurbus et al., 2003; Brillas et al., 2003; Trojanowicz et al., 2002), the main feature of them is producing  $\cdot\text{OH}$  radicals to oxidize various organic contaminants (Figure II-C-1).

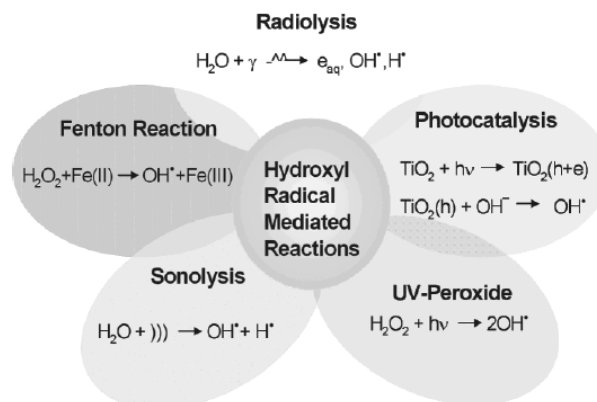


**Figure II-C-1 Advanced oxidation technologies**

Here reviewed the degradation of chlorophenols by means of advanced oxidation process in recent ten years (Pera-Titus et al., 2004). Table II-C-2 gives the data concerning the half life times and pseudo first order kinetic constants for degradation of 2,4-DCP by advanced oxidation processes.

**Table II-C-2 Degradation of 2,4-Dichlorophenol by means of advanced oxidation processes (Pera-Titus, 2004)**

Direct UV-photolysis									
[2,4-DCP] (mmol.L <sup>-1</sup> )	pH	T (°C)	Radiation intensity (einstein L <sup>-1</sup> s <sup>-1</sup> )	λ (nm)	t <sub>1/2</sub> (min)	K <sub>2,4-DCP</sub> (min <sup>-1</sup> )	Ref.		
0.3	2.0	Room	4.80 × 10 <sup>-4</sup>	185–436	17.5	3.80 × 10 <sup>-2</sup>	Benítez, 2000		
0.3	2.0	25	3.52 × 10 <sup>-5</sup>	185–436	-	3.80 × 10 <sup>-2</sup>	Benítez, 2001		
0.3	9.0	25	3.52 × 10 <sup>-5</sup>	185–436	-	0.173			
0.78	6.0	Room	5.97 × 10 <sup>-5</sup>	320–400	10.3	5.90 × 10 <sup>-4</sup>	Kuo, 1999		
0.78	9.0	Room	5.97 × 10 <sup>-5</sup>	320–400	62.0	7.00 × 10 <sup>-4</sup>			
0.40	2.5	Room	6.45 × 10 <sup>-7</sup>	250	70.0	6.95 × 10 <sup>-3</sup>	Trapido, 1997		
0.40	9.5	Room	6.45 × 10 <sup>-7</sup>	250	14.7	4.98 × 10 <sup>-2</sup>			
0.40	-	Room	2.04 × 10 <sup>-4</sup>	-	20.0	0.130	Baum, 1995		
Fenton's reagent (H <sub>2</sub> O <sub>2</sub> /Fe <sup>2+</sup> )									
[2,4-DCP] (mmol.L <sup>-1</sup> )	pH	T (°C)	[H <sub>2</sub> O <sub>2</sub> ] (mmol.L <sup>-1</sup> )	[Fe <sup>2+</sup> ] (mmol.L <sup>-1</sup> )	t <sub>1/2</sub> (min)	K <sub>2,4-DCP</sub> (min <sup>-1</sup> )	Ref.		
0.50	3.5	Room	5.0	0.20	-	0.995	Tang, 1996		
0.30	2.0	Room	7.5	0.01	2.4	0.209	Benítez, 2000		
0.51	7.1	22	5.9	0.20	4.0	-			
0.51	7.1	22	5.9	2.00	87.0	-			
0.30	2.0	25	0.5	0.01	Not reached	7.00 × 10 <sup>-4</sup>	Benítez, 2001		
photo Fenton's reagent									
[2,4-DCP]	pH	T	Radiation	[H <sub>2</sub> O <sub>2</sub> ]	[Fe <sup>2+</sup> ]	λ (nm)	t <sub>1/2</sub>	k <sub>2,4-DCP</sub>	Ref.

(mmol.L <sup>-1</sup> )	(°C)	intensity (einstein L <sup>-1</sup> s <sup>-1</sup> )	(mmol. L <sup>-1</sup> )	(mmo L.L <sup>-1</sup> )	(min)	(min <sup>-1</sup> )			
0.80	2.0	25	-	4.00	0.02	>300	25.0	-	Shul'pin, 1997
0.30	2.0	25	$4.80 \times 10^{-4}$	0.50	0.01	185–436	0.9	$8.8 \times 10^{-2}$	Benítez, 2000
0.30	2.0	25	$3.52 \times 10^{-5}$	0.50	0.01	185–436	-	$8.8 \times 10^{-2}$	Benítez, 2001
<b>H<sub>2</sub>O<sub>2</sub>/UV reagent</b>									
[2,4-DCP] (mmol.L <sup>-1</sup> )	pH	T(°C)	Radiation intensity (einstein L <sup>-1</sup> s <sup>-1</sup> )	[H <sub>2</sub> O <sub>2</sub> ] (mmol. L <sup>-1</sup> )	λ (nm)	t <sub>1/2</sub> (min)	K <sub>2,4-DCP</sub> (min <sup>-1</sup> )		Ref.
0.30	2.0	Room	$4.80 \times 10^{-4}$	0.5	185–436	14.5	$4.40 \times 10^{-2}$		Benítez, 2000
0.30	2.0	25	$4.80 \times 10^{-4}$	0.5	185–436	-	$2.54 \times 10^{-2}$		Benítez, 2001
0.40	2.5	Room	$6.45 \times 10^{-7}$	40.0	250	7.9	$8.64 \times 10^{-2}$		Trapido, 1997
0.40	9.5	Room	$6.45 \times 10^{-7}$	40.0	250	11.0	$5.22 \times 10^{-2}$		Hugül, 2000
0.74	-	25	$4.87 \times 10^{-4}$	0.74	240-570	110.0	-		
<b>Ozone reagent</b>									
[2,4-DCP] (mmol.L <sup>-1</sup> )	pH	O <sub>3</sub> feed flow rate (mg min <sup>-1</sup> )	t <sub>1/2</sub> (min)	K <sub>2,4-DCP</sub> (min <sup>-1</sup> )	k <sub>O<sub>3</sub></sub> (min <sup>-1</sup> )				Ref.
0.3	2.0	-	30.4	-	$2.40 \times 10^{-2}$				Benítez, 2000
0.3	9.0	-	3.3	-	0.315				
0.4	2.0	-	-	-	45.3				Benítez, 2000
0.78	6.0	5.0	6.0	$3.67 \times 10^{-3}$	-				Kuo,1999
0.18	3.4	8.3	22.4	-	-				Abe,1997
-	7.0	1.2	300.0	$1.07 \times 10^{-2}$	-				Chang,1995
<b>O<sub>3</sub>/UV reagent</b>									
[2,4-DCP] (mmol.L <sup>-1</sup> )	pH	O <sub>3</sub> feed flow rate (mg min <sup>-1</sup> )	Radiation intensity (einstein L <sup>-1</sup> s <sup>-1</sup> )	λ (nm)	t <sub>1/2</sub> (min)	K <sub>2,4-DCP</sub> (min <sup>-1</sup> )			Ref.
0.30	2.0	-	$1.76 \times 10^{-5}$	185–436	15.6	$6.5 \times 10^{-2}$			Benítez, 2000
0.78	6.0	5	$5.97 \times 10^{-5}$	320-400	8.8	$8.59 \times 10^{-3}$			Kuo,1997
0.40	2.5	107.3	$6.45 \times 10^{-7}$	250	-	$5.16 \times 10^{-2}$			Trapido,199 7
0.18	3.4	8.3	$2.50 \times 10^{-5}$	-	16.8	-			Abe,1997
<b>Photocatalysis</b>									
[2,4-DCP] (mmol.L <sup>-1</sup> )	Catalyst	pH	Lamp	t <sub>1/2</sub> (min)	K <sub>2,4-DCP</sub> (min <sup>-1</sup> )				Ref.

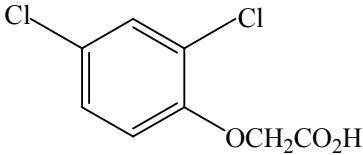
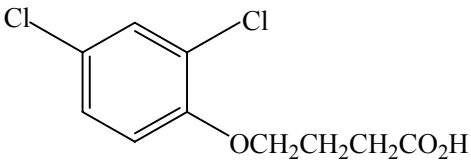
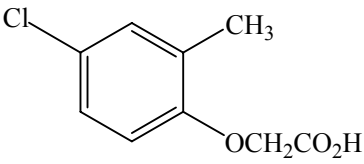
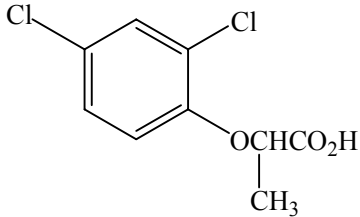
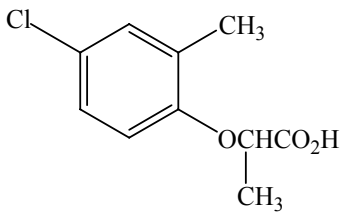
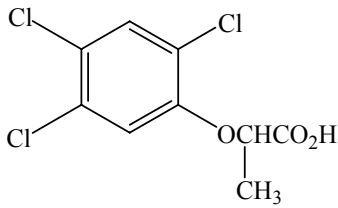
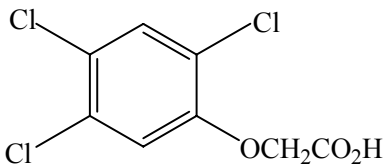
0.12	TiO <sub>2</sub> (0.1 g L <sup>-1</sup> )	6.0	125 W high pressure Hg lamp	22	4.03 × 10 <sup>-6</sup>	Jardim,1997
0.34	TiO <sub>2</sub> (0.1 g L <sup>-1</sup> )	6.6	Solar light in flat reactor	845	2.82 × 10 <sup>-7</sup>	Giménez, 1999
0.59	0.1	6.2		1368	2.98 × 10 <sup>-7</sup>	
0.57	0.2	5.9		634	6.24 × 10 <sup>-7</sup>	
0.56	0.5	6.2		433	8.93 × 10 <sup>-7</sup>	
0.60	0.5	7.6		1061	3.93 × 10 <sup>-7</sup>	
0.59	1.0	5.9		499	8.17 × 10 <sup>-7</sup>	
0.58	2.0	5.6		416	9.59 × 10 <sup>-7</sup>	
0.55	0.1	4.6	Solar light in CPCs modules	252	1.50 × 10 <sup>-6</sup>	
0.55	0.1	5.9		354	1.07 × 10 <sup>-6</sup>	
0.53	0.2	4.2		173	2.11 × 10 <sup>-6</sup>	
0.56	0.5	4.2		145	2.66 × 10 <sup>-6</sup>	
0.58	0.5	5.9		528	7.56 × 10 <sup>-7</sup>	
0.56	1.0	6.0		234	1.65 × 10 <sup>-6</sup>	
0.55	2.0	5.1		238	1.61 × 10 <sup>-6</sup>	
0.50	α-Fe <sub>2</sub> O <sub>3</sub> (1.5 gL <sup>-1</sup> )	6.0	Solar simulator	300	2.68 × 10 <sup>-6</sup>	Bandara, 2001
1.00	PW <sub>12</sub> O <sub>40</sub> <sup>3-</sup> (7.0 × 10 <sup>-4</sup> mol L <sup>-1</sup> )	1.0	Oriel 1000W Xe arc lamp	8.4	8.60 × 10 <sup>-5</sup>	Androulaki, 2000

## **D-The 2, 4-Dichlorophenoxyacetic acid (2, 4-D)**

### **D-1-Physicochemical properties of 2,4-D and contamination potential in the environment**

The chemical formula for 2,4-D is C<sub>8</sub>H<sub>6</sub>Cl<sub>2</sub>O<sub>3</sub>, and it occurs as a white crystalline powder that is almost insoluble in water (US EPA, US HSDB). The log K<sub>ow</sub> for 2, 4-D is 2.81. Table II-D-1 lists the molecular structure of 2,4-D and some chemically related herbicides.

**Table II-D-1 Structures of 2, 4-D and chemically related phenoxy herbicides.**

	
2, 4-Dichlorophenoxyacetic acid (2, 4-D)	
	
(2,4-Dichlorophenoxy) butyric acid	4-chloro-2-methylphenoxyacetic acid (MCPA)
	
2-(2,4-Dichlorophenoxy) propionic acid	$\alpha$ -(4-chloro-2-methylphenoxy) propionic acid (MCPP)
	
2-(2,4,5-trichlorophenoxy) propionic acid	2,4,5-trichlorophenoxyacetic acid (2,4,5-T)

2,4-D is used as a systemic herbicide to control broad leaf weeds in wheat, corn, rangeland/pastureland, sorghum, and barley. Over 1500 pesticide products contain 2,4-D as an active ingredient. 2,4-D, MCPA and mecoprop-p (MCPP-p) are chlorophenoxy acids developed in the 1940s and 1950s as growth regulating herbicides for use against broad leaf weeds. Since its introduction into Canada in the 1940s, 2,4-D has become one of the most widely used and studied herbicides for use in agriculture, forestry, non-crop vegetation management, turf grass, lawn care and weed resistance management. MCPA was introduced into Canada in 1952. Figure II-D-1 gives the market share in the agriculture phenoxy broad leaf weed herbicides

market in Canada (2006 Research undertaken by RIAS Inc,-regulatory impacts, alternatives and strategies).

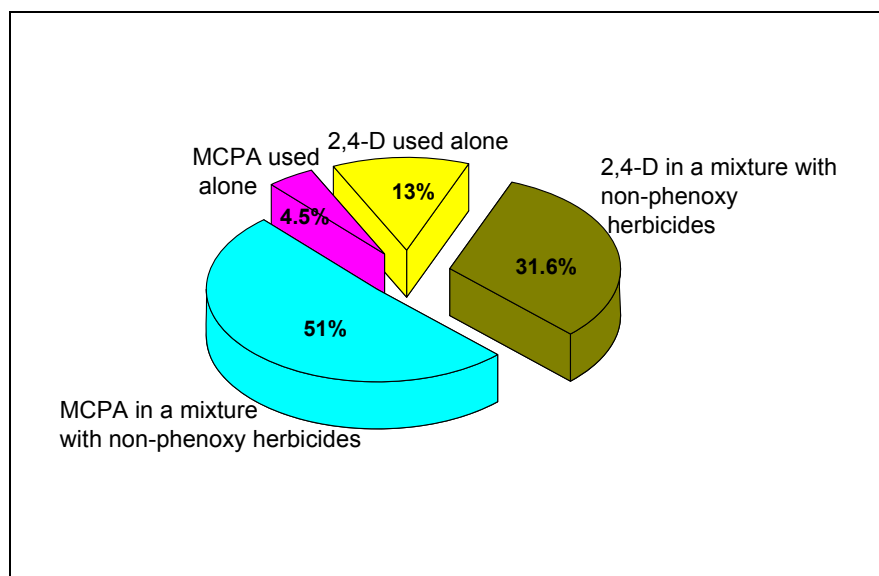


**Figure II-D-1 Market share in the agriculture phenoxy broad leaf weed herbicides market in Canada. Phenoxy market share of 25.9 million acres treated.**

Due to its relatively short half-life, 2,4-D is said to have low persistence in both soil and water. However, 2,4-D has a high potential to leach from soils, and therefore a potential for contaminating ground water. The herbicide has been detected in ground water in at least five states and Canada. Low concentrations have also been detected in surface water and drinking water in the US. Although, recently report by the European Commission (2001) United States Environmental Protection Agency (1988, 1997, 2004 and 2005) and the World Health Organization (1996, 1997, 1998 and 2003), as well as Health Canada's Pest Management Regulatory Agency (2005) conform that herbicide 2,4-D does not present a health risk. When it reach the water supply, natural degradation processes (Zepp et al., 1975), such as UV light degradation or biodegradation from microorganisms, may initiate the breakdown of 2,4-D and the major breakdown product, 2,4-DCP, is likely a more toxic compound and often more resistant to oxidative degradation. Other natural metabolic pathways of 2,4-D lead to compounds such as 2,4-dichloro-5-hydroxyacetic acid and

4-chlorophenoxyacetic acid (Hamburg et al., 2001)

### **D-2-Degradation of 2,4-D**

An increasing interest in the use of alternative processes for the pesticide oxidation has been registered in the literature. Advanced oxidation processes using titanium dioxide (Sun and Pignatello, 1995; Herrmann, 1998; Modestov and Lev, 1998) and zinc oxide (Sanches et al., 1996) as photo catalysts have been reported and the yield of 2, 4-D degradation has shown to be dependent on the mass of semiconductor, temperature and solution pH. Nevertheless, the measured TOC values remained constant during illumination, which indicates that mineralization hardly occurs. Ozonation, when catalyzed with UV light in the presence of iron ions, has presented high efficiency for the degradation of 2, 4-D (Müller et al., 1998; Piera et al., 2000; Brillas et al., 2003). Hydrogen peroxide and Fenton reagent, both accelerated by UV radiation, also have shown higher conversion rates to carbon dioxide (Sun and Pignatello, 1993; Lee et al., 2003). Direct UV irradiation method is used to degrade the 2,4-D (Kundu et al., 2005). Other photocatalysis involve various iron-mediated oxidation systems and the application ferrioxalate-exchanged resin on the removal of 2,4-D in the presence of hydrogen peroxide and UV light has been studied (Kwan and Chu, 2003, 2006). Ionizing radiation is also an efficient means for oxidative decomposition of 2,4-D (Zona et al., 1999, 2002, 2003). In some treatments, 2,4-dichlorophenol (2,4-DCP) was found as an intermediate product.(Sun and Pignatello, 1993; Herrmann, 1998).

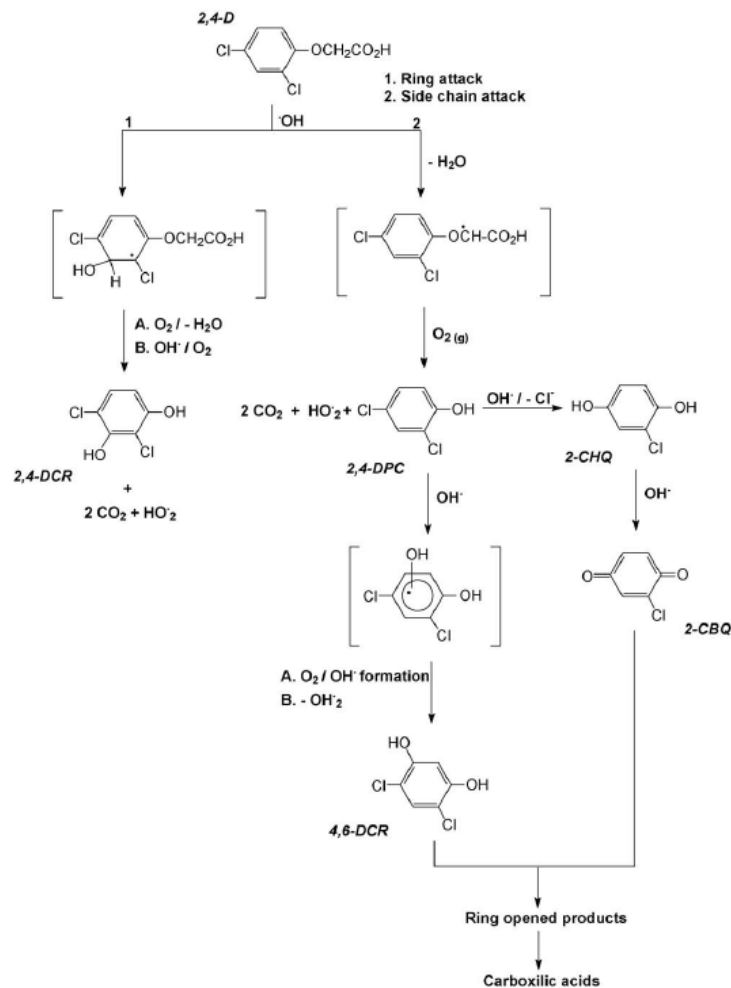


**Figure II-D-2 Proposed pathway for the degradation of 2,4-D (Carla et al., 2006)**

Figure II-D-2 presents the proposed pathway for the degradation of 2,4-D by the Fe(II)/UV/H<sub>2</sub>O<sub>2</sub> method (Carla et al., 2006). It includes the formation of 2,4-DCR by attack of hydroxyl radicals to the ring and the formation of 2,4-DPC by attack to the side chain. The compound 2-chlorobenzoquinone (2-CBQ), although not detected by all the analytical means, was included as a natural sequence of transformation of 2-chlorohydroquinone (2-CHQ).





### **III**

## **EXPERIMENTAL MATERIALS AND METHODS**



### **III-EXPERIMENTAL MATERIALS AND METHODS**

#### **A-REAGENTS**

Ferric citrate, Sigma, > 99%.

Ferric perchlorate ( $\text{Fe}(\text{ClO}_4)_3 \cdot 9\text{H}_2\text{O}$ ), Fluka, > 97%.

2,4-Dichlorophenol, Sigma, > 99%.

2,4-dichlorophenoxyacetic acid, Sigma, > 99%.

L-Tartaric acid, Sigma, > 99%.

D-Tartaric acid, Sigma, > 99%.

Pyruvic acid, Sigma, > 99%.

$\text{FeSO}_4 \cdot (\text{NH}_4)_2\text{SO}_4 \cdot 6\text{H}_2\text{O}$ , Aldrich, 99%.

5, 5-Dimethylpyrroline-N-oxide (DMPO), Aldrich, > 97%.

8-Hydroxyquinoline-5-sulfonic acid hydrate (HQSA), Aldrich, > 98%.

Benzene, Shanghai chemical reagent co. LTD, > 99%.

Phenol, Shanghai chemical reagent co. LTD, > 99%.

Sodium hydroxide, Prolabo, > 97%.

Ammonium acetate, Aldrich, > 98%.

Potassium Ferrioxalate, Merck, > 99%.

Sulfuric acid, Merck, made in EEC, > 95%.

Ferric chloride, Fluka, 99%.

Phosphoric acid, sigma-Aldrich, > 85%.

Acetic acid, Aldrich, > 99%.

Hydrochloric acid, Merck (0.1 M).

Perchloric acid, Merck, > 97%.

1,10-phenanthroline, Fluka, > 99%.

Potassium hydrogen phthalate, Nacalai tesque, Inc. KYOTO. Japan.

Sodium carbonate, Nacalai tesque, Inc. KYOTO, Japan.

Sodium hydrogen, Nacalai tesque, Inc. KYOTO, Japan.

Methanol, Carlo Erba Reagenti, HPLC grade.

Acetonitrile, Carlo Erba Reagenti, HPLC grade.

## **B-PREPARATION OF SOLUTIONS**

### **B-1-Preparation of stock solutions**

#### **(a) Fe(III) stock solution (2 mmol.L<sup>-1</sup>)**

Great care was taken to prepare the solutions of Fe(III) in order to prevent evolution and/or precipitation of Fe(III). A certain quantity of Fe(ClO<sub>4</sub>)<sub>3</sub>·9H<sub>2</sub>O (0.25817 g) was diluted to 250 ml by adding an appropriate volume of Milli-Q water to get the desired concentration of Fe(III) and the pH value of the stock solution was adjusted to pH 2.0 by perchloric acid.

#### **(b) D-Tartaric acid (D-Tar) stock solution (2 mmol.L<sup>-1</sup>)**

0.03 g of D-Tar was diluted to 100 ml by adding an appropriate volume of Milli-Q water to get the desired concentration of D-Tar.

#### **(c) L-Tartaric acid (L-Tar) stock solution (2 mmol.L<sup>-1</sup>)**

0.03 g of L-Tar was diluted to 100 ml by adding an appropriate volume of Milli-Q water to get the desired concentration of L-Tar.

#### **(d) Pyruvic acid (Pyr) stock solution (2 mmol.L<sup>-1</sup>)**

0.035 ml of Pyr was diluted to 250 ml by adding an appropriate volume of Milli-Q water to get the desired concentration of Pyr.

#### **(e) Ferric citrate stock solution (2 mmol.L<sup>-1</sup>)**

0.14045g of Ferric citrate was diluted to 250 ml by adding an appropriate volume of Milli-Q water to get the desired concentration of Ferric citrate.

#### **(f) Ferric L-Tar complex or Ferric D-Tar complex stock solution (2 mmol.L<sup>-1</sup>)**

0.3 g of L-Tar acid or D-Tar acid and 0.5164 g of  $\text{Fe}(\text{ClO}_4)_3 \cdot 9\text{H}_2\text{O}$  were mixed and diluted to 500 ml by adding an appropriate volume of Milli-Q water to get the concentration  $[\text{Fe}(\text{III})]/[\text{L-Tar}] = 2\text{mmol.L}^{-1}/4\text{mmol.L}^{-1}$  or  $[\text{Fe}(\text{III})]/[\text{D-Tar}] = 2\text{mmol.L}^{-1}/4\text{mmol.L}^{-1}$

**(g) Fe (II) stock solution (0.45 mmol.L<sup>-1</sup>)**

0.0882 g of  $\text{FeSO}_4 \cdot (\text{NH}_4)_2\text{SO}_4 \cdot 6\text{H}_2\text{O}$  was diluted to 500 ml by adding an appropriate volume of Milli-Q water to get the desired concentration of Fe (II).

**(h) 2, 4-Dichlorophenol (2,4-DCP) stock solution (1 mmol.L<sup>-1</sup>)**

0.0815 g of 2, 4-Dichlorophenol was diluted to 500 ml by adding an appropriate volume of Milli-Q water to get the desired concentration of 2, 4-Dichlorophenol.

**(i) 2,4-dichlorophenoxyacetic acid (2, 4-D) stock solution (1 mmol.L<sup>-1</sup>)**

0.05526 g of 2, 4-D was diluted to 250 ml by adding an appropriate volume of Milli-Q water to get the desired concentration of 2,4-D.

**(g) Benzene stock solution (10 mmol.L<sup>-1</sup>)**

Benzene was diluted to 1 L pure water. The solution was stirred with a magnetic bar to insure the complete dissolution of benzene.

**(k) Acetic sodium buffer**

The buffer of acetic sodium was prepared by mixing 600 mL of acetic sodium (1 N) and 360 mL of sulfuric acid (1 N) with end volume of 1 L by adding an appropriate volume of Milli-Q water.

**(l) Potassium ferrioxalate**

Potassium ferrioxalate used for actinometry was prepared from potassium oxalate and ferric chloride, according to the procedure proposed by Calvert and Pitts (Calvert et al., 1966), and carefully stored in the dark.

**(m) 8-Hydroxyquinoline-5-sulfonic acid hydrate (HQSA) solution (0.1 mol. L<sup>-1</sup>)**

The HQSA solution was prepared by dissolution of HQSA (1.21 g) in 50 mL of NaOH (0.12 mol.L<sup>-1</sup>). Great care was taken to wash the flask by HNO<sub>3</sub> to avoid that Fe adhered to the flask surface.

**B-2-Preparation of reaction solutions**

The majority of the experiments presented here were conducting under “natural” conditions, i.e. upon preparing solutions consisting of Fe(ClO<sub>4</sub>)<sub>3</sub> and 2,4-dichlorophenol without addition of further components, in particular without additional acidification. These reaction solutions were either freshly prepared from the stock sample of Fe(ClO<sub>4</sub>)<sub>3</sub>·9H<sub>2</sub>O, or by diluting aqueous stock solutions of 2 mmol L<sup>-1</sup> Fe(ClO<sub>4</sub>)<sub>3</sub> to appropriate concentrations. All the reaction solutions were all prepared with Milli-Q water. The pH values were adjusted with perchloric acid (1 N) and NaOH (1 N) by a JENWAY 3310 pH-meter to ±0.01 pH unit.

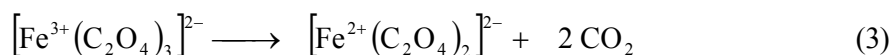
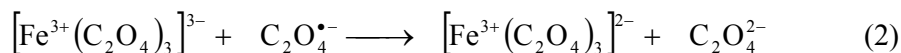
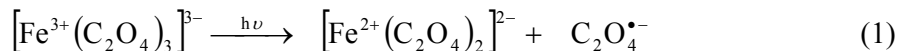
When necessary, reaction solutions were deaerated or oxygenated by purging with argon or oxygen before irradiation. The purging time depend on the solution volume: 20min for the big volume solutions (100 mL) and 10 min for the small volume solutions (5 mL).

**C-IRRADIATION**

**C-1-Ferrioxalate actinometry**

The light intensity I<sub>0</sub> was measured by ferrioxalate potassium (K<sub>3</sub>Fe(C<sub>2</sub>O<sub>4</sub>)<sub>3</sub>) actinometer (Calvert and Pitts, 1966). This method depend on the photochemical

reactivity of  $K_3Fe(C_2O_4)_3$  in the acid solution. Under irradiation, Fe(III) was reduced to Fe(II) and oxalate ion was oxidized to  $CO_2$ . The reactions are as follows:



Since  $Fe^{2+}$  can form stable red complex with 1,10-phenanthroline. Fe(II) concentrations were determined by complexometry using  $\epsilon_{510} = 1.118 \times 10^4 \text{ mol}^{-1} \text{ L cm}^{-1}$  for the complex of Fe(II) with o-phenanthroline.

The principle of this assay is the following: after irradiation of a volume ( $V_1$ ) of ferrioxalate potassium solution ( $0.006 \text{ mol. L}^{-1}$ ) for a time  $t$  (expressed in seconds), we added at 2 mL ( $V_2$ ) of this irradiated solution, 1 mL of acetate buffer, and 0.5 mL of 1.10-phenanthroline (0.1% by mass). The solution is then filled with pure water up to 5 mL ( $V_3$ ). After agitation, the solutions were kept in the dark for 1h and then the UV-vis measurement was carried out at 510nm in a cell with an optical path equal to  $\ell$ .

The number of Fe(II) formed during the photo reaction was calculated with the following formula:

$$n_{Fe^{2+}} = \frac{6.023 \cdot 10^{20} \cdot V_1 \cdot V_3 \cdot \log(I_0 / I_T)}{V_2 \cdot l_{510} \cdot \epsilon_{510}} = \frac{6.023 \cdot 10^{20} \cdot V_1 \cdot V_3 \cdot OD_{510}}{V_2 \cdot l_{510} \cdot \epsilon_{510}}$$

With  $OD_{510} = (OD_{\text{solution}} - OD_{\text{blank}})_{510}$ , the value of the absorbance at 510 nm of the blank is obtained with the same solution of potassium ferrioxalate, but not irradiated and prepared as before.

The number of  $Fe^{2+}$  formed is proportional to the fraction of absorbed light by the solution during this time  $t$ . Then the intensity emitted by the system, in photons per second for the volume  $V_1$ , is equal to:

$$I_0 = \frac{n_{Fe^{2+}}}{\phi_{Fe^{2+}} \cdot t \cdot (1 - 10^{-OD})} \text{ photons s}^{-1}$$



$(1-10^{-OD})$  is the percentage of photons absorbed by the solution at the wavelength of irradiation at time  $t = 0$ .

Then:

$$I_0 = \frac{6.023 \cdot 10^{20} \cdot V_1 \cdot V_3 \cdot OD_{510}}{V_2 \cdot l_{510} \cdot \epsilon_{510} \cdot \phi_{Fe^{2+}} \cdot t \cdot (1-10^{-DO})} \quad \text{photons s}^{-1} V_1 \text{ mL}$$

These photonic flows were expressed in photons  $s^{-1} \text{ cm}^{-2}$ , because with parallel beam,  $V_1$  can be assimilated to the length of the optical path of the cell  $l$  irr; these flows were monitored throughout this work.

So,

$$I_0 = \frac{6.023 \cdot 10^{20} \cdot V_3 \cdot l_{irr} \cdot DO_{510}}{V_2 \cdot l_{510} \cdot \epsilon_{510} \cdot \phi_{Fe^{2+}} \cdot t \cdot (1-10^{-DO})} \quad \text{photons s}^{-1} \text{ cm}^{-2}$$

### **C-2-Irradiation with monochromator**

For the determination of quantum yields, solutions were irradiated in monochromatic parallel beam in 1 cm (path length) quartz cell or 2 cm (path length) cylindrical quartz cell. The light source was a high-pressure mercury lamp Osram HBO 200W equipped with a monochromator Bausch and Lomb or Jobin Yvon. Figure III-C-1 gives a picture of the monochromatic irradiation device. The monochromatic irradiations were carried out separately at wavelength 365 nm, 313 nm and 296 nm. The light intensity was measured by ferrioxalate actinometry (Calvert and Pitts, 1966). The photon flux of the monochromatic irradiation at different wavelength is listed in Table III-C-1. Where necessary, solutions were deaerated by bubbling with argon for 10 min before irradiation.

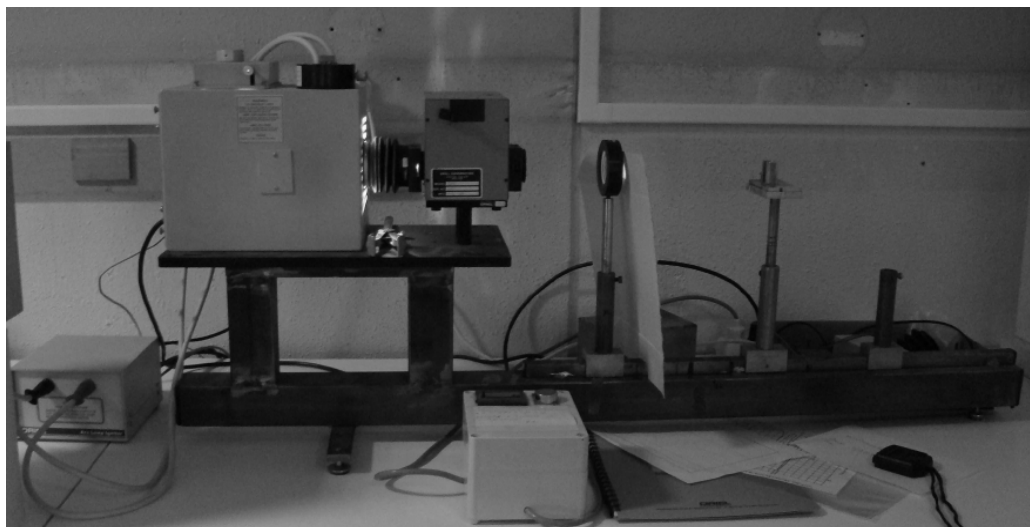


**Figure III-C-1 Monochromatic irradiation device**

**Table III-C-1 The photonic flux at 365 nm, 313 nm and 296 nm**

$\lambda_{irr}(nm)$	365	313	296
$I_0 (10^{14} \text{ photons} \cdot \text{s}^{-1} \cdot \text{cm}^{-2})$	13.7	7.46	4.39

All the quantum yield calculations depend on the following formulas (1), (2), (3) and (4):

$$\Phi = \frac{\Delta C \cdot 6.023 \cdot 10^{20} \cdot l}{I_a \cdot \Delta t} \quad (1)$$

$$\frac{I_a}{I_0} = 1 - 10^{-DO_{\lambda irr}} \quad (2)$$

Where  $(1 - 10^{-DO_{\lambda irr}})$  represents the percentage of the light absorption by the solution when  $t = 0$ ,  $I_0$  is the number of the photons entering the reaction cell per second determined by actinometry and  $l$  is the length of irradiation cell in cm.

So we can get formula (3).

$$\Phi = \frac{\Delta C \cdot 6.023 \cdot 10^{20} \cdot l}{I_0 \cdot \Delta t \cdot (1 - 10^{-DO_{\lambda irr}})} \quad (3)$$

For the organic pollutants 2, 4-DCP and 2, 4-D used in the thesis, the quantum yield can be calculated by the change of their concentrations ( $\Delta C$ ) using formula (3).

For the calculation of Fe(II) generation quantum yield, we can use formula (4),  $\Delta OD_{510nm}/\varepsilon_{510nm}$  also represents the change of the Fe(II) concentration during the irradiation.

$$\Phi = \frac{\Delta OD \cdot 6.023 \cdot 10^{20} \cdot \lambda}{\varepsilon \cdot L \cdot I_0 \cdot (1 - 10^{-OD_{\lambda irr}}) \cdot t} \quad (4)$$

L is the length of the cell used for the measurement of the optical density (OD).

### C-3-Irradiation at 365nm

The irradiation experiments were performed in a home-made photoreactor placed in a cylindrical stainless steel container. The reaction device consists of four tubes (Philips TLD 15W / 05), whose emission spectrum is from 300nm to 450nm with a maximum irradiation at 365 nm (see Figure III-C-2). These four tubes were separately placed in the four different axes, while the photoreactor, a water-jacketed Pyrex tube of 2.8 cm diameter, was placed in the center of the setup (Figure III-C-3). The solution (usually 100 mL) was continuously magnetically stirred with a magnetic bar during irradiation to insure its homogeneity. Control experiments showed that no degradation of 2, 4-DCP or 2, 4-D occurred in Fe(III) or Fe(III)-Carboxylate complexes without irradiation in this photoreactor.

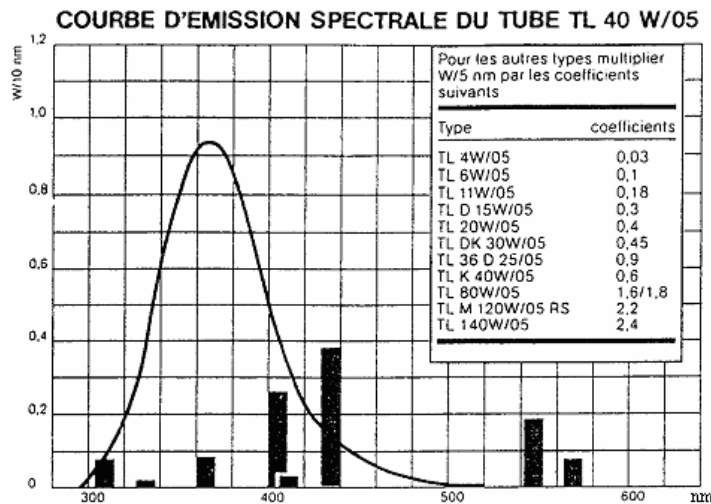
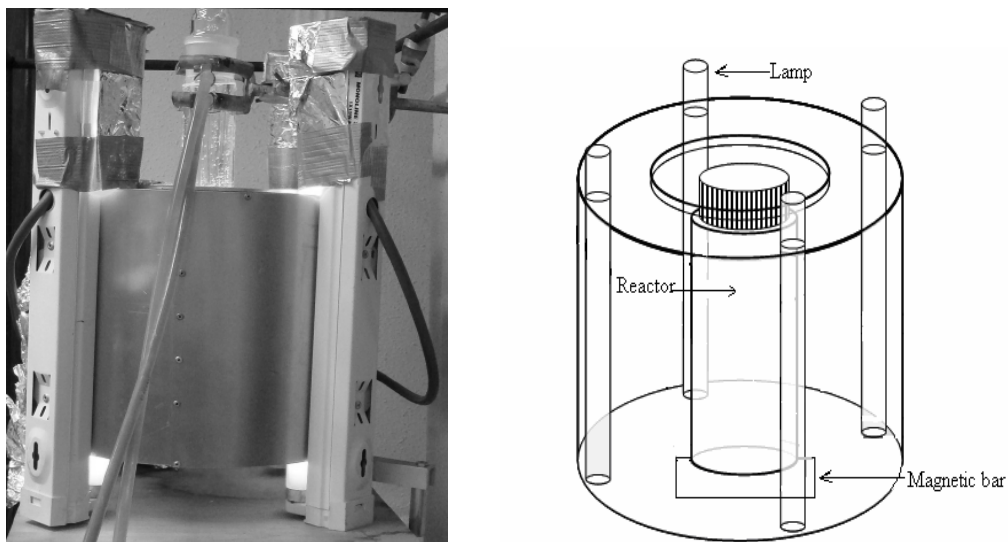


Figure III-C-2 Emission spectra of tube Philips, TLD 15W/05.



**Figure III-C-3 Home-made photoreactor with four lamps (Philips TLD 15W / 05) 1: reactor 100 mL; 2: lamps 15W× 4; 3: magnetic bar**

#### **C-4-Irradiation with Metal Halide Lamp**

In order to quantify the hydroxyl radicals generated in the reaction, irradiation experiments were performed under metal halide light ( $\lambda \geq 350$  nm, 250W, Yaming, Shanghai, China). The light intensity was  $1.2 \times 10^5$  Lux, which was detected by a digital lux meter (TES 1332, Taiwan, China). The emission spectra of lamp are shown in Figure III-C-4. The spectrum consists of several narrow bands. The light of the narrow bands with the maxima at 380, 406, 412, 438, and 452 nm could be absorbed by the Fe(III)-Carboxylate complexes. These bands were used to calculate the yields of the  $\bullet\text{OH}$  produced in the system. The fraction of the light absorbed at the major irradiation wavelengths and the light intensities incident into the reaction volume are shown in Table III-C-2.

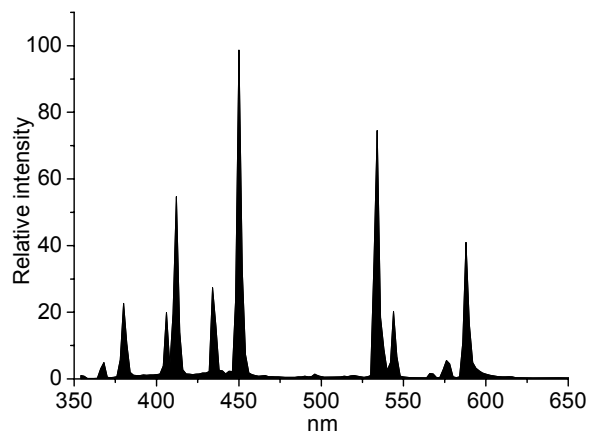


Figure III-C-4 Emission spectra of the metal halide lamp 250W.

Table III-C-2 Light intensity distribution of the metal halide lamp

$\lambda(\text{nm})$	Spectrum energy		
	Energy fraction (%)	$\text{W}\cdot\text{cm}^{-2}$	$\text{Photon}\cdot\text{s}^{-1}$
380	0.7	$2.6 \times 10^{-4}$	$4.9 \times 10^{14}$
406	0.7	$2.3 \times 10^{-4}$	$4.7 \times 10^{14}$
412	3.0	$1.0 \times 10^{-4}$	$2.1 \times 10^{14}$
438	1.3	$4.3 \times 10^{-4}$	$9.4 \times 10^{14}$
452	6.2	$2.1 \times 10^{-4}$	$4.8 \times 10^{14}$

The photochemical reactor was Pyrex tubes (each tube 1.5 cm diameter, 11.5 cm length, 1 mm wall thickness). As shown in Figure III-C-5, the homemade reaction system consisted of an electrical machine, a plate with a big hole in the center and eight small holes symmetrically around it. The metal halide lamp was positioned in the center of the plate, during the photoreaction, cooling water was used to maintain a constant temperature about  $25 \pm 1^\circ\text{C}$ . Eight identical Pyrex tubes were placed vertically in each hole of the plate, so that the lamp and the tubes were kept parallel with a fixed distance of 7 cm. The plate was kept rotating at 50 rpm by the electrical machine. Irradiation flux was well distributed throughout the tubes.

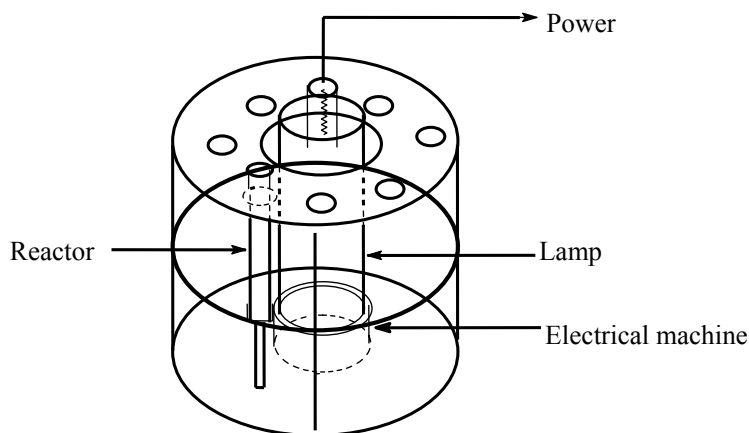


Figure III-C-5 Photoreactor with metal halide lamp 250W

## D-ANALYSIS METHODS

### D-1-Spectroscopy methods

#### UV-vis Spectrophotometer

- a. The UV–visible spectra of the solutions were recorded on a Cary 3 double beam spectrophotometer.
- b. Another UV-visible spectrophotometer, used in China, is Shimadzu model UV-1601.

#### Electron spin resonance (ESR) spectroscopy

ESR spectra were recorded at room temperature on a Bruker ER 200D, X BAND spectrometer operating at 9.6 Ghz and a cavity equipped with a quartz flat cell designed for liquid samples. Typical spectrometer parameters were: scan range, 100 G; center field set, 3440 G; time constant, 327 ms; scan time, 167 s; modulation amplitude, 1.5 G; modulation frequency, 100 kHz; receiver gain,  $1.25 \times 10^6$ ; and microwave power, 25.2 mW, frequency, 9.64 GHz.

The 5,5-Dimethylpyrroline-N-oxide (DMPO) was used as a scavenger (Figure III-D-1) in the research. The irradiation experiments were carried out under a lamp

Xe-Hg with two different filters (Figure III-D-2), which can help us to have or not the polychromatic emission between 300 to 345 nm. Cooling water was used to maintain the reaction at room temperature.

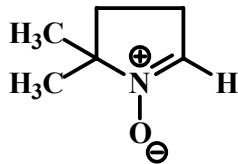


Figure III-D-1 5, 5-Dimethylpyrroline-N-oxide (DMPO)

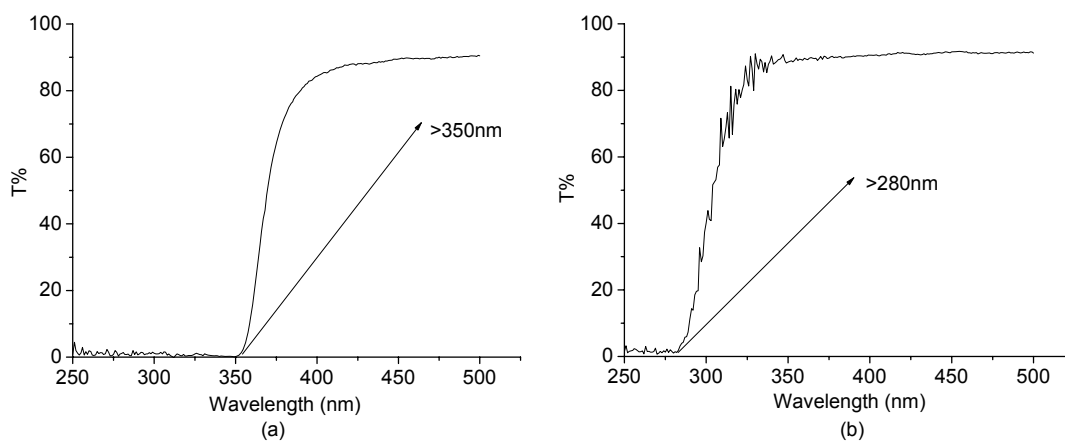


Figure III-D-2 (a) and (b) UV-visible spectra of the filters used during ESR spectroscopy experiments

## D-2-Chromatography methods

Several HPLC setups were used for products analysis:

- (1) A Waters chromatograph equipped with two pumps Waters 510, an auto-sampler 717 and a Waters 996 photodiode array detector.
- (2) A Waters chromatograph equipped with HPLC pump Waters 515 and Gilson monowavelength UV-Vis Detector.
- (3) A Shimadzu chromatograph equipped with Shimadzu LC-10AT pump and Shimadzu SPD-10A with UV-Vis detector.

Two HPLC columns were used in the work:

- a. An Agilent ZORBAX Eclipse XDB-C8 (reverse phase) of 4.6 mm (ID) × 150 mm (length) with a particle diameter of 5 μm.
- b. A Kromasil, KR100-5C18 column (reverse phase) of 4.6 mm (ID) × 150 mm (length) with a particle diameter of 5 μm.

The mobile phases used in the research are the following:

- a. To analyze the 2, 4-Dichlorophenol and its photoproducts, a mixture of pure water and methanol (40/60, v/v) was used as mobile phase and the flow rate was 1 mL min<sup>-1</sup> at 284 nm.
- b. To analyze the 2, 4-D and its photoproducts, a mixture of 0.2% acetic acid and acetonitrile (50/50, v/v) was used as mobile phase and the flow rate was 1 mL min<sup>-1</sup> at 284 nm.
- c. The formation of phenol from benzene was monitored at 270 nm and the eluent was acetonitrile/water mixture (40/60, v/v) at a flow rate of 0.8 mL min<sup>-1</sup> using Kromasil, KR100-5C18 column.

### **D-3-Dosage methods**

#### **Total organic carbon (TOC)**

The progress of the mineralization of pollutants was monitored by measuring the total organic carbon (TOC) via a Shimadzu Model TOC-5050A equipped with an automatic sample injector. The standard solutions were prepared with standard chemicals (certainty quality, Japan). 2.125 g of potassium hydrogen phthalate was dissolved in 1 L of pure water to get 1000 mg.L<sup>-1</sup> for total carbon (TC) standard solution. To get 1000 mg.L<sup>-1</sup> of inorganic carbon (IC) standard solution, 4.41 g of sodium carbonate together with 3.5 g of sodium hydrogen carbonate were dissolved in 1 L of pure water. The quantifications of TC and IC depend on the calibration curve (Figure III-D-3).



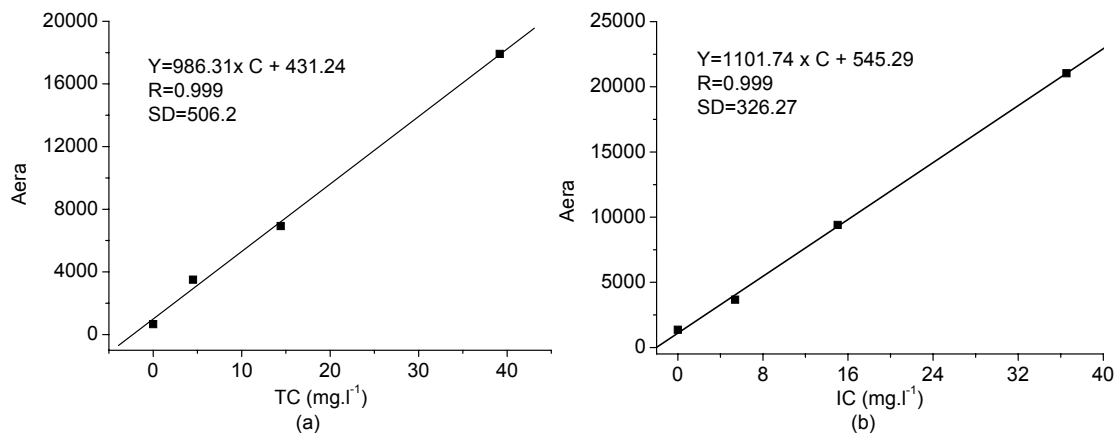


**Figure III-D-3 Calibration curves of TC (a) and IC (b)**

The total organic carbon (TOC) concentration is obtained by the difference of the concentration of TC and the concentration of IC:

$$[\text{TOC}] = [\text{TC}] - [\text{IC}]$$

### **Fe(II)**

Under irradiation, Fe(II) is formed in aqueous solutions in the presence of Fe(III). The concentration of Fe(II) was determined by complexometry with 1,10-phenanthroline taking  $\epsilon_{510 \text{ nm}} = 1.118 \times 10^4 \text{ L.mol}^{-1}.\text{cm}^{-1}$  (Calvert and Pitts, 1966).

A certain quantity of  $\text{Fe}(\text{NH}_4)_2\text{SO}_4$  solution was used as Fe(II) sources to make a calibration curve (as shown in Figure III-D-4). The molar absorption coefficient was  $11450 \text{ L.mol}^{-1}.\text{cm}^{-1}$ , which is nearly the same as the reference value  $\epsilon_{510 \text{ nm}} = 11180 \text{ L.mol}^{-1}.\text{cm}^{-1}$ . By means of the calibration curve, it was carefully checked that no interference in the analysis was observed when 2,4-D or 2,4-DCP was present in the solution.

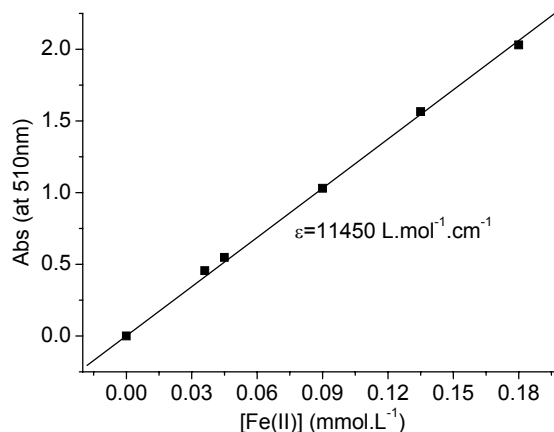


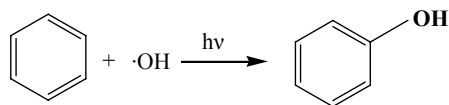
Figure III-D-4 Calibration curve of Fe(II) concentration

### *Fe(OH)<sup>2+</sup>*

The concentration of the most photoactive species,  $[\text{Fe}(\text{OH})^{2+}]$ , was determined by using 8-hydroxyquinoline-5-sulfonic acid (HQSA) (Faust et al., 1990). The absorbance of the tris complex  $\text{Fe}(\text{HQSA})_3$  was measured at  $\lambda = 572 \text{ nm}$  ( $\epsilon = 5000 \text{ mol}^{-1} \cdot \text{L} \cdot \text{cm}^{-1}$ ). The molar fraction of  $\text{Fe}(\text{OH})^{2+}$  ( $x_{\text{Fe}(\text{OH})^{2+}}$ ) was expressed as the ratio of  $[\text{Fe}(\text{OH})^{2+}]$  to total Fe in solution.

$$\% \text{Fe}(\text{OH})^{2+} = \frac{[\text{Fe}(\text{OH})^{2+}]}{[\text{Fe}]_{\text{total}}}$$

### *Hydroxyl radicals*



Scavenging of  $\cdot\text{OH}$  by high concentrations of benzene has been used to determine the yield  $\cdot\text{OH}$  radicals formation. Aromatic hydroxylation is one of the typical reactions of  $\cdot\text{OH}$  and is used for detection of  $\cdot\text{OH}$  in the case of Fenton reaction and of the photolysis of aqueous of  $\text{HNO}_2$ ,  $\text{NO}_3^-$  and  $\text{NO}_2^-$  (Arakaki et al., 1999). Benzene is very unreactive toward  $\text{O}_2(^1\Delta_g)$  (Zepp et al., 1987). The hydroxylation of benzene by  $\cdot\text{OH}$  to

produce phenol is a fairly selective process. Given the high reactivity of benzene with  $\cdot\text{OH}$  ( $k \approx 8 \times 10^9 \text{ L}\cdot\text{mol}^{-1}\cdot\text{s}^{-1}$ ) (Kochany and Bolton, 1992; Pan and Schuchmann, 1993) and under the conditions of these experiments, virtually all of the  $\cdot\text{OH}$  should have been scavenged by benzene. The retention time of phenol is 4.2 min in this work (Figure III-D-5).

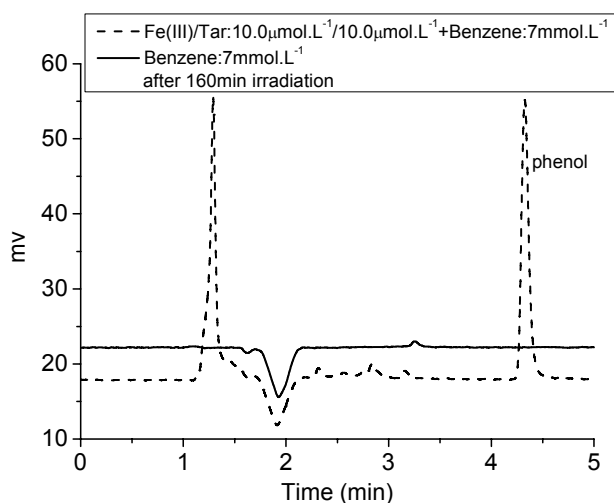


**Figure III-D-5 Formation of phenol in different conditions after 160min irradiation.**

As Figure III-D-5 and III-D-6 show, photolysis of  $7 \text{ mmol}\cdot\text{L}^{-1}$  benzene in double-distilled water showed no detectable loss of benzene and no formation of phenol after 160min of irradiation under metal halide light. The destruction rate of phenol by direct photolysis and by peroxy radicals,  $\text{O}_2(^1\Delta_g)$  and other oxidants is expected to be slow by comparison to the rate of phenol formation from the  $\cdot\text{OH}$  through the oxidation of benzene (Liu et al., 2004).

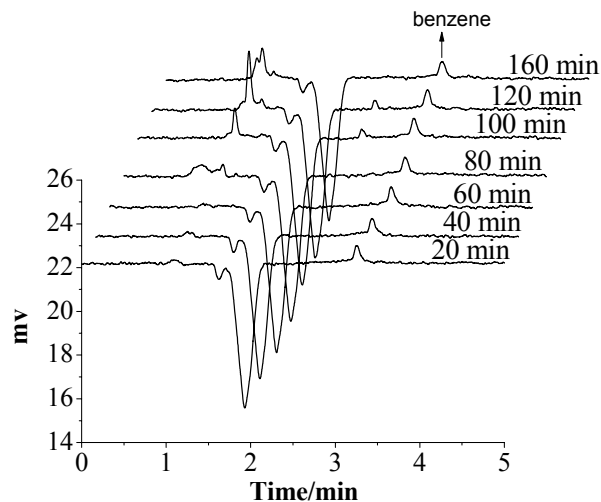


**Figure III-D-6 HPLC chromatogram of solutions with 7 mmol.L<sup>-1</sup> benzene in 160min irradiation.**

It was thought that  $\bullet\text{OH}$ -mediated oxidation of benzene forms phenol with a nearly 100% yield (Faust and Allen, 1993; Joseph et al., 2001; Wang et al., 2006), and thus the concentrations of photochemically formed hydroxyl radicals were determined as,

$$C_{\text{gOH}} = C_{\text{Phenol}}$$

Where,  $C_{\text{Phenol}}$  is the concentration of phenol at time t. Figure III-D-7 shows the calibration curve of phenol.

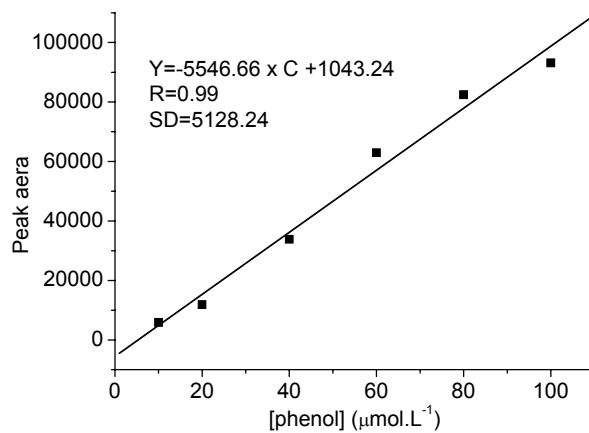


**Figure III-D-7 Calibration curve of phenol**

#### **D-4-Molar ratio method**



M represents the metal ion;

L represents the acid ions (ligand).

The method is based on the spectrophotometric measurements. We keep constant the concentration of metal ions in aqueous solution and the concentration of the relative acid is increased in the experiment. The absorbance of the aqueous solution increase with the increase of the acid concentration until it becomes stable, which indicate that the metal ions are totally complexed by the acids.

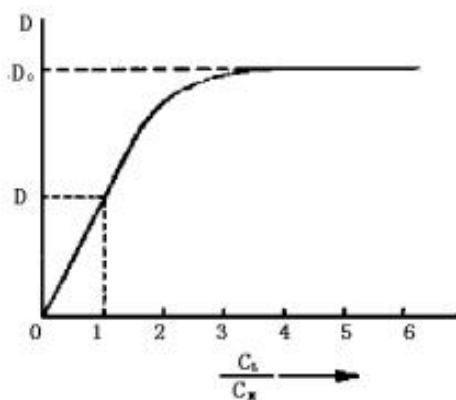


**Figure III-D-8 Measurements of the absorbance as a function of the composition of the complex  $n=C_L/C_M$**

As shown in Figure III-D-8, the absorbance of the aqueous solutions was set as *Y* axis, the corresponding ratio of  $C_L / C_M$  was set as *X* axis. Then the ratio of  $C_L / C_M$  represents the composition of the complexes. The stoichiometry of the complex corresponds to the ratio ( $C_L / C_M$ ) where the absorbance starts to be stable; no more increase is measured with the supplementary addition of acids.

## **IV**

# **RESULTS**



## IV-A Study of physicochemical properties of Fe(III)-Carboxylate complexes

Many references have reported the physical and chemical properties of Fe(III)-Carboxylate complexes, especially Fe-oxalate, Fe-EDTA, Fe-NTA and Fe-Cit complexes. However, little bibliography reports about the Fe-Tar and Fe-Pyr complexes. Here we studied the physicochemical properties of Fe-Tar and Fe-Pyr complexes.

### A-1-Properties of the carboxylic acids

Carboxylic acids are the important components of the Fe-Carboxylate complexes studied in this work. So, it is necessary to study the basic properties of these carboxylic acids used in this work before studying the physical properties of these carboxylate complexes. These acids included Citric acid, Tartaric acid (L-Tar and D-Tar acid) and Pyruvic acid. Table IV-A-1 lists the acid base dissociation constants of these acids in the form of pKa, which is the negative of the logarithm of the acid dissociation constant Ka.

Table IV-A-1 pKa of organic acids

Name	Molecular formula	Step	T(°C)	pKa
Citric acid	C <sub>6</sub> H <sub>8</sub> O <sub>7</sub>	1	20	3.14
		2	20	4.77
		3	20	6.39
Pyruvic acid	C <sub>3</sub> H <sub>4</sub> O <sub>3</sub>		25	2.39
$\alpha$ -Tartaric acid	C <sub>4</sub> H <sub>6</sub> O <sub>6</sub>	1	25	2.98
		2	25	4.34
<i>meso</i> -Tartaric acid	C <sub>4</sub> H <sub>6</sub> O <sub>6</sub>	1	25	3.22
		2	25	4.82



### A-1-1-Tartaric acid (Tar)

Tartaric acid (HOOC-CHOH-CHOH-COOH) is widely used in the industry, such as medicine, food, tannage and textile. Figure IV-A-1 presents the chemical structure of tartaric acid.

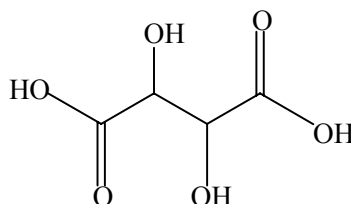


Figure IV-A-1 Chemical structure of tartaric acid

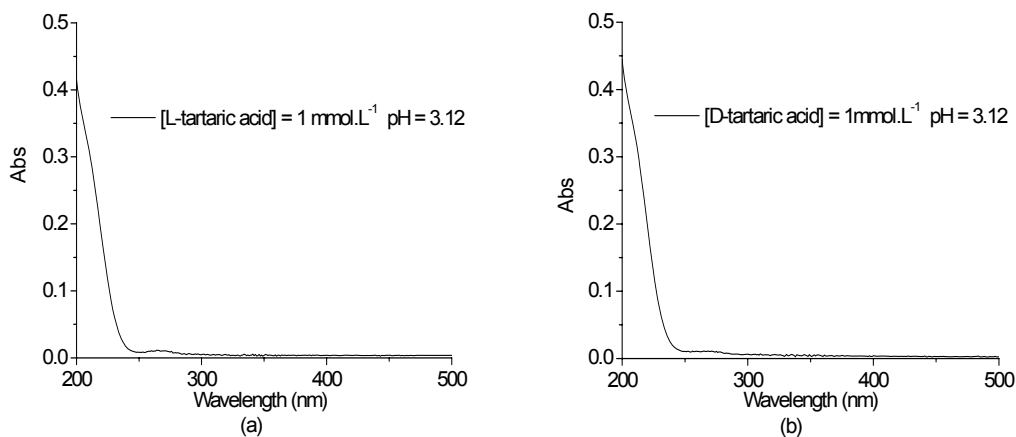
As shown in Table IV-A-2, tartaric acid has three different solid isomers: Levotartaric acid (D-Tar acid), Dextrotartaric acid (L-Tar acid) and Mesotartaric acid. When the mixture of D-Tar acid and L-Tar acid in 1:1 ratio, the polarized light will be counteracted and the mixture is called racemic acid. Mesotartaric acid does not exist in the nature and it is the chemosynthetic material.

Table IV-A-2 Forms of Tartaric Acid

levotartaric acid (D-(-)-tartaric acid)	dextrotartaric acid (L-(+)-tartaric acid)	mesotartaric acid
<p>Fischer projection: COOH at top, HO on left, H on right, COOH at bottom. Wedge-dash structure: HO on wedge, COOH on dash, HO on wedge, COOH on dash.</p>	<p>Fischer projection: COOH at top, H on left, OH on right, COOH at bottom. Wedge-dash structure: HO on wedge, COOH on dash, HO on wedge, COOH on dash.</p>	<p>Fischer projection: COOH at top, H on left, OH on right, COOH at bottom. This is equal to the mirror image: COOH at top, HO on left, H on right, COOH at bottom. Wedge-dash structures: HO on wedge, COOH on dash, HO on wedge, COOH on dash. This is equal to the mirror image: HO on wedge, COOH on dash, HO on dash, COOH on wedge.</p>
<p><b>DL-tartaric acid (racemic acid)</b> (when the ratio is 1:1)</p>		<p>HO on wedge, COOH on dash, HO on wedge, COOH on dash. This is equal to the mirror image: HO on wedge, COOH on dash, HO on dash, COOH on wedge.</p>

Two types of tartaric acid (L-tartaric acid, D-tartaric acid) were studied in this thesis. Figure IV-A-2 presents the UV-visible spectra of L-tartaric acid and D-tartaric

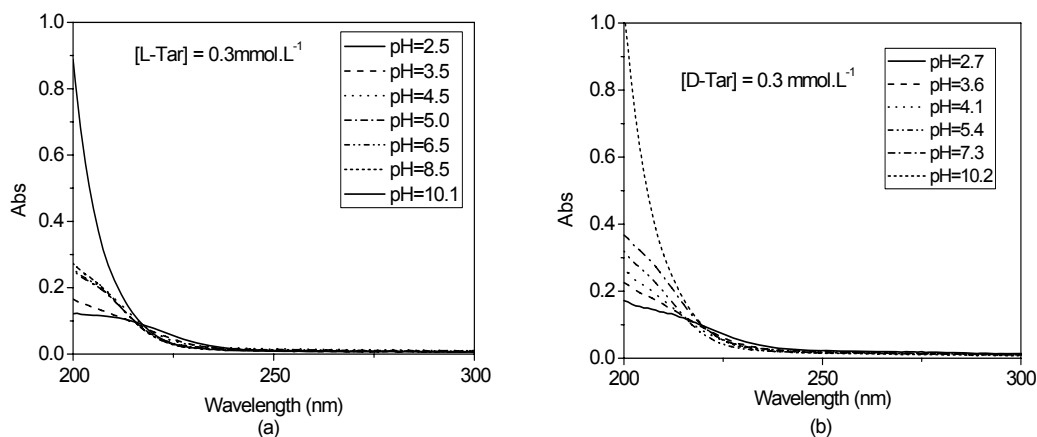
acid. These two tartaric acids have almost the same UV-vis spectrum, from 200 to 500 nm, and the relative higher absorbance is from 200 to 250 nm.



**Figure IV-A-2 UV-Visible absorption spectra of tartaric acid.**

(a) [L-Tar] = 1 mmol.L<sup>-1</sup>; (b) [D-Tar] = 1 mmol.L<sup>-1</sup>

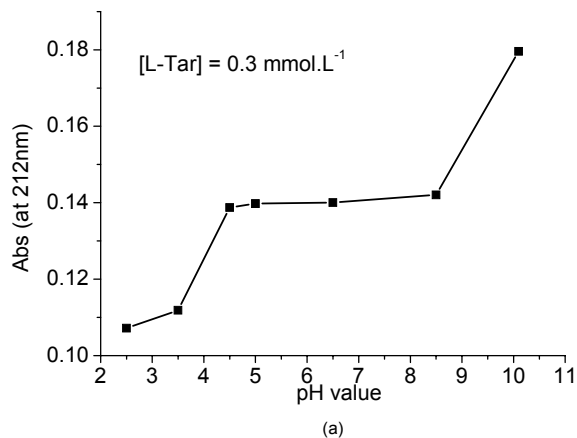
In order to evaluate the pKa of these two tartaric acids, experiments were performed under different pH values. The pH values of the solutions of L-tartaric acid (0.3 mmol.L<sup>-1</sup>) are modified between 2.5 and 10.1 and for D-tartaric acid (0.3 mmol.L<sup>-1</sup>) between 2.7 and 10.2. As shown in Figures IV-A-3, the UV-Visible absorption spectra of tartaric acid aqueous solution changed as a function of pH value.



**Figure IV-A-3 UV-Visible absorption spectra of L-Tar and D-Tar acid as function of pH.**

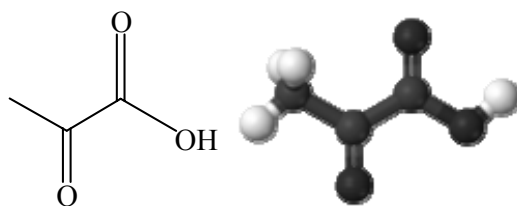
[L-Tar] = 0.3 mmol.L<sup>-1</sup>, [D-Tar] = 0.3 mmol.L<sup>-1</sup>

Figure IV-A-4 shows the variation of the absorbance at 212 nm. It contains an apparent inflexion point at pH 4.3, which is in agreement with references that indicate  $pK_{a2} = 4.32$ . The  $pK_a$  at pH higher than 9.0, which does not need study precisely the value, because it is too far away from our experimental conditions and natural conditions. The same results were obtained from the D-tartaric acid with an inflexion point observed near pH 4.3.



**Figure IV-A-4 Absorbance at 212 nm as function of aqueous solution pH value.**  
**[L-Tar] = 0.3 mmol.L<sup>-1</sup>**

### **A-1-2-Pyruvic acid (Pyr)**



**Figure IV-A-5 Chemical structure of pyruvic acid**

As shown in Figures IV-A-6(a) the UV-Visible absorption spectra of pyruvic acid aqueous solution ( $0.3 \text{ mmol.L}^{-1}$ ) are also modified as a function of pH values. The pH values of the pyruvic acid solution changed from 2.0 to 8.8, and Figure IV-A-6(b) shows the variation of the absorbance at 250 nm. There is a sharp increase of absorbance from pH 2.0 to 3.0. This is in agreement with reference indicated that the  $pK_a$  of pyruvic acid was 2.39.

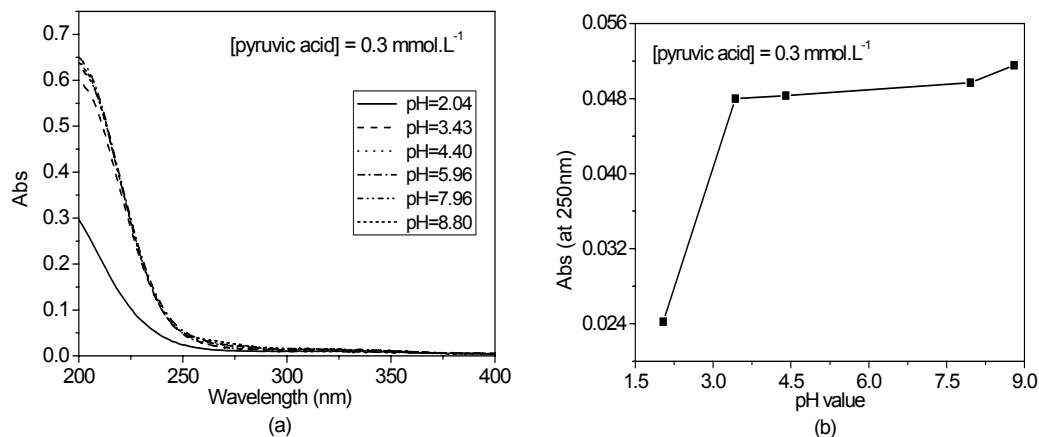


**Figure IV-A-6** The UV-visible spectra of 0.3 mmol.L<sup>-1</sup> pyruvic acid solution as a function of pH. (a) UV-visible spectra; (b) Absorbance at 250nm

### A-1-3 Citric acid (Cit)

Citric Acid (2-hydroxypropane-1,2,3-tricarboxylic acid, IUPAC name) is a colourless crystalline organic compound belong to carboxylic acid family. It exists in all plants (especially in lemons and limes) and in many animal tissues and fluids. Citric acid works as a preservative (or as an antioxidant) and cleaning agent in nature. As present in IV-A-7, it contains three carboxy groups and always used in metal-cleaning compositions as it chelates metals. Reference indicated that the pKa of Citric acid were pKa<sub>1</sub> = 3.14, pKa<sub>2</sub> = 4.77 and pKa<sub>3</sub> = 6.39 (Table IV-A-1).

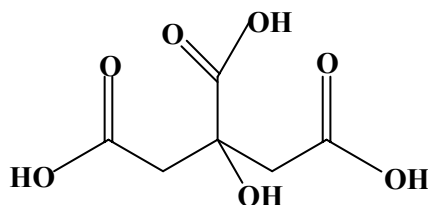


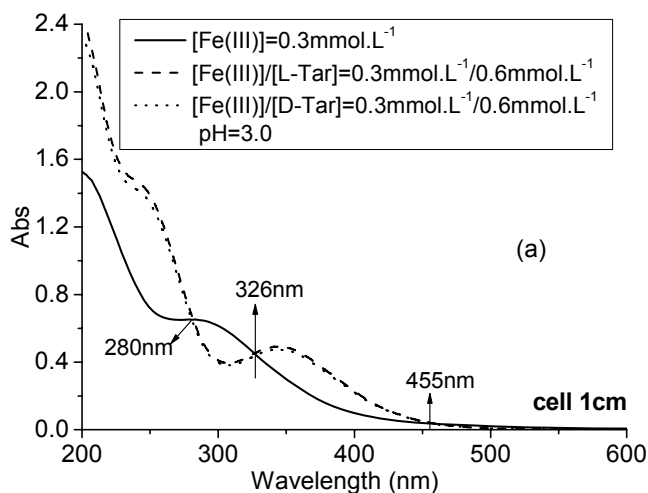
**Figure IV-A-7** Chemical structure of citric acid

## A-2-Study of the stoichiometric composition of Fe(III) in complexes with carboxylic acids

Measurements of the composition of complexes formed by Fe(III) and carboxylic acids were carried out using molar ratio method mentioned in part II experimental methods.

### A-2-1 Stoichiometry of Fe(III) in the complex with tartaric acid

D-tararic acid and L-tararic acid were separately studied in this work. The UV-vis absorbance of tartaric acid is from 200 nm to 300 nm as shown in Figure IV-A-2. The UV-visible spectra of Fe(III) and Fe(III)/Tar were presented in Figure IV-A-8. The absorbance of Fe(III)-Tar complex is around 200 to 500 nm. When Fe(III) concentration was  $0.3 \text{ mmol.L}^{-1}$ , the absorbance of Fe(III) was lower from 280 to 326 nm, at the same time the absorbance of Fe(III)/Tar was higher from 326 to 455 nm. It was obviously interpreted that Fe(III) was complexed by tartaric acid (L-Tar and D-Tar acids) in the solution. In this study, the wavelength 340 nm was chosen as the characteristic absorbance of the Fe(III)-Tar complex. The molar absorption coefficient at 340 nm are  $1200 \text{ L.mol}^{-1}.\text{cm}^{-1}$  for Fe(III);  $1960 \text{ L.mol}^{-1}.\text{cm}^{-1}$  for Fe(III)-L-Tar complex and  $1840 \text{ L.mol}^{-1}.\text{cm}^{-1}$  for Fe(III)-D-Tar complex.



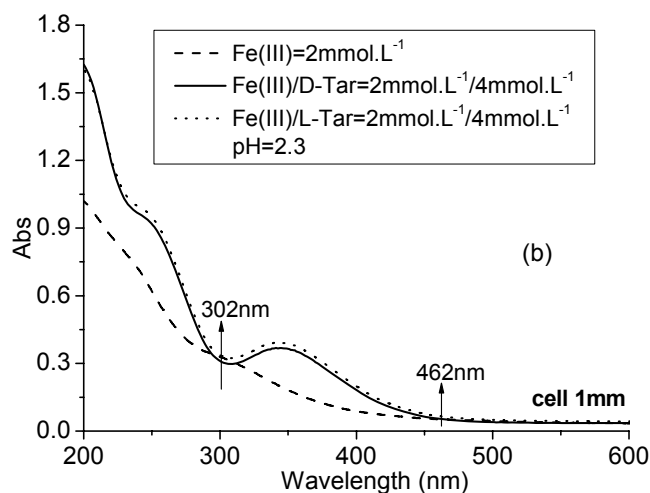


**Figure IV-A-8 UV-Visible absorption spectra of different aqueous solutions.**  
**(a) Measurement in 1 cm cell; (b) measurement in 1 mm cell**

#### A-2-1-1 Fe(III)-D-Tar complex

In this work, the concentration of Fe(III) ions was kept constant at  $0.3 \text{ mmol.L}^{-1}$  and the concentration of the D-Tar acid increased. The concentrations of D-Tar used in the experiments were 0, 0.1, 0.2, 0.3, 0.4, 0.6, 0.8 and  $1.0 \text{ mmol.L}^{-1}$ . The mixture of Fe(III) and D-Tar was adjusted to pH 2.0. Measurements were carried out by UV-visible spectra.

Figure IV-A-9 shows the variation of the UV-Visible absorption spectra of aqueous solutions with the increasing of D-Tar acid concentration. Figure IV-A-10 shows the change of the absorbance at 340 nm which increases with the increase of D-Tar acid concentration. However, it becomes stable when the D-Tar acid concentration is near  $0.6 \text{ mmol.L}^{-1}$ . This observation indicates that Fe(III) has been totally complexed by the D-Tar acid. It can be concluded that in the most stable ferric/D-Tar complexes the molar ratio between Fe(III) and D-Tar is 1:2.

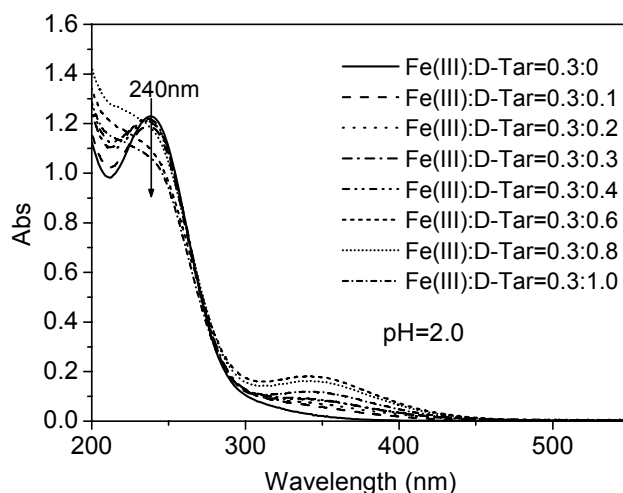


**Figure IV-A-9 UV-Visible absorption spectra of different aqueous solutions.**  
 $[\text{Fe(III)}] = 0.3 \text{ mmol.L}^{-1}$ ,  $\text{pH} = 2.0$ .

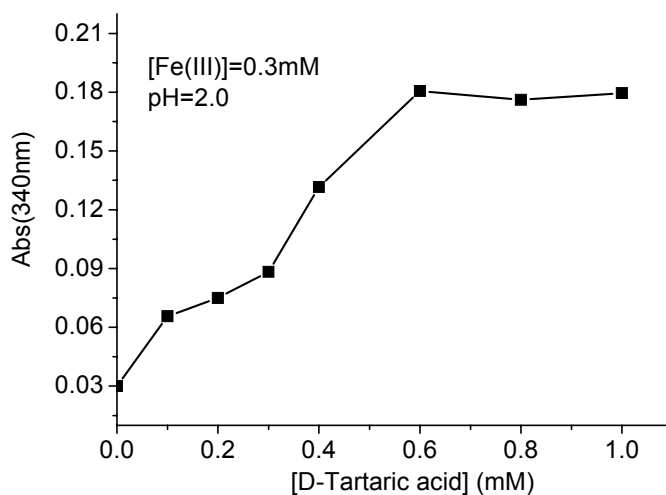


**Figure IV-A-10 Absorbance at 340 nm as a function of tartaric acid concentration.**  
 $[\text{Fe(III)}] = 0.3 \text{ mmol.L}^{-1}$ ,  $\text{pH} = 2.0$ .

### A-2-1-2 Fe(III)-L-Tar complex

Experiments were carried out to study the composition of complexes formed by Fe(III) and L-Tar acid with the same method as stated above. The concentration of Fe(III) ions was also kept constant at  $0.3 \text{ mmol.L}^{-1}$  and the concentration of the L-Tar acid was increased. The concentrations of L-Tar used in the experiments were 0, 0.1,

0.2, 0.3, 0.4, 0.6, 0.8 and 1.0 mmol.L<sup>-1</sup>. The initial pH value of the solutions was 2.0.

Figure IV-A-11 shows the variation of the UV-Visible absorption spectra of aqueous solutions with the increase of L-Tar concentration. Figure IV-A-12 shows that the absorbance at 340 nm becomes stable when the concentration of the L-Tar acid reached 0.6 mmol.L<sup>-1</sup>. We obtained the same result than for the Fe(III)-D-Tar mixture. So the most stable complexes formed between Fe(III) and tartaric acid have a molar ratio equal to 1:2.

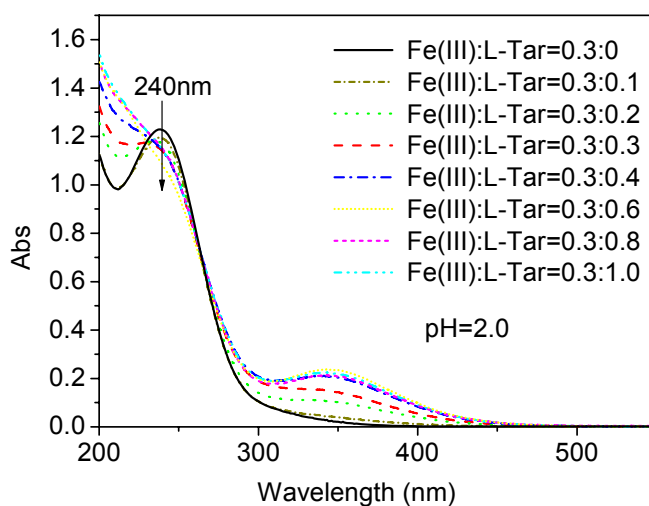


**Figure IV-A-11 UV-Visible absorption spectra of different aqueous solutions.**  
[Fe(III)] = 0.3 mmol.L<sup>-1</sup>, pH = 2.0.

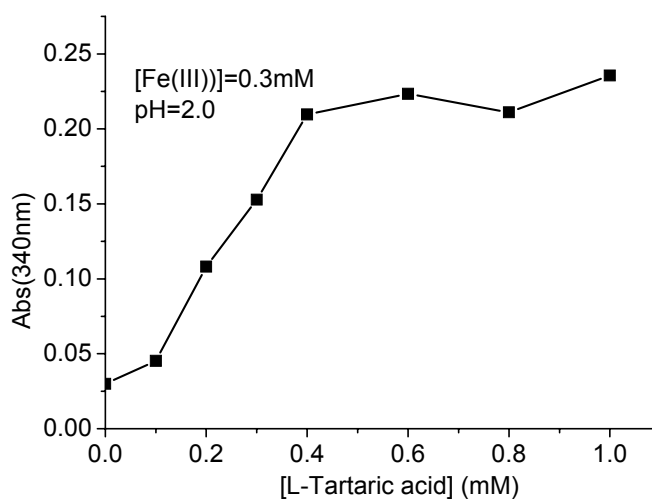


**Figure IV-A-12 Absorbance at 340 nm as a function of tartaric acid concentration.**  
[Fe(III)] = 0.3 mmol.L<sup>-1</sup>, pH = 2.0.



### A-2-2 Stoichiometry of Fe(III) in complex with pyruvic acid

The composition of complexes formed between Fe(III) and pyruvic acid was firstly studied in this work with the same method as stated above. The concentration of Fe(III) ions was also kept constant at  $0.3 \text{ mmol.L}^{-1}$  and the concentration of the Pyruvic acid was increased. The concentrations of pyruvic acid used in the experiments were 0, 0.1, 0.2, 0.3, 0.4, 0.6, 0.7, 0.8, 0.9 and  $1.0 \text{ mmol.L}^{-1}$ . The initial pH value of the solutions was 2.0. Measurements were carried out by UV-visible spectra. Experiments were carried out two times.

Figure IV-A-13 shows the variation of the UV-Visible absorption spectra of aqueous solutions with the increase of pyruvic acid concentration. The wavelength 340 nm was still chosen as the characteristic absorbance of the Fe(III)-Pyr complex (Figure IV-A-13). Figure IV-A-14 shows that the absorbance at 340nm. This absorbance becomes stable when the concentration of the pyruvic acid above  $0.8 \text{ mmol.L}^{-1}$ . It can be concluded that the most stable complexes formed between Fe(III) and Pyruvic acid is for the molar ratio equal to 1:3.

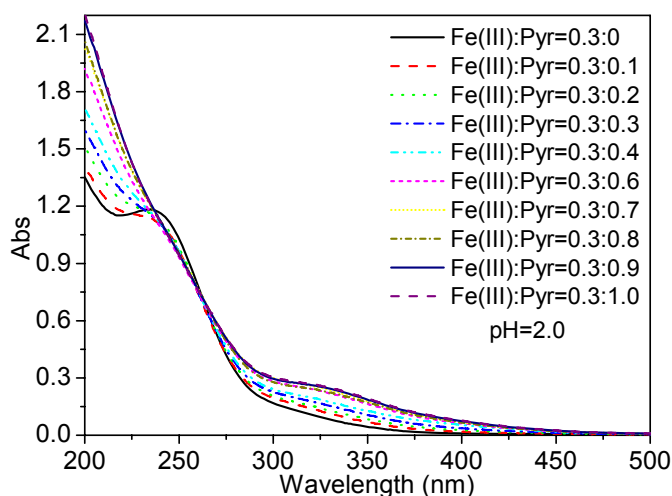
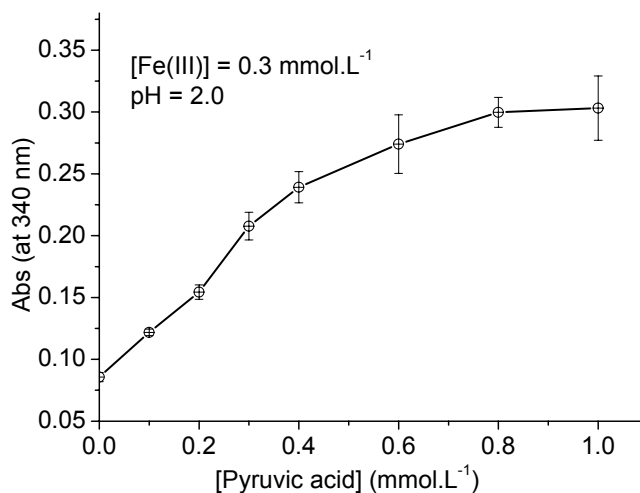


Figure IV-A-13 UV-Visible absorption spectra of different aqueous solutions.  
[Fe(III)] =  $0.3 \text{ mmol.L}^{-1}$ , pH = 2.0.



**Figure IV-A-14 Absorbance at 340 nm as a function of pyruvic acid concentration of [Fe(III)] = 0.3 mmol.L<sup>-1</sup>, pH = 2.0.**

### **A-3-Properties of Fe(III)-Carboxylate complexes**

Fe(III)-Cit, Fe(III)-Tar and Fe(III)-Pyr complexes were used in this work. So it is necessary to know their basic properties, such as their stabilities with the time at room temperature and with the variation of the pH.

#### **A-3-1 Stability of Fe(III)-Tar complexes**

In order to study the stability of the Fe-Tar complex, the stock solutions with 2 mmol.L<sup>-1</sup> Fe(III) and 4 mmol.L<sup>-1</sup> L-Tar or 4 mmol.L<sup>-1</sup> D-Tar were kept in the dark and at room temperature at least 10 days. Equilibrium was reached within 24hours for all solutions in which precipitation did not occur. Figure IV-A-15 and figure IV-A-16 show the spectrum of the solutions. The results show that Fe-Tar complex is stable in our conditions. However, Fe-Tar complex can be used as the nutrition by some bacteria, which will grow in the solutions after a long time. To limitate this phenomenon, all the stock solutions were kept in the refrigerator at 6°C. The stability of solutions used for the irradiation experiments with low concentration

$\text{Fe(III)}/\text{Tar} = 0.3 \text{ mmol.L}^{-1}/0.6 \text{ mmol.L}^{-1}$  was also measured in 2 days. As shown in Figure IV-A-15(b) and Figure IV-A-16(b), it presents the same stability as the stock solution within two days.

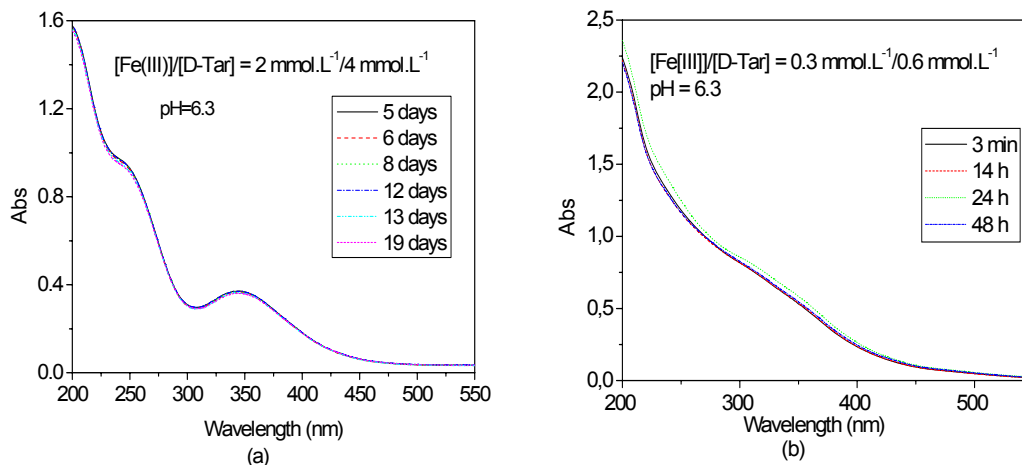


**Figure IV-A-15 Stability of the Fe(III)-D-Tar complexes as a function of time, in the dark and at room temperature**

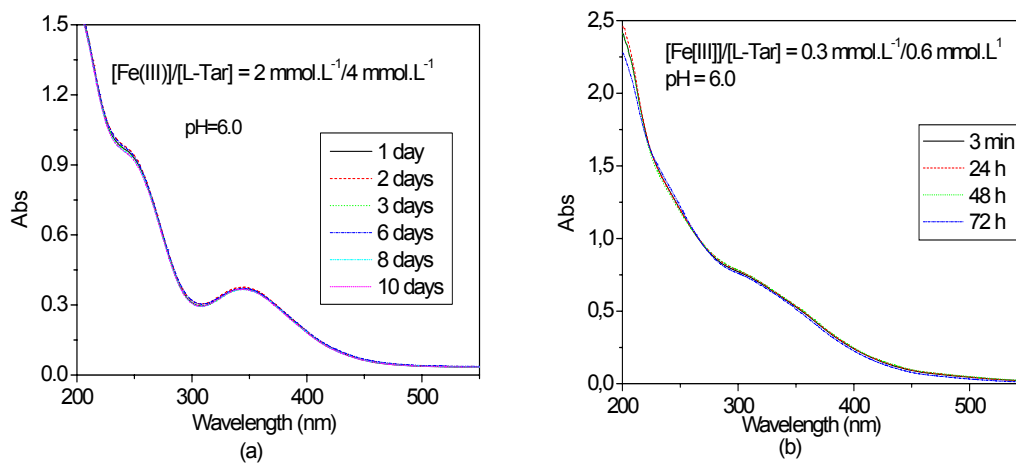
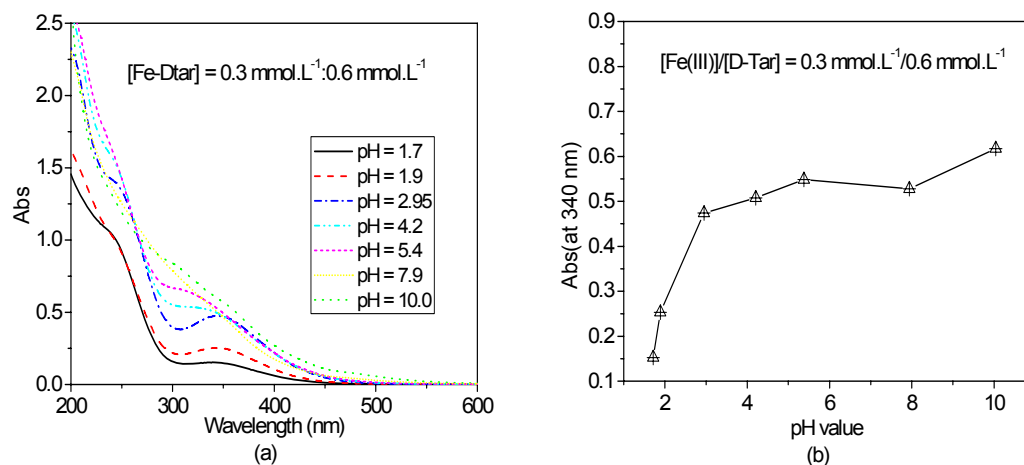


**Figure IV-A-16 Stability of the Fe(III)-L-Tar complexes as a function of time, in the dark and at room temperature**

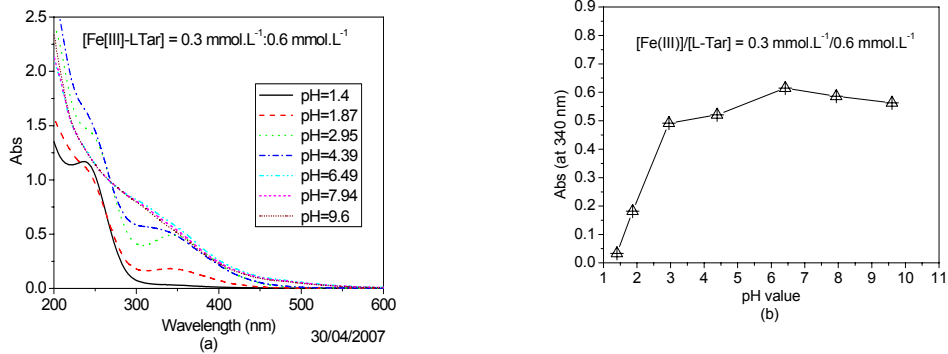
### A-3-2 pH effect

Since Fe(III) and tartaric acid can form stable complexes with a 1:2 molar ratio, all the experiments were performed with the stock solution of the complex.

Experiments were performed to study the pH effect on the stability of Fe(III)-Tar complexes. As shown in Figure IV-A-17, the UV-Visible absorption spectra of aqueous solutions with  $0.3 \text{ mmol.L}^{-1}$  Fe(III) and  $0.6 \text{ mmol.L}^{-1}$  D-Tar change according to the modification of the pH value between 1.7 to 10.0. Figure IV-A-17 (b) shows the variation of the absorbance at 340 nm. It contains an apparent inflexion point at pH 2.7. Measurement of Fe(III)-L-Tar complexes was carried out with the same method. As shown in Figure IV-A-18, the same results were obtained from the Fe(III)-L-Tar complexes. Figure IV-A-18 (b) also indicated an inflexion point near pH 2.7. In these two cases, the decrease of absorbance at lower pH ( $< 3.0$ ) could be explain by a decomplex phenomenon or by the formation of other form of the complex.

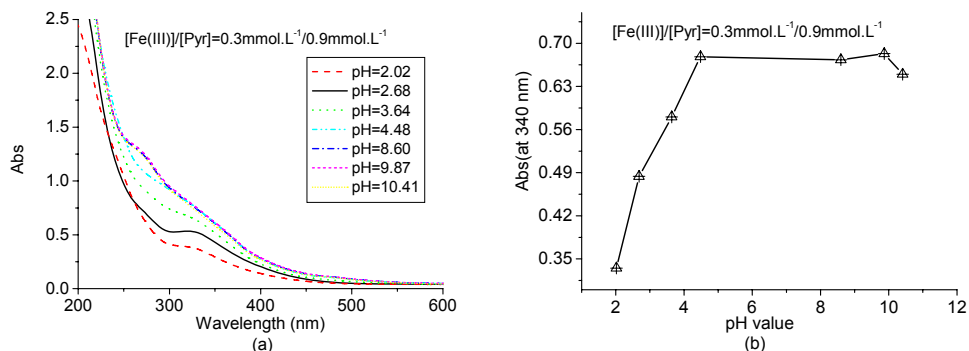


**Figure IV-A-17 UV-Visible absorption spectra of Fe-D-Tar complex solution as function of pH.  $[\text{Fe(III)}]/[\text{D-Tar}] = 0.3 \text{ mmol.L}^{-1}/0.6 \text{ mmol.L}^{-1}$  (a) UV-Visible spectra of Fe(III)-D-Tar complex; (b) Absorbance at 340 nm**



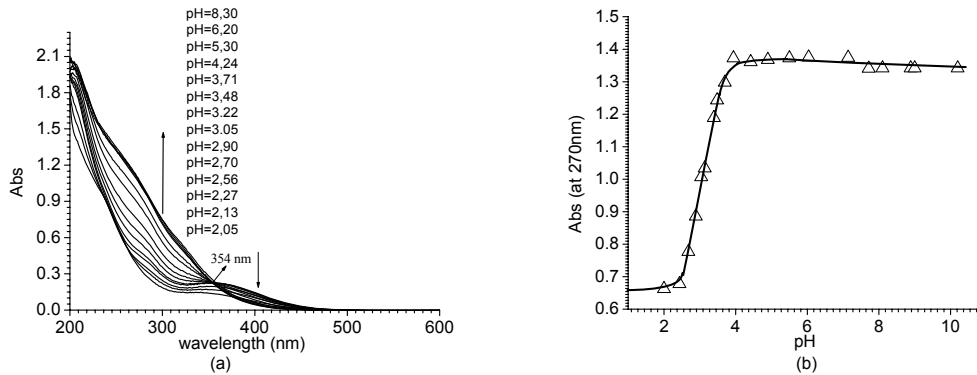
**Figure IV-A-18 UV-Visible absorption spectra of Fe(III)-L-Tar complex solution as function of pH.  $[Fe(III)]/[L-Tar] = 0.3 \text{ mmol.L}^{-1}/0.6 \text{ mmol.L}^{-1}$  (a) UV-Visible spectra of Fe(III)-L-Tar complex (b) Absorbance at 340 nm.**

We also studied the evolution of UV-visible spectra of Fe(III)-Pyr complexes as function of pH. Experiments were performed in the solutions with  $0.3 \text{ mmol.L}^{-1}$  of Fe(III)-Pyr complexes and pH between 2.02 to 10.41. Figure IV-A-19 gives the results and it indicates the pKa of Fe(III)-Pyr complex is 3.6.



**Figure IV-A-19 UV-Visible absorption spectra of Fe(III)-Pyr complex solution as function of pH.  $[Fe(III)]/[Pyr] = 0.3 \text{ mmol.L}^{-1}/0.9 \text{ mmol.L}^{-1}$  (a) UV-Visible spectra of Fe(III)-Pyr complex (b) Absorbance at 340 nm**

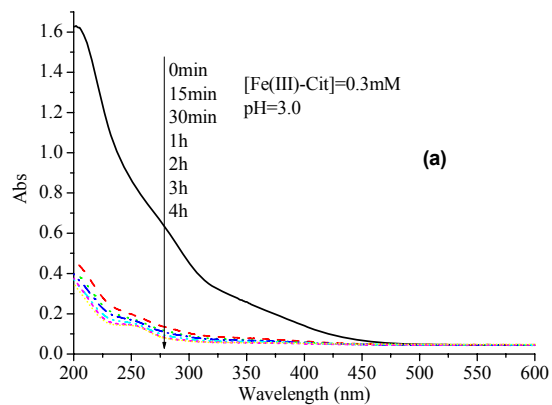
Abida (2005) has studied the evolution of UV-visible spectra of Fe(III)-Cit complexes as function of pH. Experiments were performed in the solutions with  $0.3 \text{ mmol.L}^{-1}$  of Fe(III)-Cit complexes and pH between 2.05 to 8.30. Figure IV-A-20 gives the results and it indicates the pKa of Fe(III)-Cit complex is 3.3.



**Figure IV-A-20** UV-visible spectra of Fe(III)-Cit complexes ( $0.3 \text{ mmol.L}^{-1}$ ) as function of pH. (a) UV-Visible spectra of Fe(III)-Cit complex; (b) Absorbance at 270 nm (*Abida, 2005*)

### A-3-3 Irradiation effect

Photolysis of Fe (III)-Carboxylate complexes was studied in the aqueous solution under irradiation. Results were shown in Figure IV-A-21. Only in 15 min, the UV-Visible absorbance of the aqueous solution with complexes were all apparently decreased, and these results indicated that under 365nm irradiation, these complexes were easily photolyzed and it provided the possibility for the formation of excited state complexes and further generated many kinds of radicals. Further experiments have been carried out and this conclusion has been conformed in the later part of the thesis.



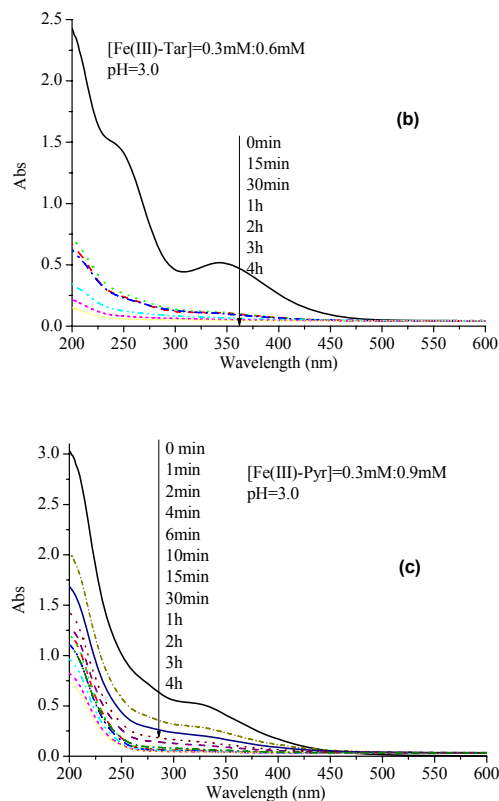


**Figure IV-A-21** Variation of UV-visible spectra of Fe(III)-Carboxylate complexes ( $0.3 \text{ mmol.L}^{-1}$ ) under irradiation (a) Fe(III)-Cit; (b) Fe(III)-Tar; (c) Fe(III)-Pyr.

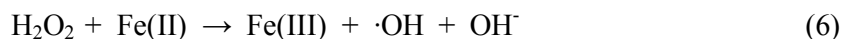
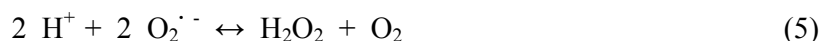
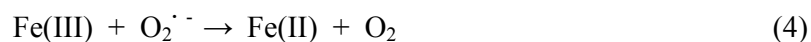
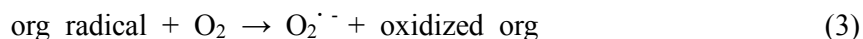
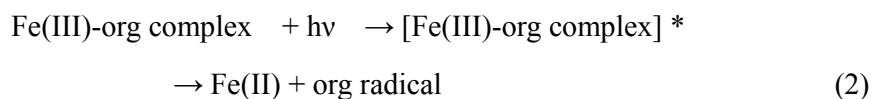
### Conclusions

In our experimental conditions, we demonstrated that Fe(III) was complexed by tartaric acid (D or L) with a ratio 1:2 and by pyruvic acid with a ratio 1:3. Some studies in the literature proposed a stoichiometry of 1:1 or 2:2 for the Fe(III)-Tar complex. This difference can be attributed to the experimental conditions used.

We check the stability of these complexes in the dark and at room temperature. Fe(III)-Tar, Fe(III)-Pyr and Fe(III)-Cit complexes are all stable in the aqueous solutions in our experimental conditions ( $\text{pH} = 3.0$ , concentration of complex  $0.3 \text{ mmol.L}^{-1}$ ). Our results show that the pH is an important parameter for the stability of the complex and its speciation. At lower pH ( $< 3.0$ ) a phenomenon of decomplexation can be proposed.

## IV-B Determination of hydroxyl radicals from photolysis of Fe(III)-Carboxylate complexes in aqueous solutions

The presence of carboxylic acids, such as oxalate, citrate and so on, has a significant effect on the speciation and the photoactivity of Fe(III) ions in acidic conditions. Because they can form stable complexes with Fe(III) ions. Free Fe(III) absorb weakly in the solar UV region (290 nm~400 nm), but the absorption spectra of hydrated or otherwise complex iron species (iron pairs) are shifted toward the visible, which might make their use in sunlight possible (Lente and Fábíán, 2001). In natural waters, photochemically induce electron transfer from the complexing organic ligand to Fe(III) in the excited Fe(III)-org complexes can take place, and subsequently, the electron deficient Fe(III)-org complexes further reduce  $O_2$  to  $O_2^{\cdot -}$ .  $O_2^{\cdot -}$  rapidly reacts to yield the hydroxyl radicals (Zuo and Hoigné, 1992; Joseph et al., 2001; Zepp et al., 1987). This pathway can be represented as the following reactions:



In this work, we studied the photogeneration of hydroxyl radicals in the aqueous solutions in the presence of Fe(III)-Carboxylate complexes.

### B-1-Photoproduction of hydroxyl radicals in the aqueous solutions with Fe(III)-Pyr complexes

Figure IV-B-1 presents the UV-Vis spectra of both the solutions containing only Fe(III) ions (pH = 3) and the solutions containing Fe(III) ions with additions of Pyr.



In the case of solution without Pyr, the spectrum belongs to the  $\text{Fe(OH)}^{2+}$  complex. The change in the spectrum after addition of Pyr indicates the formation of the Fe(III)-Pyr complex. The absorption of Fe(III)-Pyr complex in the region of 320–500 nm is sufficiently higher than that of  $\text{Fe(OH)}^{2+}$ . This allows one to assume that the Fe(III)-Pyr complex can be used in the processes of photodegradation of organic impurities in natural water systems.

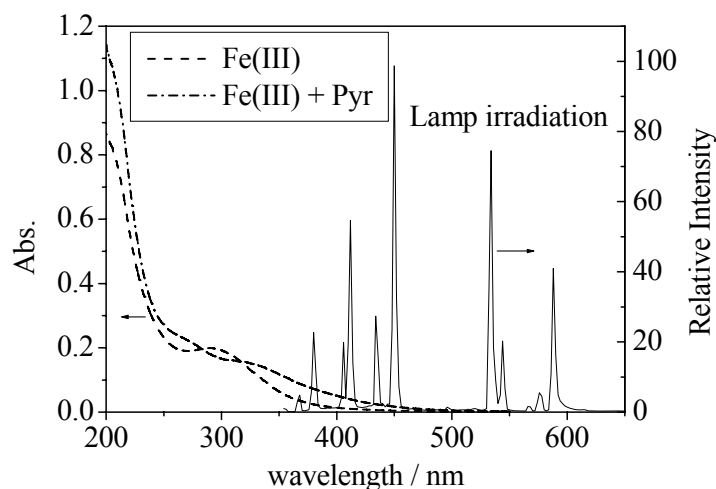


**Figure IV-B-1** UV-Visible spectrum of solutions with  $C_{\text{Fe(III)}} = 100 \mu\text{mol.L}^{-1}$  and with or without  $C_{\text{Pyr}} = 300 \mu\text{mol.L}^{-1}$ . The length of the cell was 1 cm. Initial pH of the aqueous solution was 3.0. The spectrum of the metal halide light used in this work is also shown.

Photogeneration of  $\cdot\text{OH}$  by the photolysis of Fe(III)–Pyr complexes in the aqueous solution has been determined using benzene ( $7 \text{ mmol.L}^{-1}$ ) as a scavenger and the selected typical reaction was the formation of phenol from benzene. Due to the big difference of concentration between benzene and phenol formed, we can consider that  $\cdot\text{OH}$  radicals react mainly on the benzene. Through detecting the phenol formed in the reaction solution, we can quantify  $\cdot\text{OH}$  generated in the reaction. The mechanism of photoproduction of  $\cdot\text{OH}$  in the aqueous solutions containing Fe(III)-Pyr complexes can presumably be interpreted as the following reactions scheme (Figure IV-B-2):

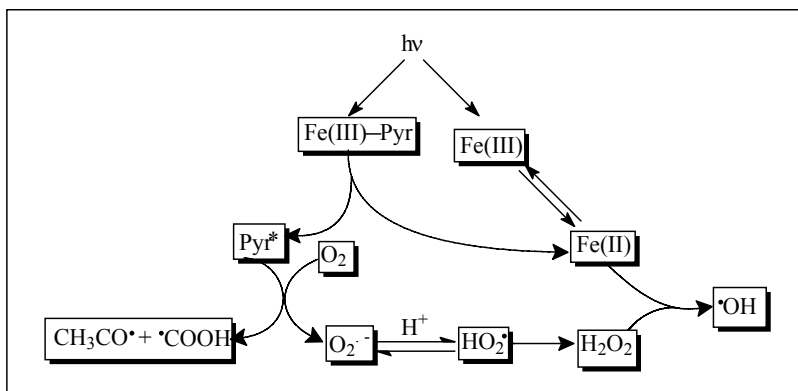
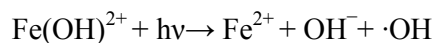
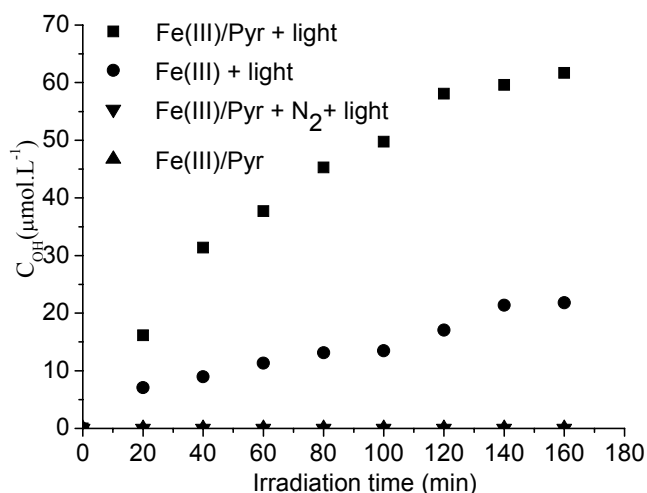


Figure IV-B-2 Photoreaction mechanism

**B-1-1 Generation of hydroxyl radicals in the irradiated aqueous solution containing Fe(III)-Pyr complexes**



The concentration of the  $\cdot\text{OH}$  radicals production by the photolysis of the Fe(III)-Pyr complex and the  $\text{Fe}(\text{OH})^{2+}$  complexes were compared. As shown in Figure IV-B-3, under the same pH and irradiation time, the concentration of  $\cdot\text{OH}$  generated in the system containing the Fe(III)-Pyr complex is higher than that in the system with  $\text{Fe}(\text{OH})^{2+}$ . The possible production of the hydroxyl radical in the thermal reaction was experimentally checked and no hydroxyl radicals were generated. The availability of oxygen in the aqueous solution was found to be an important factor for the  $\cdot\text{OH}$  production, because in anaerobic conditions, the experiments showed that no  $\cdot\text{OH}$  was generated (Figure IV-B-3).



**Figure IV-B-3 Comparison of  $\cdot\text{OH}$  formation under different conditions for an aqueous solution with  $C_{\text{Fe(III)}} = 10 \mu\text{mol.L}^{-1}$ ,  $C_{\text{Pyr}} = 90 \mu\text{mol.L}^{-1}$ . Initial pH of the aqueous solution was 3.0.**

**B-1-2 Effect of pH on the generation of hydroxyl radicals in the irradiated aqueous solution containing Fe(III)-Pyr complexes**

The experiments were performed in the homogeneous aqueous solutions at pH value of 1.5, 2.0, 3.0, 4.0 and 5.0, which were provided by an addition of hydrochloric acid. A significant effect of pH on the  $\cdot\text{OH}$  yield was observed (Figure IV-B-4). The  $\cdot\text{OH}$  concentration at pH = 3.0 appeared to be higher than that at all other pH values in the range studied. The great effect of pH on the production of  $\text{H}_2\text{O}_2$  upon the photolysis of different Fe(III)-carboxylate complexes was reported previously (Deng et al., 1998; Gao and Zepp, 1998; Wu et al., 2004).

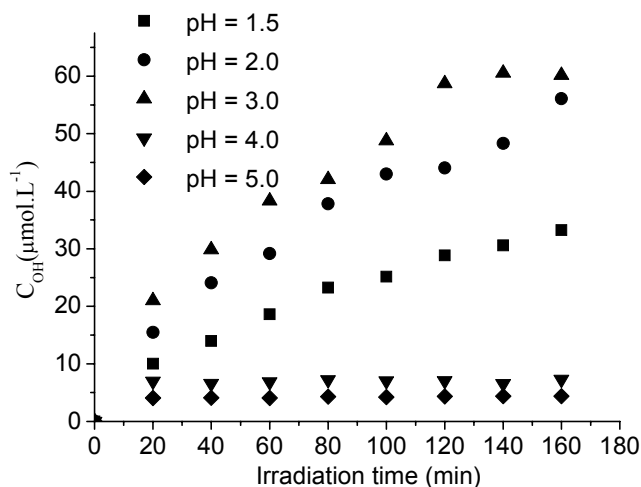


**Figure IV-B-4 Effect of the initial pH value on the total ·OH concentration for an aqueous solution with  $C_{\text{Fe(III)}} = 30 \mu\text{mol.L}^{-1}$ ,  $C_{\text{Pyr}} = 60 \mu\text{mol.L}^{-1}$ .**

We believe that the influence of pH on the photolysis of the Fe(III)-Pyr complex could be explained by two reasons. First, pH can affect the distribution of different species (Fe(III) complexes) present in the solution. These species [(Fe(III)-Pyr,  $\text{Fe}(\text{OH})^{2+}$ ,  $\text{Fe}(\text{OH})_2^+$ ,  $\text{Fe}^{3+}$  aq, pyruvic acid] possess different photochemical reactivity, and it would affect the ·OH yield. Secondly, pH can influence Fenton reaction and the equilibrium between  $\text{HO}_2\cdot/\text{O}_2^{\cdot-}$  and as a consequence the rate of ·OH radical formation.

**B-1-3 Effect of Fe(III) and Pyr concentrations on the photogeneration of hydroxyl radicals in the aqueous solution**

The concentration ratio Fe(III)/Pyr is another important factor. To evaluate this factor, the experiments in solutions with pH = 3.0 were performed. Results are shown in Figure IV-B-5 and IV-B-6. It can be concluded that both the Fe(III) and Pyr concentrations affect the ·OH yield. The ·OH concentration increased with an increase in the Pyr concentration in the range from 30.0 to 120.0  $\mu\text{mol.L}^{-1}$ , or with an increase in the Fe(III) concentration in the range from 10.0 to 60.0  $\mu\text{mol.L}^{-1}$ . At a given pH

value, a change in the Fe(III) / Pyr ratio can lead to a change in the relative content of different Fe(III)-Pyr complexes in the solution. When the Pyr concentration was much higher than that of Fe(III), the formation of  $\cdot\text{OH}$  radical is higher. When the Fe(III) concentration is relatively higher than that of Pyr, Fe(III) species in the solution can promote the  $\cdot\text{OH}$  yield in a continuous Fe(III)/ Fe(II)/Fe(III) cycle. At pH = 2.0-5.0, Fe(III) will participate in the so-called photo-Fenton reaction.  $\text{Fe}(\text{OH})^{2+}$  is thought to be the predominant photoactive species in the pH range 2.5-5.0.

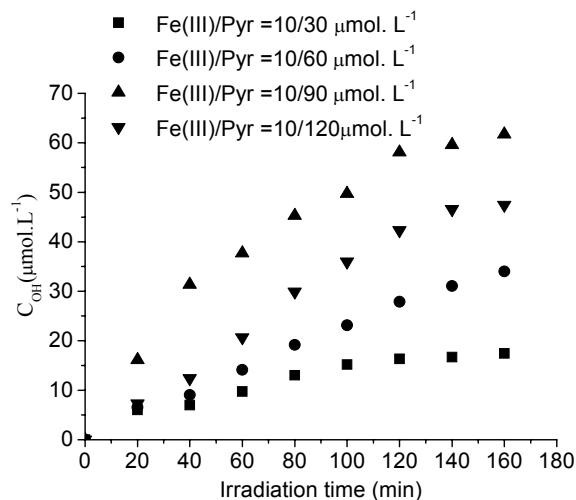


**Figure IV-B-5 Effect of the Pyr concentration on the  $\cdot\text{OH}$  total yield for aqueous solutions with  $C_{\text{Fe(III)}} = 10 \mu\text{mol.L}^{-1}$ . Initial pH of the aqueous solution was 3.0.**

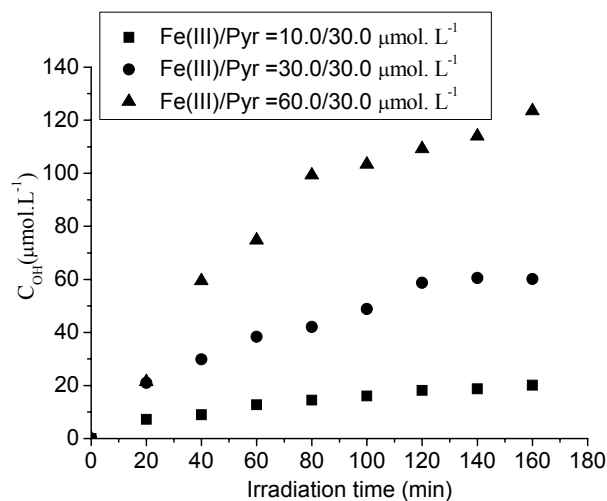


**Figure IV-B-6 Effect of the Fe(III) concentration on the  $\cdot\text{OH}$  total yield for aqueous solutions with  $C_{\text{Pyr}} = 30 \mu\text{mol.L}^{-1}$ . Initial pH of the aqueous solution was 3.0.**

### B-1-4 Effect of temperature on the photogeneration of hydroxyl radicals in the aqueous solution

To examine the effect of temperature on the quantum yield, experiments were performed at 298 and 328 K. Results are shown in Figure IV-B-7. The  $\cdot\text{OH}$  yield at 328 K was much higher than that at 298 K. Although higher temperatures will hasten the main reactions, they can also enhance side reactions. Thus, all the experiments were carried out at room temperature with cooling water.

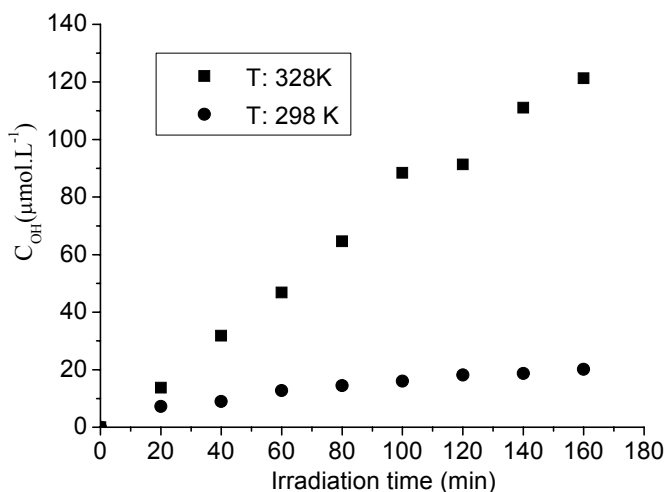
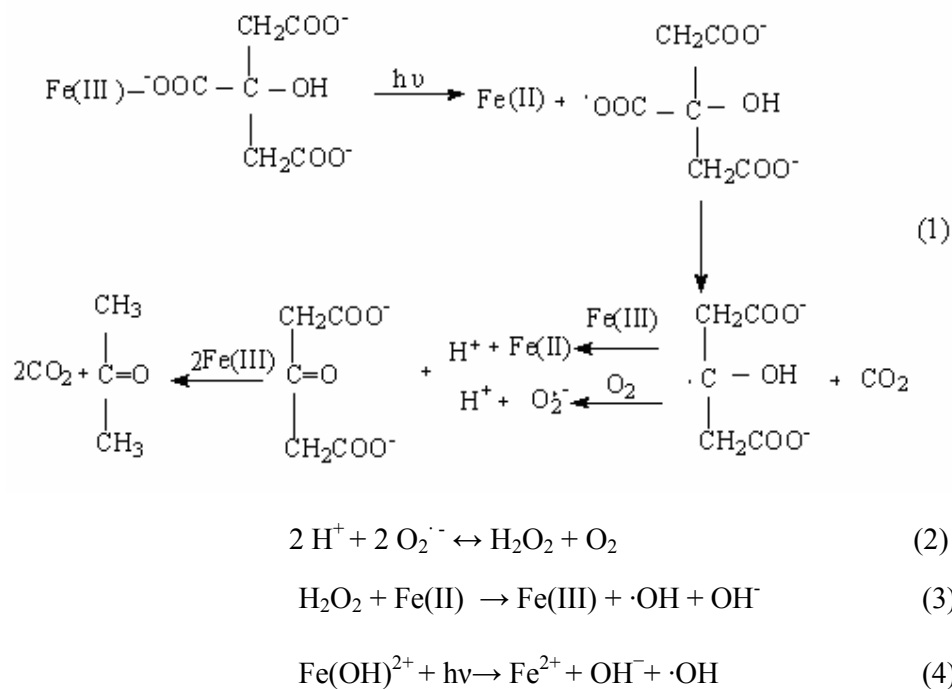


Figure IV-B-7 Effect of temperature on the  $\cdot\text{OH}$  total yield for an aqueous solution with  $C_{\text{Fe(III)}} = 10 \mu\text{mol.L}^{-1}$ , and  $C_{\text{Pyr}} = 30 \mu\text{mol.L}^{-1}$ . Initial pH of the aqueous solution was 3.0.

### **B-2-Photoproduction of hydroxyl radicals in the aqueous solutions with Fe(III)-Cit complexes**

Generation of Hydroxyl radicals in the irradiated aqueous solution containing Fe(III)-citrate complexes was confirmed by using benzene as scavenger and detection of the consequent formation of phenol. The mechanism of photoproduction of  $\cdot\text{OH}$  in the aqueous solutions containing Fe(III)-citrate complexes can be presumably

interpreted as following reactions scheme:



**B-2-1 Generation of hydroxyl radicals in the irradiated aqueous solution containing Fe(III)-Cit complexes**

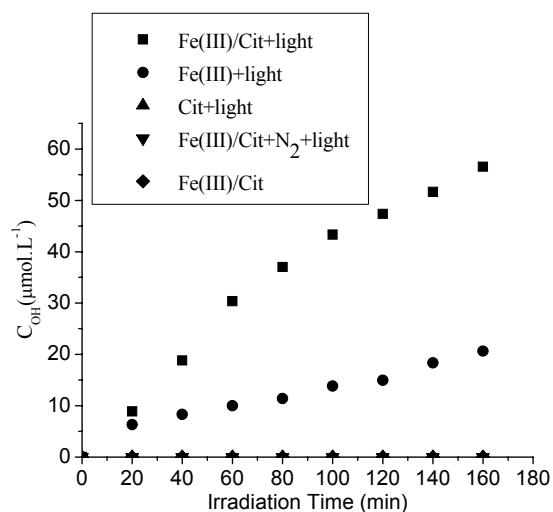


**Figure IV-B-8 Control experiments in different systems**  
 $C_{\text{Fe(III)}} = 10.0 \mu\text{mol.L}^{-1}$ ,  $C_{\text{Cit}} = 120.0 \mu\text{mol.L}^{-1}$ ,  $\text{pH} = 3.0$

Since  $\text{Fe}(\text{OH})^{2+}$  can photolyse to produce  $\cdot\text{OH}$  (reaction (4)), we did the control experiment in the solutions without citrate. As Figure IV-B-8 shows, under the same irradiation and pH value, the  $\cdot\text{OH}$  concentration generated in the irradiated aqueous solution containing Fe(III)-citrate complexes is higher than that of the solution without citrate. It can be concluded that Fe(III)-citrate complexes could enhance the photoproduction of  $\cdot\text{OH}$  in aqueous solution. Without irradiation, results show no detectable formation of phenol (see Figure IV-B-8). We also did experiment in anaerobic solution by purging the solution with  $\text{N}_2$  over ten minutes, while no  $\cdot\text{OH}$  was produced. This shows that oxygen plays an important role in the formation of active species, such as  $\text{O}_2^{\cdot-}$  and  $\cdot\text{OH}$ . The feasibility of these two solutions (with or without citric acid) for degradation of several kinds of pollutants has been examined (Deng et al., 1998; Wu and Deng, 1999 and 2000).

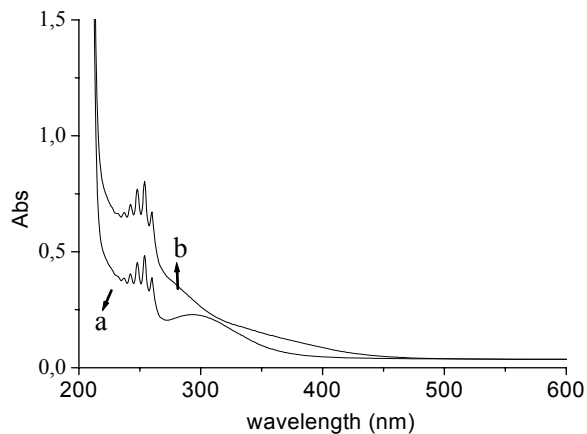


**Figure IV-B-9 UV-Vis absorption spectra of the solutions with or without citrate**  
**a: without Citrate, b: with Citrate**  
**(  $C_{\text{Fe(III)}} = 100.0 \mu\text{mol.L}^{-1}$ ,  $C_{\text{Cit}} = 300.0 \mu\text{mol.L}^{-1}$ ,  $C_{\text{benzene}} = 7 \text{ mmol.L}^{-1}$ ,  $\text{pH} = 3.0$ )**

Figure IV-B-9 presents the UV-Vis absorption spectra of the solutions in the presence of citrate or not. Fe(III)-citrate complexes absorb even more strongly than Fe(III)-OH complexes in the UV-Visible region (200-450 nm). So the Fe(III)-citrate complexes has the potential of utilizing sunlight as an irradiation source to photogenerate  $\cdot\text{OH}$ . Experiments were carried out in aerobic conditions, without oxygen no  $\cdot\text{OH}$  radicals were produced. The result shows that Fe(III)-citrate



complexes could enhance the photoproduction of  $\cdot\text{OH}$ . It is proposed that the photolysis of Fe(III)-citrate complexes has a contribution to  $\cdot\text{OH}$  production in atmospheric waters and surface water where there are high concentration ferric ions and citrate ions. Moreover,  $\cdot\text{OH}$  has high oxidizing potential for the degradation of organic pollutants in water. So we believe that the  $\cdot\text{OH}$  production from the photolysis of Fe(III)-citrate complexes in the aerobic water will play an important role in the oxidation of organic compounds in natural waters and probably in wastewater remediation by photochemical approaches.

**B-2-2 Effect of pH on the generation of hydroxyl radicals in the irradiated aqueous solution containing Fe(III)-Cit complexes**

pH is an important parameter in the chemical reaction. Experiments were carried out to study the pH effect on the photoproduction of  $\cdot\text{OH}$  radicals in the aqueous solution containing Fe(III)-citrate complexes. Irradiation experiments were carried out in aqueous solutions where the pH has been adjusted to different values of 3.0, 4.0, 5.0, 6.0 and 7.0 with hydrochloric acid ( $0.1 \text{ mol.L}^{-1}$ ). Results indicate that pH value has strong effect on the photogeneration of  $\cdot\text{OH}$  radicals. The  $\cdot\text{OH}$  concentration at pH 3.0 is higher than that at other pH values ranged from 3.0 to 7.0 (Figure IV-B-10).

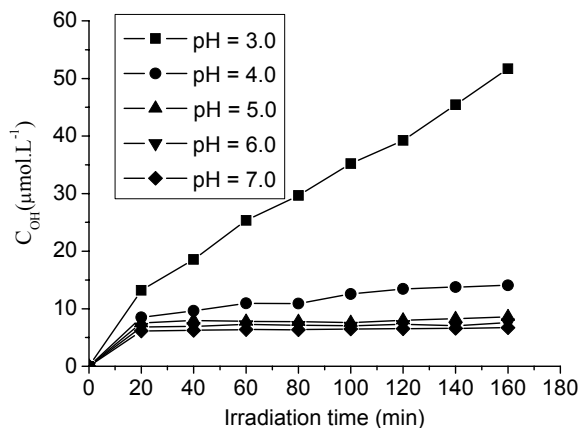


**Figure IV-B-10 Initial pH value effects on the photoproduction of  $\cdot\text{OH}$  ( $C_{\text{Fe(III)}} = 30.0 \text{ } \mu\text{mol.L}^{-1}$ ,  $C_{\text{Cit}} = 30.0 \text{ } \mu\text{mol.L}^{-1}$ )**

Previous studies have shown that the pH value of the reaction solution has great effect on the photolysis of Fe(III)-citrate complexes in producing  $\text{H}_2\text{O}_2$  and degrading organic compounds (Deng et al., 1998; Wu and Deng, 2004). The pH value may affect the distribution of Fe(III) species. So computations of the speciation of Fe(III) were carried out using Visual MINTEQ computer program in the condition with  $30.0 \mu\text{mol.L}^{-1}$  of Fe(III) and  $30.0 \mu\text{mol.L}^{-1}$  of Cit. Calculations were done at  $25^\circ\text{C}$ . The concentrations of both Fe(III) and Cit are very low, so the ionic strength is nearly zero. Results are shown in Figure IV-B-11. We can see that Fe(III)-Citrate is the predominant species when pH values range from 3.0 to 6.0. From pH 6.0~7.0,  $\text{Fe}(\text{OH})_2^+$  gradually become the major photoactive species, with almost the same quantum yield of OH radical formation that  $\text{Fe}(\text{OH})_2^{2+}$ . From Figure IV-B-11, we can conclude that pH nearly does not affect the distribution of Fe(III) species when pH values range from 3.0 to 6.0 in this work. We think that the speciation of iron is not the main reason for the pH value effect because Fe(III)-citrate is the major photoactive species in the aqueous solutions.

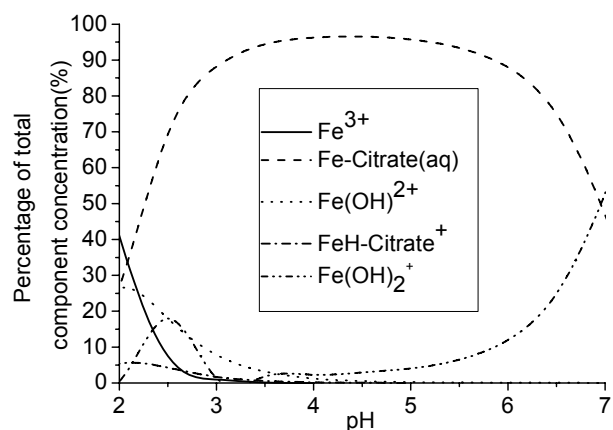


**Figure IV-B-11 pH effects on the distribution of Fe(III) species**  
 ( $C_{\text{Fe(III)}} = 30.0 \mu\text{mol.L}^{-1}$ ,  $C_{\text{Cit}} = 30.0 \mu\text{mol.L}^{-1}$ , Ionic strength= 0,  $25^\circ\text{C}$ ).

So the effect of pH may result from the pH dependency of the active intermediates  $\text{HO}_2\cdot/\text{O}_2\cdot^-$  and Fe(III)/Fe(II), which affects the formation rate of  $\text{H}_2\text{O}_2$ . Furthermore, Fenton reaction is believed to be acid-favourable and more  $\cdot\text{OH}$  is produced in water

at acidic pH values. These two reasons can be the main effect of pH on the photoreaction efficiency of producing  $\cdot\text{OH}$  in the aqueous solution containing Fe(III)-organic ligands complexes. In acid conditions, the producing efficiency of  $\cdot\text{OH}$  in the aqueous solution containing Fe(III)-citrate complexes is higher.

**B-2-3 Effect of Fe(III) and Cit concentrations on the generation of hydroxyl radicals in the irradiated aqueous solution containing Fe(III)-Cit complexes**

The concentration ratio of Fe(III) to citrate was another important factor. We have performed series of experiments to study these effects. All experiments were carried out at pH 3.0. Results are shown in Figure IV-B-12 and Figure IV-B-13, it can be concluded that Fe(III) and citrate concentrations all have effects on the photoproduction of  $\cdot\text{OH}$  radicals in the irradiated aqueous solution containing Fe(III)-citrate complexes. The  $\cdot\text{OH}$  radicals concentration increased with the increase of citrate concentration in the range of  $15.0 \mu\text{mol.L}^{-1}$  to  $120.0 \mu\text{mol.L}^{-1}$ , or the increase of Fe(III) concentration in the range of  $10.0 \mu\text{mol.L}^{-1}$  to  $60.0 \mu\text{mol.L}^{-1}$ . At a given pH value, the concentration ratio of Fe(III) to citrate can determine the species distribution of Fe(III)-citrate complexes in the aqueous solutions. Through Visual MINTEQ calculating, we obtained that at Fe(III)/Citrate ratio  $< 1$ , Fe(III)-Citrate complexes is the major photoactive species, while when the ratio is much higher than 1, the major species to produce  $\cdot\text{OH}$  radicals is  $\text{Fe}(\text{OH})^{2+}$  complexes, which is the most predominant photoactive Fe(III)-hydroxyl complex in the aqueous solution at pH 3.0.

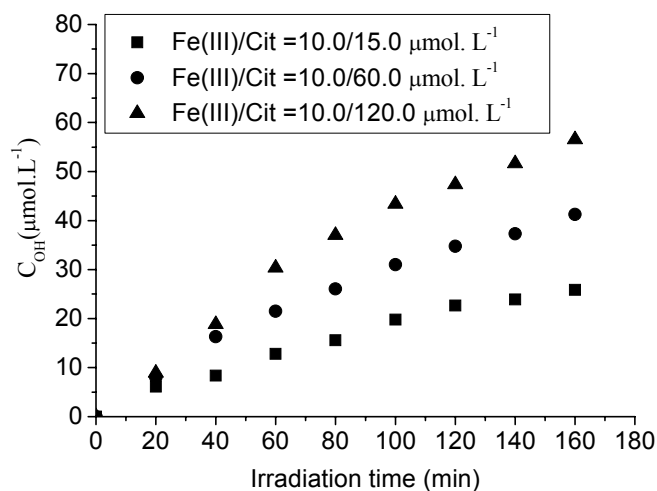


**Figure IV-B-12 Effect of citrate concentration on the photoproduction of ·OH radical (pH = 3.0, C<sub>Cit</sub> = 15.0 to 120.0 μmol.L<sup>-1</sup>, C<sub>Fe(III)</sub> = 10.0 μmol.L<sup>-1</sup>)**

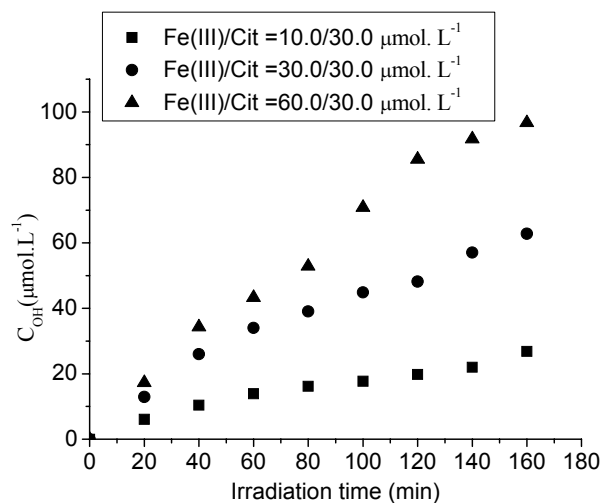


**Figure IV-B-13 Effect of ferric concentration on photoproduction of ·OH radicals (pH = 3.0, C<sub>Cit</sub> = 30.0 μmol.L<sup>-1</sup>, C<sub>Fe(III)</sub> = 10.0 to 60.0 μmol.L<sup>-1</sup>)**

### B-3-Photoproduction of hydroxyl radicals in the aqueous solutions with Fe(III)-Tar complexes

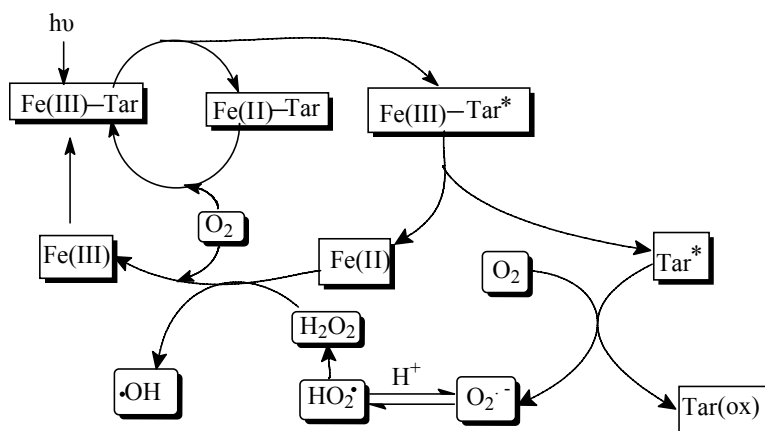
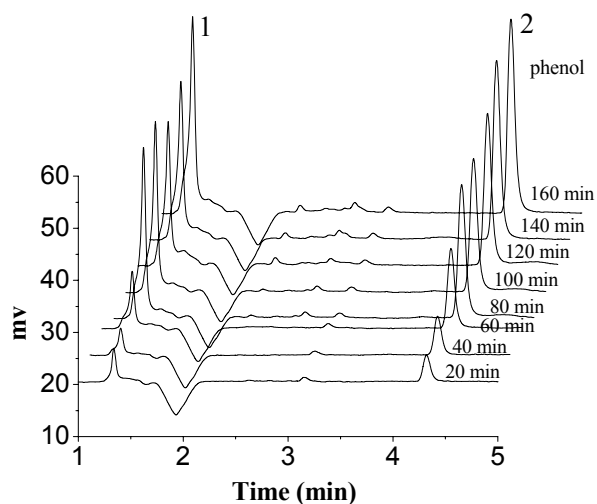


Figure IV-B-14 Photochemical reaction mechanism

In aqueous solution, the photogeneration of  $\cdot\text{OH}$  radicals can occur through different pathways shown in Figure IV-B-14. An important step is the photolysis of the Fe(III)-Tar complexes. Light absorption on the complexes results in an electronically excited state. Electron transfer via this electronically excited state leads to a reduced iron and oxidized Tar. Then carbon center radicals reduce  $\text{O}_2$  to  $\text{O}_2^{\bullet-}$ .  $\text{O}_2^{\bullet-}$  can be rapidly protonated (as function of pH) to its conjugated acid, the peroxy radicals and these radicals leads to the formation of hydrogen peroxide. The  $\cdot\text{OH}$  radicals are photoproduced by Fenton and/or photo-Fenton reactions.



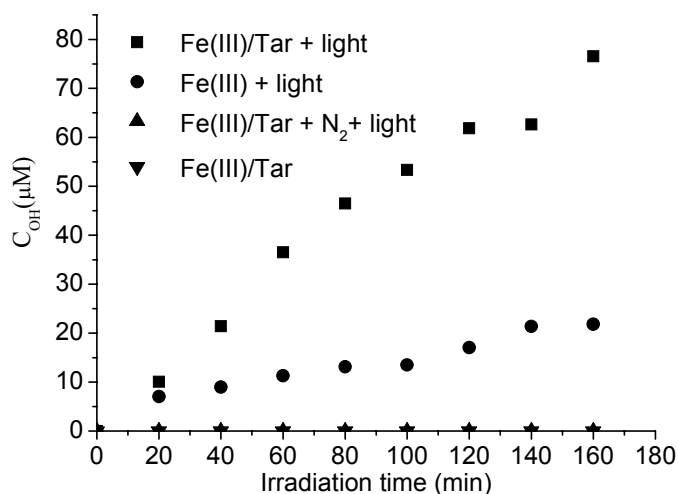
**Figure IV-B-15 HPLC chromatogram of the phenol photogeneration as a function of irradiation time ( $C_{\text{Fe(III)}} = 10.0 \mu\text{mol.L}^{-1}$ ,  $C_{\text{Tar}} = 150.0 \mu\text{mol.L}^{-1}$  and  $C_{\text{benzene}} = 7 \text{mmol.L}^{-1}$ ). The initial pH value of the aqueous solution was 3.0.  $\lambda_{\text{det}} = 270 \text{nm}$ .**

Figure IV-B-15 shows the HPLC chromatograms of the photogeneration of phenol as a function of irradiation time. The retention time of phenol is 4.2 min in this work. Peak 2 is phenol photoproduced during the illumination. We can see that the peak area of phenol increased with longer irradiation time. For the reaction between benzene and  $\cdot\text{OH}$  radicals, the formation of phenol was reported to be the major way of benzene degradation and represent almost 100% (Deister et al., 1990). Thus photochemically formed  $\cdot\text{OH}$  radicals concentrations could be determined by the phenol concentrations. It should be mentioned that the  $\cdot\text{OH}$  radicals concentrations reported here are total concentrations of  $\cdot\text{OH}$  radicals generated during the given illumination time and are not the steady-state concentrations. Peak 1 is some iron complexes with lower molecular carboxylic acids.

**B-3-1 Generation of hydroxyl radicals in the irradiated aqueous solution containing Fe(III)-Tar complexes**

Photogeneration of hydroxyl radicals by the photolysis of Fe(III)-Tar complexes

has been quantitatively determined by using benzene ( $7 \text{ mmol.L}^{-1}$ ) as a probe. Since Fe(III)-OH complexes can photolyze to produce  $\cdot\text{OH}$  radicals, we did control experiment in the aqueous solution without Tar. As Figure IV-B-16 shows, under the same irradiation and the pH value, the  $\cdot\text{OH}$  concentration generated in the systems containing Fe(III)-Tar complexes is higher than that of the system only containing Fe(III). Dark reactions were also carried out in parallel, while no  $\cdot\text{OH}$  radicals were produced.



**Figure IV-B-16 Comparing of  $\cdot\text{OH}$  radicals yield in different conditions. In an aqueous solution of  $C_{\text{Fe(III)}} = 10.0 \mu\text{mol.L}^{-1}$  and  $C_{\text{Tar}} = 150.0 \mu\text{mol.L}^{-1}$ . The initial pH value of the aqueous solution was 3.0.**

The availability of oxygen in aqueous solution was another important factor. The aqueous solution containing Fe(III)-Tar complexes were all in the presence of oxygen. Control experiments were carried out in anaerobic solution by bubbling with  $\text{N}_2$  over ten minutes. Results showed that no  $\cdot\text{OH}$  radicals are generated in the aqueous solution. Without oxygen,  $\text{O}_2^{\cdot-}$  and  $\cdot\text{OH}$  are not formed.

**B-3-2 Effect of pH on the generation of hydroxyl radicals in the irradiated aqueous solution containing Fe(III)-Tar complexes**

Experiments were carried out to investigate the initial pH value effect on the

photogeneration of  $\cdot\text{OH}$  radicals in the system containing Fe(III)-Tar complexes. Reactions were carried out in the aqueous solutions at different pH values of 1.5, 2.0, 3.0, 4.0 and 5.0 adjusted with hydrochloric acid ( $0.1 \text{ mol.L}^{-1}$ ). The results indicate that the pH value could affect the concentration of  $\cdot\text{OH}$  radicals. It can be seen that the concentration of  $\cdot\text{OH}$  radicals increases with the pH until pH = 3.0 and thereafter decrease (Figure IV-B-17).

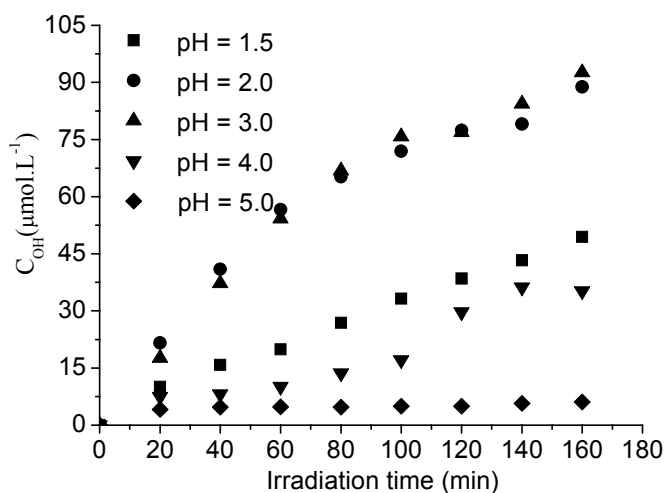
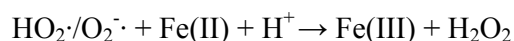


**Figure IV-B-17 Effect of initial pH value on the  $\cdot\text{OH}$  radicals yield**  
( $C_{\text{Fe(III)}} = 30.0 \text{ } \mu\text{mol.L}^{-1}$  and  $C_{\text{Tar}} = 60.0 \text{ } \mu\text{mol.L}^{-1}$ ).

Many studies have shown that the pH value has great effect on the photolysis of Fe(III)-carboxylate complexes in producing  $\text{H}_2\text{O}_2$  and degrading organic compounds.

i) The pH value could affect the efficiency the reaction of Fe(III)/Fe(II) and active intermediate  $\text{HO}_2\cdot/\text{O}_2\cdot^-$ .



ii) The pH could affect the decomposition of  $\text{H}_2\text{O}_2$ . It is known that the rate of decomposition of  $\text{H}_2\text{O}_2$  increases in the pH range from 0.0 to 3-3.2 (Gallard and De Laat, 2000). Moreover, Fenton reaction is believed to be acidic favorable and more  $\cdot\text{OH}$  radicals is generated in the system.

On the other hand, pH influence the distribution of Fe(III) species in the aqueous solutions. We computed the speciation of Fe(III) by Visual MINTEQ computer



program in the condition with  $10.0 \mu\text{mol.L}^{-1}$  of Fe(III) and  $30.0 \mu\text{mol.L}^{-1}$  of Tar. The concentrations of both Fe(III) and Tar are very low, so the ionic strength is nearly zero. Calculations were done at  $25^\circ\text{C}$ . Results showed that Fe(III)-Tar was the predominant species when pH value ranged from 2.5 to 4.0 (see Figure IV-B-18).  $\text{Fe}(\text{OH})^{2+}$  was another kind of photoactive species in the system. Ivan P. Pozdnyakov et al (2000) have investigated the mechanisms of  $\cdot\text{OH}$  radicals formation upon the excitation of  $[\text{Fe}(\text{OH})^{2+}]^*$  complex. But for pH below 2.0,  $\text{Fe}^{3+}$  became the major species which is not photoactive at the wavelength used in this work. From pH 4.5-6.0,  $\text{Fe}(\text{OH})_2^+$  gradually become the major species which as a quantum yield of OH radicals similar to that obtained with  $\text{Fe}(\text{OH})^{2+}$ . So we considered that Fe(III)-Tar was the major photoactive species in the system between pH 2.5 to 4.0.

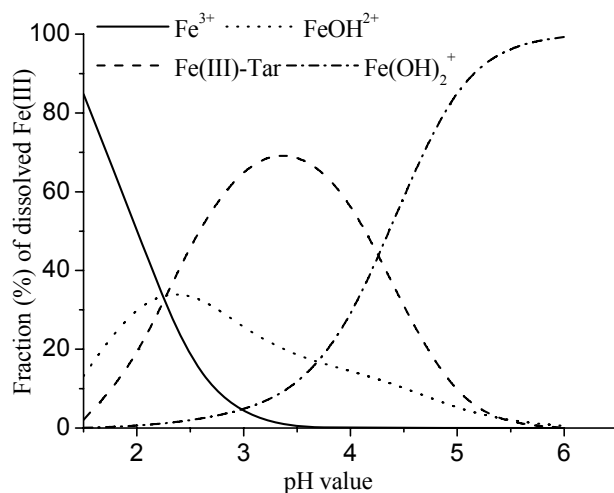


**Figure IV-B-18 Distribution of iron and Tartrate species as a function of pH in a system with  $C_{\text{Fe(III)}} = 10.0 \mu\text{mol.L}^{-1}$  and  $C_{\text{Tar}} = 30.0 \mu\text{mol.L}^{-1}$ . Ionic strength= 0. Calculations were done at  $25^\circ\text{C}$  with MINTEQ computer program.**

**B-3-3 Effect of tartaric acid concentration on the generation of hydroxyl radicals in the irradiated aqueous solution containing Fe(III)-Tar complexes**

For the effect of concentration, we chose pH 3.0 as the initial pH value of the aqueous solutions. The concentrations ratio of Fe(III) to tartaric acid was another important factor. Further experiments to study its effects were all carried out at pH 3.0.

In the Fe(III)-Tar system, reactions were carried out with the relative ratio of Fe(III) to Tar from about 1/3 to 1/12. Results are shown in Figure IV-B-19. The  $\cdot\text{OH}$  concentration generated in the system increased with increasing tartaric acid concentration. But when a certain ratio is reached (1/9), the  $\cdot\text{OH}$  concentration decrease when tartaric acid concentration increase. When tartaric acid concentration is much higher than that of Fe(III), tartaric acid become the major component in the system. We computed the speciation of tartaric acid by Visual MINTEQ computer program, results showed that  $\text{H}_2\text{Tar}$  and  $\text{HTar}^-$  instead of Fe(III)-Tar complexes were the major species in the system. So competition exists in the system, and only a part of  $\cdot\text{OH}$  can be trapped by benzene.

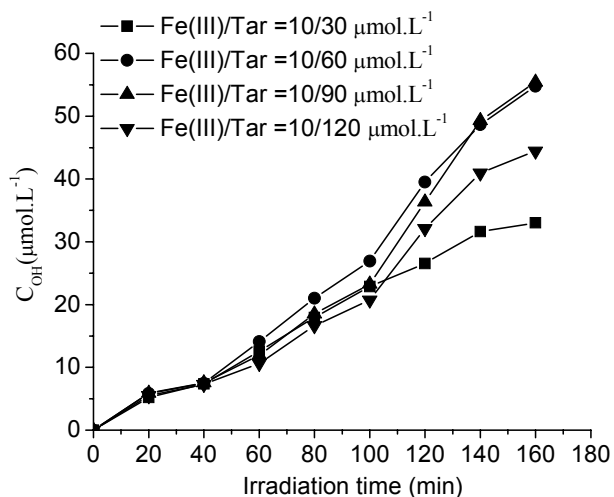


Figure IV-B-19 Effects of tartaric acid concentration on the  $\cdot\text{OH}$  radicals concentration. The initial pH value of the aqueous solution was 3.0.

**B-3-4 Effect of Fe(III) concentration on the generation of hydroxyl radicals in the irradiated aqueous solution containing Fe(III)-Tar complexes**

Fe(III) species in aqueous solution are considered to have a beneficial effect on the photogeneration of  $\cdot\text{OH}$  radicals in a continuous cycle Fe(III)/ Fe(II)/ Fe(III). The quantum yield of  $\cdot\text{OH}$  radicals is increased with increasing the initial Fe(III) concentration. Data in Figure IV-B-20 show that Fe(III) plays an important role in the

photochemical reaction. At pH between 2~5, tartaric acid can form complexes with Fe(III) in the conventional manner. When Fe(III) concentration is much higher than that of tartaric acid, Fe(III) becomes the major component in aqueous solution. It participates to the so-called photo-Fenton reaction through this photochemical reaction  $\text{Fe(III)} + \text{H}_2\text{O} + h\nu \rightarrow \text{Fe(II)} + \cdot\text{OH} + \text{H}^+$ .

$\text{Fe(OH)}^{2+}$  is considered to be the most predominant photo-active monomeric Fe(III)-hydroxy complex in the pH range 2.5 to 5.0. Irradiation of these complexes can lead to  $\cdot\text{OH}$  radicals formation.

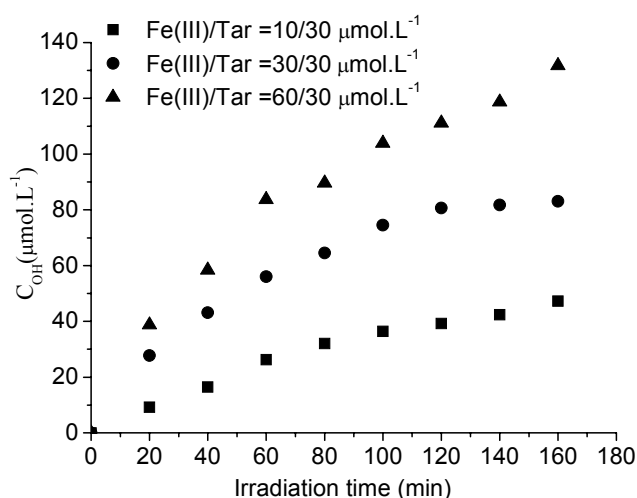


**Figure IV-B-20 Effect of the Fe(III) concentration on the  $\cdot\text{OH}$  radicals formation. The initial pH value of the aqueous solution was 3.0.**

**B-3-5 Effect of temperature on the generation of hydroxyl radicals in the irradiated aqueous solution containing Fe(III)-Tar complexes**

Finally, we also did experiments under the conditions without cooling water. Results are shown in Figure IV-B-21. Temperature could affect the generation of  $\cdot\text{OH}$  radicals. Without cooling water, the reaction temperature was about 328 K, which was higher than that with cooling water. The concentration of  $\cdot\text{OH}$  radicals at 328 K was nearly twice than at 298 K. Temperature effect mainly results from (1) some of the steps involved in the photochemical reaction process can be affected by the temperature; and

(2) with the increasing of the temperature, the average molecular kinetic energy will be increased. Reaction rate could be effectively enhanced at higher temperature. Although higher temperature can enhance the main reactions, it can also improve the subsidiary reactions. So temperature has great effect on the reaction and the following experiments were all carried out at room temperature.

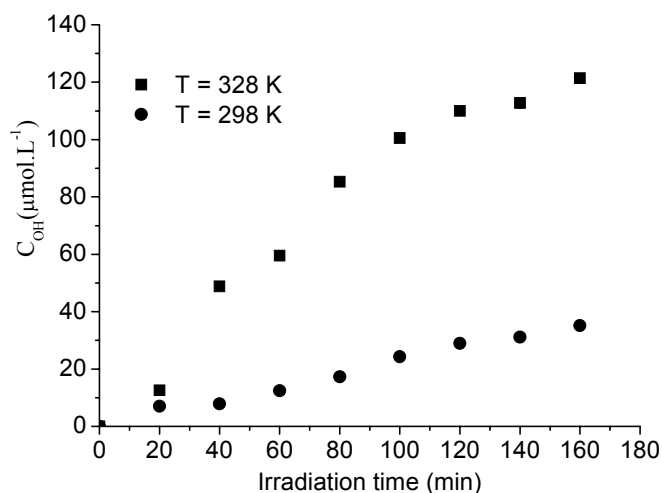


**Figure IV-B-21 Effect of temperature on the  $\cdot\text{OH}$  radicals concentration ( $C_{\text{Fe(III)}} = 10.0 \mu\text{mol.L}^{-1}$ , and  $C_{\text{Tar}} = 30.0 \mu\text{mol.L}^{-1}$ ). The initial pH value of the aqueous solution was 3.0. (a) Without cooling water the temperature is about 328 K, (b) with cooling water the temperature is about 298 K.**

## **Conclusions**

In the present study, formation of phenol from benzene was used to determine the concentration of  $\cdot\text{OH}$  radicals by the photolysis of Fe(III)-Carboxylate complexes, including Fe-Tar, Fe-Cit and Fe-Pyr complexes. Parameters, such as pH, the concentration of Fe(III), of acids, oxygen and temperature were all considered in the study. Results confirmed that the pH value has great effect on the photolysis of Fe(III)-Carboxylate complexes in producing  $\cdot\text{OH}$ . The maximum concentration of  $\cdot\text{OH}$  radicals were observed at pH 3.0 (pH ranged from 1.5 to 7.0) in all systems.

The  $\cdot\text{OH}$  concentration generated in the system increased also with the increase of Fe(III) or acids concentrations. This effect was systematically observed with Fe(III) whatever the complex. However, for the concentration of acids the increase of OH radicals concentration is observed for pyruvic and citric acid until the ratio 1:12 but for tartaric acid a decrease is observed for the ratio 1:12. The presence of high concentration of acid strongly favored the reoxidation of Fe(II) after the first photoredox process in the complex. This step (reoxidation of Fe(II)) is a limiting step in the photocatalytic process based on the couple Fe(III)/Fe(III) (Poulain et al., 2003). The fact in the case of tartaric acid the concentration of OH radicals decreases when the acid concentration increases can be surprising. In this particular case a competition for the reactivity of  $\cdot\text{OH}$  radical between benzene and organic compounds (tartaric acid or oxidized tartaric acid) can be put forward.

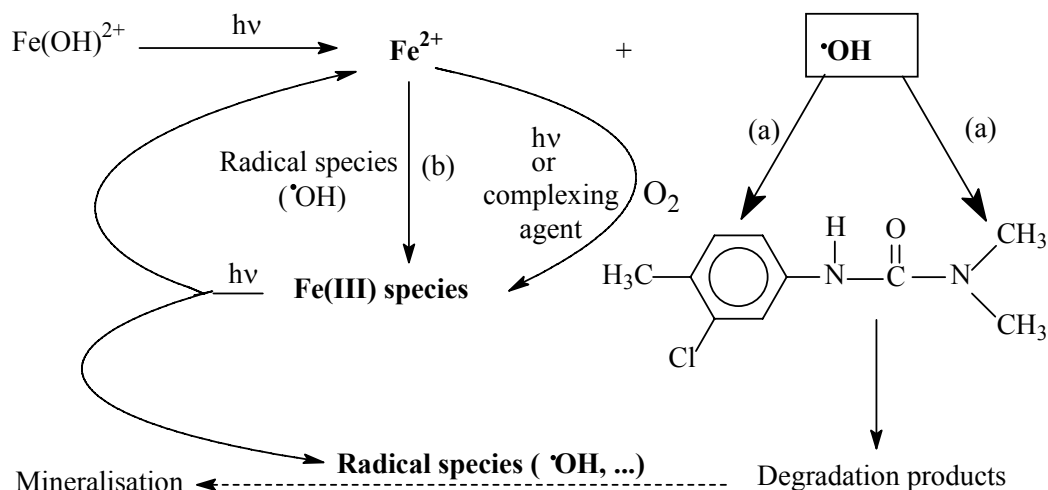


**Figure IV-B-22 Photochemical cycle Fe(III)/Fe(II) in the presence of organic pollutant (Chlortoluron), from Poulain et al, 2003.**

Oxygen is a crucial factor for the formation of active radicals in the aqueous solutions. Without oxygen no formation of  $\cdot\text{OH}$  radical is observed.

The yields of  $\cdot\text{OH}$  radicals at 328 K is much higher than at 298 K. Higher temperatures enhance the main and the side reactions of the process. So, all our experiments were carried under controlled temperature with cooling water.

Results show that the concentration of  $\cdot\text{OH}$  in the systems containing Fe(III)-Carboxylate complexes are higher than that of the system only containing Fe(III). It can be concluded that organic acids (Cit, Tar, Pyr) have positive effects on the photogeneration of  $\cdot\text{OH}$  in the aqueous solution. So, the Fe(III)-Carboxylate complexes have the potential of utilizing sunlight as an irradiation source. Especially in natural waters, which contain Fe(III)/Fe(II) and many kinds of organic acids. Photochemical reactions can be induced by sunlight, and it will play an important role in the oxidation of organic/inorganic pollutants in natural waters. Further experimental and theoretical work is needed to fully understand the system and its application in natural aquatic or atmospheric environments.

## IV-C Degradation of 2, 4-Dichlorophenol photoinduced by the Fe(III)-Carboxylate complexes

The compound 2,4-DCP (2,4-Dichlorophenol) is a key intermediate in the synthesis of the herbicide 2,4-D (2,4-dichlorophenoxyacetic acid). In this research, 2,4-DCP was used as a model and target compound to study the capacity of Fe(III)-Carboxylate complexes in the degradation of pollutants.

### C-1-Properties of 2,4-Dichlorophenol (2,4-DCP) aqueous solution

The UV-visible spectrum of the solution with  $0.1 \text{ mmol.L}^{-1}$  2,4-DCP is presented in Figure IV-C-1. It has two bands with maximum absorption at 226 and 284 nm. The molar absorption coefficients ( $\epsilon$ ) are  $6650 \text{ L.mol}^{-1}.\text{cm}^{-1}$  for 226 nm and  $2180 \text{ L.mol}^{-1}.\text{cm}^{-1}$  for 284 nm. The UV-visible spectrum of 2,4-DCP solutions according to the concentration are given in Figure IV-C-2.

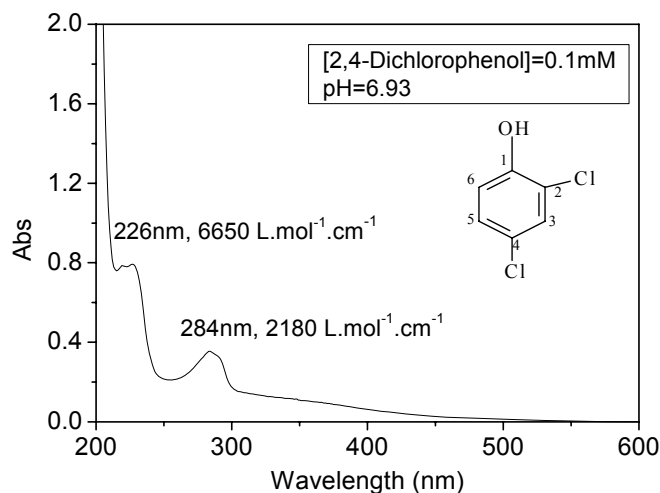
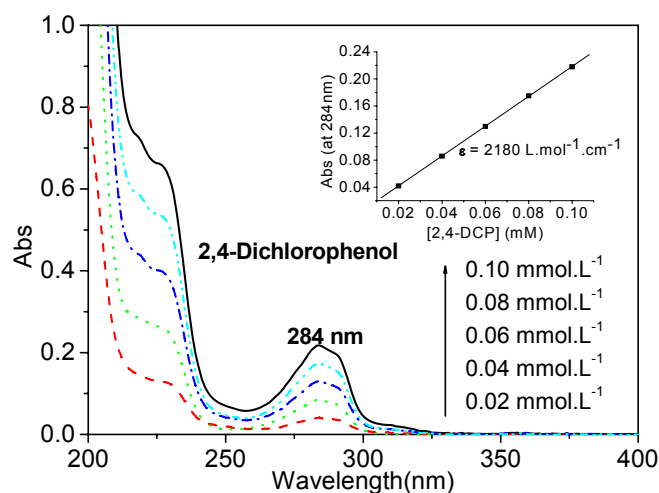


Figure IV-C-1 The UV-visible spectra of 2,4-Dichlorophenol.



**Figure IV-C-2** The UV-visible spectra of 2,4-Dichlorophenol at different concentrations.

The 2,4-DCP species in the aqueous solution usually changed as a function of pH value (Figure IV-C-3). At  $\text{pH} < 8.0$ , the main species is 2,4-DCP with maximum absorption at 284 nm. Figure IV-C-3 exhibits two bands with maximum absorption at 244 nm and 306 nm. However, the absorption of 2,4-DCP does not interfere with the main irradiation wavelength used in this work (365 nm). From the values in Figure IV-C-3, we obtain the Figure IV-C-4, which presents the absorbance at 244 nm as function of pH in aqueous solution. The  $\text{pK}_a$  of 2,4-DCP equal to 7.91 is confirmed by our curve. Figure IV-C-5 shows the protonation equilibrium between the two forms of 2,4-DCP in the aqueous solution.



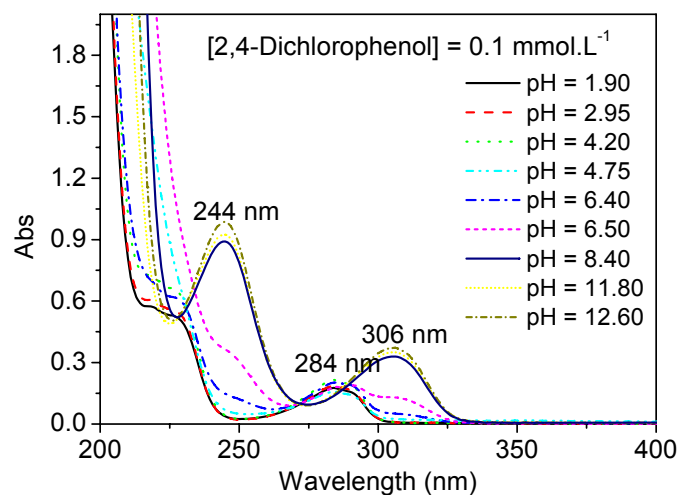


Figure IV-C-3 pH effect on the distribution of 2,4-Dichlorophenol species in aqueous solution.

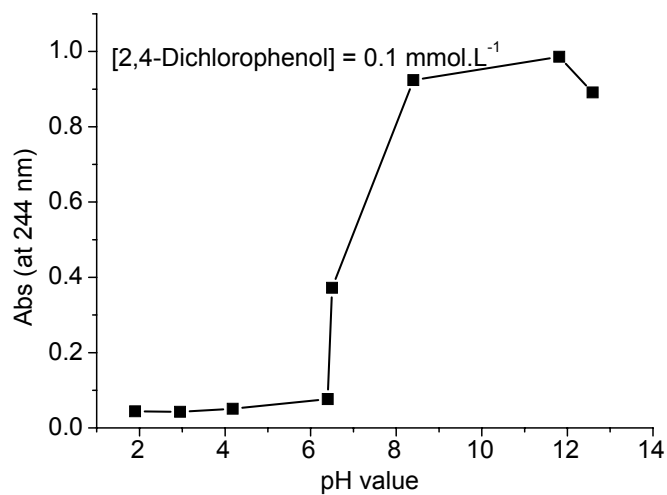


Figure IV-C-4 Absorbance at 244 nm as function of pH in aqueous solution with 0.1 mmol.L<sup>-1</sup> of 2,4-DCP

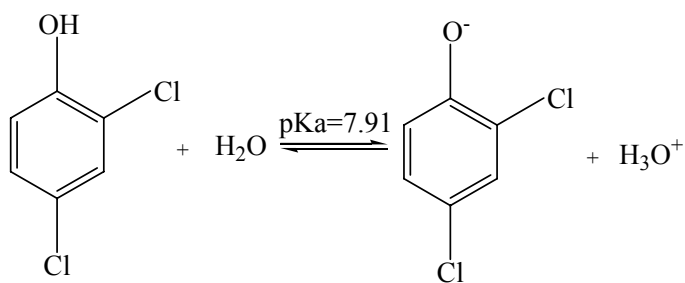


Figure IV-C-5 Protonation equilibrium of 2,4-DCP in the aqueous solution

## C-2-Photodegradation of 2,4-DCP induced by $\text{Fe}(\text{OH})^{2+}$

Experiments were first carried out to study the degradation of 2,4-DCP photoinduced by Fe(III) in aqueous solution. Before describing the photodegradation of 2,4-DCP, we present the physicochemical properties of Fe(III) in aqueous solutions.

### C-2-1 Properties of Fe(III) solutions

The absorption spectrum of an aqueous solution with  $0.3 \text{ mmol.L}^{-1} \text{ Fe}(\text{ClO}_4)_3$  as a function of time after preparation is shown in Figure IV-C-6. Freshly prepared solutions presents a maximum absorption at about 297 nm characteristic of the monohydroxy complex  $[\text{Fe}(\text{OH})(\text{H}_2\text{O})_5]^{2+}$  (also written as  $\text{Fe}(\text{OH})^{2+}$ ). Upon standing in the dark, the absorption spectrum gradually increased in intensity and shifted to longer wavelengths; this can be rationalized by assuming a gradual and irreversible conversion of monomeric iron species to oligomeric ones (Flynn, 1984).

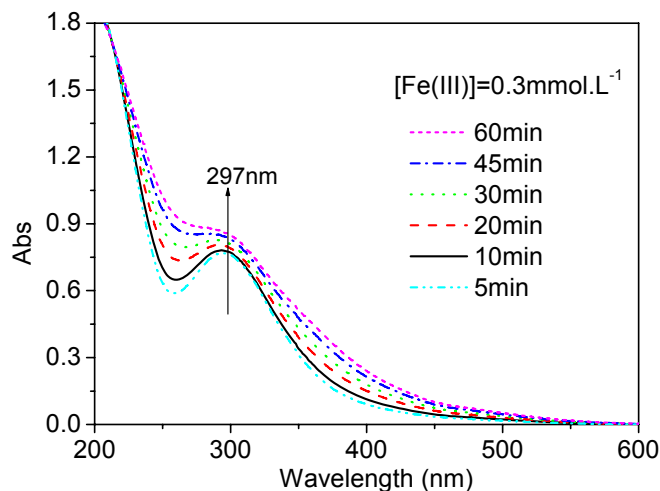


**Figure IV-C-6 UV-Visible absorption spectra of an aqueous solution of  $[\text{Fe}(\text{III})] = 0.3 \text{ mmol.L}^{-1}$  recorded at different time after the preparation.**

Since pH value plays an important role on the distribution of Fe(III) species in the

aqueous solutions, experiments to control this important effect were carried out in this work. The pH values of the aqueous solutions with  $0.3 \text{ mmol.L}^{-1}$  of  $\text{Fe}(\text{ClO}_4)_3$  were adjusted to 1.5, 2.5, 3.15, 4.3, 5.4, 6.8, 7.6 and 8.5. Figure IV-C-7 presents the variation of the UV-visible spectra as function of the pH value.  $\text{Fe}(\text{OH})^{2+}$  was the predominant species when pH value ranged from 2.5 to 4.0 (see Figure IV-C-7). Ivan P. Pozdnyakov et al (2000) have investigated the mechanisms of  $\cdot\text{OH}$  radicals formation upon the excitation of  $[\text{Fe}(\text{OH})^{2+}]$  complex. While at pH below 2.0,  $[\text{Fe}(\text{H}_2\text{O})_6]^{3+}$  become the major species. From pH 5.0 to 6.0,  $\text{Fe}(\text{OH})_2^+$  gradually become the major species but this species rapidly disappear with time. When pH is over 7.0,  $\text{Fe}(\text{OH})_3$  is formed in the aqueous solutions and precipitate.

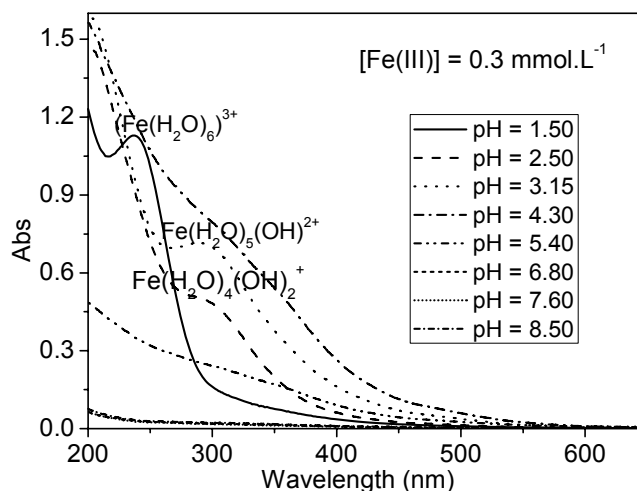


**Figure IV-C-7 pH effect on the distribution of Fe(III) species in aqueous solutions.**

### **C-2-2 Properties of Fe(III)/2,4-DCP solutions**

Experiments were performed to study UV-visible spectrum of different aqueous solutions: a)  $0.1 \text{ mmol.L}^{-1}$  Fe(III); b)  $0.1 \text{ mmol.L}^{-1}$  2,4-DCP; c) mixture of  $0.1 \text{ mmol.L}^{-1}$  Fe(III) and  $0.1 \text{ mmol.L}^{-1}$  2,4-DCP. Figure IV-C-8 shows the spectrum of the solution 3 min after the preparation.

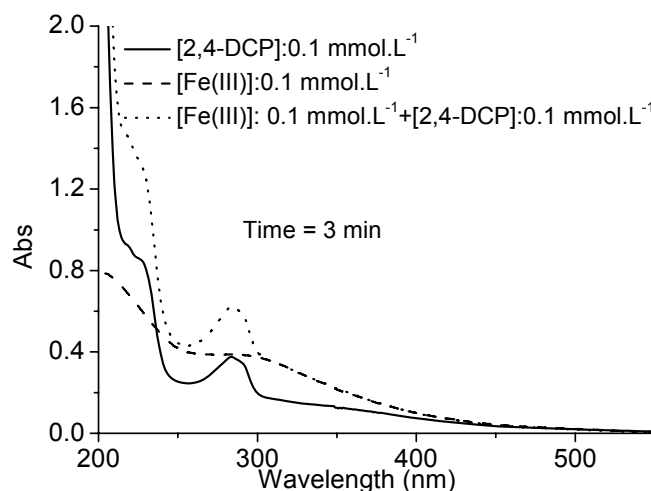


**Figure IV-C-8 UV-Visible absorption spectra of aqueous solution after 3 min preparation with  $0.1 \text{ mmol.L}^{-1}$  Fe(III) and  $0.1 \text{ mmol.L}^{-1}$  2,4-DCP.**

Figure IV-C-9 shows spectra of an aqueous solution with  $0.1 \text{ mmol.L}^{-1}$  of Fe(III) and  $0.3 \text{ mmol.L}^{-1}$  of 2,4-DCP recorded at different time of ageing of the solution. The absorption spectrum gradually increased in intensity and this can be rationalized by assuming a gradual and irreversible conversion of monomeric Fe(III) species to oligomeric ones. But no overall changes in the absorption spectrum of 2,4-DCP with a peak at  $\lambda = 284 \text{ nm}$  were observed since no complex formation between Fe(III) and 2,4-DCP occurs. Since  $\text{Fe}(\text{OH})^{2+}$  was thought to be the main monomeric species in the Fe(III) solutions, determination was carried out in two different aqueous solutions, with  $0.3 \text{ mmol.L}^{-1}$  of Fe(III) and with or without  $0.1 \text{ mmol.L}^{-1}$  of 2,4-DCP. Figure IV-C-10 presents the results. There is no significant impact of the presence of 2,4DCP on the evolution of the  $\text{Fe}(\text{OH})^{2+}$  concentration. It also indicated that there is no interference of 2,4-DCP on the distribution of iron species in the aqueous solutions. This experiment show again that there is no complex formation between 2,4-DCP and the different Fe(III) species.

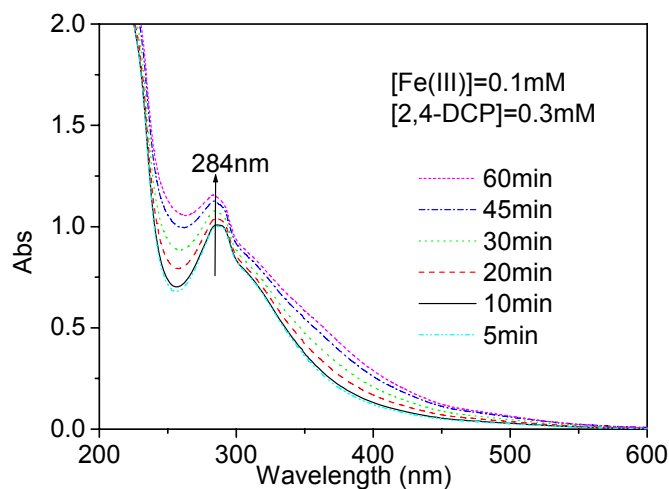


**Figure IV-C-9** UV-Visible absorption spectra of an aqueous solution with  $0.1 \text{ mmol.L}^{-1}$  of Fe(III) and  $0.3 \text{ mmol.L}^{-1}$  of 2,4-DCP recorded at different time after the preparation.

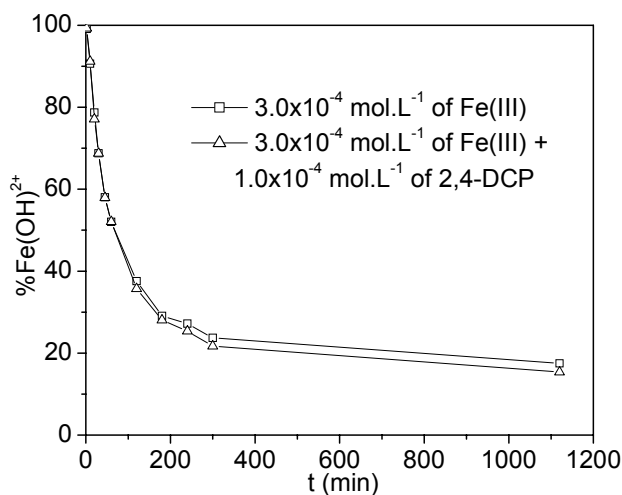


**Figure IV-C-10** Determination of  $\text{Fe(OH)}^{2+}$  species in different solutions as function of time.  $T = 22^\circ\text{C}$ .

### C-2-3 Degradation of 2,4-DCP photoinduced by Fe(III)

Irradiation experiments were performed in aqueous solutions with  $0.1 \text{ mmol.L}^{-1}$  of 2,4-DCP under 365 nm. Two concentrations of Fe(III) ( $0.3 \text{ mmol.L}^{-1}$  and  $0.21 \text{ mmol.L}^{-1}$ ) were studied in this work. Figure IV-C-11 shows the variation of the

UV-visible spectra of the solution before and after 240 min of irradiation. The absorbance of solution, especially at 284 nm, was apparently decreased after 240min irradiation. As shown in Figure IV-C-12, the concentration of 2,4-DCP was evidently decreased at two different reaction conditions and it was totally photodegraded after 300min irradiation. Better results were obtained with higher Fe(III) concentration.

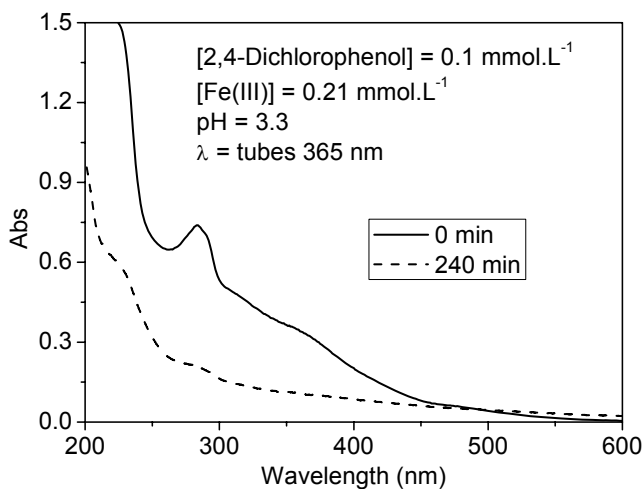


Figure IV-C-11 Variation of the UV-visible spectra of the reaction solutions as a function of the irradiation time. [Fe(III)] = 0.21 mmol.L<sup>-1</sup>, initial pH value is 3.3.

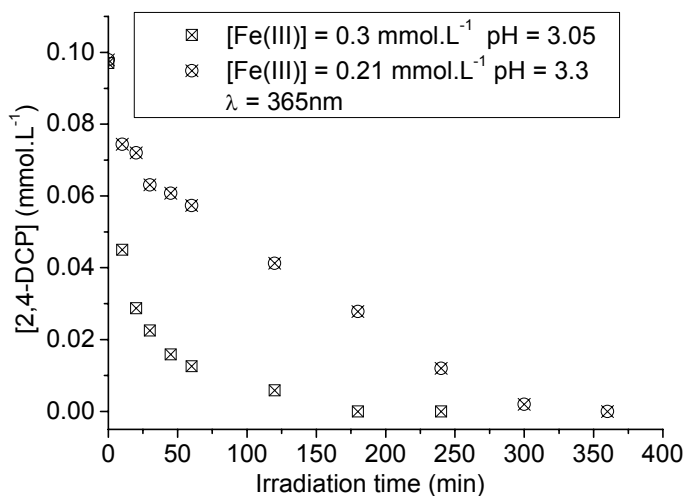


Figure IV-C-12 Photodegradation of 2,4-DCP in the aqueous solutions with Fe(ClO<sub>4</sub>)<sub>3</sub>.

The important difference observed at the beginning of the irradiation, between

the two concentrations of iron, can be surprising. But both the difference of pH and of the iron concentration can explain this phenomenon.

#### **C-2-4 Quantum yields of Fe(II) and 2,4-DCP in the Fe(III) solution ( $\lambda_{\text{irr}} = 365\text{nm}$ )**

Quantum yields of Fe(II) generation were studied in the aqueous solution with  $0.3 \text{ mmol.L}^{-1}$  of Fe(III) perchlorate at pH 3.0. Monochromatic irradiation experiments were carried out under 365 nm. The initial quantum yield of Fe(II) was calculated by taking 2 ml of the solution during irradiation at intervals of 1 min. The concentration of Fe(II) was determined by complexometry with *ortho*-phenanthroline (at conversion  $< 10\%$ ). The quantum yield  $\Phi_{\text{Fe(II)}}$  was 0.027.

Irradiation of 2,4-DCP was also carried under 365 nm in the aqueous solution with  $0.1 \text{ mmol.L}^{-1}$  of 2,4-DCP at pH 3.0 and in the absence of Fe(III). Quantum yield of 2,4-DCP ( $\Phi_{2,4\text{-DCP}}$ ) disappearance was equal to zero in the absence of Fe(III) after 10 min of irradiation. Because the absorbance of 2,4-DCP is negligible at 365 nm, so there is no direct photodegradation of 2,4-DCP at that wavelength.

The solution with  $0.3 \text{ mmol.L}^{-1}$  of Fe(III) and  $0.1 \text{ mmol.L}^{-1}$  of 2,4-DCP was irradiated at 365nm. Measurements were carried out to study the formation of Fe(II) and the degradation of 2,4-DCP. The results were  $\Phi_{\text{Fe(II)}} = 0.046$  and  $\Phi_{2,4\text{-DCP}} = 0.050$ , which were higher than the two cases listed above. It can be concluded that Fe(III) could induce the photolysis of 2,4-DCP, simultaneously 2,4-DCP could enhance the conversion of Fe(III) to Fe(II). The dark reaction was carried out in parallel, but no formation of Fe(II) and no degradation of 2,4-DCP were observed. The reaction could not occur without irradiation.

#### **C-3-Degradation of 2,4-DCP induced by the photolysis of Fe(III)-Carboxylate complexes**

Degradation of 2,4-DCP photoinduced by Fe(III)-Carboxylate complexes was studied in this work. Irradiation experiments were carried out separately under monochromatic irradiation for short times and under irradiation in the photoreactor (emission centred at 365 nm) for long times. Parameters affecting the photoreaction, such as irradiation wavelength, pH, oxygen, concentrations of Fe(III)-Carboxylate complexes and 2,4-DCP, were all studied in the experiments.

### **C-3-1 Quantum yields of 2, 4-DCP degradation and Fe(II) formation**

The reaction times were well controlled to make sure that all the degradation of reagents and the generation of products not exceed 10%. This condition permits to determine the number of photons absorbed in the initial reaction period. Therefore, the quantum yields of 2, 4-DCP degradation ( $\Phi_{2,4\text{-DCP}}$ ) and Fe(II) generation ( $\Phi_{\text{Fe(II)}}$ ) were calculated with an error less than 5%. Parameters that may influence the reaction were all studied.

#### **C-3-1-1 Influence of the irradiation wavelength on the quantum yields of Fe(II) and 2,4-DCP in different Fe(III)-Carboxylate complexes systems**

Quantum yields of Fe(II) generation was studied in the aqueous solutions with different Fe(III)-Carboxylate complexes, which were Fe(III)-LTar, Fe(III)-DTar, Fe(III)-Pyr and Fe(III)-Cit complexes. All of the experiments were carried out at pH 3.0. The monochromatic irradiation was separately carried out at 296, 313 and 365 nm. Table IV-C-1 presents the results. With the increase of wavelength, the quantum yields of Fe(II) was obviously decreased. This phenomenon can be explained by the well established result that the excess of energy at shorter wavelength favors the photoredox process. The quantum yields of Fe(II) generation are higher in the presence of 0.3 mmol.L<sup>-1</sup> of Fe(III)-Carboxylate complexes than in the condition just



with 0.3 mmol.L<sup>-1</sup> of Fe(III). It can be concluded that the carboxylic acid as a ligand can enhance the photo-reduction of Fe(III) to Fe(II) when compared to water molecule. The  $\Phi_{\text{Fe(II)}}$  generation was almost the same in the presence of two different Fe(III)-Tar complexes. Moreover, Fe(III)-D-Tar and Fe(III)-L-Tar complexes have almost the same ability to photoinduced the degradation of pollutants in the solutions.

Experiments also studied the quantum yields of Fe(II) and 2,4-DCP in the aqueous solutions with 0.1 mmol.L<sup>-1</sup> of 2,4-DCP and 0.3 mmol.L<sup>-1</sup> of Fe(III)-Carboxylate complexes. Results are presented in Table IV-C-1. The wavelength has a strong effect on the quantum yields.  $\Phi_{\text{Fe(II)}}$  and  $\Phi_{2,4\text{-DCP}}$  increased with the decrease of wavelength in different reaction systems. However quantum yields of Fe(II) formation and 2,4-DCP degradation for different Fe(III) complexes have a opposite tendency. For the  $\Phi_{\text{Fe(II)}}$ , the tendency is Fe(III)-Pyr > Fe(III)-Cit > Fe(III)-Tar > Fe(OH)<sup>2+</sup>, and for the  $\Phi_{2,4\text{-DCP}}$ , the tendency is Fe(III)-Pyr~Fe(OH)<sup>2+</sup> > Fe(III)-Cit > Fe(III)-Tar. In the presence of ligands and pollutant,  $\Phi_{\text{Fe(II)}}$  are higher because Fe(II) formed is less reoxidized, and radical species attack the pollutant as well. But the lower  $\Phi_{2,4\text{-DCP}}$  is because of the competition between organic substrates, less radicals are available for the 2,4-DCP degradation.

**Table IV-C-1 Quantum yields of Fe(II) and 2,4-DCP as a function of wavelength in different systems.**

$\lambda$ , nm	$I_0, 10^{14}$ photons·s <sup>-1</sup> . cm <sup>-2</sup>	<sup>a)</sup> $\Phi_{\text{Fe(II)}}$ $\Delta t=60\text{s}$	<sup>b)</sup> $\Phi_{\text{Fe(II)}}$ $\Delta t=60\text{s}$	$\Phi_{2,4\text{-DCP}}$ $\Delta t=15\text{min}$
(a)[Fe(III)] = 0.3 mmol.L <sup>-1</sup> , pH = 3.0				
296	4.39	0.021	0.072	0.089
313	7.46	0.016	0.043	0.052
365	13.7	0.027	0.046	0.014
(b)[Fe(III)-Pyr] = 0.3 mmol.L <sup>-1</sup> ; 0.9 mmol.L <sup>-1</sup> , pH = 3.0				
296	4.39	0.33	0.36	0.090
313	7.46	0.25	0.31	0.039
365	13.7	0.21	0.31	0.027
(c)[Fe(III)-Dtar] = 0.3 mmol.L <sup>-1</sup> ; 0.6 mmol.L <sup>-1</sup> , pH = 3.0				
296	4.39	0.31	0.40	0.020
313	7.46	0.24	0.29	0.010
365	13.7	0.14	0.23	0.014

(d)[Fe(III)-LTar] = 0.3 mmol.L <sup>-1</sup> : 0.6 mmol.L <sup>-1</sup> , pH = 3.0				
296	4.39	0.32	0.39	0.033
313	7.46	0.25	0.28	0.013
365	13.7	0.14	0.22	0.009
(e)[Fe(III)-Cit] = 0.3 mmol.L <sup>-1</sup> , pH = 3.0				
296	4.39	0.23	0.26	0.066
313	7.46	0.16	0.19	0.022
365	13.7	0.25	0.27	0.019

a) without 2,4-DCP

b) with 0.1 mmol.L<sup>-1</sup> of 2,4-DCP

$I_0$  is the number of the photons entering the cell per second.

*For the quantum yield the experimental error was estimated to 10%.*

**C-3-1-2 Effect of oxygen on the quantum yields of Fe(II) and 2,4-DCP in different reaction systems ( $\lambda_{irr}= 365nm$ )**

Oxygen generally is an important parameter in the photochemical process. Experiments were carried out to study the oxygen effects on the quantum yield of Fe(II) formation and on the quantum yield of 2,4-DCP degradation. Different gas were used by bubbling oxygen or argon 10 min into the solutions before irradiation. Fe(III)-LTar, Fe(III)-DTar, Fe(III)-Pyr and Fe(III)-Cit complexes were all studied in the experiments. All the experiments were carried out at pH 3.0 with monochromatic irradiation at 365 nm. Results are shown in Table IV-C-2. In the deoxygenated solution, the quantum yield of 2,4-DCP was near zero whatever the nature of the investigated carboxylate. The quantum yields of Fe(II) were also very low compared to that in the presence of oxygen. It can be concluded that oxygen plays a very important role in the reaction process.

Oxygen can enhance the photolysis of Fe(III)-Carboxylate complexes by trapping the electron on the carbon centered radical formed after the photoredox process. Then the formed  $O_2^{\bullet -}$  radicals rapidly react to finally leads to the formation of hydroxyl radical. This radical is the major radical responsible of the the pollutant (2,4-DCP) degradation. In the absence of oxygen, less reactive species are formed in the reaction, thus oxygen is quite necessary to rproduce the reactive species that cause

2,4-DCP degradation. In these experiments, the quantum yield of 2,4-DCP degradation was higher in the presence of Fe(III)-Pyr than with other complexes.

**Table IV-C-2 Oxygen effect on the quantum yields of Fe(II) and 2,4-DCP. In the aqueous solutions with 0.1 mmol.L<sup>-1</sup> 2,4-DCP and the initial pH value was 3.0. ( $\lambda_{irr}$ =365nm)**

Different reaction systems  Concentration in mmol.L <sup>-1</sup>	$\Phi_{Fe(II)}$			$\Phi_{2,4-DCP}$		
	Deaerated solution	Aerated solution	Oxygen saturated solution	Deaerated solution	Aerated solution	Oxygen saturated solution
[Fe(III)-Pyr] = 0.3:0.9	0.040	0.31	0.53	0.001	0.028	0.096
[Fe(III)-LTar] = 0.3:0.6	0.083	0.22	0.23	0.003	0.010	0.019
[Fe(III)-DTar] = 0.3:0.6	0.086	0.23	0.25	0.003	0.014	0.018
[Fe(III)-Cit]=0.3 (commercial product)	0.093	0.27	0.30	0.003	0.019	0.032

**C-3-1-3 Effect of pH on the quantum yields of Fe(II) and 2,4-DCP in different reaction systems ( $\lambda_{irr}$ = 365 nm)**

The pH value was another very important parameter in the photochemical reaction. Experiments were carried out to study the pH effect on the quantum yields of Fe(II) formation and 2,4-DCP degradation. All of the reactions were carried out under monochromatic irradiation at 365nm. During the experiments, the Fe(III)-Carboxylate complex concentration was kept constant as shown in Figure IV-C-13-a, and the concentration of 2,4-DCP was 0.1 mmol.L<sup>-1</sup>. The pH value of the reaction solutions were changed and adjusted to the desired value. Results about the quantum yields of Fe(II) formation are presented in Figure IV-C-13-a and Figure IV-C-13-b. In these cases, the highest quantum yields of Fe(II) were obtained at pH 3.0. Many references indicated that the photoactive species Fe(OH)<sup>2+</sup> was the main species at pH 3.0. pH could affect the reactions in the aqueous solutions, as following,

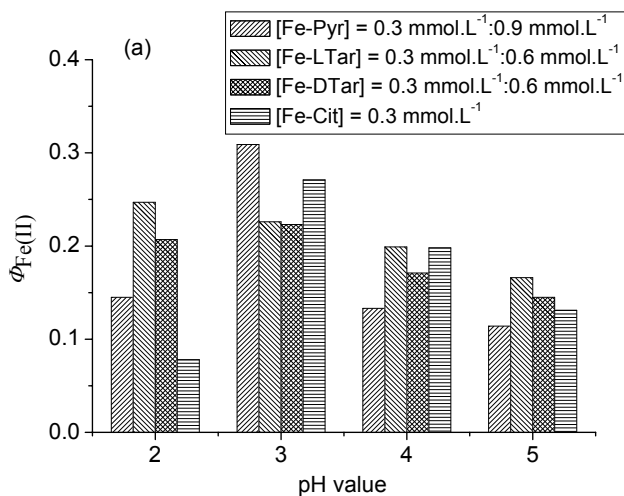
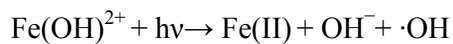
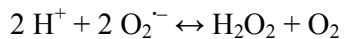
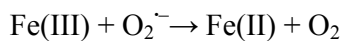
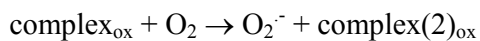
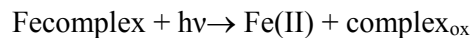


**Figure IV-C-13-a pH effect on the quantum yields of Fe(II). In the aqueous solutions with 0.1 mmol.L<sup>-1</sup> 2,4-DCP. ( $\lambda_{\text{irr}} = 365 \text{ nm}$ )**

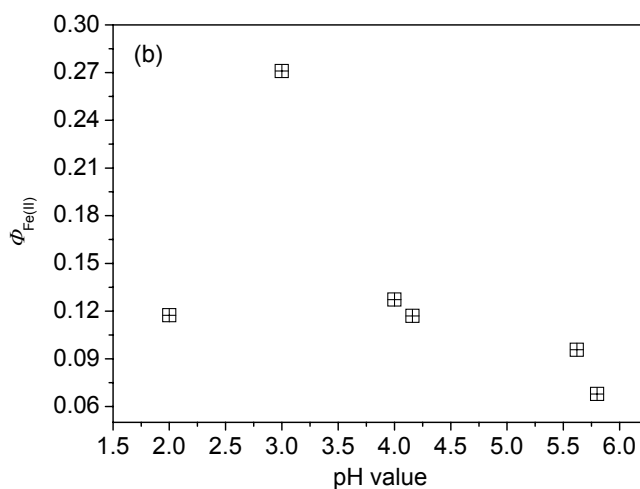


**Figure IV-C-13-b pH effect on the quantum yields of Fe(II). In the aqueous solutions with 0.3 mmol.L<sup>-1</sup> of Fe(III)-Cit and 0.1 mmol.L<sup>-1</sup> of 2,4-DCP. ( $\lambda_{\text{irr}} = 365 \text{ nm}$ )**

The pH effect on the quantum yields of 2,4-DCP degradation was also studied. In order to simulate the early stages of the reaction, irradiation period was 10 min to make sure that the degradation rate of 2,4-DCP was less than 10%. Results are shown in Table IV-C-3. The quantum yields of 2,4-DCP disappearance at different pH's showed similar phenomenon, that  $\Phi_{2,4\text{-DCP}}$  was decreased with the increase of the pH value. It can be concluded that acidic condition is more effective for the pollutant degradation in the presence of Fe(III)-carboxylate complexes. The quantum yields of 2,4-DCP degradation was optimal at pH 2.0 for Fe(III)-Tar and Fe(III)-Cit complexes, and at pH 3.0 for Fe(III)-Pyr complexes. In all cases, the quantum yields of 2,4-DCP degradation is negligible at pH 5.0.

**Table IV-C-3 pH effects on the quantum yields of 2,4-DCP, with 0.1 mmol.L<sup>-1</sup> of 2,4-DCP. ( $\lambda_{\text{irr}} = 365\text{nm}$ )**

pH	$\Phi_{2,4\text{-DCP}}$
(a) [Fe(III)-Pyr] = 0.3 mmol.L <sup>-1</sup> : 0.9 mmol.L <sup>-1</sup> *	
2.0	0.026
3.0	0.028
4.0	0.004
5.0	0.002
(b) [Fe(III)-LTar] = 0.3 mmol.L <sup>-1</sup> :0.6 mmol.L <sup>-1</sup> *	
2.0	0.026
3.0	0.010
4.1	0.005
5.8	0.005
(c) [Fe(III)-DTar] = 0.3 mmol.L <sup>-1</sup> :0.6 mmol.L <sup>-1</sup> *	
2.0	0.024
3.0	0.014
4.0	0.004
5.6	0.004
(d) [Fe(III)-Cit] = 0.3 mmol.L <sup>-1</sup> *	
2.0	0.021
3.0	0.019
4.2	0.015
5.6	0.011
5.8	0.009

*\*The ratio Fe(III)/Ligand in the iron carboxylate complexes are 1/3, 1/2, 1/2, 1/1 for pyruvic, tartaric L and D and citric acids respectively.*

**C-3-1-4 Effect of complexes concentration on the quantum yields of Fe(II) and 2,4-DCP in different reaction systems ( $\lambda_{irr} = 365 \text{ nm}$ )**

The effects of the Fe(III)-Carboxylate complexes concentration on the quantum yields of Fe(II) and 2,4-DCP were studied at pH 3.0 with monochromatic irradiation (365nm). Fe(III)-Pyr, Fe(III)-Tar and Fe(III)-Cit complexes were all studied. Results are presented in the following Table IV-C-4.

The quantum yields of Fe(II) generation was strongly influenced by the concentration of Fe(III)-Carboxylate complexes. When the concentration of complexes increases, the quantum yield of  $\Phi_{\text{Fe(II)}}$  increases too. In these cases, the  $\Phi_{2,4\text{-DCP}}$  was also increased when the complexes concentration increased. However, this effect is less pronounced than for quantum yield of Fe(II). For example it is important to note that the quantum yields of 2,4-DCP at low Fe(III)-LTar concentration was almost the same than at 10 times higher Fe(III)-LTar complex concentration. This phenomenon can be explained by a competition between 2,4-DCP and the organic part of the complex for the reactivity of the formed hydroxyl radical. At higher Fe(III)-complex concentration this competition could be not negligible and has a negative effect on the 2,4-DCP degradation.

**Table IV-C-4 Effects of Fe(III)-Carboxylate complexes concentration on the quantum yields of Fe(II) and 2,4-DCP. The initial pH value was 3.0. ( $\lambda_{irr} = 365 \text{ nm}$ )**

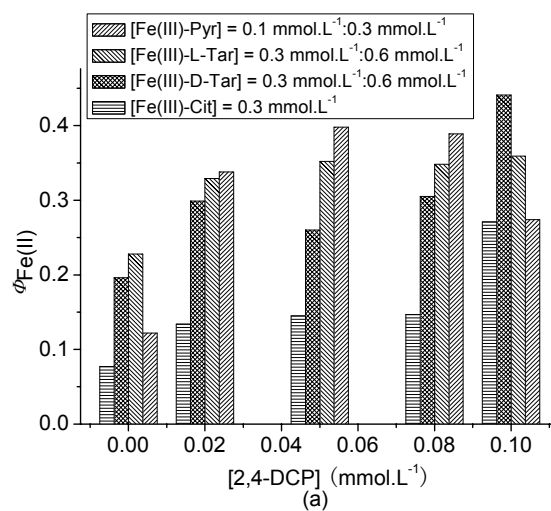
Different conditions	$\Phi_{\text{Fe(II)}}$	$\Phi_{2,4\text{-DCP}}$
[Fe(III)-LTar] (mmol.L <sup>-1</sup> )		
0.01:0.02	0.13	0.011
0.02:0.04	0.18	0.014
0.10:0.20	0.18	0.013
0.30:0.60	0.23	0.010
[Fe(III)-DTar] (mmol.L <sup>-1</sup> )		
0.10:0.20	0.17	0.010
0.30:0.60	0.22	0.014
[Fe(III)-Cit] (mmol.L <sup>-1</sup> )		
0.10	0.088	0.004

0.20	0.12	0.018
0.30	0.27	0.019
<hr/>		
[Fe(III)-Pyr] (mmol.L <sup>-1</sup> )		
0.1: 0.3	0.27	0.021
0.3: 0.9	0.31	0.028

**C-3-1-5 Effect of 2,4-DCP concentration on the quantum yields of Fe(II) and 2,4-DCP in different reaction systems ( $\lambda_{irr} = 365\text{nm}$ )**

2,4-DCP is used as a model compound in this work, so we studied its effects on the reaction. Monochromatic irradiation was 365 nm. The solutions were adjusted to pH 3.0 with constant Fe(III)-Carboxylate complexes concentration. The concentration of 2,4-DCP are 0, 0.02, 0.05, 0.08 and 0.10 mmol.L<sup>-1</sup>. Results are presented in Figure IV-C-14. The presence of 2,4-DCP obviously enhanced the quantum yields of Fe(II) formation in all the complex systems. As shown in Figure IV-C-14 (a), with the increase of 2,4-DCP concentration,  $\Phi_{\text{Fe(II)}}$  increases. Photolysis of Fe(III)-Carboxylate complexes can form Fe(II) and generate reactive species, which quickly react with the pollutant, thus, the reaction will continue in the way that Fe(III) is reduced to Fe(II).

As evidenced by the values in Figure IV-C-14 (b), the quantum yields of 2,4-DCP disappearance increases with the increase of the 2,4-DCP concentration in all cases. High concentration of 2,4-DCP can increase the probability of reaction with the radical species photogenerated in the solutions.



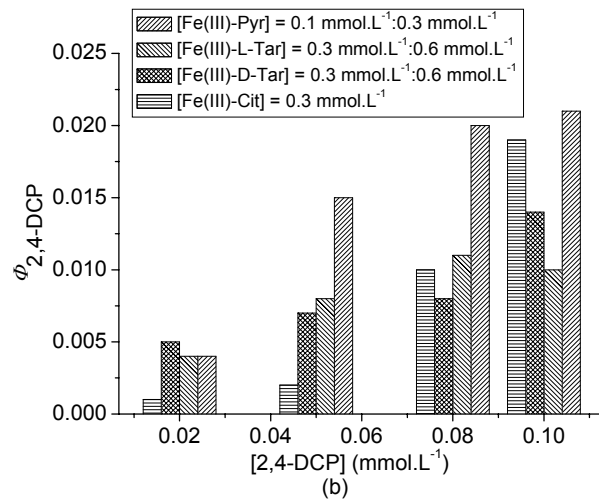


Figure IV-C-14 Effects of 2,4-DCP concentration on the quantum yields of Fe(II) and 2,4-DCP. The initial pH value was 3.0. ( $\lambda_{irr} = 365 \text{ nm}$ )

### C-3-2 Photodegradation of 2,4-DCP at 365 nm in the presence of Fe(III)-Carboxylate complexes

#### C-3-2-1 Degradation of 2,4-DCP photoinduced by Fe(III)-Cit complex

The UV-visible spectra of solution with  $0.1 \text{ mmol.L}^{-1}$  Fe(III)-Cit complex is shown in Figure IV-C-15. The natural pH is 4.4. Figure IV-C-16 gives the structure of Fe(III)-Cit. The pKa is equal to 3.3.

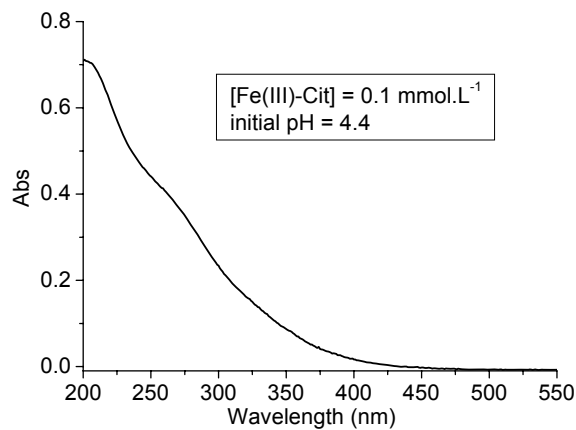
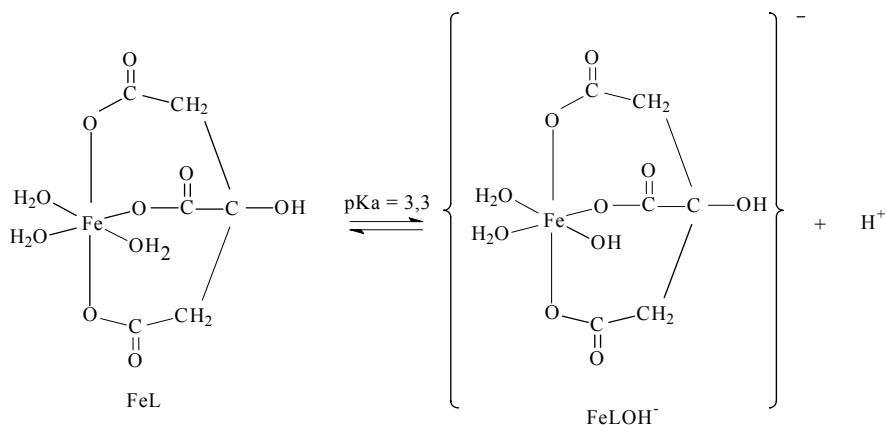


Figure IV-C-15 UV-Visible spectra of aqueous solution with  $0.1 \text{ mmol.L}^{-1}$  Fe(III)-Cit





**Figure IV-C-16 Structure of Fe(III)-Cit.(Abida, 2005)**

Experiments were performed to study UV-visible spectrum of different aqueous solutions: a) 0.1 mmol.L<sup>-1</sup> Fe(III)-Cit; b) 0.1 mmol.L<sup>-1</sup> 2,4-DCP; c) mixture of 0.1 mmol.L<sup>-1</sup> Fe(III)-Cit and 0.1 mmol.L<sup>-1</sup> 2,4-DCP. Figure IV-C-17 shows the spectrum of the solution 3 min after the preparation.

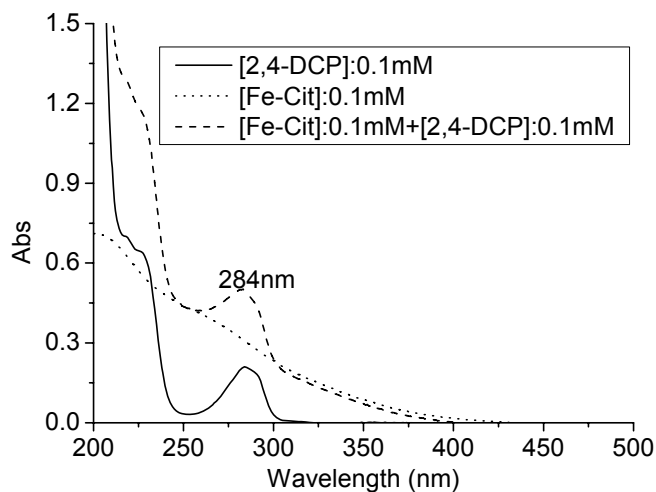
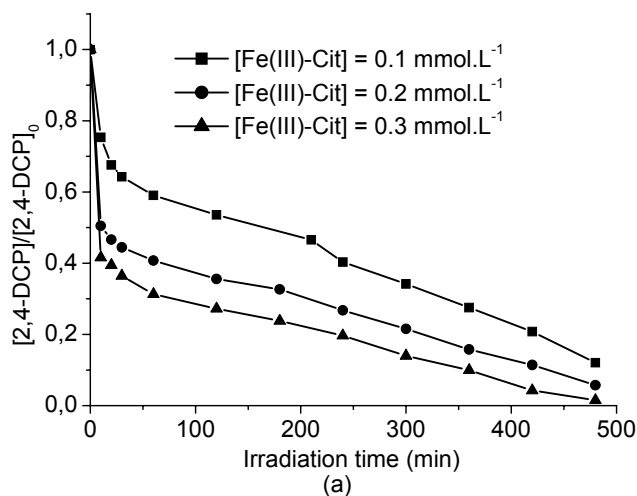


**Figure IV-C-17 Comparing of the UV-visible spectra of different aqueous solutions.**

The spectrum of the mixture corresponds to the sum of the both spectrum of the two components (2,4-DCP and Fe-Cit). This result shows that there is no interaction between the two components at the fundamental state.

### C-3-2-1-1 Effects of Fe(III)-Cit concentration

Experiments were carried out to study the effect of Fe(III)-Cit concentration on the photodegradation of 2,4-DCP. The initial concentration of Fe(III)-Cit complex used in the work are 0.1, 0.2 and 0.3 mmol.L<sup>-1</sup>. The solutions contain 0.1 mmol.L<sup>-1</sup> of 2,4-DCP with an initial pH value equal to 3.0. Results are shown in Figure IV-C-18(a), the photodegradation efficiency of 2,4-DCP increased with the increase of Fe-Cit complex concentration. After 6h of irradiation, the 2,4-DCP had almost disappear in the solution with 0.3 mmol.L<sup>-1</sup> Fe(III)-Cit complex. However, it is not fair to conclude that the higher the complex concentration, the higher the photodegradation rate is. Actually, if the complex concentration is too high, competition reactions will strongly exist between the organic substances (acid carboxylic and 2,4-DCP) in aqueous solutions. Less active species is available for the degradation of 2,4-DCP. That why the photodegradation efficiency of 2,4-DCP is almost the same in the presence of 0.3 and 0.6 mmol.L<sup>-1</sup> of Fe(III)-Cit complexes (Figure IV-C-18(b)).



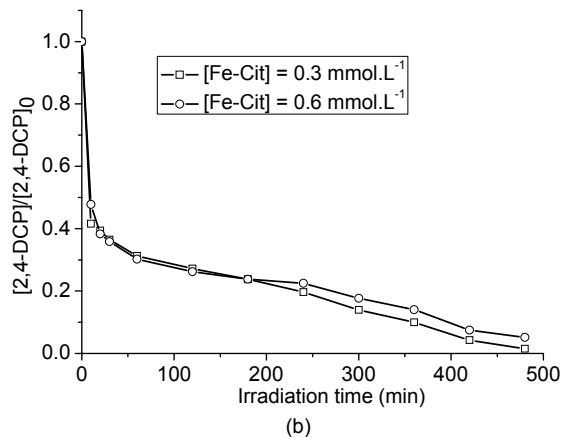


**Figure IV-C-18 Degradation of 2,4-DCP as a function of Fe(III)-Cit concentration in solution with an initial pH = 3.0. [2,4-DCP] = 0.1 mmol.L<sup>-1</sup>.**

During the irradiation process, the iron species especially Fe(II) was also detected. Figure IV-C-19 presents the photogeneration of Fe(II) in the experiments. In the beginning of the reaction, the concentration of Fe(II) increased very fast whatever the starting concentration in complex. Fe(III) has been totally photoreduced to Fe(II) after 20 min of irradiation. The reaction then continues (photocatalytic cycle Fe(III)/Fe(II)) consuming Fe(II) and formed  $\cdot\text{OH}$ , which is the main reason for the degradation of 2,4-DCP. In the presence of 0.3 mmol.L<sup>-1</sup> Fe(III)-Cit, the concentration of Fe(II) slightly decreased from 99% to 85% of total iron after 8h of irradiation.

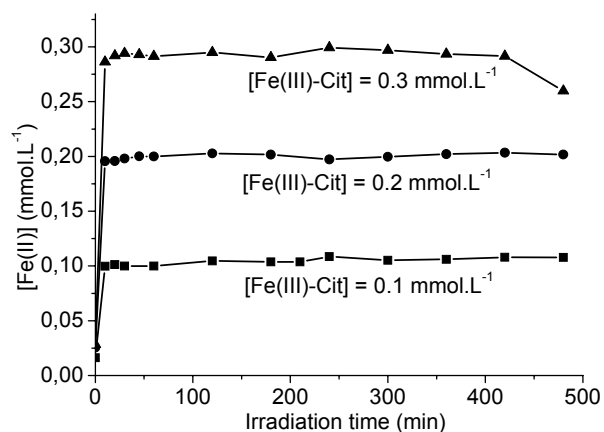


**Figure IV-C-19 The photogeneration of Fe(II) as a function of Fe(III)-Cit concentration in solution with an initial pH = 3.0. [2,4-DCP] = 0.1 mmol.L<sup>-1</sup>.**

### C-3-2-1-2 Effect of pH

The pH is a very important parameter in many kinds of reactions. Experiments were carried out to study the pH effect on the photodegradation of 2,4-DCP in the solution with  $0.3 \text{ mmol.L}^{-1}$  of Fe(III)-Cit complex and  $0.1 \text{ mmol.L}^{-1}$  of 2,4-DCP under irradiation at 365 nm. pH was adjusted to the desired value. From the results presented in Figure IV-C-20, it appears that the pH has a strong effect on the photodegradation reaction. The optimal photodegradation efficiency of 2,4-DCP was observed at pH = 3.0. For example, after 60 min irradiation, approximately 70% of 2,4-DCP was degraded at pH = 3.0, but only 45% at pH = 3.6 and 42% at pH = 6.0. Fe(II) concentrations were also determined at the same time. Results are presented in Figure IV-C-21, pH presents also a strong effect on the formation of Fe(II) species. Especially at pH = 6.0, the maximum concentration of Fe(II) was only 40% of total iron in the aqueous solution after 60 min of irradiation, and it decreased to 25% after 8 h of irradiation. Lower concentration of Fe(II) in the solutions, lower formation of radicals species, thus, the photodegradation efficiency of 2,4-DCP is low.

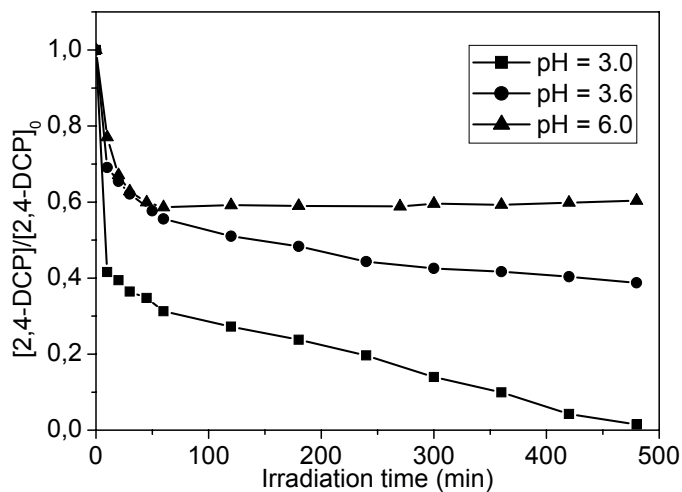


**Figure IV-C-20 Influence of pH on the photodegradation of 2,4-DCP in the presence of Fe(III)-Cit complexes.  $[\text{Fe(III)-Cit}] = 0.3 \text{ mmol.L}^{-1}$ ,  $[\text{2,4-DCP}] = 0.1 \text{ mmol.L}^{-1}$ .**

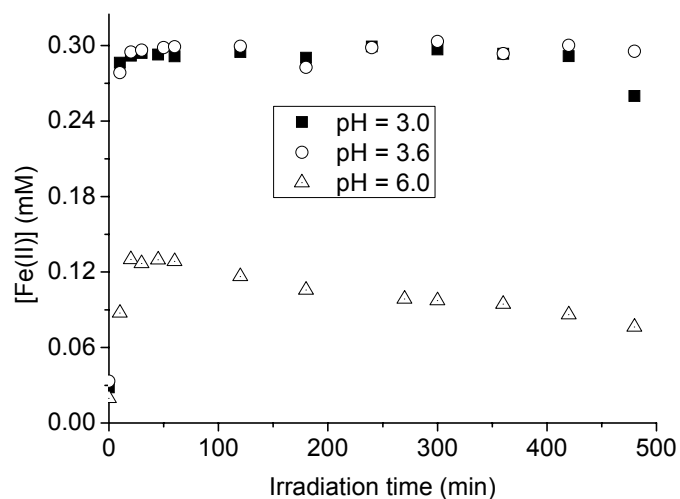


**Figure IV-C-21 Influence of pH on the photogeneration of Fe(II) in the presence of Fe(III)-Cit complexes.  $[\text{Fe(III)-Cit}] = 0.3 \text{ mmol.L}^{-1}$ ,  $[\text{2,4-DCP}] = 0.1 \text{ mmol.L}^{-1}$ .**

#### **C-3-2-1-2 Effect of oxygen**

Oxygen is another very important factor in the photochemical reactions. So it is necessary to study its effect on the photodegradation of 2,4-DCP. Experiments were carried out in deaerated and aerated solutions separately. Results are presented in Figure IV-C-22. Oxygen has a strong effect on the reaction. The photodegradation efficiency of 2,4-DCP is much higher in the aerated solution than in the deaerated solution. In the presence of oxygen, more reactive species ( $\text{O}_2^-$ ,  $\text{H}_2\text{O}_2$  and then  $\cdot\text{OH}$ ) will be generated in the aqueous solutions, which has been determined in the previous research. In the absence of oxygen a non negligible fraction of 2,4-DCP is degraded (more than 20%). This result show that the first radical formed (the degradation is very fast at the beginning) are capable to degrade 2,4-DCP.

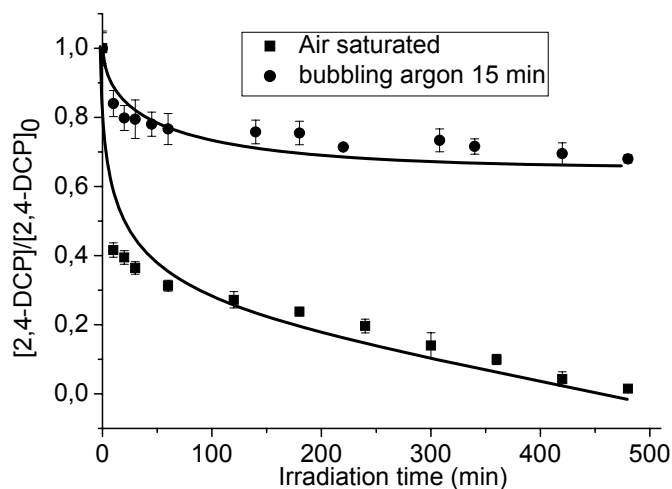


**Figure IV-C-22 Effects of oxygen on the photodegradation of 2,4-DCP in the presence of Fe(III)-Cit complexes. [Fe(III)-Cit] = 0.3 mmol.L<sup>-1</sup>, [2,4-DCP] = 0.1 mmol.L<sup>-1</sup>, pH = 3.0**

Determination of Fe(II) was also performed. Results are presented in the Figure IV-C-23. The formation of Fe(II) is very fast at the beginning of the reaction. The oxygen has no significant effect on the formation of Fe(II) (Figure IV-C-23). Fe(III) was almost totally reduced to Fe(II) species after 30 min of irradiation in all conditions. The concentration of Fe(II) species is stable in the absence of oxygen. However, the concentration of Fe(II) decreased to the final value of 85% of total iron in the air saturated solution after 8 h of irradiation. Some Fe(II) can be reoxidized into Fe(III) by oxygen or oxygenated reactive species.

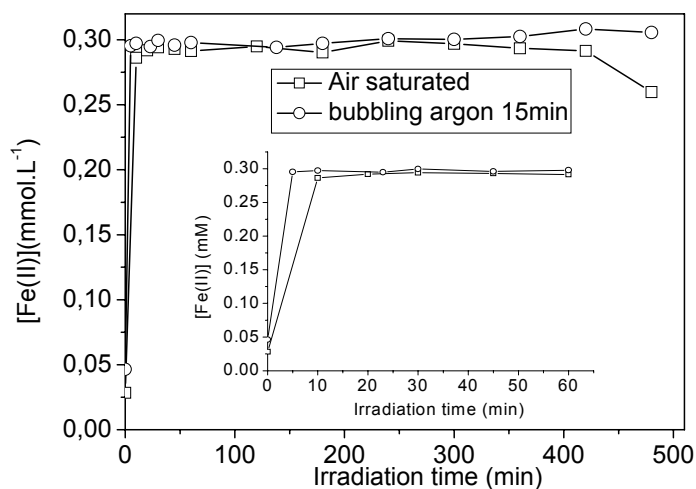


**Figure IV-C-23 Effects of oxygen on the photogeneration of Fe(II) in the presence of Fe(III)-Cit complexes.  $[\text{Fe(III)-Cit}] = 0.3 \text{ mmol.L}^{-1}$ ,  $[\text{2,4-DCP}] = 0.1 \text{ mmol.L}^{-1}$ ,  $\text{pH} = 3.0$**

### **C-3-2-2 Degradation of 2,4-DCP photoinduced by Fe(III)-D or L-Tar complex**

All the results obtained with tartaric acid are similar whatever the isomer D or L. Fe(III)-D or L-Tar complex was used to study the photodegradation of 2,4-DCP.

#### **C-3-2-2-1 Effect of Fe(III)-D or L-Tar concentration**

Effect of Fe(III)-D or L-Tar concentration on the photodegradation of 2,4-DCP was studied with initial concentrations of Fe(III)-complex equal to 0.05, 0.1, 0.2 and 0.3  $\text{mmol.L}^{-1}$ . The solutions contain 0.1  $\text{mmol.L}^{-1}$  of 2,4-DCP with an initial pH value adjusted at 3.0. Results about the photodegradation efficiency of 2,4-DCP are presented in Figure IV-C-24 a and b. It has two subsequent steps. In the first step, before 30min of irradiation, the photodegradation efficiency of 2,4-DCP increased with the increase of Fe(III)-complex concentration. In the second step the photodegradation efficiency appears to be the opposite tendency with the photodegradation efficiency of 2,4-DCP higher in the presence of lower complex concentration of Fe-complex. This result is due to the fact that at the beginning of the

irradiation, higher concentration of active radicals is formed in the solutions with the higher concentration of complexes. At the same time, the photolysis of Fe(III)-D or L-Tar complexes, will generate some low molecular weight organic substances, at higher concentration when the concentration of Fe(III)-complex is higher. These organic species also consume active radicals and competition reactions is present between 2,4-DCP and organic substances photogenerated from the Fe(III)-complexes. This competition is more acute in solutions with high concentration of complexes and so less active radicals are available for the degradation of 2,4-DCP.

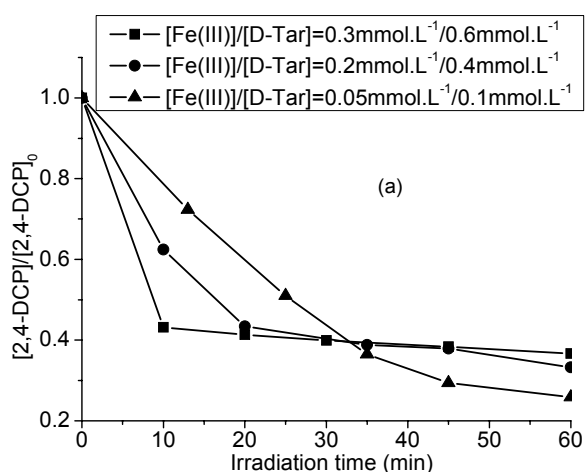


**Figure IV-C-24 a Photodegradation of 2,4-DCP as a function of Fe(III)-D-Tar concentration in solutions with an initial pH = 3.0.  $[2,4\text{-DCP}]_0 = 0.1 \text{ mmol.L}^{-1}$ .**

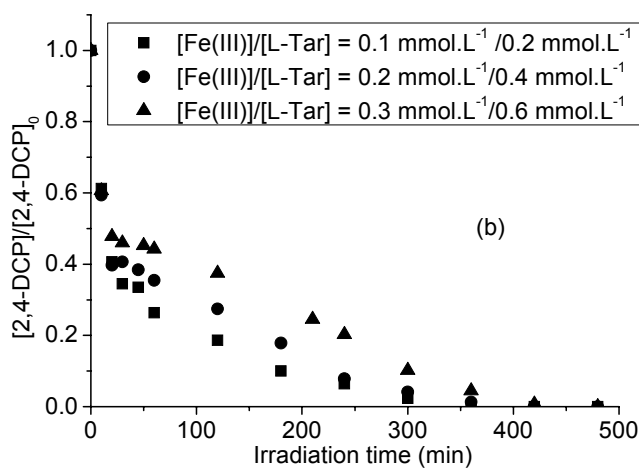


**Figure IV-C-24 b Photodegradation of 2,4-DCP as a function of Fe(III)-L-Tar concentration in solutions with an initial pH = 3.0.  $[2,4\text{-DCP}]_0 = 0.1 \text{ mmol.L}^{-1}$ .**



The concentration of Fe(II) was detected during the same reaction. Figure IV-C-25 presents the results about the determination of Fe(II). After 45 min of irradiation, the concentration of Fe(II) corresponded approximately to 100% of initial concentration of total iron added in the solutions. However, the concentration of Fe(II) decreased to 70%~75% of total iron after 8 h of irradiation in the solutions with concentrations in complex equal to 0.2 and 0.3 mmol.L<sup>-1</sup>. It also indicated that the photoreaction intermediates interfere in the photocatalytic cycle Fe(III)/Fe(II) in the solution.

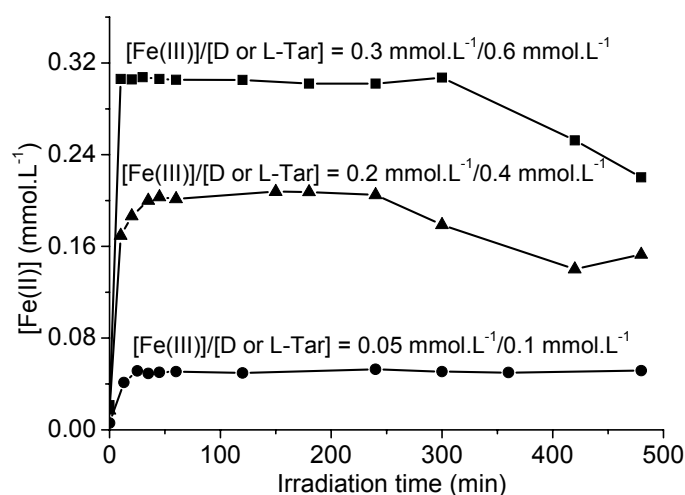


**Figure IV-C-25 Photogeneration of Fe(II) as a function of Fe(III)-D or L-Tar concentration in solutions with an initial pH = 3.0. [2,4-DCP]<sub>0</sub> = 0.1 mmol.L<sup>-1</sup>.**

Since the concentration of Fe(III)-D-Tar has a complicate effect on the photodegradation of 2,4-DCP. Experiments were performed with a group of low concentrations in complex from 0.01 mmol.L<sup>-1</sup> to 0.05 mmol.L<sup>-1</sup>, which are all lower than the concentration of 2,4-DCP 0.1 mmol.L<sup>-1</sup>. The pH of the solution is 3.0 in all the experiments. Results about the photodegradation of 2,4-DCP are presented in Figure IV-C-26. According to the results, at lower concentration of complex ( $\leq 0.1$  mmol.L<sup>-1</sup>) the photodegradation efficiency of 2,4-DCP increased with the increase of complex concentration over the value used in this experiment. The photodegradation

of 2,4-DCP and formation of Fe(II) proceed rapidly at the beginning of the irradiation. After 1 h of irradiation 75% of 2,4-DCP has disappeared in the presence of 0.05 mmol.L<sup>-1</sup> Fe(III)-D or L-Tar complex. As shown in Figure IV-C-27, the concentration of Fe(II) reach 80% of the total iron in the solutions after 10 min of irradiation.

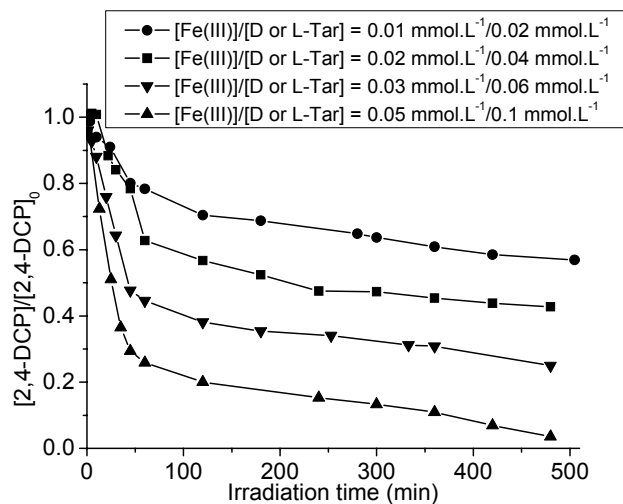


**Figure IV-C-26 Photodegradation of 2,4-DCP as a function of Fe(III)-D or L-Tar concentration with an initial pH = 3.0. [2,4-DCP]<sub>0</sub> = 0.1 mmol.L<sup>-1</sup>.**

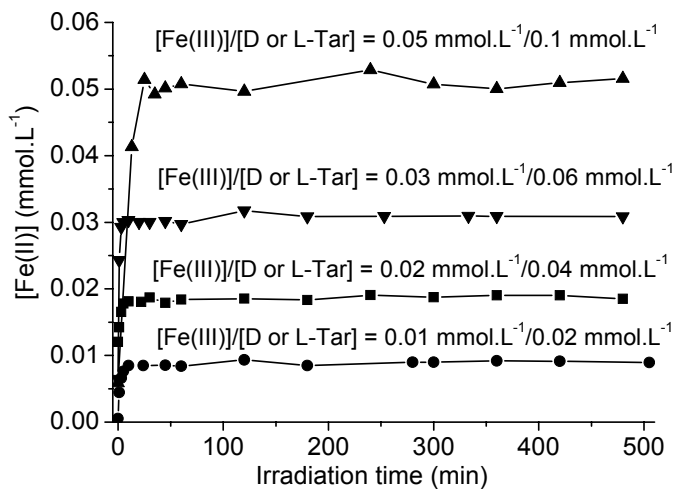


**Figure IV-C-27 Photogeneration of Fe(II) as a function of Fe(III)-D or L-Tar concentration in solutions with an initial pH = 3.0. [2,4-DCP]<sub>0</sub> = 0.1 mmol.L<sup>-1</sup>.**

### C-3-2-2-2 Effect of pH

pH effect was investigated in the solution with  $0.3 \text{ mmol.L}^{-1}$  Fe(III)-D or L-Tar complex and  $0.1 \text{ mmol.L}^{-1}$  2,4-DCP under irradiation at 365 nm. pH was adjusted to the desired value with perchloric acid (1N). Results about the photodegradation of 2,4-DCP are presented in Figure IV-C-28. pH has a strong effect on the reaction. The optimal photodegradation efficiency of 2,4-DCP was observed at pH 3.0. After 2 h of irradiation, 70% of 2,4-DCP was degraded at pH 3.0, 57% at pH 3.6 and only 11% at pH 5.0 or 6.0. After 6 h, 2,4-DCP was totally degraded at pH 3.0. Acidic conditions is favorable for the degradation of 2,4-DCP.

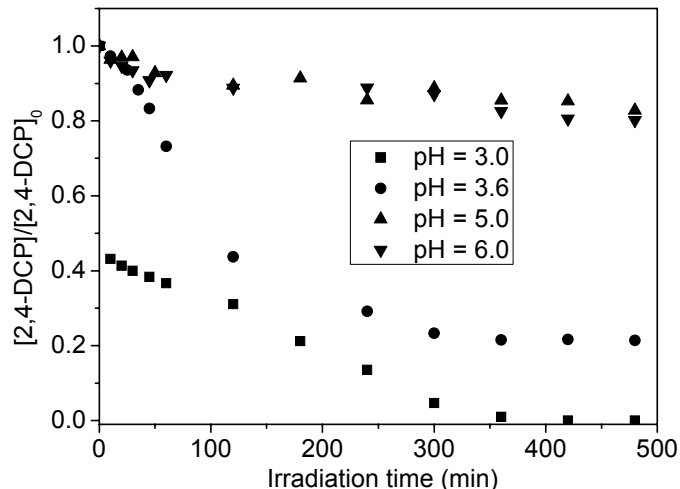


**Figure IV-C-28** pH effect on the photodegradation of 2,4-DCP.  $[\text{Fe(III)}]/[\text{D or L-Tar}] = 0.3 \text{ mmol.L}^{-1}/0.6 \text{ mmol.L}^{-1}$ ,  $[\text{2,4-DCP}]_0 = 0.1 \text{ mmol.L}^{-1}$ .

Fe(II) species was also determined at the same time. Results are presented in Figure IV-C-29, pH presents a strong effect on the formation of Fe(II) species. Low pH is favorable for the formation of Fe(II). At pH 3.0 and 3.6, total irons are almost totally and quickly transformed to Fe(II).after 10 min of irradiation. But for the relative higher pH value, the transformation of iron species was slower. The results are presented in the Figure IV-C-29, the evolution of Fe(II) seems to have three reaction steps. First step, before 2 h of irradiation the concentration of Fe(II) was increased until a plateau value, 80% of total iron concentration for pH 5.0 and 70%

for pH 6.0. In the second step, the concentration of Fe(II) was stable from 2 h to 5 h of irradiation. And then in the third step concentration of Fe(II) gradually decreased to a final value corresponding to 73% of total iron for pH 3.0, 60% for pH 5.0 and 43% for pH 6.0.

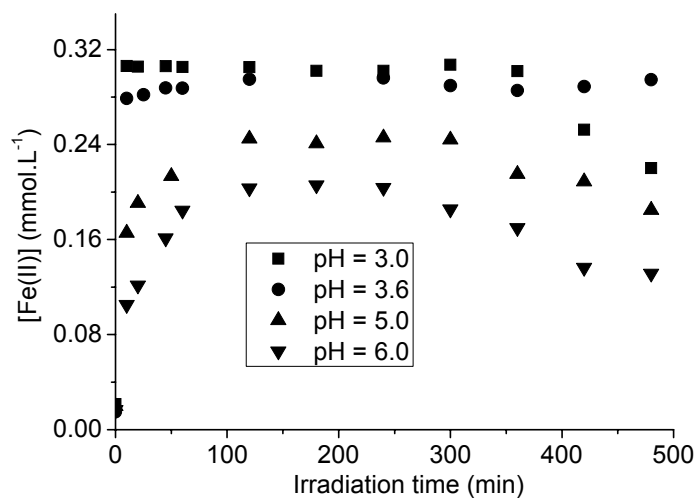


**Figure IV-C-29 Photogeneration of Fe(II) as function of pH value.  $[\text{Fe(III)}]/[\text{D or L-Tar}] = 0.3 \text{ mmol.L}^{-1}/0.6 \text{ mmol.L}^{-1}$ ,  $[\text{2,4-DCP}]_0 = 0.1 \text{ mmol.L}^{-1}$ .**

Figure IV-C-30 a and b presents the UV-visible spectra of the solutions with 0.2 and 0.01 mmol.L<sup>-1</sup> of Fe(III)-D-Tar complex and 0.1 mmol.L<sup>-1</sup> of 2,4-DCP as a function of the irradiation time. Irradiation was carried out at 365 nm and the starting pH of the solution is equal to 3.0. From the variation of the spectrum, the absorbance of 2,4-DCP at 284 nm was apparently decreased according to the time in the two conditions. This decrease was very fast at the beginning of the irradiation at higher concentration in iron complex. The absorbance of Fe(III)-D or L-Tar complex from 300 to 500 nm was also apparently decreased according to the irradiation time. After 8 h of irradiation and at higher concentration of complex, the pH value of solution increased from 3.0 to 3.4. It is well established that the oxidative degradation of the pollutant consumes H<sup>+</sup>. At lower concentration of complex, the variation of UV-vis spectrum is very interesting and in Figure IV-C-30 b two isosbestic points appear very clearly. This evolution shows very well the simultaneous disappearance of 2,4-DCP

and the complex and the formation of a new product with higher absorption near 250 nm.

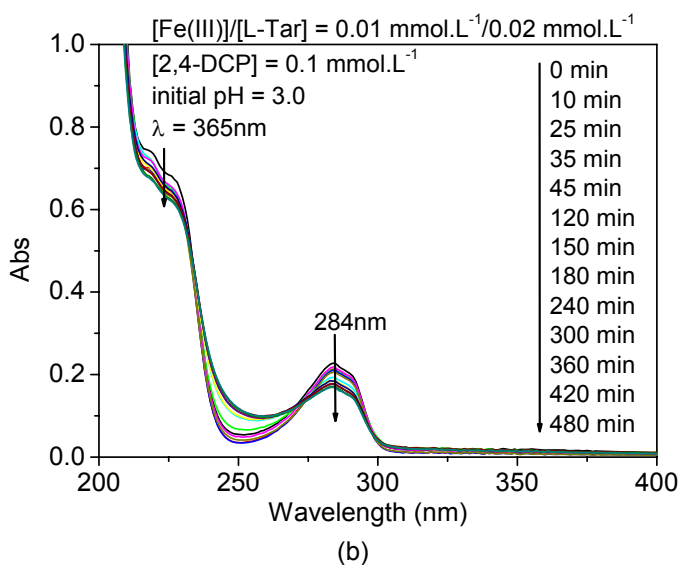
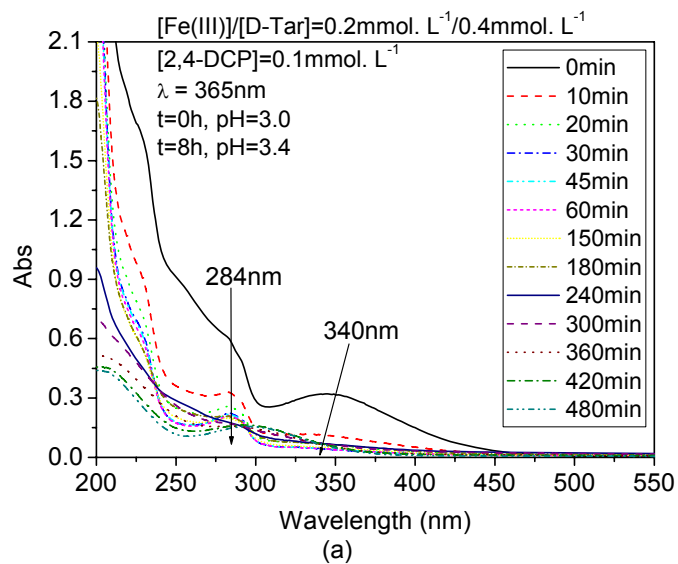


**Figure IV-C-30** Variation of the UV-visible spectra of the reaction solutions as a function of the irradiation time. (a)  $[\text{Fe(III)}]/[\text{D or L-Tar}] = 0.2 \text{ mmol.L}^{-1}/0.4 \text{ mmol.L}^{-1}$  (b)  $[\text{Fe(III)}]/[\text{D or L-Tar}] = 0.01 \text{ mmol.L}^{-1}/0.02 \text{ mmol.L}^{-1}$ .  $\lambda_{\text{irr}} = 365 \text{ nm}$ ; Initial pH value was 3.0.

### C-3-2-2-3 Effect of oxygen

Oxygen effect on the photoreaction was studied in the solution with  $0.3 \text{ mmol.L}^{-1}$  Fe(III)-D or L-Tar and  $0.1 \text{ mmol.L}^{-1}$  2,4-DCP at pH= 3.0. Deoxygenated condition was obtained by bubbling argon into the solutions before irradiation. Figure IV-C-31 presents the results. The curves show that oxygen is an important parameter for the photodegradation efficiency of 2,4-DCP. In the oxygen rich condition, the photodegradation efficiency of 2,4-DCP has reached 63% after 1h irradiation, and only 11% 2,4-DCP was degraded in the deaerated condition. Oxygen is a crucial parameter for the formation of reactive species in the aqueous solutions. The degradation observed in deaerated condition can be attributed to primary radicals photogenerated in the photoredox process or due to a not complete deoxygenation of the solutions.

Determination of Fe(II) was performed at the same time. Results are presented in the Figure IV-C-32. The formation of Fe(II) is very fast at the beginning of the reaction in both conditions. The concentration of Fe(II) has reached over 90% of the total iron in the solutions after 10 min of irradiation. Iron was almost totally reduced to Fe(II) species after 10 min of irradiation. Oxygen effect present the same tendency as in the presence of Fe(III)-Cit complex. Fe(II) species was stable in the absence of oxygen all along the experiment. However, the concentration of Fe(II) decreased to the final value of 70% of total iron in the air saturated solution after 8 h of irradiation.

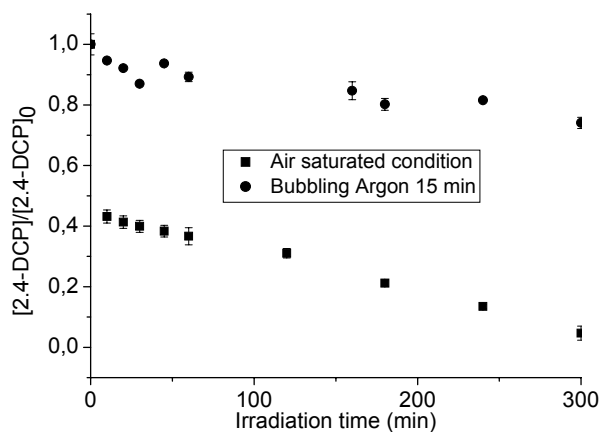


**Figure IV-C-31 Effects of oxygen on the photodegradation of 2,4-DCP in the presence of Fe(III)-D or L-Tar complexes. [Fe(III)-D or L-Tar] =  $0.3 \text{ mmol.L}^{-1}$ , [2,4-DCP] =  $0.1 \text{ mmol.L}^{-1}$ , pH = 3.0**

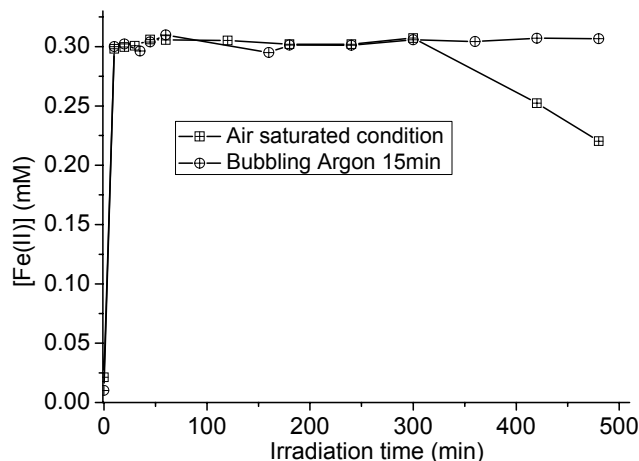


**Figure IV-C-32 Effects of oxygen on the photogeneration of Fe(II) in the presence of Fe(III)-D or L-Tar complexes. [Fe(III)-D or L-Tar] = 0.3 mmol.L<sup>-1</sup>, [2,4-DCP] = 0.1 mmol.L<sup>-1</sup>, pH = 3.0**

### **C-3-2-3 Degradation of 2,4-DCP photoinduced by Fe(III)-Pyr complex**

Fe(III)-Pyr complex was also used to study the photodegradation of 2,4-DCP.

#### **C-3-2-3-1 Effect of Fe(III)-Pyr concentration**

Effect of Fe(III)-Pyr concentration on the photodegradation of 2,4-DCP was studied. The initial concentration of Fe(III)-Pyr complex used in the work are 0.1, 0.2 and 0.3 mmol.L<sup>-1</sup>. The reaction solutions contain 0.1 mmol.L<sup>-1</sup> of 2,4-DCP with an initial pH value equal to 3.0. Figure IV-C-33 presents the experimental results about the photodegradation efficiency of 2,4-DCP. The photodegradation efficiency of 2,4-DCP was increased with the increase of Fe(III)-Pyr concentration all along the experiments. It is different from the results obtained in the presence of Fe(III)-Tar complexes for long irradiation time where the degradation of 2,4-DCP decreased for higher concentration of Fe(III)-Tar complexes.

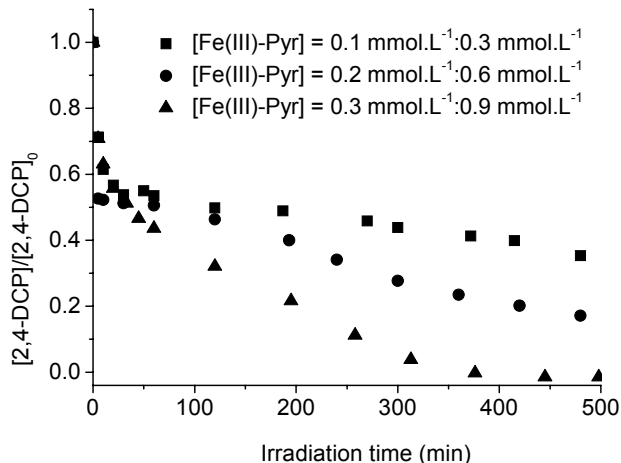


**Figure IV-C-33 Photodegradation of 2,4-DCP as a function of Fe-Pyr concentration in solution with an initial pH = 3.0.  $[2,4\text{-DCP}]_0 = 0.1 \text{ mmol.L}^{-1}$ .**

The formation of Fe(II) species was determined at the same time. Results are presented in Figure IV-C-34. In the presence of 0.1 and 0.2 mmol.L<sup>-1</sup> Fe(III)-Pyr complexes, the concentration of Fe(II) was over 94% of the total irons after 10 min of irradiation. In the presence of 0.3 mmol.L<sup>-1</sup> of Fe(III)-Pyr, the iron was totally transformed to Fe(II) after 45 min of irradiation. The concentrations of Fe(II) are all stable according to the irradiation time. These results are similar to those obtained with the author iron complexes (Fe-Cit and Fe-Tar).

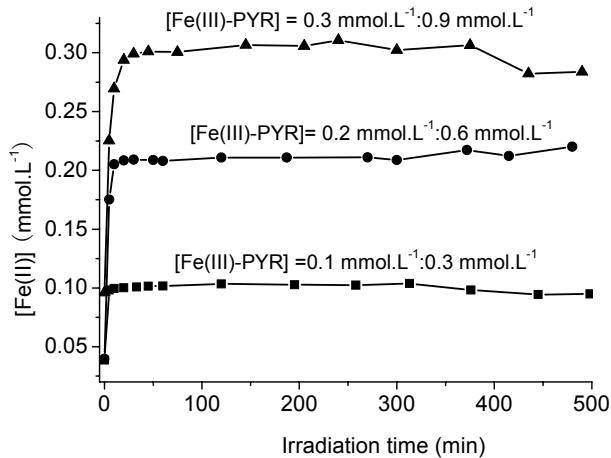


**Figure IV-C-34 Photogeneration of Fe(II) as a function of Fe-Pyr concentration in solutions with an initial pH = 3.0.  $[2,4\text{-DCP}]_0 = 0.1 \text{ mmol.L}^{-1}$ .**



### C-3-2-3-2 Effect of pH

pH as an important parameter was studied in the solution with  $0.1 \text{ mmol.L}^{-1}$  Fe(III)-Pyr complex and  $0.1 \text{ mmol.L}^{-1}$  2,4-DCP under irradiation at 365 nm. The pH was adjusted to the desired value by perchloric acid (1 N). Figure IV-C-35 presents the experiment results. The pH plays an important role in the photodegradation of 2,4-DCP. More than 80% of the 2,4-DCP disappeared at pH 3.0 and 4.0 after 8 h of irradiation. The photodegradation was slow in the relative high pH. Only 42% of 2,4-DCP disappeared at pH 5.35 after 8 h of irradiation. Acidic conditions is favorable for the formation of active species, which is the main reason for the degradation of 2,4-DCP.

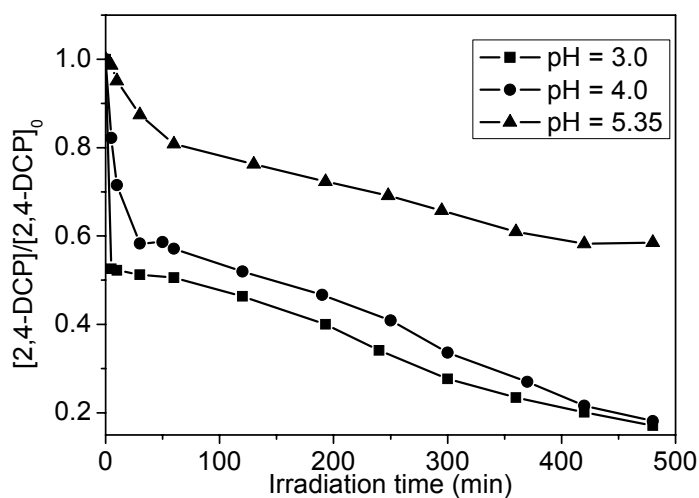


**Figure IV-C-35 pH effect on the photodegradation of 2,4-DCP.  $[\text{Fe(III)}]/[\text{Pyr}] = 0.1 \text{ mmol.L}^{-1}/0.3 \text{ mmol.L}^{-1}$ ,  $[\text{2,4-DCP}]_0 = 0.1 \text{ mmol.L}^{-1}$ .**

Detection of Fe(II) species was also performed at the same time. Results are presented in Figure IV-C-36, pH presents a strong effect on the formation of Fe(II) species. Lower pH is favorable for the formation of Fe(II). At pH 3.0 the concentration of Fe(II) corresponded to approximately 100% of the total iron concentration after 10 min of irradiation. However, at relative high pH, the reduction

of Fe(III) species was slower but around 100% of the total iron concentration was also obtained after 1 h of irradiation at pH 4.0. However, at higher pH (5.35) only 68% of the total iron concentration is reduced into Fe(II) after 1h of irradiation. For longer irradiation times, there is an apparent decrease of Fe(II) concentration at pH 4.0 and the concentration of Fe(II) gradually decreased to reach a final value of 85% of the total iron after 8 h of irradiation.

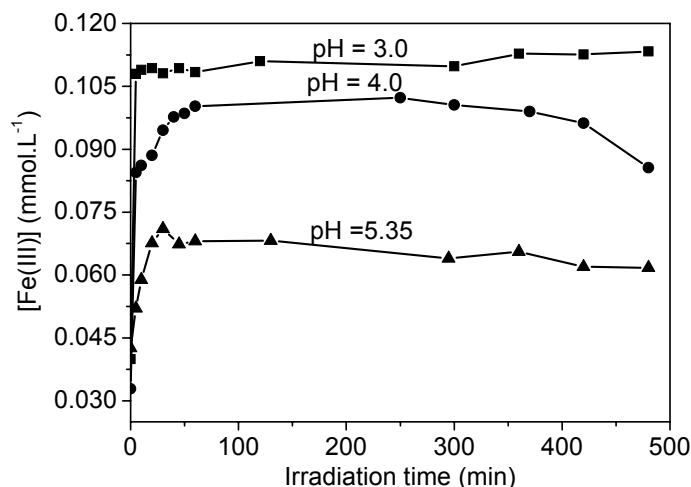


**Figure IV-C-36 Photogeneration of Fe(II) as function of pH value.  $[\text{Fe(III)}]/[\text{Pyr}] = 0.1 \text{ mmol.L}^{-1}/0.3 \text{ mmol.L}^{-1}$ ,  $[\text{2,4-DCP}]_0 = 0.1 \text{ mmol.L}^{-1}$ .**

### C-3-2-3-3 Effect of oxygen

Oxygen effect on the photodegradation of pollutants was performed in the solutions with  $0.3 \text{ mmol.L}^{-1}$  Fe(III)-Pyr complex and  $0.1 \text{ mmol.L}^{-1}$  2,4-DCP at pH = 3.0. Results are presented in Figure IV-C-37. Oxygen can enhance the photodegradation of 2,4-DCP in the presence of Fe(III)-Pyr complex. In the air saturated condition, the photodegradation efficiency of 2,4-DCP is higher than in the deaerated conditions. After 8 h of irradiation, 2,4-DCP has been totally degraded in the air saturated condition, and only 28% of the 2,4-DCP was degraded in the deaerated solution. In deaerated condition the rate of the degradation of 2,4-DCP seems to be faster after 350 min of irradiation. It is difficult to explain this observation

and it can be due to enter of oxygen in the solution during the experiment.

As shown in the Figure IV-C-38, the formation of Fe(II) is very fast at the beginning of the reaction in both conditions. Iron was almost totally reduced to Fe(II) species after 30 min of irradiation. The same conclusions as before for the author iron complexes were obtained. The concentration of Fe(II) species is stable in the deaerated solution and there is a small decrease in the aerated solution with a final value of 94% of total iron concentration after 8 h of irradiation.

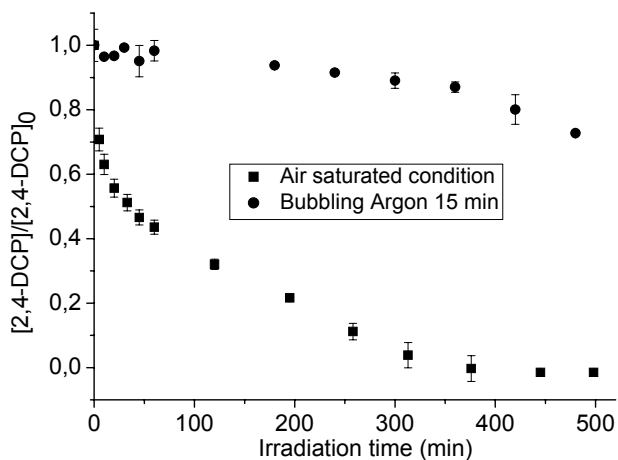


**Figure IV-C-37 Effect of oxygen on the photodegradation of 2,4-DCP in the presence of Fe(III)-Pyr complexes.  $[\text{Fe(III)-Pyr}] = 0.3 \text{ mmol.L}^{-1}$ ,  $[\text{2,4-DCP}] = 0.1 \text{ mmol.L}^{-1}$ ,  $\text{pH} = 3.0$**

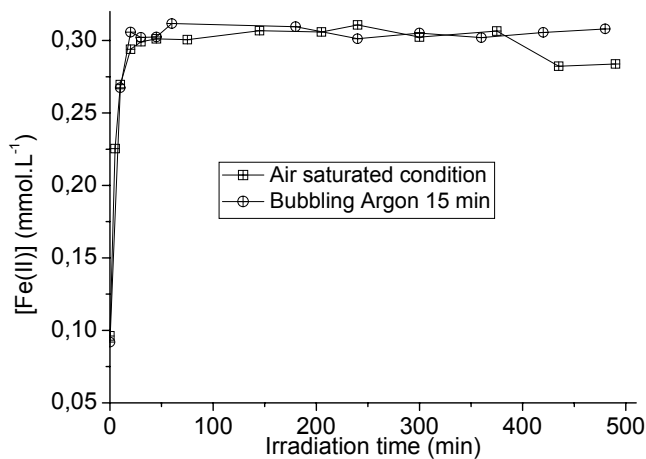


**Figure IV-C-38 Effect of oxygen on the photogeneration of Fe(II) in the presence of Fe(III)-Pyr complexes.  $[\text{Fe(III)-Pyr}] = 0.3 \text{ mmol.L}^{-1}$ ,  $[\text{2,4-DCP}] = 0.1 \text{ mmol.L}^{-1}$ ,  $\text{pH} = 3.0$**

#### **C-3-2-4 Comparing of the photodegradation of 2,4-DCP in different systems**

The photochemical properties of Fe(III) and Fe(III)-Carboxylate complexes have been systemically studied in this work. The studied complexes are comparable in the photoreaction efficiency of Fe(II) formation and 2,4-DCP degradation. Results about the photodegradation efficiency of 2,4-DCP are presented in the Figure IV-C-39. However, a slight difference is observed and the efficiency of Fe(III) complexes to degrade 2,4-DCP is in the order of  $\text{Fe}(\text{OH})^{2+} < \text{Fe}(\text{III})\text{-Pyr} < \text{Fe}(\text{III})\text{-Tar} < \text{Fe}(\text{III})\text{-Cit}$  after 2 h of irradiation. After 3 h of irradiation an for longer times, the photodegradation efficiency is changed into an opposite order that is  $\text{Fe}(\text{III})\text{-Cit} < \text{Fe}(\text{III})\text{-Tar} < \text{Fe}(\text{III})\text{-Pyr} < \text{Fe}(\text{OH})^{2+}$ . This very important observation indicates that there is a competition between organic compounds in the solutions. After 2h~3h of irradiation, iron was totally reduced to Fe(II) and as a consequence Fe(III) complexes was completely disappeared at the same time. Many organic substances simultaneously exist in the solutions. Hydroxyl radical is an unselective active species for the degradation of pollutants. That is why the OH radical is less available for the degradation of 2,4-DCP in the aqueous solution in the presence of acid ligands and for longer irradiation time the aquacomplexes of iron become more efficient for the degradation of the pollutant (2,4-DCP).

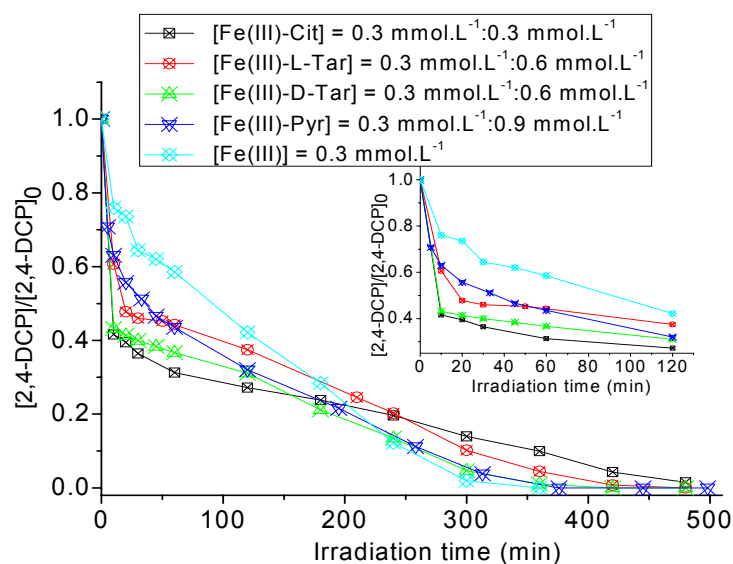


**Figure IV-C-39 Photodegradation of 2,4- DCP in different systems.**  
 $[\text{2,4-DCP}] = 0.1 \text{ mmol.L}^{-1}$ ,  $\text{pH} = 3.0$

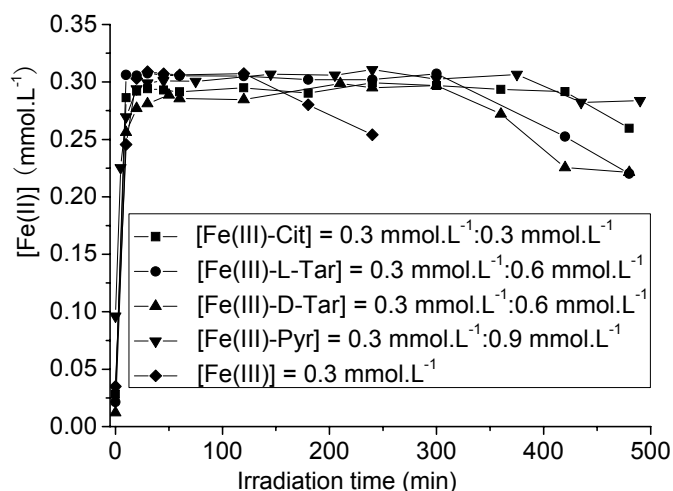


**Figure IV-C-40 Photogeneration of Fe(II) in different systems.**  
**[2,4-DCP] = 0.1 mmol.L<sup>-1</sup>, pH = 3.0**

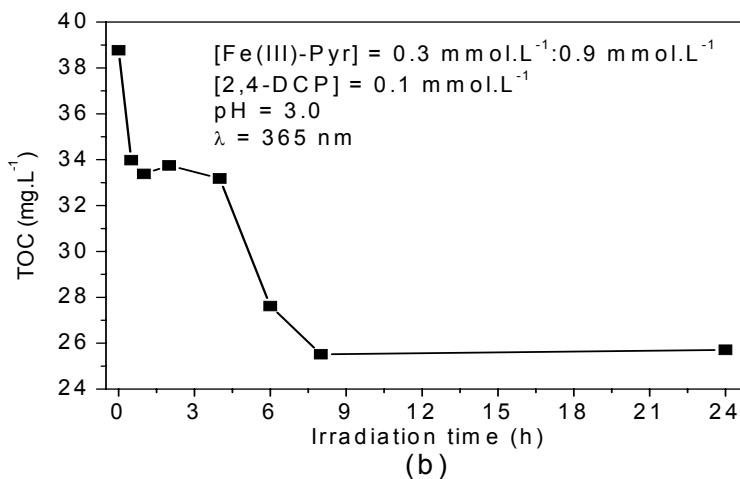
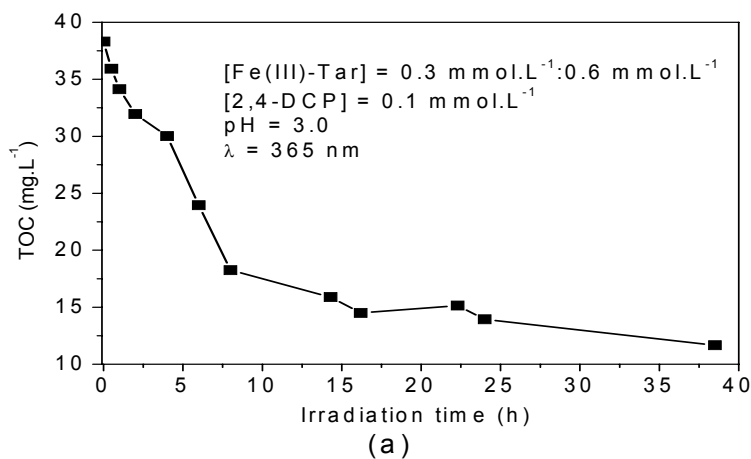
Figure IV-C-40 presents the formation of Fe(II) species. Whatever Fe(III)-Carboxylate complexes, Fe(III) is reduced very fast. After 30 min of irradiation approximately all Fe(III) species are reduced. 2,4-DCP is rapidly degraded in the initial period which correspond to the fast Fe(II) formation. Results demonstrate that all of the iron systems can effectively induce the photodegradation of 2,4-DCP.

The Fe(II) concentration starts to decrease for longer irradiation time, different as a function of the Fe(III) complexes used. This decrease of Fe(II) can be explained by the reactivity of OH radical on Fe(II). This reaction becomes significant when the concentration of starting pollutant or organic species in general decreases. This phenomenon has been already described in the literature (Mestankova et al, 2004).

### C-3-3 Mineralization analysis by TOC

Total organic carbon (TOC) experiments were undertaken in order to make evidence for the mineralization of pollutants. The mixture of 0.1 mmol.L<sup>-1</sup> of 2,4-DCP and 0.3 mmol.L<sup>-1</sup> of Fe(III)-Carboxylate complexes was analysed as a function of irradiation time by TOC analyser. Results are presented in the Figure IV-C-41. The concentration of TOC decreased according to the irradiation time. The decrease can

be partly attributed to the photodegradation of 2,4-DCP and partly to the photoredox process in the iron complexes. During the irradiation process, the Fe(III) complexes was decomposed under irradiation accompanied by the formation of active radicals, which directly induced the photodegradation of 2,4-DCP. Many experiments presented above also indicated that 2,4-DCP completely disappeared after 8 h of irradiation. The second reason for the TOC concentration decrease is the photodegradation of organic acids used as a complexing agent of iron. It is well known and presented in the bibliography that in the first step of the photochemical process of iron-carboxylic acid complexes, a decarboxylation is systematically observed.



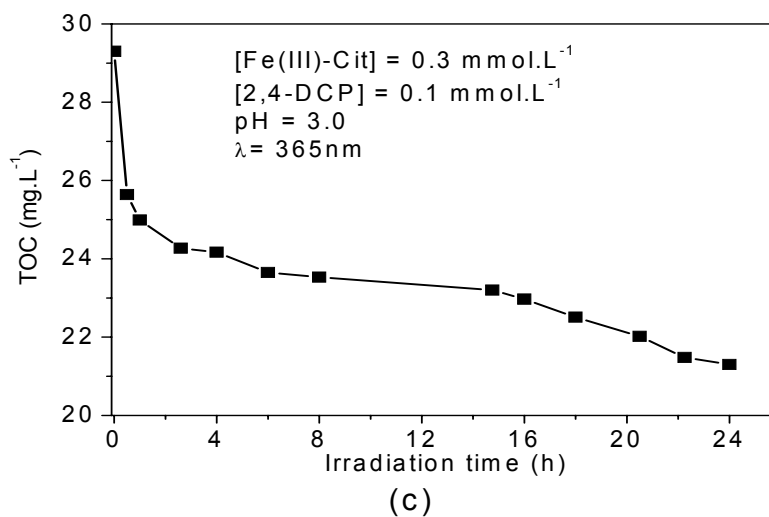


**Figure IV-C-41** Time courses of TOC values during irradiation of mixtures of 0.1 mmol.L<sup>-1</sup> of 2,4-DCP and 0.3 mmol.L<sup>-1</sup> of Fe(III)-Carboxylate complexes. (a) Fe(III)-Tar; (b) Fe(III)-Pyr; (c) Fe(III)-Cit,  $\lambda_{irr} = 365$  nm

Systemically with the three iron-complexes a decrease of TOC concentration is observed. However, this decrease is much more important in the presence of Fe(III)-Tar complex. This difference can be attributed to the structure of the different carboxylic acid. But this more important mineralization observed with Fe(III)-tar complex is surprising when we know that the quantum yield of 2,4-DCP degradation is the smallest of the four iron complexes. Anyway, it is difficult to go further in the discussion. Indeed, more experiments will be necessary to know if the mineralization observed is mainly due to the organic ligand degradation or to the 2,4-DCP degradation.

## Conclusions

Photodegradation of 2,4-DCP was investigated in the presence of different Fe(III)-Carboxylate complexes, including Fe-D or L-Tar, Fe-Pyr and Fe-Cit complexes. Irradiation experiments were carried out separately under monochromatic irradiation for short times and under polychromatic irradiation (between 300 and 500 nm) for longer times. The results indicate that irradiation wavelength, pH, oxygen, Fe(III)-Carboxylate complexes and 2,4-D concentrations, all have an impact on the quantum yields of Fe(II) formation and 2,4-DCP disappearance and also on the kinetic of 2,4-DCP degradation.

However, the first important remark is that evolution of quantum yields of Fe(II) formation and 2,4-DCP disappearance as a function of the different Fe(III) complexes have a different tendency. For the  $\Phi_{\text{Fe(II)}}$ , the tendency is Fe(III)-Pyr > Fe(III)-Cit > Fe(III)-Tar > Fe(OH)<sup>2+</sup>, and for the  $\Phi_{2,4\text{-DCP}}$ , the tendency is Fe(III)-Pyr~Fe(OH)<sup>2+</sup> > Fe(III)-Cit > Fe(III)-Tar. The main difference is due to the fact that Fe(OH)<sup>2+</sup> is the most photoactive complex for the degradation of 2,4-DCP and the less photoactive complex for the formation of Fe(II). These results indicate that at the beginning of the reaction, organic acids can enhance photoformation of Fe(II) as well as active species, however, they also quench active radicals at the same time. Thus, competition reactions coexist in the reaction solutions, less radicals is available for the degradation of 2,4-DCP.

Longer irradiation times results indicate that Fe(III)-Carboxylate complexes can effectively induced the degradation of 2,4-DCP. However, the photodegradation processes are more complicated in the presence of organic ligands. Competition reactions exist in the aqueous solutions. After 3 h of irradiation, many kinds of intermediate products originated from 2,4-DCP and from Fe(III)-Carboxylate complexes coexist in the aqueous solutions. That is why total mineralization is hard to obtain in comparison with iron aquacomplexes.

Results indicate that both lower pH and higher concentration of oxygen are



favorable for the photodegradation of 2,4-DCP and are very important parameter for the efficiency of the pollutant degradation. The effect of iron-complexes concentration is more complicated. Indeed, at higher concentrations of Fe-Carboxylate complexes the degradation of 2,4-DCP is increase in many cases. But, in the case of Fe-Tar complex and at higher concentration ( $> 0.1 \text{ mmol.L}^{-1}$ ), the degradation of 2,4-DCP is strongly reduced after 20 min of irradiation and as a conclusion the total efficiency is lower than for lower Fe(III)-Tar concentration ( $< 0.1 \text{ mmol.L}^{-1}$ ). This phenomenon very sensitive, in our experimental condition ( $[\text{Fe(III)-complexes}] < 0.3 \text{ mmol.L}^{-1}$ ) with tartaric acid is attributed to the competition between organic ligand and pollutant for the reactivity of hydroxyl radicals. The difference of concentration, between the Fe(III)-complexes, to reach the competition for the hydroxyl radical can be attributed to the difference of reactivity of  $\cdot\text{OH}$  radical on the different organic acids. This observation is in agreement with the rate constant of different organic acids with hydroxyl radicals:

**Table IV-C-5 Rate constants of  $\cdot\text{OH}$  radicals on the different organic acids (Buxton et al, 1988).**

Organic acids	Rate constants ( $\text{L.mol}^{-1}.\text{s}^{-1}$ )
Tartaric acid (pH = 2.0)	$7 \times 10^8$
Tartrate ion (pH= 9.0)	$6.8 \times 10^8$
Citric acid (pH = 1.0)	$5.0 \times 10^7$
Pyruvate ion (pH = 9.0)	$3.1 \times 10^7$

$\cdot\text{OH}$  radicals have a higher reactivity on the tartaric acid, that is why we observed a competition for  $\cdot\text{OH}$  reaction at lower concentration for this acid.

## IV-D Degradation of 2,4-Dichlorophenoxyacetic acid (2,4-D) photoinduced by the Fe(III)-Carboxylate complexes

Experiments were carried out to study the photodegradation of 2,4-D induced by the Fe(III)-Carboxylate complexes, such as Fe(III)-Cit, Fe(III)-Tar and Fe(III)-Pyr complexes, which have been used in the previous part of this thesis. Parameters such as wavelength irradiation, complexes concentration, pH and oxygen, were all studied in the work.

### D-1-Properties of 2,4-D in aqueous solution

The UV-visible spectrum of the solutions with different concentrations of 2,4-D is presented in Figure IV-D-1. It has two bands with maximum absorption at 230 nm and 284 nm. The molar absorption coefficients ( $\epsilon$ ) are  $8725 \text{ L}\cdot\text{mol}^{-1}\cdot\text{cm}^{-1}$  at 230 nm and  $1920 \text{ L}\cdot\text{mol}^{-1}\cdot\text{cm}^{-1}$  at 284 nm (determined with the figure IV-D-2). The pKa of 2,4-D is equal to 2.64.

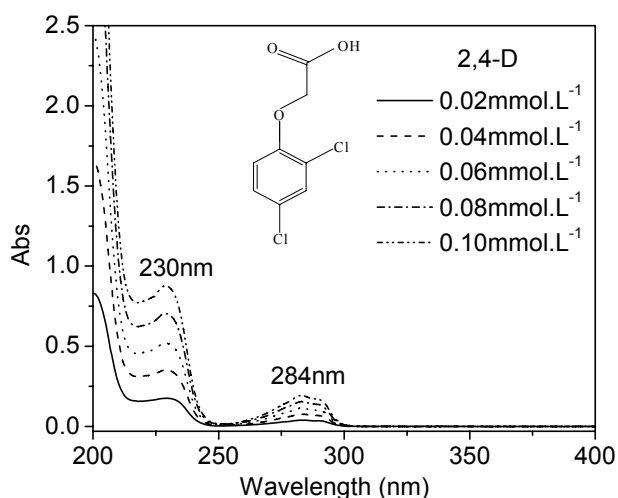
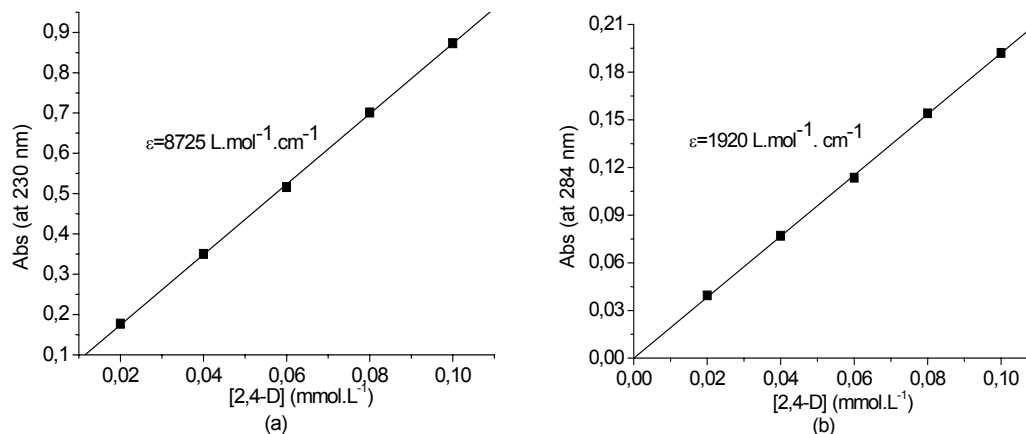
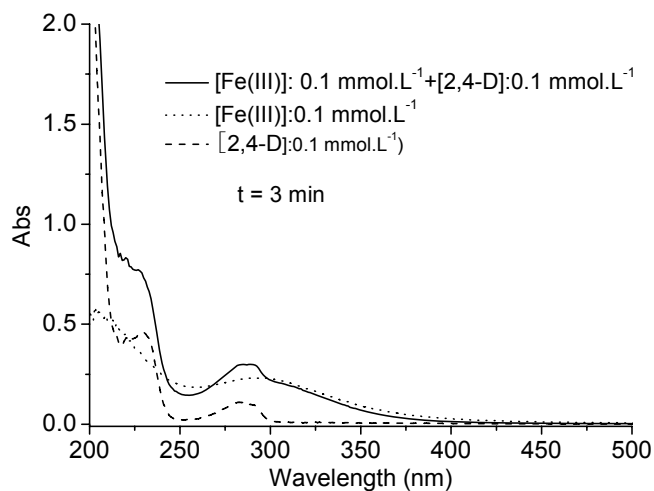


Figure IV-D-1 UV-visible spectra of 2,4-D at different concentrations.



**Figure IV-D-2 Molar absorption coefficients at different wavelength.**  
**(a) 230 nm, (b) 284 nm.**

Experiments were performed to study UV-visible spectra of different aqueous solutions: a) 0.1 mmol.L<sup>-1</sup> Fe(III); b) 0.1 mmol.L<sup>-1</sup> 2,4-D; c) mixture of 0.1 mmol.L<sup>-1</sup> Fe(III) and 0.1 mmol.L<sup>-1</sup> 2,4-D. Figure IV-D-3 shows the spectra of the solutions 3 min after the preparation.



**Figure IV-D-3 UV-Visible absorption spectra of aqueous solution 3 min after the preparation with 0.1 mmol.L<sup>-1</sup> of Fe(III) and 0.1 mmol.L<sup>-1</sup> of 2,4-D**

The spectrum of the mixture (Fe(III) + 2,4-D) correspond to the sum of the spectra of the both components. This result shows that there is no interaction

(complexation) between 2,4-D and Fe(III) in the aqueous solution.

## **D-2-Quantum yields of 2, 4-D degradation and Fe(II) formation**

The quantum yield has been evaluated in the method that for 2,4-DCP (< at 10% of the reaction progress).

### **D-2-1 Influence of the irradiation wavelength on the quantum yields of Fe(II) and 2,4-D in different Fe(III)-Carboxylate complexes systems**

The quantum yields of Fe(II) formation and 2,4-D disappearance has been evaluated at different wavelength (296, 313 and 365 nm) in the aqueous solutions with 0.1 mmol.L<sup>-1</sup> of 2,4-D and 0.3 mmol.L<sup>-1</sup> Fe(III)-Carboxylate complexes. All of the experiments were carried out at pH 3.0. Table IV-D-1 presents the results. Wavelength has a strong effect on the quantum yields.  $\Phi_{\text{Fe(II)}}$  and  $\Phi_{2,4\text{-D}}$  all increased with the decrease of the wavelength in different reaction systems. However if we compare the quantum yields as a function of iron-complex used, quantum yields of Fe(II) formation and 2,4-D disappearance have an opposite tendency excepted in the presence of Fe(III)-Pyr where the quantum yields the highest for both, Fe(II) and 2,4-D. For the  $\Phi_{\text{Fe(II)}}$ , the tendency is Fe(III)-Pyr > Fe(III)-Tar > Fe(III)-Cit > Fe(OH)<sup>2+</sup>, but for the  $\Phi_{2,4\text{-D}}$ , the tendency is Fe(III)-Pyr > Fe(OH)<sup>2+</sup> > Fe(III)-Cit > Fe(III)-Tar. The photoreduction of Fe(III) is enhanced in the presence of ligands. So the  $\Phi_{\text{Fe(II)}}$  are much higher in the presence of acid carboxylic as ligands than in the presence of water or hydroxide group as ligands (Fe(OH)<sup>2+</sup>). This difference can be attributed to the fact that in the case of organic ligands Fe(II) formed is less reoxidized, and radical species formed under irradiation attack pollutants as well. However, in the case of Fe(III)-Tar and Fe(III)-Cit, the  $\Phi_{2,4\text{-D}}$  is lower in the presence than with Fe(OH)<sup>2+</sup>. This surprising result, if you take into account  $\Phi_{\text{Fe(II)}}$ , can be due to the competition between organic substrates and less radicals are available for the 2,4-D degradation at the beginning of the irradiation.

**Table IV-D-1 Quantum yields of disappearance of 2,4-D and generation of Fe(II) as a function of the irradiation wavelength.**

$\lambda$	$I_0, 10^{14}$ photons $\cdot$ s $^{-1}$ $\cdot$ cm $^{-2}$	$\Phi_{\text{Fe(II)}}$ $\Delta t=40\text{s}$	$\Phi_{2,4\text{-D}}$ $\Delta t=10\text{min}$
(a)Fe(III) = 0.3 mmol.L $^{-1}$ , pH = 3.0			
296	4.39	0.070	0.037
313	7.46	0.029	0.029
365	13.7	0.025	0.012
(b)Fe(III)-Pyr = 0.3 mmol.L $^{-1}$ :0.9 mmol.L $^{-1}$ , pH = 3.0			
296	4.39	0.47	0.135
313	7.46	0.28	0.060
365	13.7	0.30	0.046
(c)Fe(III)-Tar = 0.3 mmol.L $^{-1}$ :0.6 mmol.L $^{-1}$ , pH = 3.0			
296	4.39	0.25	0.007
313	7.46	0.22	0.002
365	13.7	0.15	0.008
(d)Fe(III)-Cit = 0.3 mmol.L $^{-1}$ , pH = 3.0			
296	4.39	0.22	0.024
313	7.46	0.17	0.009
365	13.7	0.16	0.010

**D-2-2 Influence of oxygen on the quantum yields of Fe(II) and 2,4-D with different Fe(III)-Carboxylate complexes systems ( $\lambda_{\text{irr}}= 365\text{nm}$ )**

Oxygen plays a very important role in the photochemical process. Its effects on the quantum yield of Fe(II) formation and on the quantum yield of 2,4-D degradation were studied in this work. Different gas medium of reaction solutions were obtained by bubbling oxygen or argon 10 min into the solutions before irradiation. All the experiments were carried out in the presence of Fe(III)-Carboxylate complexes (Fe(III)-Tar, Fe(III)-Pyr and Fe(III)-Cit) at pH = 3.0 with monochromatic irradiation at 365 nm. Results are collected in Table IV-D-2. In deaerated solution, the quantum yield of 2,4-D is negligible, especially in the presence of Fe(III)-Cit and Fe(III)-Tar complexes. The quantum yield of Fe(II) formation in oxygenated solution is almost five times higher than those obtained in the absence of oxygen. In these experiments, the quantum yields of Fe(II) formation and 2,4-D disappearance were higher in the presence of Fe(III)-Pyr than with other complexes.

**Table IV-D-2 Quantum yields of disappearance of 2,4-D and generation of Fe(II) as a function of oxygen. The initial pH value was 3.0. ( $\lambda_{irr}=365\text{nm}$ )**

Different reaction systems Concentration in mmol.L <sup>-1</sup>	$\Phi_{\text{Fe(II)}}$			$\Phi_{2,4\text{-D}}$		
	Deaerated solution	Aerated solution	Oxygen saturated solution	Deaerated solution	Aerated solution	Oxygen saturated solution
[Fe(III)-Cit] = 0.3	0.041	0.16	0.23	0.001	0.010	0.014
[Fe(III)-Pyr] = 0.3:0.9	0.063	0.30	0.32	0.008	0.046	0.048
[Fe(III)-Tar] = 0.3:0.6	0.046	0.15	0.22	0.001	0.008	0.014

It can be concluded that oxygen has a strong effect on the reaction. Oxygen enhance the photoredox process involving Fe(III)-Carboxylate complexes, thus, more Fe(II) and reactive species ( $\cdot\text{OH}$  radicals) are generated in the reaction. Moreover, in the absence of oxygen, necessary to form the reactive species, 2,4-D degradation is strongly inhibited.

**D-2-3 Influence of pH on the quantum yields of Fe(II) and 2,4-D in different Fe(III)-Carboxylate complexes systems ( $\lambda_{irr}= 365 \text{ nm}$ )**

As we have seen before, the pH is also a very important parameter in the photochemical reaction with Fe(III)-complexes. All of the reactions were carried out under monochromatic irradiation at 365 nm. In the experiments, the concentration of Fe(III)-Cit was 0.3 mmol.L<sup>-1</sup>, Fe(III)/Tar was 0.3 mmol.L<sup>-1</sup>/0.6 mmol.L<sup>-1</sup>, Fe(III)/Pyr was 0.3 mmol.L<sup>-1</sup>/0.9 mmol.L<sup>-1</sup> and 2,4-D was 0.1 mmol.L<sup>-1</sup>. The pH values of the solutions were changed from 2.0 to 5.0. Results about the quantum yields of Fe(II) are presented in Figure IV-D-4. In these cases, the higher quantum yields of Fe(II) were obtained at pH 3.0 in all the systems. Fe(III)-Pyr presents the higher quantum yield of Fe(II) formation  $\Phi_{\text{Fe(II)}} = 0.295$ .

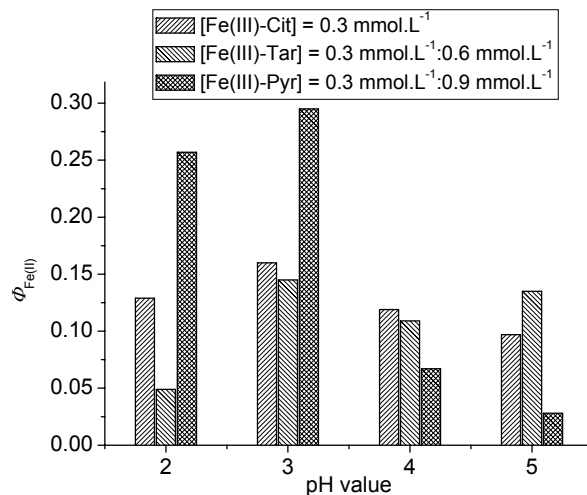


**Figure IV-D-4 pH effect on the quantum yields of Fe(II) formation in the presence of 0.1 mmol.L<sup>-1</sup> of 2,4-D. ( $\lambda_{irr} = 365$  nm)**

The pH effect on the quantum yields of 2,4-D disappearance was also studied. Results are shown in Table IV-D-3. According to the values in Table IV-D-3, the quantum yields of 2,4-D disappearance were decreased with the increase of the pH value. It can be concluded that acidic condition is more favourable for the degradation of 2,4-D in the presence of Fe(III)-carboxylate complexes. The quantum yields of 2,4-D disappearance were optimal at pH 3.0 in the presence of Fe(III)-Pyr complexes ( $\Phi_{2,4-D} = 0.046$ ).

**Table IV-D-3 Quantum yields of disappearance of 2,4-D as a function of pH. In the aqueous solutions with 0.1 mmol.L<sup>-1</sup> 2,4-D. ( $\lambda_{irr} = 365$  nm)**

pH	$\Phi_{2,4-D}$		
	Fe(III)-Cit	Fe(III)-Tar	Fe(III)-Pyr
2.0	0.008	0.009	0.044
3.0	0.010	0.008	0.046
4.0	0.013	0.002	0.001
5.0	0.008	0.005	0.007

**D-2-4 Influence of 2, 4-D concentration on the quantum yields of Fe(II) and 2,4-D with different Fe(III)-Carboxylate complexes ( $\lambda_{irr}= 365 \text{ nm}$ )**

Effects of 2,4-D concentration on the quantum yields of Fe(II) and 2,4-D was studied in the solutions with  $0.3 \text{ mmol.L}^{-1}$  Fe(III)-Carboxylate complexes (Fe(III)-Cit, Fe(III)-Pyr and Fe(III)-Tar). Monochromatic irradiation was 365 nm. The solutions were adjusted to pH 3.0. The concentration of 2,4-D were 0, 0.02, 0.04, 0.08 and 0.10  $\text{mmol.L}^{-1}$ . Quantum yields of Fe(II) formation are presented in Figure IV-D-5, which shows a tendency that with the increase of the 2,4-D concentration, the  $\Phi_{\text{Fe(II)}}$  increases. The presence of 2,4-D enhanced the quantum yields of Fe(II) in all the systems. The values of  $\Phi_{\text{Fe(II)}}$  are in the following order Fe(III)-Pyr > Fe(III)-Cit ~ Fe(III)-Tar. Photolysis of Fe(III)-Carboxylate complexes can form Fe(II) and generate reactive species, which quickly can react with the pollutant. Thus, in the low concentration of pollutant  $\cdot\text{OH}$  radicals can react on the Fe(II) formed giving rise Fe(III). This reaction can explain the fact that the quantum yield of Fe(II) increases with the increase of the 2,4-D concentration. This phenomenon is more evident with Fe(III) aquacomplexes where no other organic compounds are present in solution (Christensen and Sehested, 1988 and Mestankova et al., 2004).



As evidenced by the values in Figure IV-D-6, the quantum yields of 2,4-D disappearance increases with the increase of 2,4-D concentration in all the cases. The value of  $\Phi_{2,4-D}$  are also in the following order Fe(III)-Pyr > Fe(III)-Cit ~ Fe(III)-Tar, identical to that of  $\Phi_{\text{Fe(II)}}$ . High concentrations of 2,4-D can increase the probability of reaction with the radical species photogenerated in the reaction.



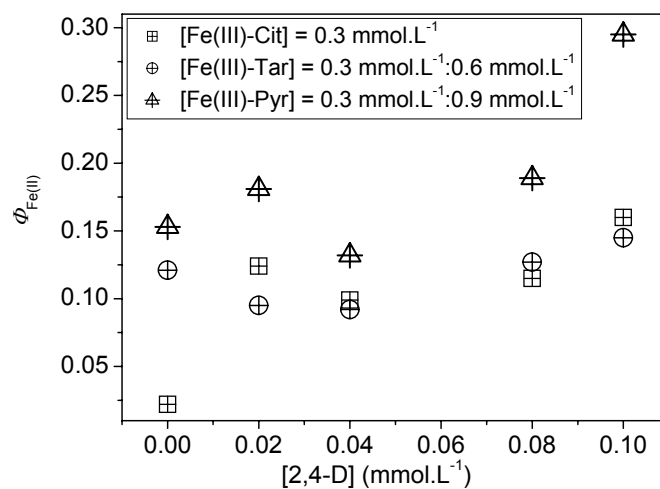


**Figure IV-D-5 Effects of 2,4-D concentration on the quantum yields of Fe(II) formation. The initial pH of the aqueous solutions is 3.0. ( $\lambda_{\text{irr}}=365\text{nm}$ )**

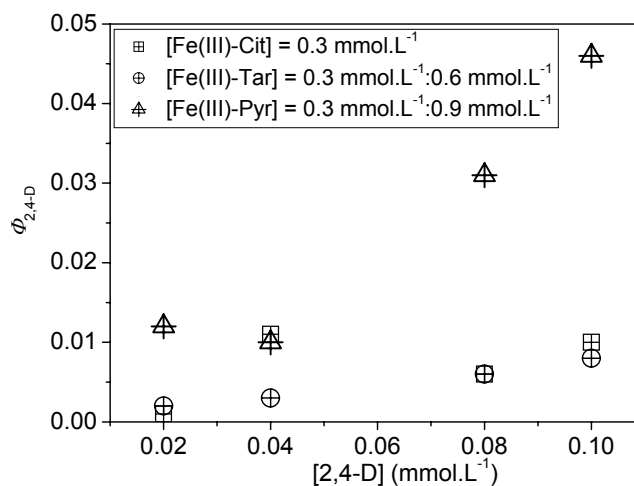


**Figure IV-D-6 Effects of 2,4-D concentration on the quantum yields of 2,4-D disappearance. The initial pH of the aqueous solutions is 3.0. ( $\lambda_{\text{irr}} = 365 \text{ nm}$ )**

These results show that in such system there a competition for the reactivity of OH radicals between the pollutant (2,4-D), the organic ligands of the complex (Citric, tartaric and pyruvic acids) and Fe(II).

## **D-3-Photodegradation of 2,4-D at 365 nm in the presence of Fe(III)-Carboxylate complexes**

### **D-3-1 Degradation of 2,4-D photoinduced by Fe(III)-Cit complex**

The photodegradation of 2,4-D was studied in the presence of Fe(III)-Cit complexes. Irradiation was with polychromatic tubes emitting between 300 and 500 nm. Concentration of complex, pH and oxygen were all studied in this work.

#### **D-3-1-1 Effect of Fe(III)-Cit concentration**

Fe(III)-Cit concentration effect on the photodegradation of 2,4-D was studied in the aqueous solution with  $0.1 \text{ mmol.L}^{-1}$  of 2,4-D at pH 3.0. The initial concentration of Fe(III)-Cit complex used in the work were 0.1, 0.2 and  $0.3 \text{ mmol.L}^{-1}$ . Figure IV-D-7 presents the photodegradation efficiency of 2,4-D. The disappearance of 2,4-D increase with the increase of Fe-Cit complex concentration. The reaction is very fast in the initial period, After 1 h of irradiation, 60% of the 2,4-D has been degraded in the solution with  $0.3 \text{ mmol.L}^{-1}$  of Fe(III)-Cit complex, 45% with  $0.2 \text{ mmol.L}^{-1}$ , and only 30% with  $0.1 \text{ mmol.L}^{-1}$  of Fe(III)-Cit complex. Then the systems keep the ability to degrade 2,4-D with slower reaction rate. After 8 h of irradiation, the photodegradation efficiency of 2,4-D have reached 80%, 63% and 38% in the solutions with 0.3, 0.2 and  $0.1 \text{ mmol.L}^{-1}$  of Fe(III)-Cit complexes respectively.

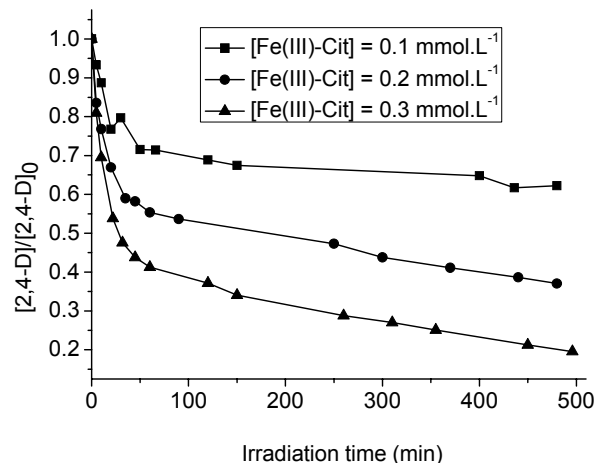


**Figure IV-D-7 Degradation of 2,4-D as a function of Fe-Cit concentration in solution with an initial pH = 3.0.  $[2,4-D]_0 = 0.1 \text{ mmol.L}^{-1}$ .**

During the reaction process, Fe(III) was reduced to Fe(II) species. Thus, the concentration of Fe(II) was also detected at the same time. Figure IV-D-8 presents the results, which indicate that the Fe(III) was reduced very fast at the beginning, more than 90% of Fe(III) has been reduced to Fe(II) after 30 min of irradiation. After that the photochemical process continues with a stable concentration of Fe(II) species. There is no significant variation of the concentration of Fe(II) from 1 h to 8 h of irradiation in all the conditions. The concentration of Fe(II) represents between 89% to 97% of the total iron concentration after 8 h of irradiation.

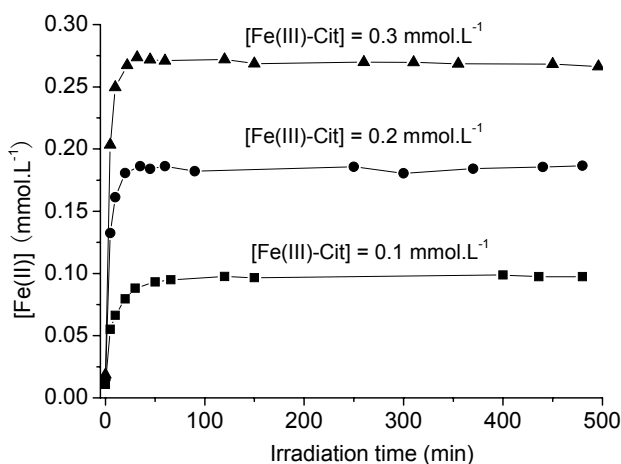


**Figure IV-D-8 Photogeneration of Fe(II) as a function of Fe(III)-Cit concentration in solution with an initial pH = 3.0.  $[2,4-D]_0 = 0.1 \text{ mmol.L}^{-1}$ .**

### D-3-1-2 Effect of oxygen

Oxygen is a very important parameter in the reaction. A lot of experiments have proved its effects on the photodegradation of pollutants in the previous study. Experiments were performed in the solutions with  $0.1 \text{ mmol.L}^{-1}$  of Fe(III)-Cit complex and  $0.1 \text{ mmol.L}^{-1}$  of 2,4-D at pH 3.0. Different reaction medium was obtained by bubbling oxygen or argon into the solutions before irradiation. Results are presented in Figure IV-D-9. Oxygen has again a strong effect on the photodegradation of 2,4-D. In the oxygen saturated condition, the photodegradation efficiency of 2,4-D is higher than in the air saturated and deaerated conditions. At the beginning of the reaction, the degradation rate is also faster in the oxygen saturated condition than in the other conditions. The photodegradation efficiencies of 2,4-D after 7 h of irradiation are 70% in the oxygen saturated solution, 40% in the air saturated solution and 25% in the deaerated solution.

Like with 2,4-DCP, 2,4-D is slightly degraded in the absence of oxygen. The first radical species are capable to react with 2,4-D to induced is degradation without the interaction of oxygen.

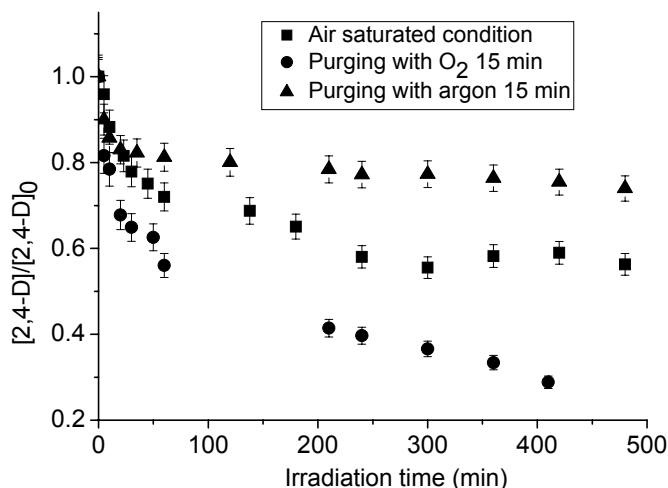


**Figure IV-D-9 Degradation of 2,4-D as function of oxygen in solutions with an initial pH = 3.0.  $[\text{Fe-Cit}]_0 = 0.1 \text{ mmol.L}^{-1}$ ,  $[\text{2,4-D}]_0 = 0.1 \text{ mmol.L}^{-1}$ .**

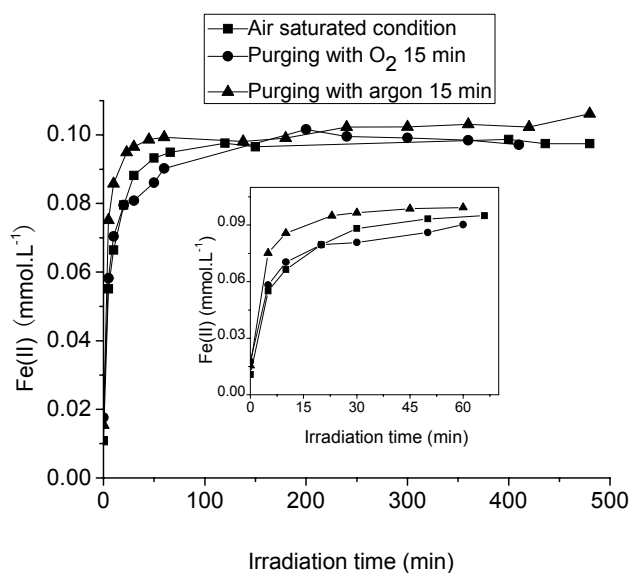


**Figure IV-D-10 Photogeneration of Fe(II) as function of oxygen in solutions with an initial pH = 3.0.  $[\text{Fe-Cit}]_0 = 0.1 \text{ mmol.L}^{-1}$ ,  $[\text{2,4-D}]_0 = 0.1 \text{ mmol.L}^{-1}$ .**

Oxygen effects on the formation of Fe(II) was studied in the same reaction. Figure IV-D-10 presents the results. The formation of Fe(II) is very fast at the beginning of the reaction. Oxygen presents a slight negative effect on the formation of Fe(II) before 60 min of irradiation. However we can conclude that it does not appear any significant effect of oxygen on Fe(II) formation.

### **D-3-1-3 Effect of pH**

Experiments were carried in the solution with  $0.3 \text{ mmol.L}^{-1}$  of Fe(III)-Cit complex and  $0.1 \text{ mmol.L}^{-1}$  of 2,4-D. With the increase of pH, the photodegradation efficiency of 2,4-D decreased. The optimal photodegradation process of 2,4-D was obtained at pH 3.0. As shown in Figure IV-D-11, the photodegradation rate is fast before 1 h of irradiation in all pH values and then the degradation continues with a slower rate. At pH 5.7, no further degradation of 2,4-D occurred and only 26% of 2,4-D was degraded after 8 h of irradiation. The photodegradation efficiency is about 80% at pH 3.0 and 56% at pH 3.65 after 8 h of irradiation.

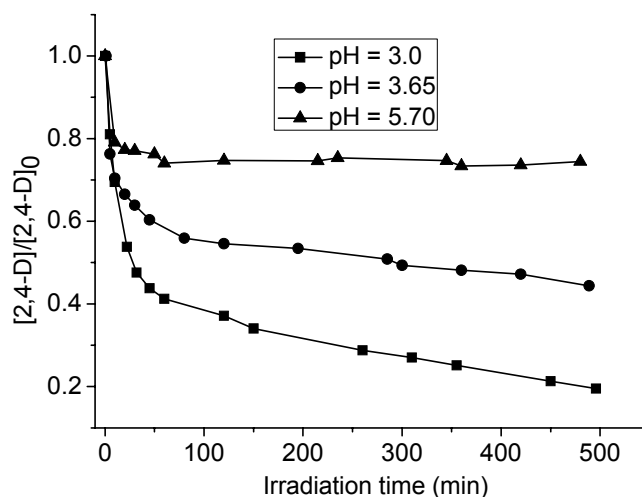


**Figure IV-D-11 Influence of pH on the photodegradation of 2,4-D in the presence of Fe(III)-Cit complexes.  $[\text{Fe(III)-Cit}]_0 = 0.3 \text{ mmol.L}^{-1}$ ,  $[\text{2,4-D}]_0 = 0.1 \text{ mmol.L}^{-1}$ .**

Fe(II) formation was strongly affected by the pH (Figure IV-D-12). Especially at relative higher pH 5.7, the formation of Fe(II) was obviously lower, the maximum concentration of Fe(II) corresponded to only 50% of total Fe in the aqueous solution after 60 min of irradiation. This value decreased to 30% after 6 h of irradiation. The lower the concentration of Fe(II) formed, the lower the formation of radicals species was and thus, the photodegradation ratio of 2,4-DCP was low at higher pH.

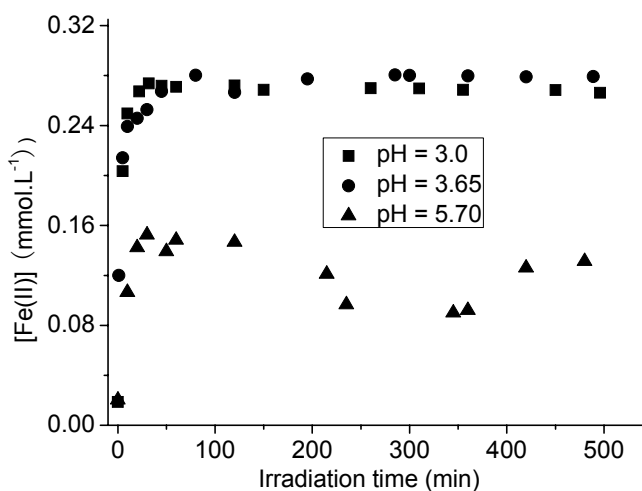


**Figure IV-D-12 Influence of pH on the photogeneration of Fe(II) in the presence of Fe-Cit complexes.  $[\text{Fe(III)-Cit}]_0 = 0.3 \text{ mmol.L}^{-1}$ ,  $[\text{2,4-D}]_0 = 0.1 \text{ mmol.L}^{-1}$ .**

## D-3-2 Degradation of 2,4-D photoinduced by Fe(III)-Pyr complex

### D-3-2-1 Effect of Fe(III)-Pyr concentration

Fe(III)-Pyr concentration effect on the photodegradation of 2,4-D in the aqueous solution was studied with  $0.1 \text{ mmol.L}^{-1}$  of 2,4-D at pH 3.0 under polychromatic irradiation (300-500 nm). Three different concentrations of Fe(III)-Pyr complex were tested ( $0.1$ ;  $0.2$  and  $0.3 \text{ mmol.L}^{-1}$ ). Irradiation time was 8 h in all the experiments. From the results in Figure IV-D-13, the same conclusion was obtained; the photodegradation efficiency of 2,4-D increased with the increase of Fe(III)-Pyr complex concentration. The reaction is fast in the initial period, After 1 h of irradiation, 74% of the 2,4-D has been degraded in the solution with  $0.3 \text{ mmol.L}^{-1}$  in Fe(III)-Pyr complex, 60% in the presence of  $0.2 \text{ mmol.L}^{-1}$  of Fe(III)-Pyr, 47% and for  $0.1 \text{ mmol.L}^{-1}$  in Fe(III)-Pyr solution. Then the reaction becomes slow. After 8 h of irradiation, the photodegradation efficiency of 2,4-D have reached 98%, 90% and 75% with  $0.3$ ,  $0.2$  and  $0.1 \text{ mmol.L}^{-1}$  Fe(III)-Pyr complexes respectively.

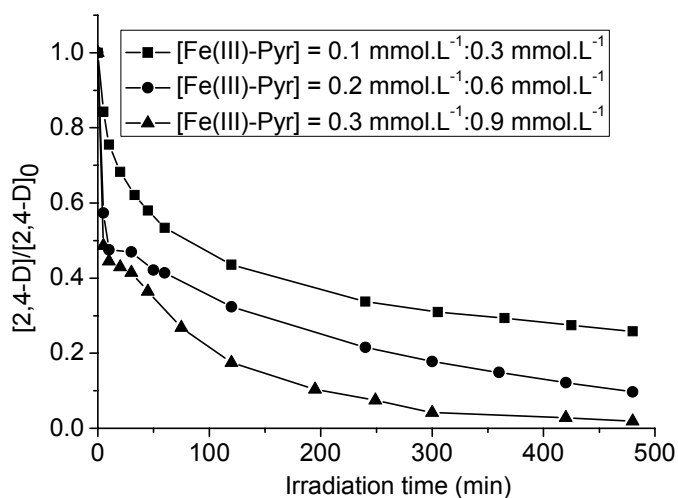


**Figure IV-D-13 Degradation of 2,4-D as a function of Fe(III)-Pyr concentration with an initial pH = 3.0.  $[2,4-D]_0 = 0.1 \text{ mmol.L}^{-1}$ .**

The concentration of Fe(II) was also detected in the these experiments. Results are presented in Figure IV-D-14. Fe(III) was reduced very fast and it has been

approximately totally reduced to Fe(II) after 30 min of irradiation. After that the reaction continues and the concentration of Fe(II) species keep stable. There is no apparent variation of the concentration of Fe(II) from 1 h to 8 h of irradiation whatever the concentration in Fe(III)-pyruvate complex.

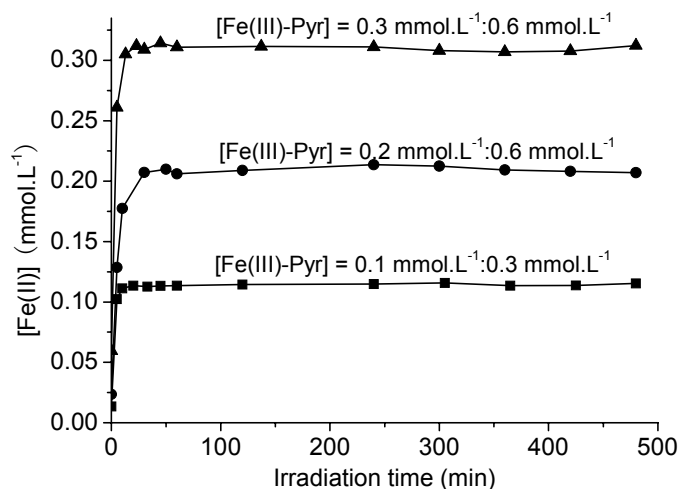


**Figure IV-D-14 Photogeneration of Fe(II) as a function of Fe(III)-Pyr concentration with an initial pH = 3.0. [2,4-D]<sub>0</sub> = 0.1 mmol.L<sup>-1</sup>.**

The spectra of the solutions as a function of the irradiation times are presented in the Figure IV-D-15. The solution is a mixture of 0.1 mmol.L<sup>-1</sup> of 2,4-D and (a) 0.1 mmol.L<sup>-1</sup> of Fe(III)-Pyr or (b) 0.2 mmol.L<sup>-1</sup> Fe(III)-Pyr, the pH = 3.0. There is a sharp decrease after 5 min of irradiation in both conditions. This observation is due to the very efficient photoredox process taking place in the Fe(III)-complex under irradiation. The absorbance of complex from 300 to 500 nm decreased. It is in agreement with the fact that the Fe(II) formation, resulting from the photoredox process, is very fast at the beginning of the irradiation.



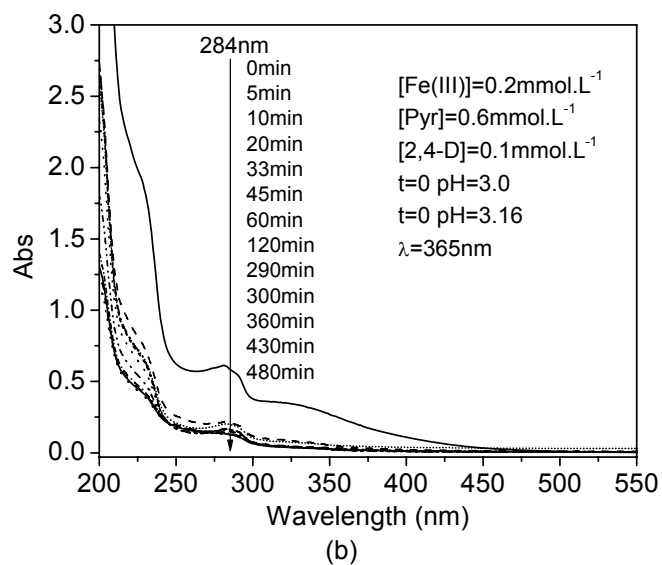
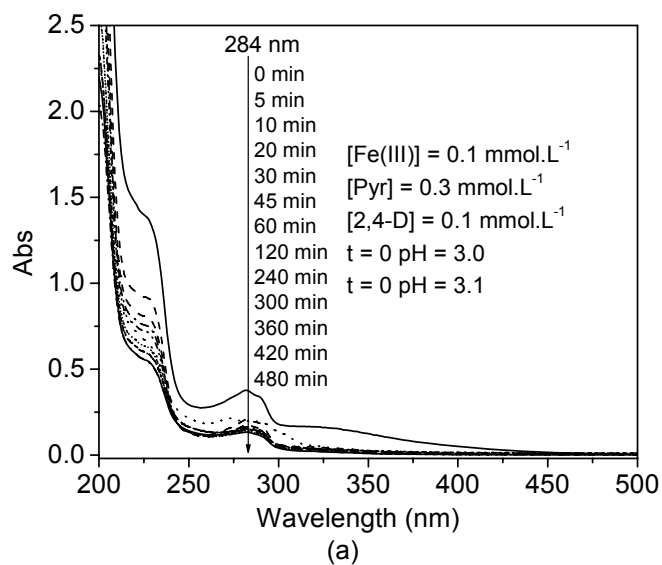


**Figure IV-D-15** UV-visible spectrum of the solutions as a function of the irradiation time. (a) [Fe(III)-Pyr] = 0.1 mmol.L<sup>-1</sup>/0.3 mmol.L<sup>-1</sup>, (b) [Fe(III)-Pyr] = 0.2 mmol.L<sup>-1</sup>/0.6 mmol.L<sup>-1</sup>

### D-3-2-2 Effect of oxygen

Oxygen effects on the photodegradation of pollutants was performed in the solutions with 0.1 mmol.L<sup>-1</sup> of Fe(III)-Pyr complex and 0.1 mmol.L<sup>-1</sup> of 2,4-D at pH = 3.0. Different reaction medium was obtained by bubbling oxygen or argon into the

solutions before irradiation. Figure IV-D-16 shows the experiment results. Oxygen can enhance the photodegradation of 2,4-D in the presence of Fe(III)-Pyr complex. In the oxygen rich condition, the photodegradation efficiency of 2,4-D is higher than in the air saturated and deaerated conditions. The oxygen also accelerated the photoreaction rate. At the beginning of the reaction, the degradation rate is faster in the oxygen rich condition than the other conditions. The photodegradation efficiency of 2,4-D are 68% in the oxygen saturated solution, 47% in the air saturated solution and 22% in the deaerated solution after 1 h of irradiation.

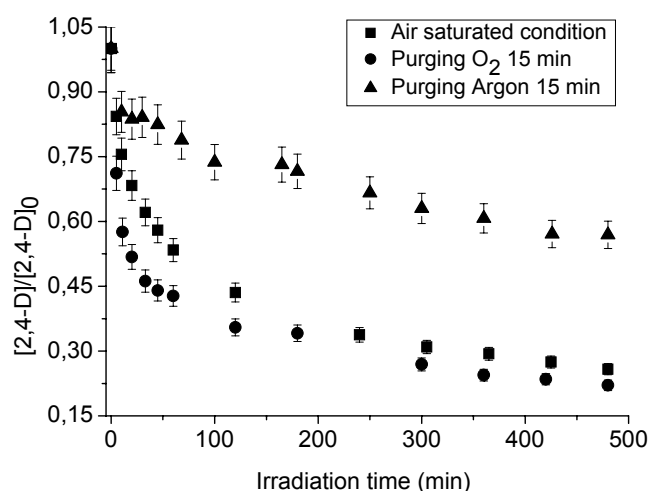


**Figure IV-D-16 Degradation of 2,4-D as function of oxygen in solutions with an initial pH = 3.0.  $[\text{Fe(III)-Pyr}]_0 = 0.1 \text{ mmol.L}^{-1}$ ,  $[\text{2,4-D}]_0 = 0.1 \text{ mmol.L}^{-1}$ .**

Oxygen effects on the formation of Fe(II) was also studied at the same time. The same results, than for Fe(III)-Cit complex are observed. No significant effect of oxygen is observed on the formation of Fe(II).

### **D-3-2-3 Effect of pH**

Experiments were carried to study the pH effect in the solution with 0.1 mmol.L<sup>-1</sup> of Fe(III)-Pyr complex and 0.1 mmol.L<sup>-1</sup> of 2,4-D. Results are presented in Figure IV-D-18. As always, pH presents a strong effect on the photodegradation of 2,4-D and the optimal photodegradation ratio of 2,4-D was obtained at pH = 3.0. 74%

of 2,4-D was degraded after 8 h of irradiation. As shown in Figure IV-D-18, the photodegradation rate is faster at low pH values. As I mentioned before, acidic condition is favorable for the reaction. The photodegradation efficiency is very low at pH 5.6 and 4.5 and only 10% to 15% of 2,4-D are degraded after 8 h of irradiation.

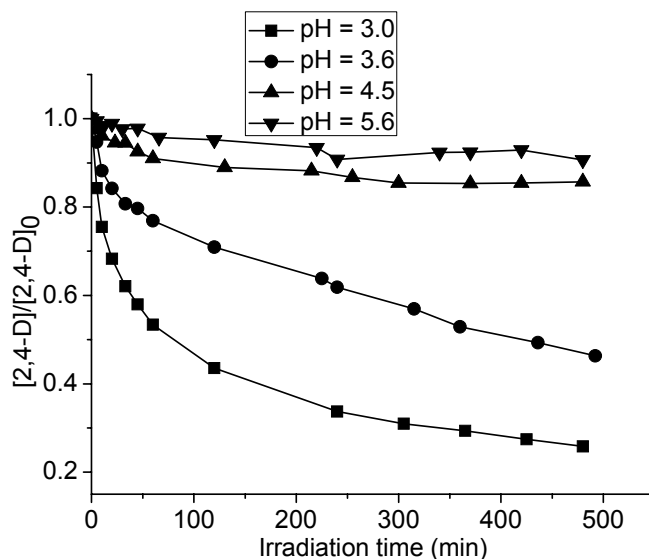


**Figure IV-D-17 Influence of pH on the photodegradation of 2,4-D in the presence of Fe(III)-Pyr complexes.  $[\text{Fe(III)-Pyr}]_0 = 0.1 \text{ mmol.L}^{-1}$ ,  $[\text{2,4-D}]_0 = 0.1 \text{ mmol.L}^{-1}$ .**

As shown in Figure IV-D-18, The formation rate and the concentration of Fe(II) are all obviously affected by the pH. At lower pH, Fe(III) species are very fast reduced to Fe(II). At pH 3.0, Fe(III) is approximately totally reduced to Fe(II) after 5 min of irradiation. The reduction efficiency represents only 80% at pH 4.5 and 56% at pH 5.6 after 1 h of irradiation. From 1 h to 8 h of irradiation, there is no further significant evolution of Fe(II) concentration.

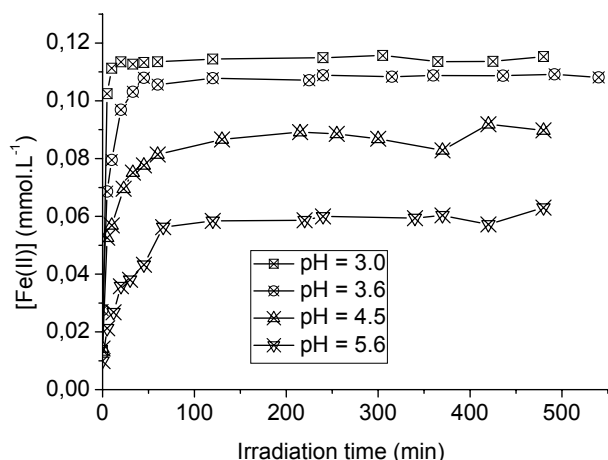


**Figure IV-D-18 Influence of pH on the photogeneration of Fe(II) in the presence of Fe(III)-Pyr complexes.  $[\text{Fe(III)-Pyr}]_0 = 0.1 \text{ mmol.L}^{-1}$ ,  $[\text{2,4-D}]_0 = 0.1 \text{ mmol.L}^{-1}$ .**

Figure IV-D-19 presents the UV-visible spectra of the solutions at different complex concentrations and pH as a function of the irradiation time. Figure IV-D-19 presents the spectra with higher concentration of Fe(III)-Pyr complexes ( $0.3 \text{ mmol.L}^{-1}$ ) at pH 3.9. The absorbance of the solution decreases with the increase of the irradiation time. The pH was increased to 5.8 after 437 min of irradiation.  $\text{H}^+$  is consumed during the photoredox process; hydroxyl radicals and other radical species are formed at the same time and attack the pollutant making its absorption decreasing.

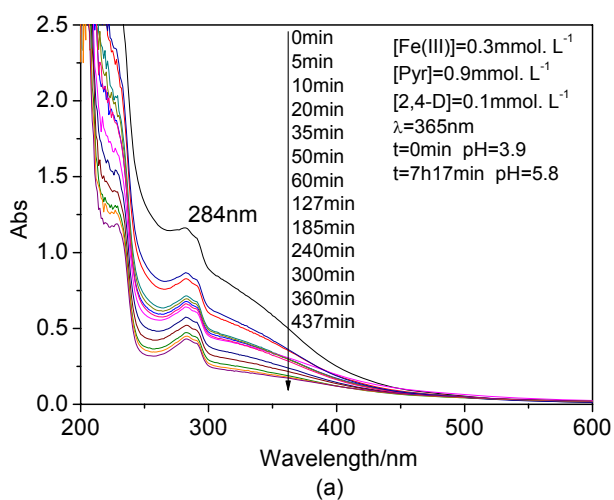


**Figure IV-D-19 UV-visible spectrum as a function of the irradiation time.  $[\text{Fe(III)-Pyr}] = 0.3 \text{ mmol.L}^{-1}/0.9 \text{ mmol.L}^{-1}$ , pH = 3.9.**

### D-3-3 Degradation of 2,4-D photoinduced by Fe(III)-Tar complex

#### D-3-3-1 Effects of Fe(III)-Tar concentration

Fe(III)-Tar concentration effect was studied in the solution with  $0.1 \text{ mmol.L}^{-1}$  of 2,4-D, with an initial pH value at 3.0 and under polychromatic irradiation (300-500 nm). The concentrations of Fe(III)-Tar complex are 0.1, 0.2 and 0.3  $\text{mmol.L}^{-1}$ . The results presented Figure IV-D-20, show that the degradation of 2,4-D is not strongly affected by the concentration of Fe(III)-Tar complex, a slight better efficiency is observed at higher concentration. After 6 h of irradiation, the 2,4-D has been totally degraded in the presence of 0.2 and 0.3  $\text{mmol.L}^{-1}$  of iron-complexes and more than 90% is degraded with 0.1  $\text{mmol.L}^{-1}$  of this complex. With the other Fe(III)-complexes (Cit and Pyr) the effect of Fe(III)-complex concentration is much more important.

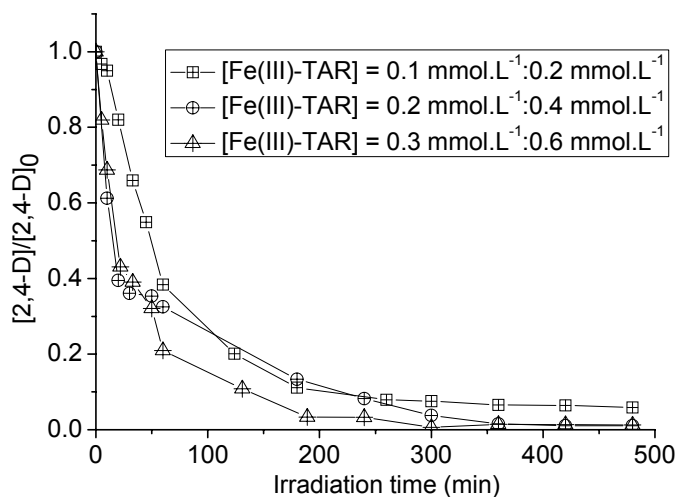


**Figure IV-D-20 Degradation of 2,4-D as a function of Fe(III)-Tar concentration with an initial pH = 3.0.  $[2,4-D]_0 = 0.1 \text{ mmol.L}^{-1}$ .**

Figure IV-D-21 presents the results about the photogeneration of Fe(II) in these experiments. Fe(III) has been totally reduced to Fe(II) after 10 min of the irradiation. The concentration of Fe(II) keeps stable in the following reaction. The important

formation of Fe(II) can be a good parameter for the Fenton reaction. This point will be discussed later in the conclusion/discussion part.

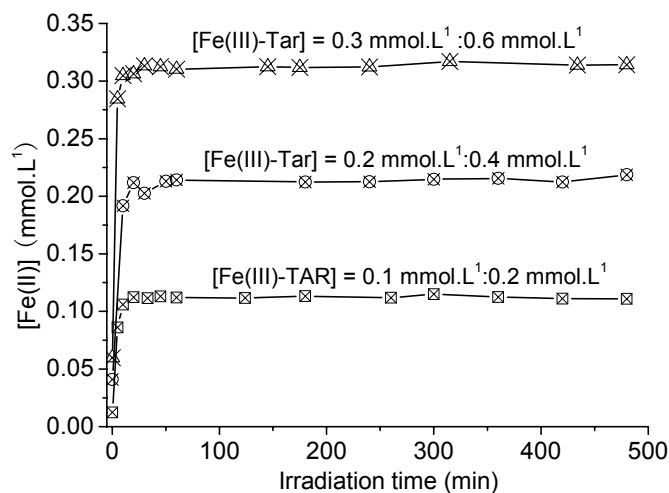


**Figure IV-D-21 Photogeneration of Fe(II) as a function of Fe-Tar concentration in solution with an initial pH = 3.0. [2,4-D]<sub>0</sub> = 0.1 mmol.L<sup>-1</sup>.**

The UV-visible spectra of the solution with 0.3 mmol.L<sup>-1</sup> of Fe(III)-Tar and 0.1 mmol.L<sup>-1</sup> of 2,4-D at pH 3.0 as a function of irradiation time are presented in Figure IV-D-22. There is a sharp decrease in 5 min of irradiation. It means that as we mentioned before, the photoredox of the complex is very fast at pH = 3.0. It can be seen from the decrease of the absorbance from 300 to 500 nm. This decrease of absorbance is attributed both to the degradation of the complex and of the pollutant 2,4-D.

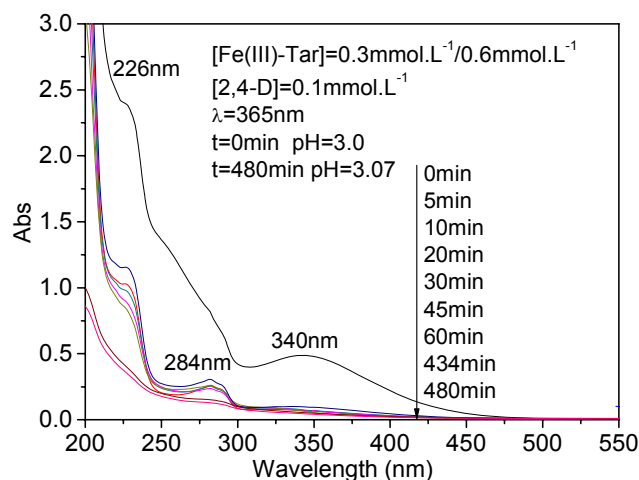


Figure IV-D-22 UV-visible spectra of the solutions as a function of the irradiation time.  
 $[\text{Fe(III)-Tar}] = 0.3 \text{ mmol.L}^{-1}/0.6 \text{ mmol.L}^{-1}$ ,  $\text{pH} = 3.0$ .

### D-3-3-2 Effect of pH

pH effect on the reaction was studied in the solution with  $0.1 \text{ mmol.L}^{-1}$  of Fe(III)-Tar complex and  $0.1 \text{ mmol.L}^{-1}$  of 2,4-D. The results presented in Figure IV-D-23 show that the pH has a strong effect on the photodegradation reaction. The optimal photodegradation efficiency of 2,4-D is obtained at pH 3.0. After 8 h of irradiation, 94% 2,4-D is degraded at pH 3.0, 82% at pH 3.5, but only 15% at pH 5.8.

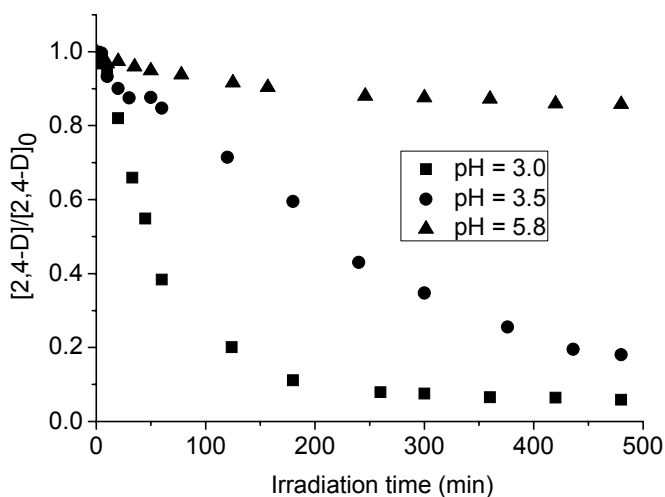
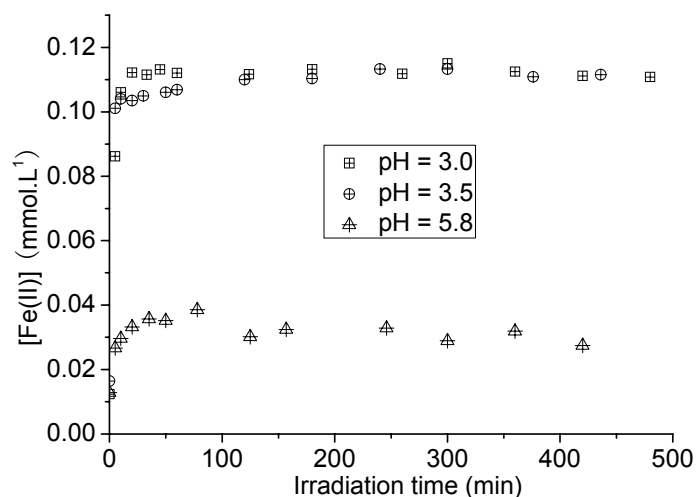


Figure IV-D-23 Influence of pH on the photodegradation of 2,4-D in the presence of Fe-Tar complexes.  $[\text{Fe(III)-Tar}]_0 = 0.1 \text{ mmol.L}^{-1}$ ,  $[\text{2,4-D}]_0 = 0.1 \text{ mmol.L}^{-1}$ .



**Figure IV-D-24 Influence of pH on the photogeneration of Fe(II) in the presence of Fe(III)-Tar complexes.  $[\text{Fe(III)-Tar}]_0 = 0.1 \text{ mmol.L}^{-1}$ ,  $[\text{2,4-D}]_0 = 0.1 \text{ mmol.L}^{-1}$ .**

At low pH 3.0 and 3.5, Fe(III) is totally reduced to Fe(II) species very quickly (after 10 min of irradiation). However at higher pH 5.8, the maximum concentration of Fe(II) represents only 38% of total iron in the aqueous solution after 80 min of irradiation. The Fe(II) represents only 27% of total iron after 8 h of irradiation.

The UV-visible spectra of the solution with  $0.1 \text{ mmol.L}^{-1}$  of Fe(III)-Tar and  $0.1 \text{ mmol.L}^{-1}$  of 2,4-D at pH 3.0 as a function of irradiation time are presented in Figure IV-D-25. There is a sharp decrease of the absorbance, all along the spectrum, after 5 min of irradiation already observed with the Fe(III)-Tar complexes. These important decrease reflects that the photoredox process in the Fe(III)-Tar complex is very fast at the beginning. As a consequence the degradation of 2,4-D is also very fast at the beginning of the irradiation as shown in figure IV-D-20.



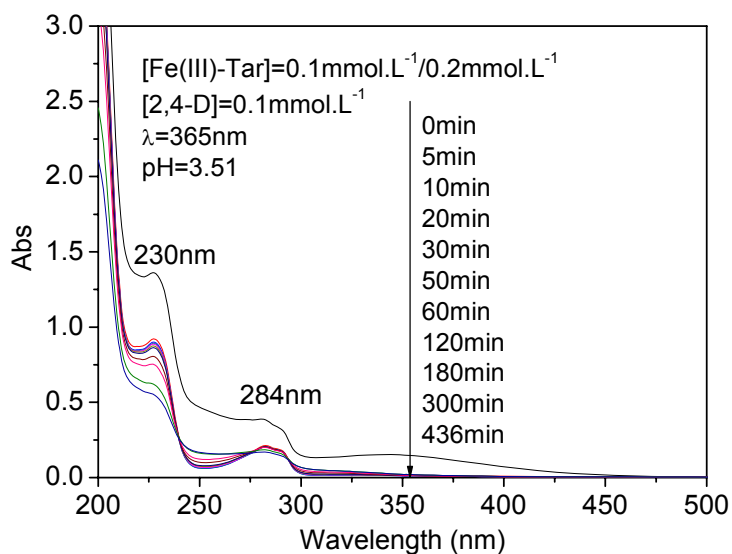


**Figure IV-D-25 UV-visible spectrum of the solutions according to the time.**  
 $[\text{Fe(III)-Tar}] = 0.1 \text{ mmol.L}^{-1}/0.2 \text{ mmol.L}^{-1}$ ,  $\text{pH} = 3.5$

### **D-3-3 Comparison of the photodegradation of 2,4-D with different complexes**

The photochemical properties of Fe(III)-Carboxylate complexes have been systemically studied in the presence of 2,4-D. It is necessary to compare the photoreaction efficiency of Fe(II) formation and 2,4-D degradation in the presence of the different iron-complexes. Results about the photodegradation efficiency of 2,4-D are presented in the Figure IV-D-26. The efficiency of Fe(III) complexes to degrade 2,4-D is in the order of  $\text{Fe(III)-Cit} < \text{Fe(III)-Tar} < \text{Fe(III)-Pyr}$  before 45 min of irradiation. After 1 h of irradiation, the photodegradation efficiency is changed into another order that is  $\text{Fe(III)-Cit} < \text{Fe(III)-Pyr} < \text{Fe(III)-Tar}$ .

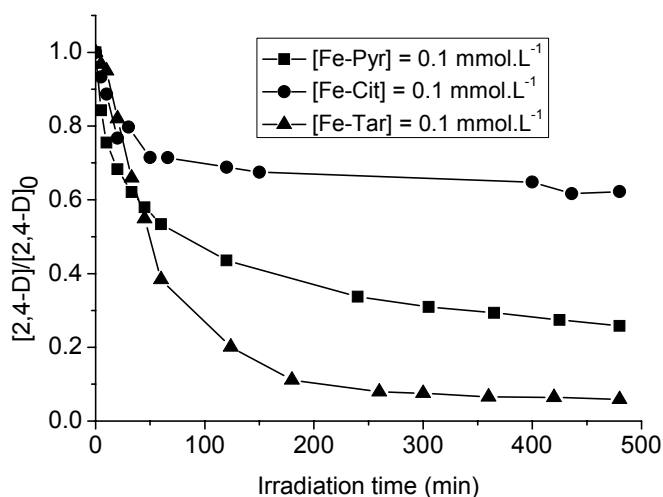


**Figure IV-D-26 Photodegradation of 2,4-D with different complexes.**  
**[2,4-D] = 0.1 mmol.L<sup>-1</sup>, pH = 3.0**

Figure IV-D-27 presents the formation of Fe(II) species with different complexes. Fe(III) is reduced very fast in the solutions with Fe(III)-Tar or Fe(III)-Pyr, and after 10 min of irradiation approximately all Fe(III) species are reduced. However, in the solution with Fe(III)-Cit, 94% of Fe(III) are reduced to Fe(II) after 1 h of irradiation. This result is correlated with a relative low photodegradation efficiency of 2,4-D in the presence of Fe(III)-Cit complexes.

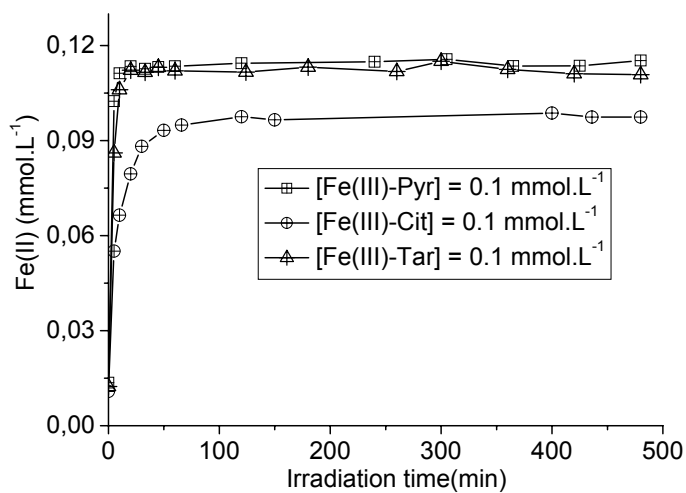


**Figure IV-D-27 Photogeneration of Fe(II) with different iron-complexes.**  
**[2,4-D] = 0.1 mmol.L<sup>-1</sup>, pH = 3.0**

### D-3-4 Total organic carbon analysis

One of the aims of the work is study the efficiency of 2,4-D disappearance in the solution, when the degradation was photoinduced by Fe(III) complexes. Total organic carbon experiments were undertaken in order to make evidence for the mineralization of the pollutants. From the results in Figure IV-D-28, the concentration of TOC decreases when the irradiation times increases. It appears that oxygen favors the mineralization process like the degradation of the starting pollutant. These observation are in agreement with the previous results obtained with 2,4-DCP.

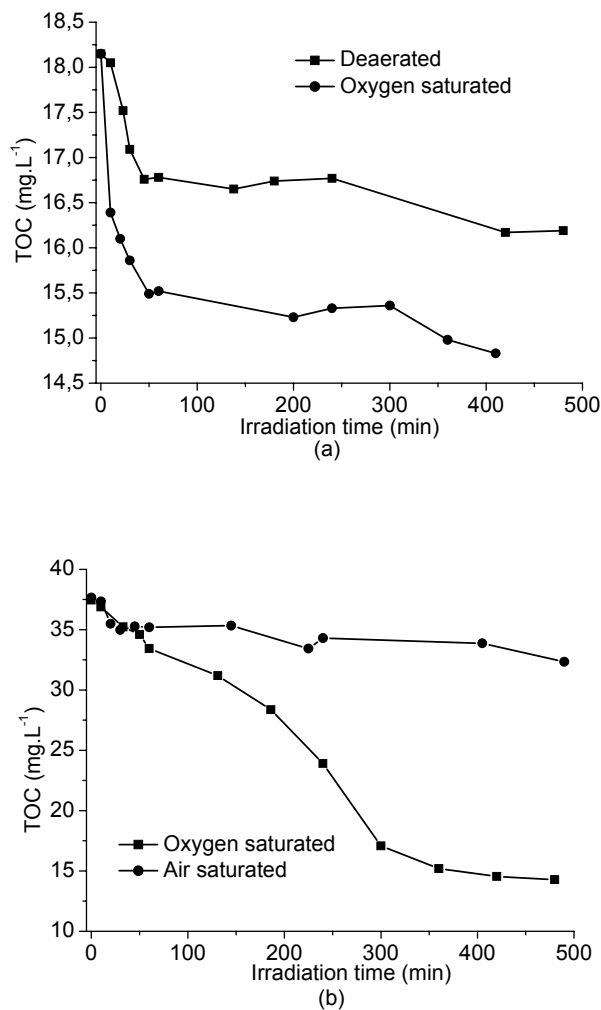


**Figure IV-D-28 Evolution of total organic carbon as function of oxygen concentration. (a) Mixture of 0.1 mmol.L<sup>-1</sup> in Fe(III)-Cit and 0.1 mmol.L<sup>-1</sup> in 2,4-D, (b) mixture of 0.3 mmol.L<sup>-1</sup> in Fe(III)-Tar and 0.1 mmol.L<sup>-1</sup> in 2,4-D, pH = 3.0.**

Total organic carbon experiments were also undertaken in the solutions with different pH. As shown in Figure IV-D-29, the higher mineralization efficiency of pollutant was obtained at lower pH = 3.0. It is correlated with the result that the optimal photodegradation efficiency of 2,4-D is also at pH = 3.0.

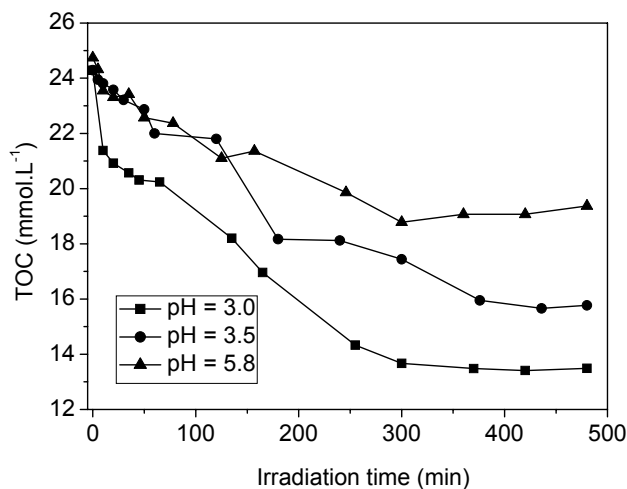


**Figure IV-D-29 Evolution of total organic carbon in the solution with 0.1 mmol.L<sup>-1</sup> in Fe(III)-Tar and 0.1 mmol.L<sup>-1</sup> in 2,4-D as function of pH.**

In the solutions and after the photoredox process, different kind of organic substances are present. The decrease of the TOC concentration can be partly attributed to the degradation of 2,4-D but also to the transformation of the organic ligands. During the irradiation process, high reactivity radicals were generated by the photoredox process of the Fe(III) complexes and these radicals can attack 2,4-D and its degradation products but also Fe(III)-complexes and the transformation products of the organic ligands.

## Conclusions

Degradation of 2,4-D photoinduced by Fe(III)-Carboxylate complexes were investigated in this study. Results indicate that irradiation wavelength, pH, oxygen, concentrations of Fe(III)-Carboxylate complexes and 2,4-D, all have effect on the quantum yields of Fe(II) formation and 2,4-D degradation.

Irradiation wavelength has a great effect on the quantum yields, both  $\Phi_{\text{Fe(II)}}$  and  $\Phi_{2,4\text{-D}}$  increase with the decrease of wavelength of irradiation in the different reaction systems. The low pH and high concentration of oxygen are all favorable for the photodegradation of 2,4-D. In the presence of high concentration in oxygen and at pH 3.0 the total degradation of 2,4-D is observed after 8 h of irradiation. Oxygen is necessary for an efficient degradation of 2,4-D.

In the different reaction systems, quantum yields of Fe(II) formation and 2,4-D degradation have not the same tendency. For the  $\Phi_{\text{Fe(II)}}$ , the tendency is Fe(III)-Pyr > Fe(III)-Tar > Fe(III)-Cit > Fe(OH)<sup>2+</sup>, but for the  $\Phi_{2,4\text{-D}}$ , the tendency is Fe(III)-Pyr > Fe(OH)<sup>2+</sup> > Fe(III)-Cit > Fe(III)-Tar. For Fe(III)-Pyr complexes the quantum yields of Fe(II) formation and 2,4-D disappearance are the highest. The charge transfer of the photoredox process in this complex seems to be very efficient. Other Fe(III) complexes have an opposite tendency for the both quantum yields. This observation is due to the fact that for the degradation of 2,4-D and in the presence of organic ligands there is a competition for the reactivity of ·OH radicals. The quantum yield of 2,4-D degradation becomes higher with Fe(III) aquacomplexes than with Fe(III)-Cit and than with Fe(III)-Tar. This is in agreement with the higher rate constant of ·OH radical with tartaric acid. The same results were observed with the case of 2,4-DCP.

In terms of kinetics of 2,4-D degradation, the best efficiency is found for the Fe(III)-Tar complexes (figure IV-D-28). This is the opposite of the quantum yield. In the system with tartaric acid we suppose that some organic compounds formed by oxidation of tartrate ligand enhance the reoxidation of Fe(II) into Fe(III). This step is the rate limiting in photochemical process with Fe(III) species (Catastini et al, 2002).

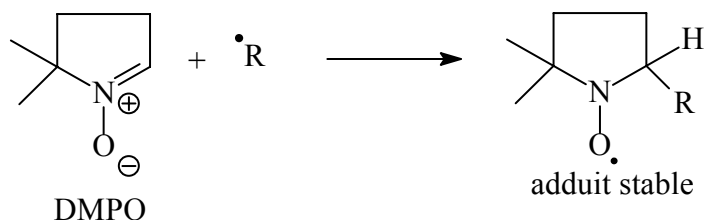
The better oxidation of Fe(II) leads to higher concentration of radical species and as a consequence to higher degradation of organic pollutants present in the solution.

## IV-E-Photodegradation mechanism

### IV-E-1-Study of Fe(III)-Carboxylate complexes by ESR (electron spin resonance) spectroscopy in aqueous solution under irradiation

In order to understand the photochemical processes in the aqueous solutions with iron carboxylate complexes under irradiation, experiments were carried out by ESR spin trapping techniques. DMPO ( $1\text{mg}\cdot\text{mL}^{-1}$ ) was used as a scavenger for different species radicals formed in solution. The irradiations were carried out directly in the cavity ESR using a xenon lamp and appropriate filters to select the wavelengths.

However, in the ESR measurements, we did not find good signals about the DMPO-OH EPR spectrum.



In our experiments, the four-line EPR spectrum (1:2:2:1) of the DMPO-OH spin adduct was only observed in the presence of Fe(III)-Cit after 50 min of irradiation ( $\lambda \geq 280\text{nm}$ ) (Figure IV-E-1). The four-line signal with the intensity of 1:2:2:1 is due to the same value of coupling constant between the hydrogen and the nitrogen with the radical centred on the oxygen ( $a_{\text{N}} = a_{\text{H}} = 14.9\text{ G}$ ). These coupling constants depend on the nature of R. The fact that this signal is not systematically observed could be explained by oxidation of the DMPO-OH adduct by iron complexes. A study of Burkitt (1993) demonstrated that both EDTA/Fe(II) and EDTA/Fe(III) are capable to degrade the DMPO-OH adduct.

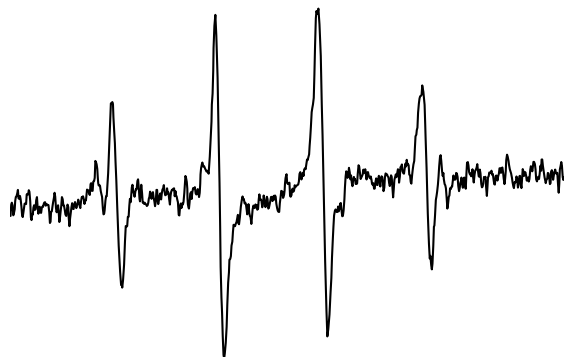


**Figure IV-E-1 ESR spectra of the aqueous solution with  $1 \text{ mg.mL}^{-1}$  DMPO and  $0.3 \text{ mmol.L}^{-1}$  Fe(III)-Cit complex at pH 3.0 after 50min irradiation  $\lambda \geq 280 \text{ nm}$ . Cell quartz has 1 mm path length.**

In each experiment, the ESR spectrum was recorded after the same number of scans. We present in detail the various signals obtained by ESR during irradiation by changing parameters such as iron-carboxylate complexes, wavelength excitation, as well as the pH of the solution.

Irradiation experiments were carried out at two different wavelengths  $\lambda \geq 280\text{nm}$  and  $\lambda \geq 350\text{nm}$  in the solution with Fe(III)-Cit complexes. The ESR signals observed are different as a function of irradiation wavelength (Figure IV-E-2). At shorter wavelengths OH radicals are trapped at the beginning of irradiation and for longer irradiation time a more complicated signal is observed. This signal was attributed before to the combination of the classical 1:2:2:1 signal of  $\cdot\text{OH}$  adduct and of the  $\text{CO}_3^{\cdot-}$  adduct (Abida et al, 2006). At longer irradiation wavelength, a nice signal corresponding to dedoublet triplet is observed. According to the literature this signal correspond to  $\text{CO}_2^{\cdot-}$  or  $\text{RCO}_2^{\cdot-}$  adduct (Abida et al, 2006).



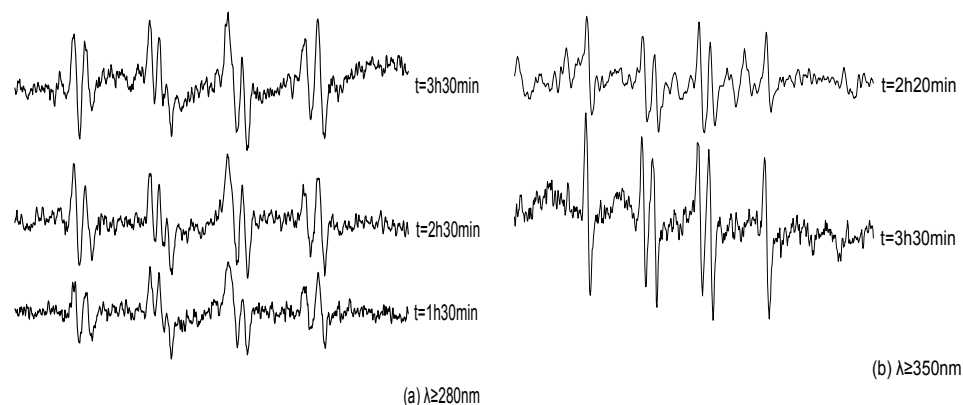


**Figure IV-E-2 ESR spectra of the aqueous solution with 1 mg.mL<sup>-1</sup> DMPO and 0.3 mmol.L<sup>-1</sup> Fe(III)-Cit complex at pH 3.0 during irradiation (a)  $\lambda \geq 280$  nm, (b)  $\lambda \geq 350$  nm**

As shown in Figure IV-E-3 and IV-E-4, the same ESR spectra signals were obtained in the presence of Fe(III)-Tar and Fe(III)-Pyr complexes. Results are presented in the following figures. These signals correspond to a mixture of radical types,  $\cdot\text{OH}$ ,  $\text{CO}_3^{\cdot-}$ ,  $\text{CO}_2^{\cdot-}$  and  $\text{RCO}_2^{\cdot}$  trapped by the DMPO.

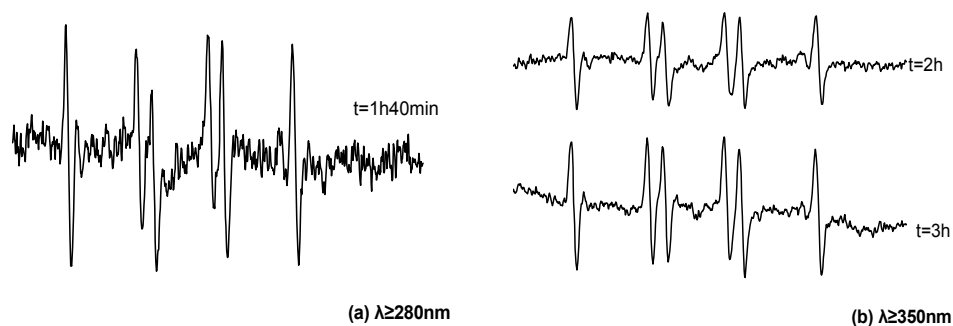


**Figure IV-E-3 ESR spectra of the aqueous solution with 1 mg.mL<sup>-1</sup> in DMPO and 0.3 mmol.L<sup>-1</sup> in Fe(III)-Tar complex at pH = 3.0 during irradiation (a)  $\lambda \geq 280$  nm, (b)  $\lambda \geq 350$  nm**

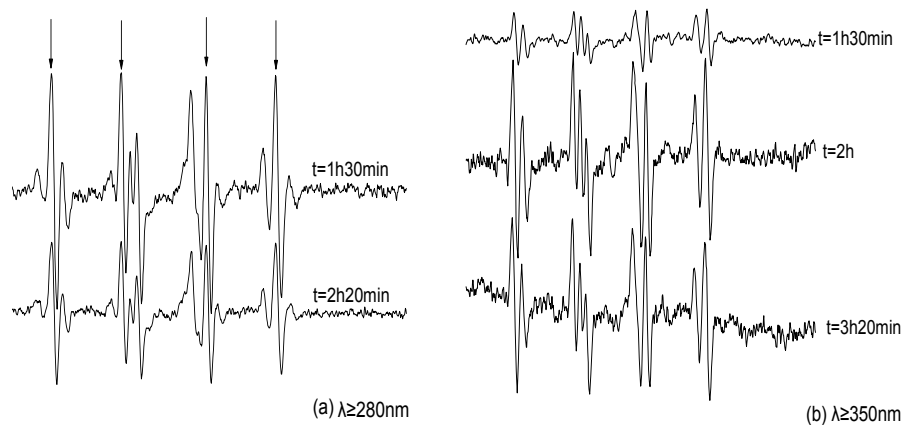
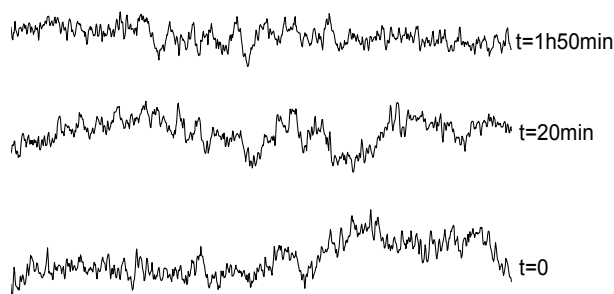
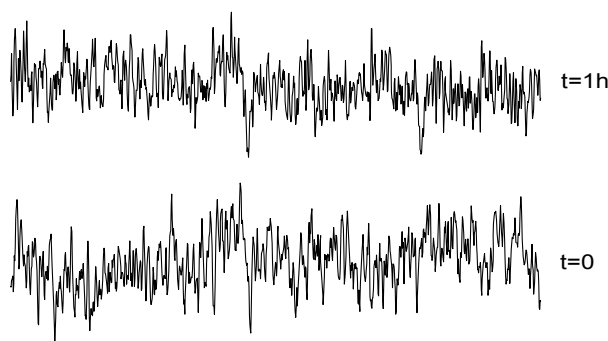


**Figure IV-E-4 ESR spectra of the aqueous solution with 1 mg.mL<sup>-1</sup> in DMPO and 0.3 mmol.L<sup>-1</sup> in Fe(III)-Pyr complex at pH = 3.0 during irradiation (a)  $\lambda \geq 280$  nm, (b)  $\lambda \geq 350$  nm**

However, in the present study, there is no ESR signals indicated the formation of radicals for a starting pH = 6.0 in the aqueous solutions with Fe(III)-Tar and Fe(III)-Pyr complex under irradiation at  $\lambda \geq 280$ nm (Figure IV-E-5). This is in agreement with the results obtained at pH 6.0 where no degradation of pollutant is observed.



**(a) 0.3mM Fe(III)-Tar**



**(b) 0.3mM Fe(III)-Pyr**

**Figure IV-E-5 ESR spectra of the aqueous solution with  $1\text{mg}\cdot\text{mL}^{-1}$  in DMPO and (a)  $0.3\text{mmol}\cdot\text{L}^{-1}$  in Fe(III)-Tar complex, (b)  $0.3\text{mmol}\cdot\text{L}^{-1}$  in Fe(III)-Pyr complex at pH 6.0 under irradiation at  $\lambda \geq 280\text{nm}$ .**

The DMPO/ $\cdot\text{OH}$  adduct can be produced not only by  $\cdot\text{OH}$ , but also by the decomposition of the DMPO adduct with superoxide radicals (Finkelstein et al., 1979). However, if the DMPO/ $\cdot\text{OH}$  signal observed is due to trapping of  $\cdot\text{OH}$  by DMPO, then addition of  $\cdot\text{OH}$  scavengers will diminish the signal and leads to new DMPO adducts. In the present work, both iron-carboxylate complexes and organic ligands can effectively quench the DMPO/ $\cdot\text{OH}$ . In such systems with carboxylate complexes the detection of all radicals which can be produced are very complicated. To elucidate in details the primary mechanisms of the different radical formation, the use of more

specific radical scavenger will be useful. Therefore, detection of the corresponding DMPO spin adducts is a strong indicator for  $\cdot\text{OH}$  formation. Moreover, in our previous work the formation of hydroxyl radicals have been confirmed and determined by using benzene as a scavenger in the aqueous solutions with iron-carboxylate complexes under irradiation.

#### **IV-E-2-Identification of photoproducts and degradation mechanism**

##### **2,4-D**

The photodegradation of 2,4-DCP and 2,4-D in the presence of three kinds of Fe(III)-Carboxylate complexes have been studied in the previous parts of this work. Results indicate that hydroxyl radicals are the origin of the degradation of pollutants. However, the photodegradation processes are very complicated in the presence of organic ligands. Competition reactions exist in the aqueous solutions. Here we identify the photoproducts generated after irradiation and propose the degradation mechanism. 2,4-DCP is the most prevalent primary photoproduct during the photodegradation of 2,4-D in the presence of Fe(III)-complexes, no hydroxylated products of 2,4-D were observed by mass spectrometry. The same major photoproduct was found also in systems utilising different advanced oxidation processes (AOT's are the technologies based on producing of hydroxyl radicals).  $\cdot\text{OH}$  first attacks on carbon 1 of the aromatic ring followed by the loss of an alkoxy group. The formation of this major intermediate implies a high degree of selectivity for  $\cdot\text{OH}$  addition to the 2,4-D ring. (Peller et al., 2004).

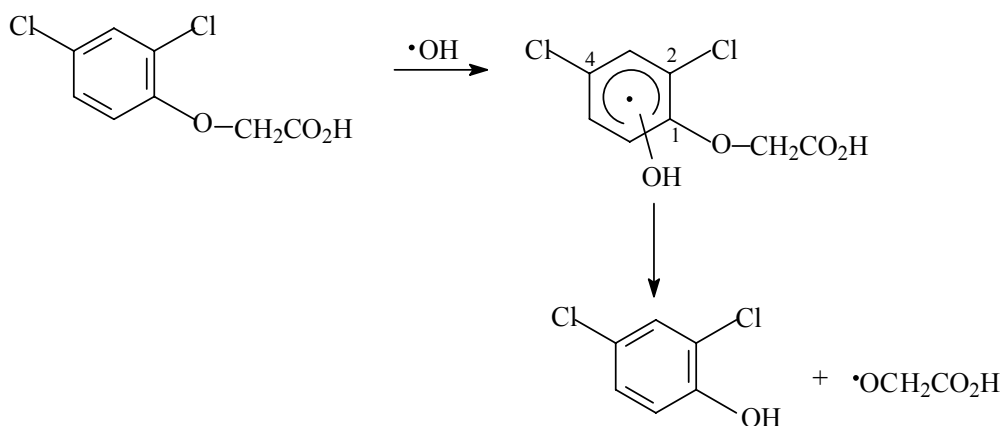
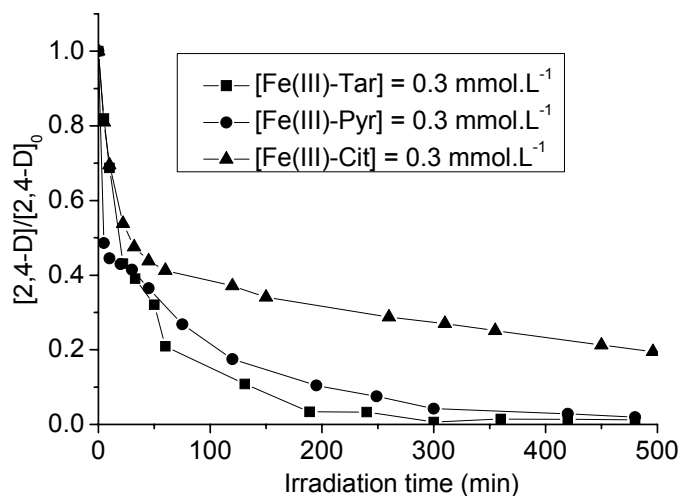
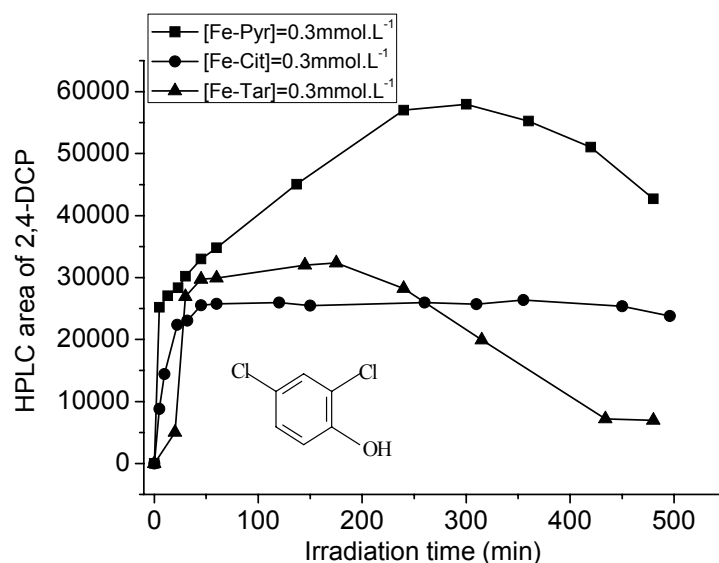


Figure IV-E-6 presents the photodegradation efficiency of 2,4-D in three different complexes systems. At the initial reaction period (45 min), the efficiency of Fe(III) complexes to degrade 2,4-D is in the order of Fe(III)-Cit < Fe(III)-Tar < Fe(III)-Pyr. After 1 h of irradiation, the photodegradation efficiency is changed into another order that is Fe(III)-Cit < Fe(III)-Pyr < Fe(III)-Tar. From these results, it can be concluded that Fe(III)-Pyr has high activity to degrade 2,4-D under irradiation, however, Fe(III)-Cit always presents a relative slow degradation efficiency of 2,4-D. Fe(III)-Tar also presents a relative higher activity to degrade 2,4-D.



**Figure IV-E-6 Photodegradation of 2,4-D with different complexes in different systems with 0.1 mmol.L<sup>-1</sup> of 2,4-D at pH = 3.0.**

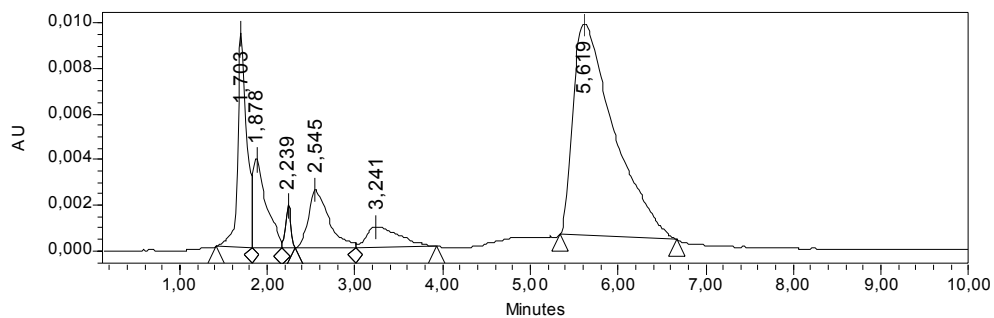


**Figure IV-E-7 Evolution of HPLC area of product 2,4-DCP in different systems with 0.1 mmol.L<sup>-1</sup> of 2,4-D at pH = 3.0.**

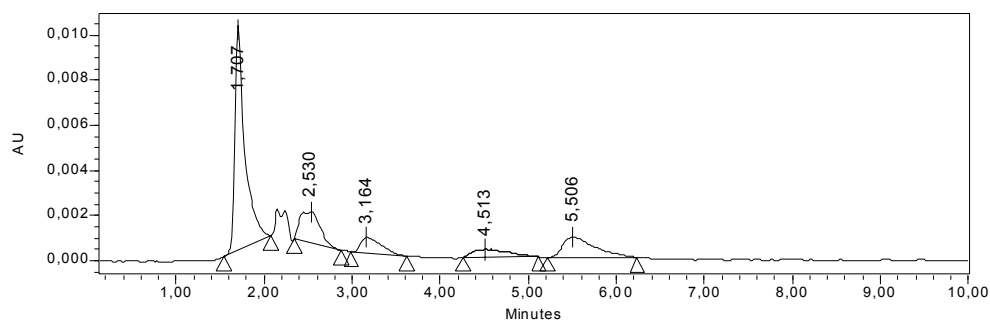
On the figure IV-E-7 the kinetics of 2,4-DCP formation, the major photoproduct of 2,4-D, are presented in the three different systems, Fe(III)-Pyr, Fe(III)-Tar and Fe(III)-Cit. In the presence of Fe-Pyr complex the concentration of 2,4-DCP is higher than with other complexes. The concentration of 2,4-DCP is maximum after 5 h of irradiation. This observation can be explained by the higher quantum yield of 2,4-D disappearance (0.046) than the quantum yield of 2,4-DCP disappearance (0.027) in the presence of Fe(III)-Pyr. Opposite efficiency is observed for the other complexes Fe(III)-Tar and Fe(III)-Cit. In the presence of Fe(III)-Tar a maximum concentration of 2,4-DCP is reached after 3 h of irradiation and after a fast decrease takes place. This is consistent with the above 2,4-D degradation results that the 2,4-D have almost disappeared after 3h irradiation. In the presence of Fe(III)-Cit a surprising constant concentration is reached after approximately 1 h of irradiation. From the results in Figure IV-E-6, the 2,4-D degradation efficiency is relative low in the presence of Fe(III)-Cit than they other two Fe complexes. So less 2,4-D was degraded to 2,4-DCP during the reaction procedure and with a low degradation efficiency of 2,4-DCP. Thus, the concentration of intermediate 2,4-DCP was stable after 1 h of irradiation.

## 2,4-DCP

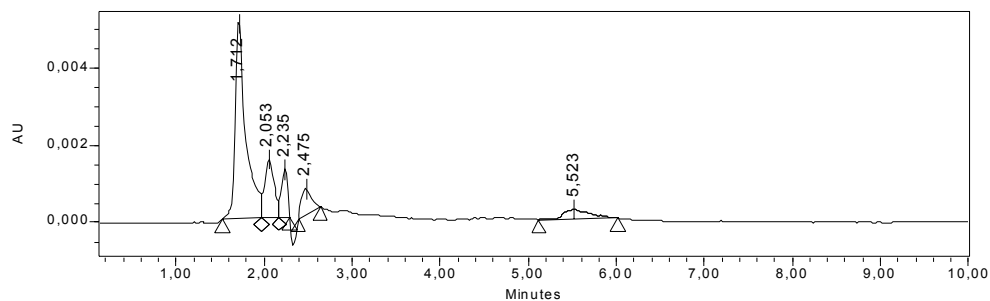
In order to study the photodegradation process of 2,4-DCP, long time irradiation were performed in the aqueous solution of Fe(III)-Tar complex at pH 3.0. Figure IV-E-8 presents the HPLC chromatogram of the reaction solution according to irradiation time. 2,4-DCP (retention time = 5.6 min) was degraded and totally disappeared after 24 h of irradiation. The aromatic intermediate products also disappeared after 24 h of irradiation.



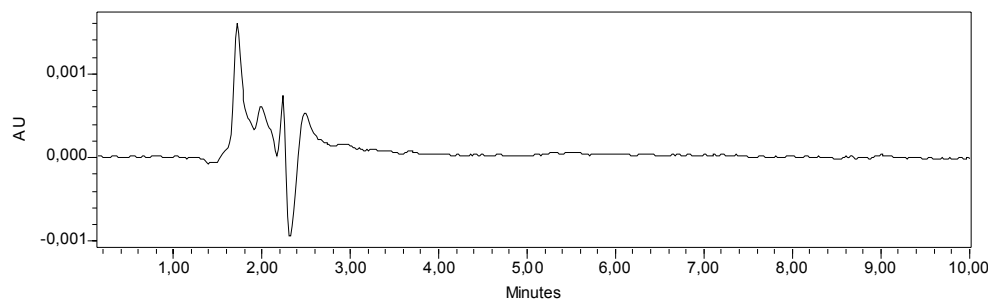
(a) 1 h irradiation



(b) 18 h irradiation



(c) 22 h irradiation



(d) 24 h irradiation

**Figure IV-E-8 Evolution of the HPLC chromatograms of solution as a function of the irradiation time with  $0.3 \text{ mmol.L}^{-1}$  in Fe(III)-Tar and  $0.1 \text{ mmol.L}^{-1}$  in 2,4-DCP at pH = 3.0.**

The same photoproducts are observed in the system with Fe(III)-Tar at higher pH = 3.9, after 8h of irradiation (Figure IV-E-9).

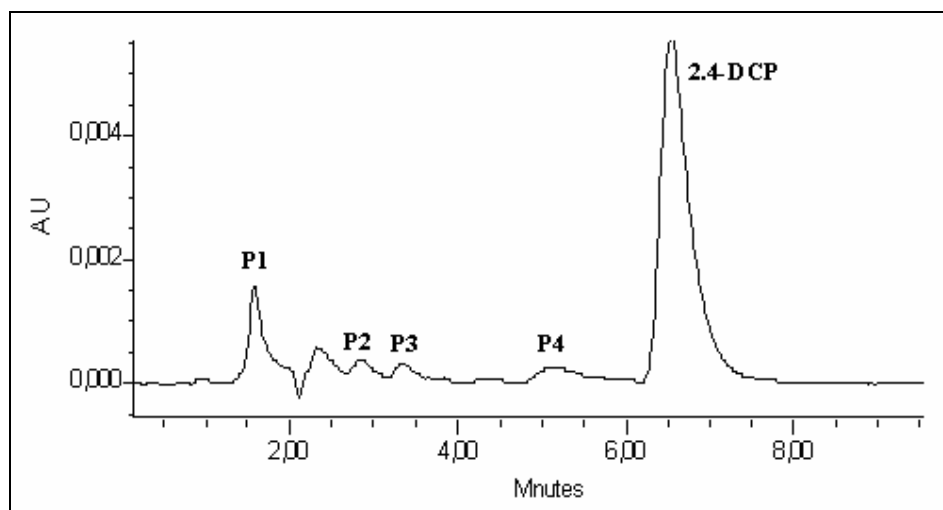


**Figure IV-E-9 HPLC chromatogram of solution of  $0.3 \text{ mmol.L}^{-1}$  Fe(III)-Tar and  $0.1 \text{ mmol.L}^{-1}$  2,4-DCP at pH = 3.9, after 8 h of irradiation.**

Figure IV-E-10 presents the HPLC chromatograms of the solutions with Fe(III)-Pyr complex ( $0.1 \text{ mmol.L}^{-1}$ ) and 2,4-DCP ( $0.1 \text{ mmol.L}^{-1}$ ) at pH 3.0 in 8 h of irradiation. The main photoproducts detected in our experimental conditions were P1, P2, P3 and P4. The same photoproducts were detected in the previous experiments with Fe(III)-Tar. The difference of the retention time, observed between these two experiments, is due to the different HPLC instruments used. For Fe(III)-Cit the same photoproducts are obtained.



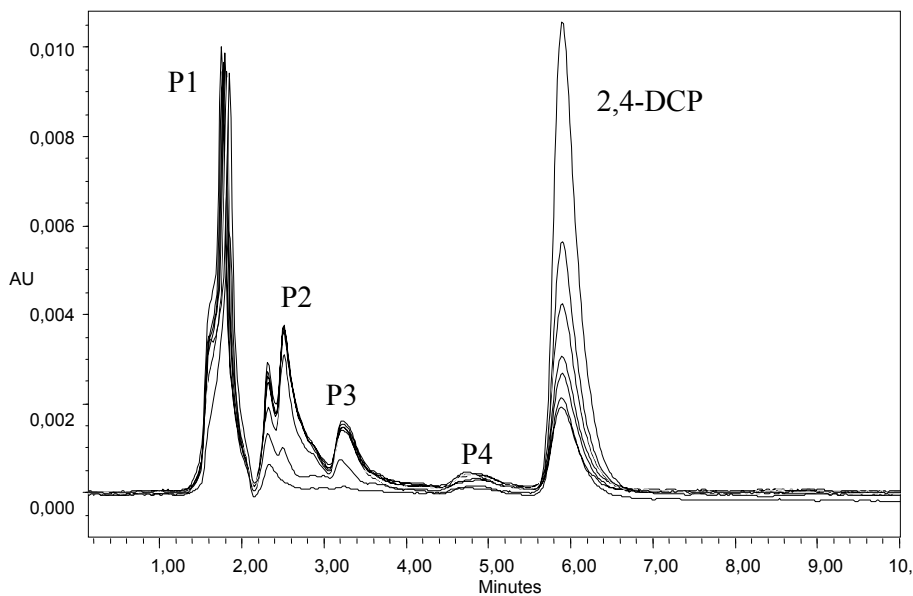


**Figure IV-E-10 Evolution of HPLC spectrum of reaction solution with  $0.1 \text{ mmol.L}^{-1}$  Fe(III)-Pyr and  $0.1 \text{ mmol.L}^{-1}$  2,4-DCP at pH = 3.0**

The evolutions of the concentration of the 4 different photoproducts as a function of irradiation time are presented in Figure IV-E-11. The photoproduct P1 with a shorter retention time can be attributed to different Fe(II) or Fe(III) complexes formed with oxidized products of organic ligands or of 2,4-DCP.

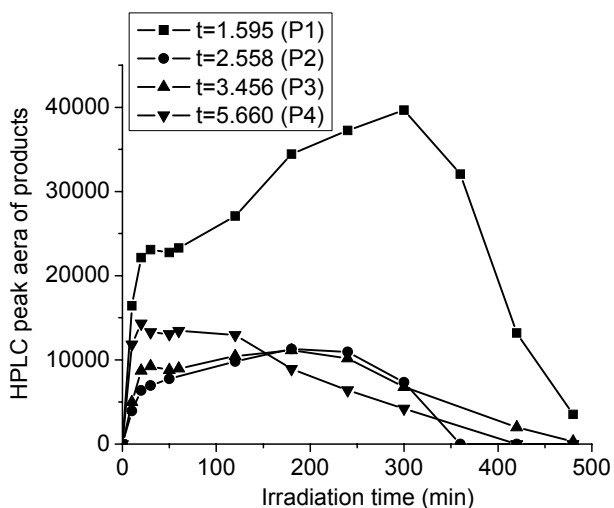
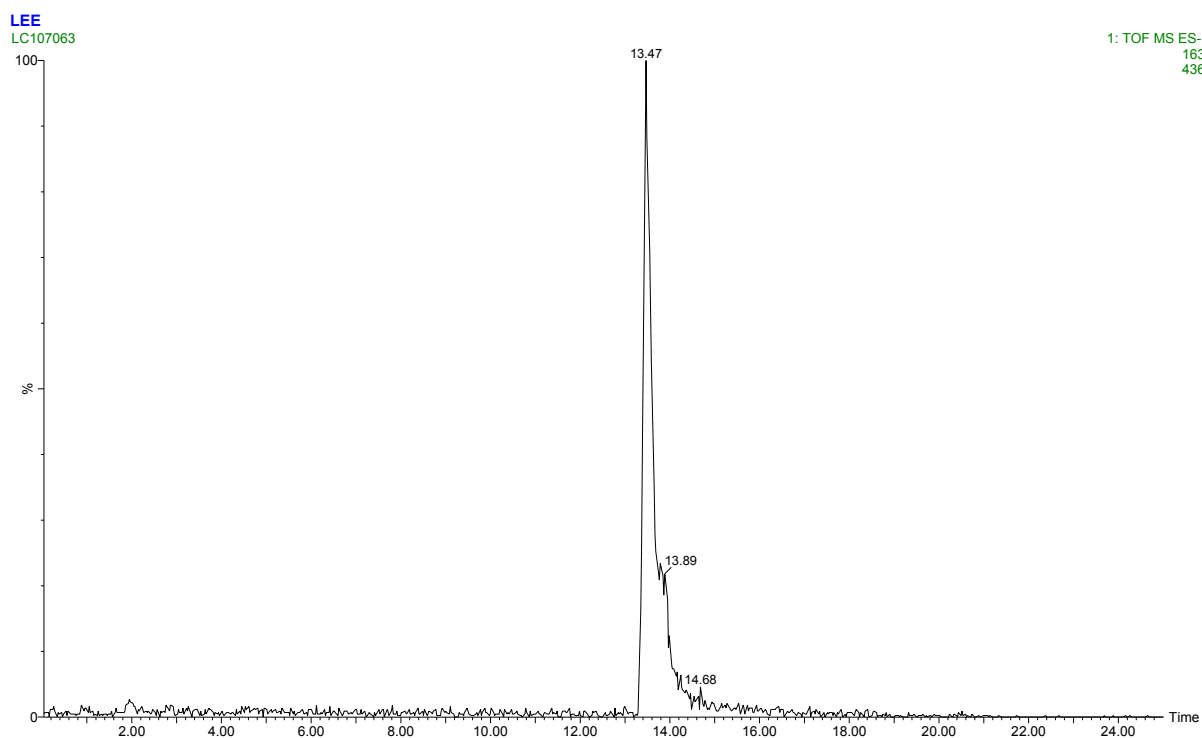
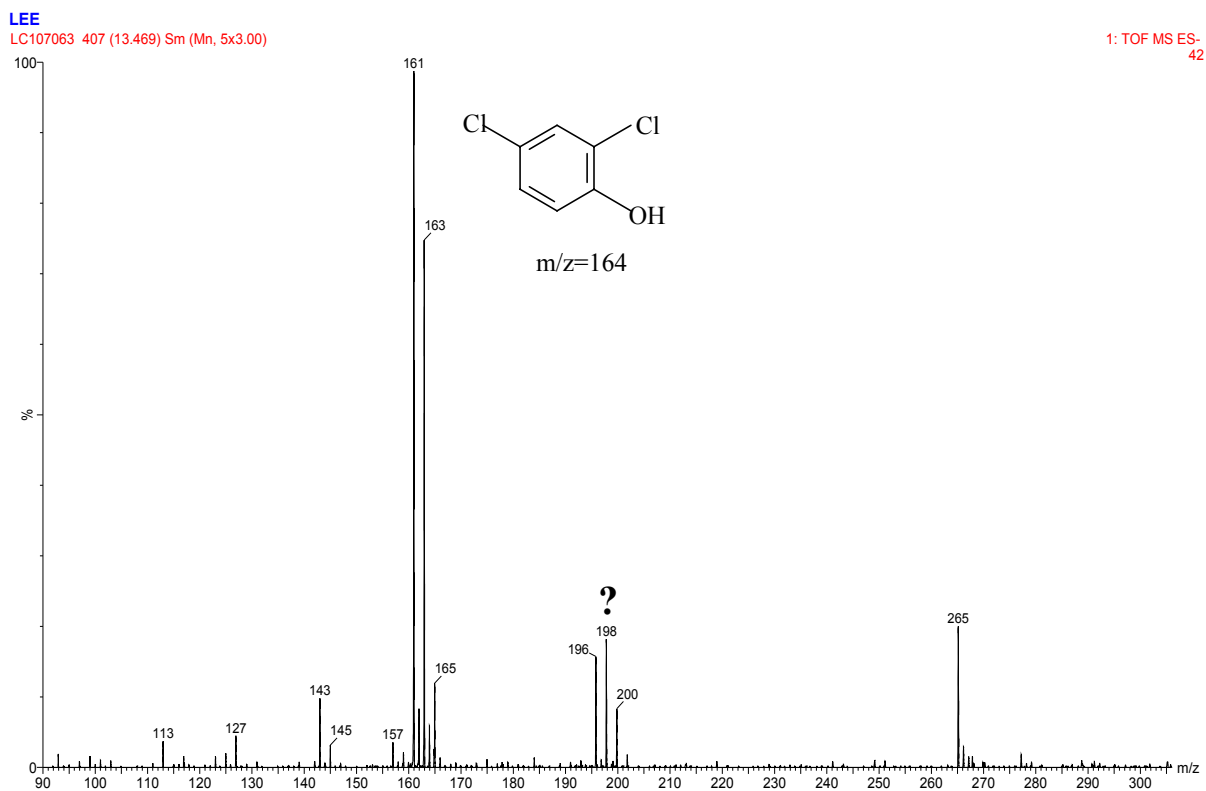


**Figure IV-E-11 Time evolution of HPLC area of photoproducts generated in the solutions of  $0.3 \text{ mmol.L}^{-1}$  Fe(III)-Tar and  $0.1 \text{ mmol.L}^{-1}$  2,4-DCP at pH = 3.9**

For the identification of the primary photoproducts experiments of HPLC/ES/MS were carried out at the centre of chemical analysis of the chemistry department at the Blaise Pascal University. The electro-spray (ES) mode with negative ionization was used for our analysis. First of all, in figure IV-E-12 total ions chromatogram and mass spectrum of a solution of 2,4-DCP are presented. The masses observed at 161, 163 and 165  $m/z$  correspond to the 2,4-DCP with two chlorine atoms.



**(a) Total ion chromatogram**



(b) Mass spectra

Figure IV-E-12 LC-MS spectra of 2,4-DCP (0.1 mmol.L<sup>-1</sup>)

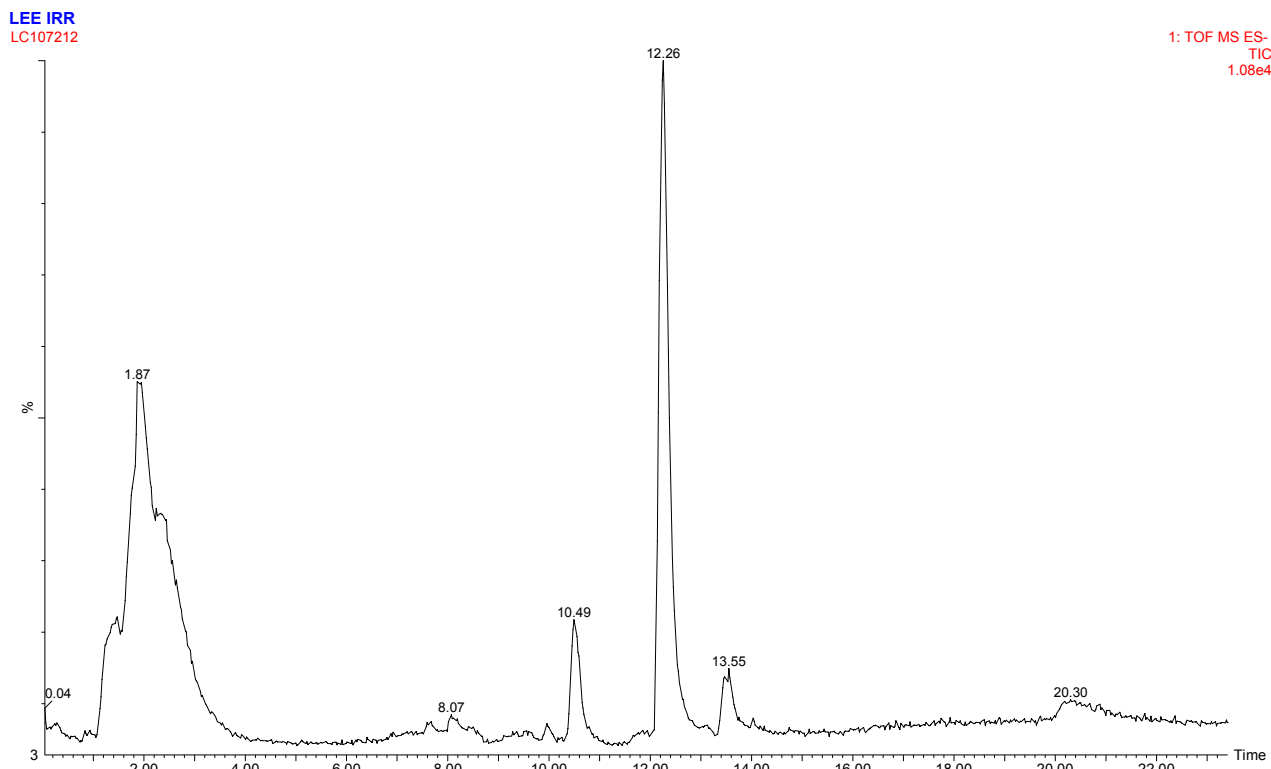
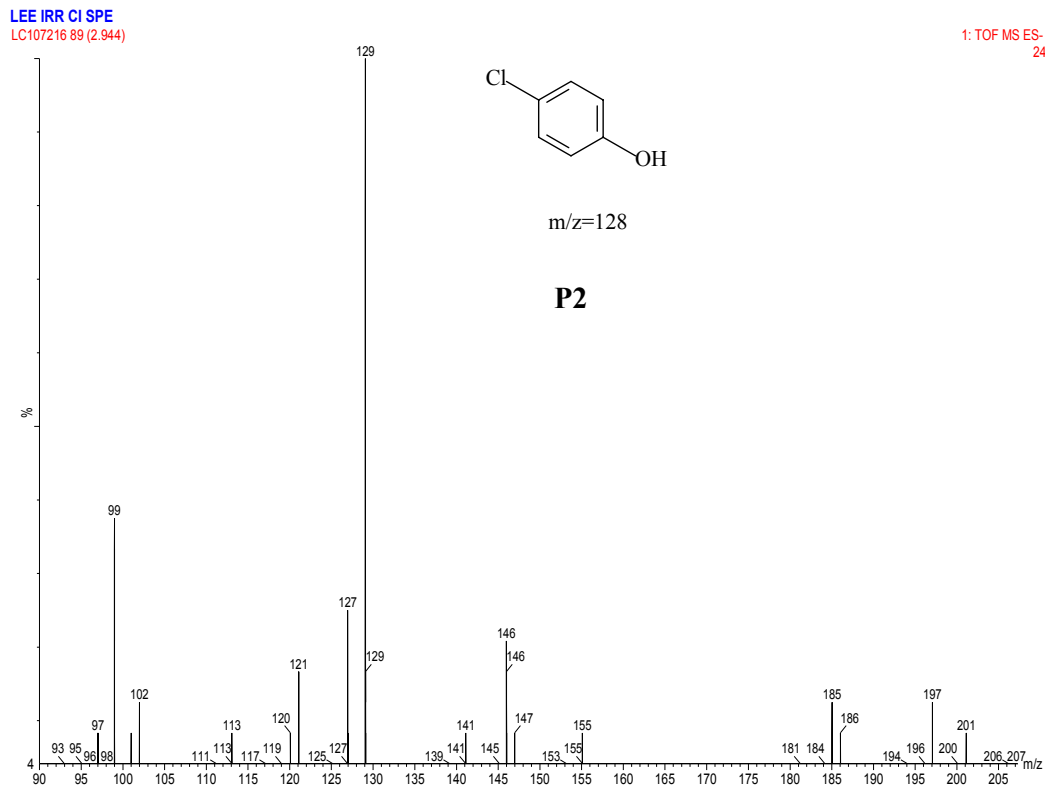


Figure IV-E-13-a Total ion chromatogram

Figure IV-E-13-a presents the total ions chromatogram of reaction solution of 2,4-DCP and Fe complexes after 3h irradiation.

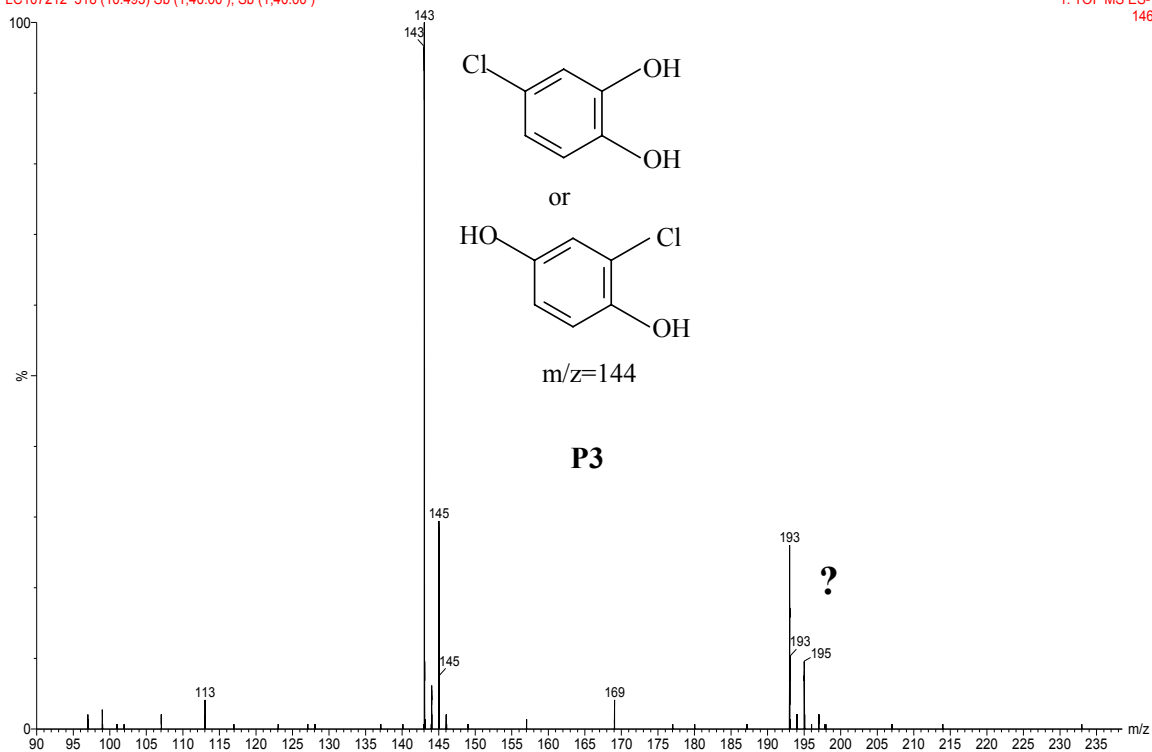
The mass spectra of the three main photoproducts are presented in figure IV-E-13-b. P3 and P4 are hydroxylated products with the substitution of one chlorine atom for P3 and the addition of ·OH group for P4. The photoproduct P2 corresponds to an elimination of a chlorine atom.



LEE IRR

LC107212 318 (10.493) Sb (1,40.00); Sb (1,40.00)

1: TOF MS ES-  
146



LEE IRR

LC107212 371 (12.258)

1: TOF MS ES-  
728

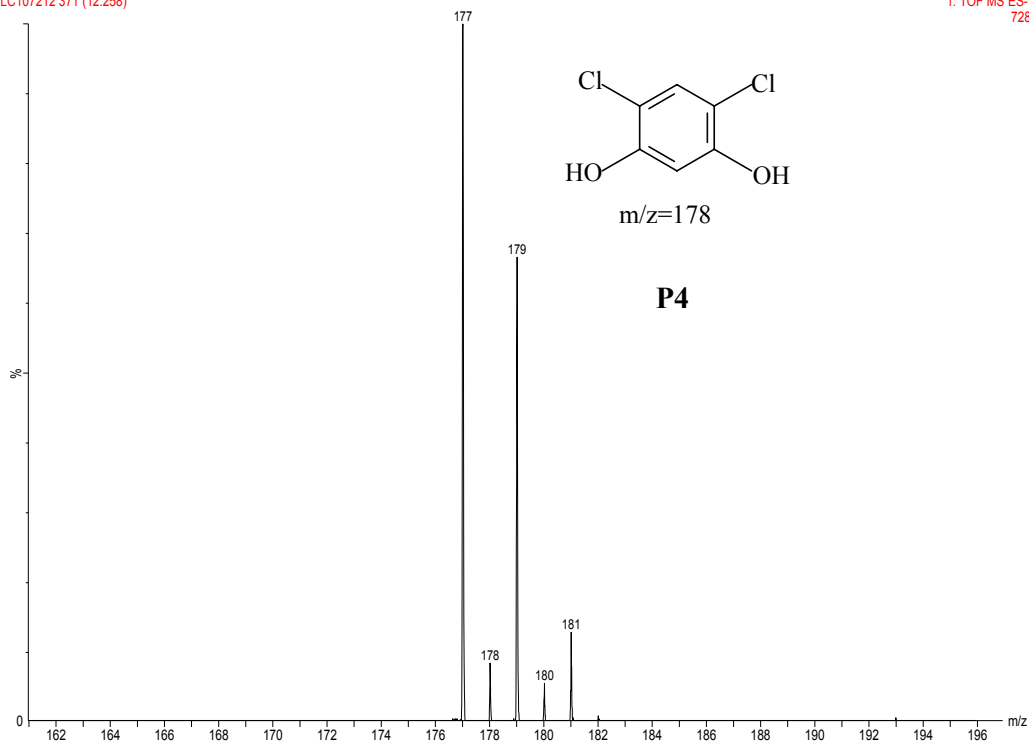
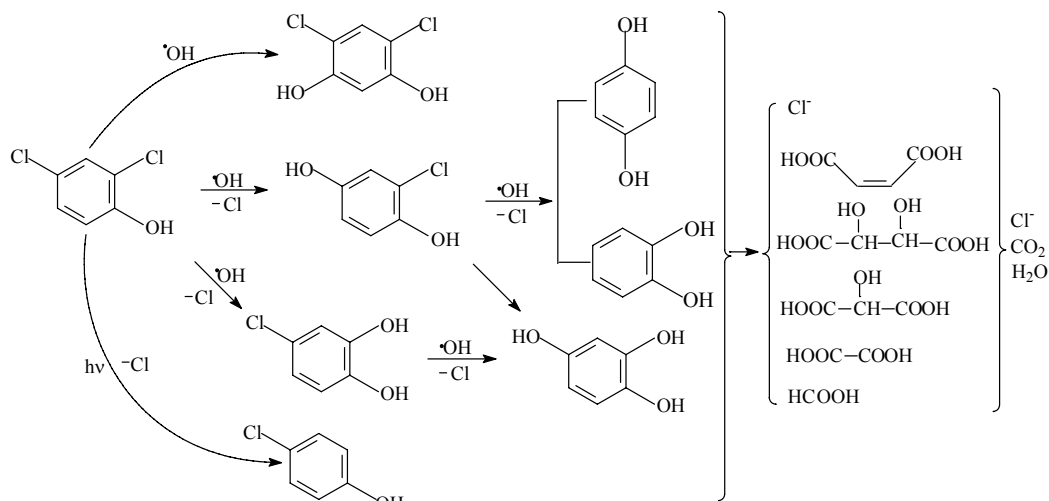


Figure IV-E-13-b LC-MS spectra of photoproducts

After these identifications of products we can propose a photodegradation mechanism of 2,4-DCP in the presence Fe(III)-complexes. The reactivity with hydroxyl radicals, the main reactive species photogenerated from Fe(III)-complexes is presented in the following scheme.



**Figure IV-E-14 Proposed photodegradation scheme of 2,4-DCP**

For longer irradiation time the primary photoproducts disappeared and small organic acids molecules are formed. The degradation can continue until the total mineralization of the 2,4-DCP.

**V**

**GENERAL CONCLUSIONS**





## **V-General conclusions**

In the present study the photodegradation of the herbicide 2,4-D (2,4-dichlorophenoxyacetic acid) and its main photoproduct (2,4-DCP) in the presence of three Fe(III)-carboxylate complexes (citrate, pyruvate and tartrate) have been investigated. This type of complexes can be formed in the natural aquatic environment due to the presence of such acids and iron in water. Thus, such complexes can influence the fate of pollutants spread in the environment. 2,4-D belongs to the class of herbicide heavily used in the worldwide area.

The experiments carried out with benzene used as a trap of hydroxyl radicals clearly show that hydroxyl radicals are the reactive species photogenerated from Fe(III)-carboxylate complexes under solar light. These radicals are well known to be very reactive on the big majority of organic pollutants and they can oxidize the pollutants until its complete mineralization.

In order to estimate the photochemical efficiency of the different Fe(III)-complexes a detailed work has been performed on the evaluation of the quantum yields. The quantum yields of 2,4-D disappearance increases in the following order of Fe(III)-complexes: Fe(III)-Tar < Fe(III)-Cit < Fe(OH)<sup>2+</sup> < Fe(III)-Pyr. In these systems, for the quantum yields of Fe(II) formation an opposite tendency is observed excepted for the Fe(III)-Pyr which has also the highest quantum yield of Fe(II) formation. It is important to mention that the quantum yields of Fe(II) formation is much higher with the three Fe(III)-carboxylate complexes than with Fe(III) aquacomplexes (Fe(OH)<sup>2+</sup>). This high difference could be attributed to a better delocalisation of the electron, after the charge transfer, on the carboxylate group in comparison with hydroxide group. Thus the photoredox process is more efficient in Fe(II)-carboxylate complexes than in Fe(III) aquacomplexes. These tendencies can be also explained by the competition between 2,4-D and carboxylic ligand for the reaction of ·OH radicals. So in the presence of other organic compounds the degradation of 2,4-D will be reduced. On the contrary Fe(II) formation, in the

presence of higher organic compounds concentration, will be increased. Indeed, in the presence of organic substrate the reaction of  $\cdot\text{OH}$  radical on Fe(II) will be less important. So, concentration of Fe(II) and as a consequence quantum yield will be higher. The same tendencies for the quantum yields of Fe(II) formation and the pollutant degradation were found in the systems with 2,4-dichlorophenol (2,4-DCP) as the pollutant. The particularity or singularity of Fe(III)-Pyr is confirmed also for 2,4-DCP. The quantum yield of 2,4-DCP degradation and Fe(II) formation are the highest than for the other complexes. We can explain this particularity by the lower reactivity of hydroxyl radicals with pyruvate or pyruvic acid than with another substrate. This lower reactivity can be also considered for oxidised ligand of pyruvate obtained after the photoredox process. Moreover, the intramolecular charge transfer is favoured by the delocalisation of electron present in the pyruvic acid, and therefore the efficiency of photoredox processes is higher than in other complexes.

On the basis of the quantum yields measurements, the efficiency of photodegradation of 2,4-D and 2,4-DCP in the systems with Fe(III) complexes can be compared. In general, the quantum yields of 2,4-DCP degradation are higher than in the case of 2,4-D.

pH = 3.0 [Fe(III)-complex] = 0.3 mmol.L <sup>-1</sup> $\lambda_{\text{exc}} = 365 \text{ nm}$	$\Phi_{2,4\text{-D}}$	$\Phi_{2,4\text{-DCP}}$
Fe(III)-Cit	0.010	0.019
Fe(III)-Tar	0.008	0.014
Fe(III)-Pyr	0.046	0.027

Once more, we observe the singularity for Fe(III)-pyruvate, the efficiency of the photodegradation is higher for 2,4-D than for 2,4-DCP.

The effect of different parameters on the efficiency of 2,4-D and 2,4-DCP degradation was studied in details in system with monochromatic light for primary reaction or for longer irradiation time in photoreactor with polychromatic light (300-500nm). The presence of oxygen is primordial for the reactive species formation;

in the absence of oxygen the degradation of our pollutants is negligible. The other important parameter is the pH. The distribution of species in the solution of Fe(III) complexes strongly depends on pH. The reactivity of each species is highly different, thus the efficiency of the photoredox process is influenced by pH. pH plays also an important role in Fenton reaction; reaction supposed taking place in such system. The optimum pH for 2,4-D and 2,4-DCP degradation is around at pH 3.0, increase of pH decreases the efficiency of the pollutant photodegradation. Unfortunately, the degradation rate of our pollutant at pH higher than 5.0 is very slow. The influence of Fe(III) complex concentration on the degradation of our pollutants was studied in detail. At first, the photodegradation of our pollutants increases with the concentration of Fe(III)-complexes. But the degradation rate reach a maximum value and additional increase of Fe(III)-complex concentration decreases the degradation rate. The maximum degradation rate is obtained then the concentration of Fe(III) complexes is optimal for the formation of the reactive species and it is not too high to act as a scavenger of hydroxyl radicals formed. The optimal concentration depends on the nature of the ligand. Our results show an optimal concentration equal to 0.3 mmol.L<sup>-1</sup> (in iron) for the Fe(III)-Cit complex and 0.1 mmol.L<sup>-1</sup> for the Fe(III)-Tar complex. For Fe(III)-Pyr complex the optimal concentration is not really determined but  $\geq 0.3$  mmol.L<sup>-1</sup>. The difference between tartrate and citrate ligand is due to the higher capacity of tartrate ligand to react with hydroxyl radical and to act as a scavenger of these radicals.

Ligand	Pyruvate	Citrate	Tartrate
Rate constant with ·OH radical (L.mol <sup>-1</sup> .s <sup>-1</sup> )	3.1×10 <sup>7</sup>	5.0×10 <sup>7</sup>	6.9×10 <sup>8</sup>

In our system with Fe(III)-carboxylate complexes we observe the same mechanism of 2,4-D degradation for all complexes and it corresponds totally to the mechanism described in the previous work on the degradation of 2,4-D by Advanced Oxidation Processes (generating ·OH radicals). 2,4-D is selectively degraded to

2,4-DCP, which through different photodegradation products could be mineralized into  $\text{H}_2\text{O}$ ,  $\text{Cl}^-$  and  $\text{CO}_2$ . The formation of hydroxyl radicals in the solutions of Fe(III) complexes is confirmed by ESR spectroscopy measurements. Further experiments with another type of radical scavenger could be helpful for elucidate the mechanism of the radical formation via detection of different radicals in our system. Some additional theoretical work could explain the particularity of Fe(III)-pyruvate complex.

Our work shows that the presence of Fe(III)-carboxylate complexes could have a considerable impact on the fate of organic pollutant in aquatic environment. . In this work we studied three different carboxylic acid, one tri-carboxylic (citric), one di-carboxylic (tartaric) and one mono-carboxylic (pyruvic). The reactivity of chosen complexes reflect some similarities in photochemical properties, the most distinguished complex is Fe(III)-pyruvate. The particularity of pyruvic acid can be due to the fact that it is a mono-carboxylic acid and that the charge transfer is easier in such iron complexes than with complexes with di- or tri-carboxylic acids. A study of other carboxylic acid will be necessary to conclude on this aspect of reactivity as a function of the number of carboxylic group.

# **VI**

## **APPENDIX**



## VII-1-List of tables

Table II-A-1:	Concentrations of the total iron and dissolved iron in the rain, snow, fog or seawater systems in different locations.	11
Table II-A-2:	Reactions and rate constants in (S=35) sea water at 298 K	15
Table II-B-1:	Monocarboxylic acids and Dicarboxylic acids investigated in aerosols at different sites	21
Table II-B-2:	The effect of chelation on the rate of Fe(II) oxidation. $[\text{Fe(II)}] = 110 \mu\text{mol.L}^{-1}$ , $[\text{chelator}] = 550 \mu\text{mol.L}^{-1}$ , $50 \text{ mmol.L}^{-1}$ Tris buffer, pH 7.0	25
Table II-C-1:	Structures of common chlorophenols	34
Table II-C-2:	Degradation of 2,4-Dichlorophenol by means of advanced oxidation processes (Pera-Titus, 2004)	37
Table II-D-1:	Structures of 2, 4-D and chemically related phenoxy herbicides.	40
Table III-C-1:	The photon flux at 365nm, 313nm and 296nm	53
Table III-C-2:	Light intensity distribution of the metal halide lamp	56
Table IV-A-1:	pKa of organic acids	67
Table IV-A-2:	Forms of Tartaric Acid	68
Table IV-C-1:	Quantum yields of Fe(II) and 2,4-DCP as a function of wavelength in different systems.	116
Table IV-C-2:	Oxygen effect on the quantum yields of Fe(II) and 2,4-DCP. In the aqueous solutions with $0.1 \text{ mmol.L}^{-1}$ 2,4-DCP and the initial pH value was 3.0. ( $\lambda_{\text{irr}}=365\text{nm}$ )	118
Table IV-C-3:	pH effects on the quantum yields of 2,4-DCP, with $0.1 \text{ mmol.L}^{-1}$ of 2,4-DCP. ( $\lambda_{\text{irr}} = 365\text{nm}$ )	120
Table IV-C-4:	Effects of Fe(III)-Carboxylate complexes concentration on the	121

	quantum yields of Fe(II) and 2,4-DCP. The initial pH value was 3.0. ( $\lambda_{irr}=365\text{nm}$ )	
Table IV-C-5:	Rate constants of $\cdot\text{OH}$ radicals on the different organic acids (Buxton et al, 1988).	148
Table IV-D-1:	Quantum yields of disappearance of 2,4-D and generation of Fe(II) as a function of the irradiation wavelength.	152
Table IV-D-2:	Quantum yields of disappearance of 2,4-D and generation of Fe(II) as a function of oxygen. The initial pH value was 3.0. ( $\lambda_{irr}=365\text{nm}$ )	153
Table IV-D-3:	Quantum yields of disappearance of 2,4-D as a function of pH. In the aqueous solutions with $0.1\text{ mmol.L}^{-1}$ 2,4-D. ( $\lambda_{irr}=365\text{nm}$ )	154



## VII-2-List of Figures

Figure II-A-1:	Speciation of Fe(III) in seawater as a function of pH (Millero et al., 1995)	8
Figure II-A-2:	Transformation of iron in different aqueous phases in the remote marine aerosols (zhuang et al., 1992)	10
Figure II-A-3:	The scheme of iron recycling in the atmospheric water Behra and Sigg (1990)	14
Figure II-A-4:	Photochemical transformation of iron	15
Figure II-A-5:	Structure of octahedral $[\text{Fe}(\text{H}_2\text{O})_6]^{3+}$	16
Figure II-A-6:	Proposed structure of dimer species Fe(III) by Sommer et Margerum (1970)	16
Figure II-A-7:	Proposed structure of trimeric species Fe(III) by Sommer et Margerum (1970)	16
Figure II-A-8:	The distribution of Fe(III) complexes as function of pH $[\text{Fe}(\text{III})] = 0.03 \text{ mol.L}^{-1}$ , $T = 298 \text{ k}$ (Mestankova, 2004)	18
Figure II-A-9:	Approximate predominance-area pH vs $\log C_{\text{Fe(III)}} \text{ (M)}$ diagram, $25^\circ\text{C}$ , ionic strength 0. The dashed lines labeled a, b, and c are the saturation lines for goethite, aged amorphous hydrous oxide, and fresh amorphous hydrous oxide, respectively.	19
Figure II-A-10:	UV-visible spectra of Fe(III) aqueous complexes	20
Figure II-B-1:	Figure II-B-1 The mechanism of photochemical redox cycling of iron in the aqueous solution. Fe(II)-L and Fe(III)-L represent Fe(II) and Fe(III) complexed with Ligand. (Abida, 2005)	23
Figure II-B-2:	Reaction scheme for the photolysis of Fe(III)-polycarboxylate complexes	24
Figure II-B-3:	Logarithm of the reaction rate constant ( $\text{M}^{-1} \text{ s}^{-1}$ ) of oxidation of Fe(II) species by $\text{O}_2$ , as a function of the redox potential, EH0 (vs. NHE), for the corresponding Fe(III)/Fe(II) redox	26

	couples (Sulzberger et al., 1995)	
Figure II-B-4:	Light-induced iron cycling, and surface (--) and solution (s) reactions in heterogeneous photo-Fenton systems. (Mazellierp and Sulzberger, 2001)	27
Figure II-B-5:	Possible reactions in illuminated solution containing Cr(VI), Oxalate, and Fe(II, III) (Hug et al., 1997).	29
Figure II-B-6:	Oxidation and hydrolysis of tridentate Fe(II)-Citrate complex to bidentate Fe(III)-Citrate complex.	30
Figure II-B-7:	Diagram of distribution of complexes in the system Fe(NO <sub>3</sub> ) <sub>3</sub> -Tartaric acid (1:1): 1) Fe <sub>aq</sub> ; 2) FeH <sub>3</sub> tar; 3) Fe <sub>2</sub> -(H <sub>3</sub> Tar)(H <sub>2</sub> Tar); 4) FeH <sub>2</sub> Tar; 5) Fe <sub>2</sub> (H <sub>2</sub> Tar) <sub>2</sub> ; 6) FeHTar; 7) Fe <sub>2</sub> (HTar) <sub>2</sub> ; 8) FeTar; 9) Fe <sub>2</sub> (Tar) <sub>2</sub> .(Kostromina et al., 1988)	31
Figure II-B-8:	Dimer complexes	32
Figure II-B-9:	Proposed monomer complexes	32
Figure II-B-10:	Figure II-B-10 Distribution of complexes in Fe(III)-meso-dl tartaric acid systems. [Fe(III)] : [meso-Tar] : [DL-Tar] = 2.458 : 2.484 : 2.493×10 <sup>-3</sup> mol.L <sup>-1</sup> . X represent DL-Tar and Y represent meso-Tar.	33
Figure II-C-1:	Advanced oxidation technologies	37
Figure II-D-1:	Market share in the agriculture phenoxy broadleaf weed herbicides market in Canada. Phenoxy market share of 25.9 million acres treated.	41
Figure II-D-2:	Proposed pathway for the degradation of 2,4-D (Carla B et al., 2006)	43
Figure III-C-1:	Monochromatic irradiation device	53
Figure III-C-2:	Emission spectra of lamp Philips, TLD 15W/05.	54
Figure III-C-3:	Home-made photoreactor with four lamps (Philips TLD 15W / 05) 1: reactor 100 mL; 2: lamps 15W× 4; 3: magnetic bar	55

Figure III-C-4:	Emission spectra of the metal halide lamp 250 W.	56
Figure III-C-5:	Photochemical reactor with metal halide lamp 250W	57
Figure III-D-1:	5, 5-Dimethylpyrroline-N-oxide (DMPO)	58
Figure III-D-2:	(a) and (b) UV-visible spectra of the filters used during ESR spectroscopy experiments	58
Figure III-D-3:	Calibration curve of TC (a) and IC (b).	60
Figure III-D-4:	Calibration curve of Fe(II) concentration	61
Figure III-D-5:	Formation of phenol in different conditions after 160min irradiation.	62
Figure III-D-6:	HPLC chromatogram of solutions with 7 mmol.L <sup>-1</sup> benzene in 160min irradiation.	63
Figure III-D-7:	Calibration curve of phenol	63
Figure III-D-8:	Measurements of the absorbance as a function of the composition of the complex $n=C_L/C_M$	64
Figure IV-A-1:	Chemical structure of Tartaric acid	68
Figure IV-A-2:	UV-Visible absorption spectra of tartaric acid. (a) [L-Tar] = 1 mmol.L <sup>-1</sup> ; (b) [D-Tar] = 1 mmol.L <sup>-1</sup>	69
Figure IV-A-3:	UV-Visible absorption spectra of L-Tar and D-Tar acid as function of pH. [L-Tar]=0.3mmol.L <sup>-1</sup> , [D-Tar]=0.3 mmol.L <sup>-1</sup>	69
Figure IV-A-4:	Absorbance at 212 nm as function of aqueous solution pH value. [L-Tar]=0.3 mmol.L <sup>-1</sup> , [D-Tar]=0.3 mmol.L <sup>-1</sup>	70
Figure IV-A-5:	Chemical structure of Pyruvic acid	70
Figure IV-A-6:	The UV-visible spectra of 0.3 mmol.L <sup>-1</sup> Pyruvic acid solution as a function of pH. (a) UV-visible spectra; (b) Absorbance at 250nm	71
Figure IV-A-7:	Chemical structure of Citric acid	71

Figure IV-A-8:	UV-Visible absorption spectra of different aqueous solution. (a) measurement in 1cm cell; (b) measurement in 1mm cell	73
Figure IV-A-9:	UV-Visible absorption spectra of different aqueous solutions. $[\text{Fe(III)}]=0.3\text{mmol.L}^{-1}$ , $\text{pH}=2.0$ .	74
Figure IV-A-10:	Absorbance at 340 nm as a function of tartaric acid concentration. $[\text{Fe(III)}]=0.3\text{ mmol.L}^{-1}$ , $\text{pH}=2.0$ .	74
Figure IV-A-11:	UV-Visible absorption spectra of different aqueous solutions. $[\text{Fe(III)}]=0.3\text{ mmol.L}^{-1}$ , $\text{pH}=2.0$ .	75
Figure IV-A-12:	Absorbance at 340 nm as a function of tartaric acid concentration. $[\text{Fe(III)}] = 0.3\text{ mmol.L}^{-1}$ , $\text{pH} = 2.0$ .	75
Figure IV-A-13:	UV-Visible absorption spectra of different aqueous solutions. $[\text{Fe(III)}]=0.3\text{ mmol.L}^{-1}$ , $\text{pH}=2.0$ .	76
Figure IV-A-14:	Absorbance at 340 nm as a function of pyruvic acid concentration of. $[\text{Fe(III)}] = 0.3\text{ mmol.L}^{-1}$ , $\text{pH} = 2.0$ .	77
Figure IV-A-15:	Stability of the Fe(III)-D-Tar complexes as a function of time, in the dark and at room temperature	78
Figure IV-A-16:	Stability of the Fe(III)-L-Tar complexes as a function of time, in the dark and at room temperature	78
Figure IV-A-17:	UV-Visible absorption spectra of Fe-D-Tar complex solution as function of pH. $[\text{Fe(III)}]/[\text{D-Tar}] = 0.3\text{ mmol.L}^{-1}/0.6\text{ mmol.L}^{-1}$ (a) UV-Visible spectra of Fe(III)-D-Tar complex; (b) Absorbance at 340 nm	79
Figure IV-A-18:	UV-Visible absorption spectra of Fe(III)-L-Tar complex solution as function of pH. $[\text{Fe(III)}]/[\text{L-Tar}] = 0.3\text{ mmol.L}^{-1}/0.6\text{ mmol.L}^{-1}$ (a) UV-Visible spectra of Fe(III)-L-Tar complex (b) Absorbance at 340 nm.	80
Figure IV-A-19:	UV-Visible absorption spectra of Fe(III)-Pyr complex solution as function of pH. $[\text{Fe(III)}]/[\text{Pyr}] = 0.3\text{ mmol.L}^{-1}/0.9\text{ mmol.L}^{-1}$ (a) UV-Visible spectra of Fe(III)-Pyr complex (b) Absorbance at 340 nm	80
Figure IV-A-20:	UV-visible spectra of Fe(III)-Cit complexes ( $0.3\text{ mmol.L}^{-1}$ ) as function of pH. (a) UV-Visible spectra of Fe(III)-Cit	81

complex; (b) Absorbance at 270 nm (Abida, 2005)

Figure IV-A-21:	Variation of UV-visible spectra of Fe(III)-Carboxylate complexes ( $0.3 \text{ mmol.L}^{-1}$ ) under irradiation (a) Fe(III)-Cit; (b) Fe(III)-Tar; (c) Fe(III)-Pyr.	82
Figure IV-B-1:	UV-Visible spectrum of solutions with $C_{\text{Fe(III)}} = 100 \text{ } \mu\text{mol.L}^{-1}$ and with or without $C_{\text{Pyr}} = 300 \text{ } \mu\text{mol.L}^{-1}$ . The length of the cell was 1 cm. Initial pH of the aqueous solution was 3.0. The spectrum of the metal halide light used in this work is also shown.	84
Figure IV-B-2:	Photoreaction mechanism	85
Figure IV-B-3:	Comparison of $\cdot\text{OH}$ formation under different conditions for an aqueous solution with $C_{\text{Fe(III)}} = 10 \text{ } \mu\text{mol.L}^{-1}$ , $C_{\text{Pyr}} = 90 \text{ } \mu\text{mol.L}^{-1}$ . Initial pH of the aqueous solution was 3.0.	86
Figure IV-B-4:	Effect of the initial pH value on the total $\cdot\text{OH}$ concentration for an aqueous solution with $C_{\text{Fe(III)}} = 30 \text{ } \mu\text{mol.L}^{-1}$ , $C_{\text{Pyr}} = 60 \text{ } \mu\text{mol.L}^{-1}$ .	87
Figure IV-B-5:	Effect of the Pyr concentration on the $\cdot\text{OH}$ total yield for aqueous solutions with $C_{\text{Fe(III)}} = 10 \text{ } \mu\text{mol.L}^{-1}$ . Initial pH of the aqueous solution was 3.0.	88
Figure IV-B-6:	Effect of the Fe(III) concentration on the $\cdot\text{OH}$ total yield for aqueous solutions with $C_{\text{Pyr}} = 30 \text{ } \mu\text{mol.L}^{-1}$ . Initial pH of the aqueous solution was 3.0.	88
Figure IV-B-7:	Effect of temperature on the $\cdot\text{OH}$ total yield for an aqueous solution with $C_{\text{Fe(III)}} = 10 \text{ } \mu\text{mol.L}^{-1}$ , and $C_{\text{Pyr}} = 30 \text{ } \mu\text{mol.L}^{-1}$ . Initial pH of the aqueous solution was 3.0.	89
Figure IV-B-8:	Control experiments in different systems $C_{\text{Fe(III)}} = 10.0 \text{ } \mu\text{mol.L}^{-1}$ , $C_{\text{Cit}} = 120.0 \text{ } \mu\text{mol.L}^{-1}$ , $\text{pH} = 3.0$	90
Figure IV-B-9:	UV-Vis absorption spectra of the solutions with or without citrate a: without Citrate, b: with Citrate ( $C_{\text{Fe(III)}} = 100.0 \text{ } \mu\text{mol.L}^{-1}$ , $C_{\text{Cit}} = 300.0 \text{ } \mu\text{mol.L}^{-1}$ , $C_{\text{benzene}} = 7 \text{ mmol.L}^{-1}$ , $\text{pH} = 3.0$ )	91
Figure IV-B-10:	Initial pH value effects on the photoproduction of $\cdot\text{OH}$ ( $C_{\text{Fe(III)}} = 30.0 \text{ } \mu\text{mol.L}^{-1}$ , $C_{\text{Cit}} = 30.0 \text{ } \mu\text{mol.L}^{-1}$ )	92

Figure IV-B-11:	pH effects on the distribution of Fe(III) species ( $C_{\text{Fe(III)}}=30.0\mu\text{mol.L}^{-1}$ , $C_{\text{Cit}}=30.0\mu\text{mol.L}^{-1}$ , Ionic strength= 0, 25°C)	93
Figure IV-B-12:	Effect of citrate concentration on the photoproduction of $\cdot\text{OH}$ radical (pH = 3.0, $C_{\text{Cit}} = 15.0$ to $120.0 \mu\text{mol.L}^{-1}$ , $C_{\text{Fe(III)}} = 10.0\mu\text{mol.L}^{-1}$ )	95
Figure IV-B-13:	Effect of ferric concentration on photoproduction of $\cdot\text{OH}$ radicals (pH = 3.0, $C_{\text{Cit}} = 30.0 \mu\text{mol.L}^{-1}$ , $C_{\text{Fe(III)}} = 10.0$ to $60.0 \mu\text{mol.L}^{-1}$ )	95
Figure IV-B-14:	Photochemical reaction mechanism	96
Figure IV-B-15:	HPLC chromatogram of the phenol photogeneration as a function of irradiation time ( $C_{\text{Fe(III)}} = 10.0 \mu\text{mol.L}^{-1}$ , $C_{\text{Tar}} = 150.0 \mu\text{mol.L}^{-1}$ and $C_{\text{benzene}} = 7 \text{ mmol.L}^{-1}$ ). The initial pH value of the aqueous solution was 3.0. $\lambda_{\text{det}} = 270 \text{ nm}$ .	97
Figure IV-B-16:	Comparing of $\cdot\text{OH}$ radicals yield in different conditions. In an aqueous solution of $C_{\text{Fe(III)}} = 10.0\mu\text{mol.L}^{-1}$ and $C_{\text{Tar}} = 150.0\mu\text{mol.L}^{-1}$ . The initial pH value of the aqueous solution was 3.0.	98
Figure IV-B-17:	Effect of initial pH value on the $\cdot\text{OH}$ radicals yield ( $C_{\text{Fe(III)}}= 30.0 \mu\text{mol.L}^{-1}$ and $C_{\text{Tar}} = 60.0 \mu\text{mol.L}^{-1}$ ).	99
Figure IV-B-18:	Distribution of iron and Tartrate species as a function of pH in a system with $C_{\text{Fe(III)}} = 10.0\mu\text{mol.L}^{-1}$ and $C_{\text{Tar}} = 30.0\mu\text{mol.L}^{-1}$ . Ionic strength= 0. Calculations were done at 25°C with MINTEQA2 computer program.	100
Figure IV-B-19:	Effects of tartaric acid concentration on the $\cdot\text{OH}$ radicals concentration. The initial pH value of the aqueous solution was 3.0.	101
Figure IV-B-20:	Effect of the Fe(III) concentration on the $\cdot\text{OH}$ radicals formation. The initial pH value of the aqueous solution was 3.0.	102
Figure IV-B-21:	Effect of temperature on the $\cdot\text{OH}$ radicals concentration ( $C_{\text{Fe(III)}} = 10.0 \mu\text{mol.L}^{-1}$ , and $C_{\text{Tar}} = 30.0 \mu\text{mol.L}^{-1}$ ). The initial pH value of the aqueous solution was 3.0. (a) Without cooling water the temperature is about 328 K, (b) with	103

cooling water the temperature is about 298 K.

Figure IV-B-22	Photochemical cycle Fe(III)/Fe(II) in the presence of organic pollutant (Chlortoluron), from Poulain et al, 2003.	105
Figure IV-C-1:	The UV-visible spectra of 2,4-Dichlorophenol.	106
Figure IV-C-2:	The UV-visible spectra of 2,4-Dichlorophenol at different concentrations.	107
Figure IV-C-3:	pH effect on the distribution of 2,4-Dichlorophenol species in aqueous solution.	108
Figure IV-C-4:	Absorbance at 244 nm as function of pH in aqueous solution with 0.1mM 2,4-DCP	108
Figure IV-C-5:	Protonation equilibrium of 2,4-DCP in the aqueous solution	108
Figure IV-C-6:	UV-Visible absorption spectra of an aqueous solution of [Fe(III)] = 0.3 mmol.L <sup>-1</sup> recorded at different time after the preparation.	109
Figure IV-C-7:	pH effect on the distribution of Fe(III) species in aqueous solutions.	110
Figure IV-C-8:	UV-Visible absorption spectra of aqueous solution after 3 min preparation with 0.1 mmol.L <sup>-1</sup> Fe(III) and 0.1 mmol.L <sup>-1</sup> 2,4-DCP.	111
Figure IV-C-9:	UV-Visible absorption spectra of an aqueous solution with 0.1 mmol.L <sup>-1</sup> of Fe(III) and 0.3 mmol.L <sup>-1</sup> of 2,4-DCP recorded at different time after the preparation.	112
Figure IV-C-10:	Determination of Fe(OH) <sup>2+</sup> species in different solutions as function of time. T = 22°C.	112
Figure IV-C-11:	Variation of the UV-visible spectra of the reaction solutions as a function of the irradiation time. [Fe(III)] = 0.21 mmol.L <sup>-1</sup> , initial pH value is 3.3.	113
Figure IV-C-12:	Photodegradation of 2,4-DCP in the aqueous solutions with Fe(ClO <sub>4</sub> ) <sub>3</sub> .	113
Figure IV-C-13-a:	pH effect on the quantum yields of Fe(II). In the aqueous	119

solutions with 0.1 mmol.L<sup>-1</sup> 2,4-DCP. ( $\lambda_{irr} = 365 \text{ nm}$ )

- Figure IV-C-13-b: pH effect on the quantum yields of Fe(II). In the aqueous solutions with 0.3 mmol.L<sup>-1</sup> of Fe(III)-Cit and 0.1 mmol.L<sup>-1</sup> of 2,4-DCP. ( $\lambda_{irr} = 365 \text{ nm}$ ) 119
- Figure IV-C-14: Effects of 2,4-DCP concentration on the quantum yields of Fe(II) and 2,4-DCP. The initial pH value was 3.0. ( $\lambda_{irr}=365\text{nm}$ ) 123
- Figure IV-C-15: UV-Visible spectra of aqueous solution with 0.1 mmol.L<sup>-1</sup> Fe(III)-Cit 123
- Figure IV-C-16: Structure of Fe(III)-Cit.(Abida, 2005) 124
- Figure IV-C-17: Comparing of the UV-visible spectra of different aqueous solutions. 124
- Figure IV-C-18: Degradation of 2,4-DCP as a function of Fe(III)-Cit concentration in solution with an initial pH = 3.0. [2,4-DCP] = 0.1 mmol.L<sup>-1</sup> 126
- Figure IV-C-19: The photogeneration of Fe(II) as a function of Fe(III)-Cit concentration in solution with an initial pH = 3.0. [2,4-DCP] = 0.1 mmol.L<sup>-1</sup>. 126
- Figure IV-C-20: Influence of pH on the photodegradation of 2,4-DCP in the presence of Fe(III)-Cit complexes. [Fe(III)-Cit] = 0.3 mmol.L<sup>-1</sup>, [2,4-DCP] = 0.1 mmol.L<sup>-1</sup>. 127
- Figure IV-C-21: Influence of pH on the photogeneration of Fe(II) in the presence of Fe(III)-Cit complexes. [Fe(III)-Cit] = 0.3 mmol.L<sup>-1</sup>, [2,4-DCP] = 0.1 mmol.L<sup>-1</sup>. 128
- Figure IV-C-22: Effects of oxygen on the photodegradation of 2,4-DCP in the presence of Fe(III)-Cit complexes. [Fe(III)-Cit] = 0.3 mmol.L<sup>-1</sup>, [2,4-DCP] = 0.1 mmol.L<sup>-1</sup>, pH=3.0 129
- Figure IV-C-23: Effects of oxygen on the photogeneration of Fe(II) in the presence of Fe(III)-Cit complexes. [Fe(III)-Cit] = 0.3 mmol.L<sup>-1</sup>, [2,4-DCP] = 0.1 mmol.L<sup>-1</sup>, pH=3.0 130
- Figure IV-C-24a: Photodegradation of 2,4-DCP as a function of Fe(III)-D-Tar concentration in solutions with an initial pH=3.0. 131



$[2,4\text{-DCP}]_0 = 0.1 \text{ mmol.L}^{-1}$ .

- Figure IV-C-24b: Photodegradation of 2,4-DCP as a function of Fe(III)-L-Tar concentration in solutions with an initial pH=3.0.  $[2,4\text{-DCP}]_0 = 0.1 \text{ mmol.L}^{-1}$ . 131
- Figure IV-C-25: Photogeneration of Fe(II) as a function of Fe(III)-D or L-Tar concentration in solutions with an initial pH=3.0.  $[2,4\text{-DCP}]_0 = 0.1 \text{ mmol.L}^{-1}$ . 132
- Figure IV-C-26: Photodegradation of 2,4-DCP as a function of Fe(III)-D or L-Tar concentration with an initial pH = 3.0.  $[2,4\text{-DCP}]_0 = 0.1 \text{ mmol.L}^{-1}$ . 133
- Figure IV-C-27: Photogeneration of Fe(II) as a function of Fe(III)-D or L-Tar concentration in solutions with an initial pH = 3.0.  $[2,4\text{-DCP}]_0 = 0.1 \text{ mmol.L}^{-1}$ . 133
- Figure IV-C-28: pH effect on the photodegradation of 2,4-DCP.  $[\text{Fe(III)}]/[\text{D or L-Tar}] = 0.3 \text{ mmol.L}^{-1}/0.6 \text{ mmol.L}^{-1}$ ,  $[2,4\text{-DCP}]_0 = 0.1 \text{ mmol.L}^{-1}$ . 134
- Figure IV-C-29: Photogeneration of Fe(II) as function of pH value.  $[\text{Fe(III)}]/[\text{D or L-Tar}] = 0.3 \text{ mmol.L}^{-1}/0.6 \text{ mmol.L}^{-1}$ ,  $[2,4\text{-DCP}]_0 = 0.1 \text{ mmol.L}^{-1}$ . 135
- Figure IV-C-30: Variation of the UV-visible spectra of the reaction solutions as a function of the irradiation time. (a)  $[\text{Fe(III)}]/[\text{D or L-Tar}] = 0.2 \text{ mmol.L}^{-1}/0.4 \text{ mmol.L}^{-1}$  (b)  $[\text{Fe(III)}]/[\text{D or L-Tar}] = 0.01 \text{ mmol.L}^{-1}/0.02 \text{ mmol.L}^{-1}$ .  $\lambda_{\text{irr}} = 365\text{nm}$ ; Initial pH value was 3.0. 136
- Figure IV-C-31: Effects of oxygen on the photodegradation of 2,4-DCP in the presence of Fe(III)-D or L-Tar complexes.  $[\text{Fe(III)-D or L-Tar}] = 0.3 \text{ mmol.L}^{-1}$ ,  $[2,4\text{-DCP}] = 0.1 \text{ mmol.L}^{-1}$ , pH = 3.0 137
- Figure IV-C-32: Effects of oxygen on the photogeneration of Fe(II) in the presence of Fe(III)-D or L-Tar complexes.  $[\text{Fe(III)-D or L-Tar}] = 0.3 \text{ mmol.L}^{-1}$ ,  $[2,4\text{-DCP}] = 0.1 \text{ mmol.L}^{-1}$ , pH = 3.0 138
- Figure IV-C-33: Photodegradation of 2,4-DCP as a function of Fe-Pyr concentration in solution with an initial pH = 3.0.  $[2,4\text{-DCP}]_0 = 0.1 \text{ mmol.L}^{-1}$ . 139

Figure IV-C-34:	Photogeneration of Fe(II) as a function of Fe-Pyr concentration in solutions with an initial pH = 3.0. [2,4-DCP] <sub>0</sub> = 0.1 mmol.L <sup>-1</sup> .	139
Figure IV-C-35:	pH effect on the photodegradation of 2,4-DCP. [Fe(III)]/[Pyr] = 0.1 mmol.L <sup>-1</sup> /0.3 mmol.L <sup>-1</sup> , [2,4-DCP] <sub>0</sub> = 0.1 mmol.L <sup>-1</sup> .	140
Figure IV-C-36:	Photogeneration of Fe(II) as function of pH value. [Fe(III)]/[Pyr] = 0.1 mmol.L <sup>-1</sup> /0.3 mmol.L <sup>-1</sup> , [2,4-DCP] <sub>0</sub> = 0.1 mmol.L <sup>-1</sup> .	141
Figure IV-C-37:	Effect of oxygen on the photodegradation of 2,4-DCP in the presence of Fe(III)-Pyr complexes. [Fe(III)-Pyr] = 0.3 mmol.L <sup>-1</sup> , [2,4-DCP] = 0.1 mmol.L <sup>-1</sup> , pH = 3.0	142
Figure IV-C-38:	Effect of oxygen on the photogeneration of Fe(II) in the presence of Fe(III)-Pyr complexes. [Fe(III)-Pyr] = 0.3 mmol.L <sup>-1</sup> , [2,4-DCP] = 0.1 mmol.L <sup>-1</sup> , pH = 3.0	142
Figure IV-C-39:	Photodegradation of 2,4- DCP in different systems. [2,4-DCP] = 0.1 mmol.L <sup>-1</sup> , pH = 3.0	143
Figure IV-C-40:	Photogeneration of Fe(II) in different systems. [2,4-DCP] = 0.1 mmol.L <sup>-1</sup> , pH = 3.0	144
Figure IV-C-41:	Time courses of TOC values during irradiation of mixtures of 0.1 mmol.L <sup>-1</sup> of 2,4-DCP and 0.3 mmol.L <sup>-1</sup> of Fe(III)-Carboxylate complexes. (a) Fe(III)-Tar; (b) Fe(III)-Pyr; (c) Fe(III)-Cit, λ <sub>irr</sub> = 365 nm	146
Figure IV-D-1:	The UV-visible spectra of 2,4-D at different concentrations.	149
Figure IV-D-2:	Molar absorption coefficients at different wavelength. (a) 230nm, (b) 284nm.	150
Figure IV-D-3:	UV-Visible absorption spectra of aqueous solution 3 min after the preparation with 0.1 mmol.L <sup>-1</sup> of Fe(III) and 0.1 mmol.L <sup>-1</sup> of 2,4-D	150
Figure IV-D-4:	pH effect on the quantum yields of Fe(II) formation in the presence of 0.1 mmol.L <sup>-1</sup> of 2,4-D. (λ <sub>irr</sub> = 365 nm)	154
Figure IV-D-5:	Effects of 2,4-D concentration on the quantum yields of	156

Fe(II) formation. The initial pH of the aqueous solutions is 3.0. ( $\lambda_{irr}=365\text{nm}$ )

- Figure IV-D-6: Effects of 2,4-D concentration on the quantum yields of 2,4-D disappearance. The initial pH of the aqueous solutions is 3.0. ( $\lambda_{irr} = 365 \text{ nm}$ ) 156
- Figure IV-D-7: Degradation of 2,4-D as a function of Fe-Cit concentration in solution with an initial pH = 3.0.  $[2,4-D]_0 = 0.1 \text{ mmol.L}^{-1}$ . 158
- Figure IV-D-8: Photogeneration of Fe(II) as a function of Fe(III)-Cit concentration in solution with an initial pH = 3.0.  $[2,4-D]_0 = 0.1 \text{ mmol.L}^{-1}$ . 158
- Figure IV-D-9: Degradation of 2,4-D as function of oxygen in solutions with an initial pH = 3.0.  $[\text{Fe-Cit}]_0 = 0.1 \text{ mmol.L}^{-1}$ ,  $[2,4-D]_0 = 0.1 \text{ mmol.L}^{-1}$ . 159
- Figure IV-D-10: Photogeneration of Fe(II) as function of oxygen in solutions with an initial pH = 3.0.  $[\text{Fe-Cit}]_0 = 0.1 \text{ mmol.L}^{-1}$ ,  $[2,4-D]_0 = 0.1 \text{ mmol.L}^{-1}$ . 160
- Figure IV-D-11: Influence of pH on the photodegradation of 2,4-D in the presence of Fe(III)-Cit complexes.  $[\text{Fe(III)-Cit}]_0 = 0.3 \text{ mmol.L}^{-1}$ ,  $[2,4-D]_0 = 0.1 \text{ mmol.L}^{-1}$ . 161
- Figure IV-D-12: Influence of pH on the photogeneration of Fe(II) in the presence of Fe-Cit complexes.  $[\text{Fe(III)-Cit}]_0 = 0.3 \text{ mmol.L}^{-1}$ ,  $[2,4-D]_0 = 0.1 \text{ mmol.L}^{-1}$ . 161
- Figure IV-D-13: Degradation of 2,4-D as a function of Fe(III)-Pyr concentration with an initial pH = 3.0.  $[2,4-D]_0 = 0.1 \text{ mmol.L}^{-1}$ . 162
- Figure IV-D-14: Photogeneration of Fe(II) as a function of Fe(III)-Pyr concentration with an initial pH = 3.0.  $[2,4-D]_0 = 0.1 \text{ mmol.L}^{-1}$ . 163
- Figure IV-D-15: UV-visible spectrum of the solutions as a function of the irradiation time. (a)  $[\text{Fe(III)-Pyr}] = 0.1 \text{ mmol.L}^{-1}/0.3 \text{ mmol.L}^{-1}$ , (b)  $[\text{Fe(III)-Pyr}] = 0.2 \text{ mmol.L}^{-1}/0.6 \text{ mmol.L}^{-1}$  164
- Figure IV-D-16: Degradation of 2,4-D as function of oxygen in solutions with an initial pH = 3.0.  $[\text{Fe(III)-Pyr}]_0 = 0.1 \text{ mmol.L}^{-1}$ ,  $[2,4-D]_0 =$  165

0.1 mmol.L<sup>-1</sup>.

- Figure IV-C-17: Influence of pH on the photodegradation of 2,4-D in the presence of Fe(III)-Pyr complexes. [Fe(III)-Pyr]<sub>0</sub> = 0.1 mmol.L<sup>-1</sup>, [2,4-D]<sub>0</sub> = 0.1 mmol.L<sup>-1</sup>. 166
- Figure IV-D-18: Influence of pH on the photogeneration of Fe(II) in the presence of Fe(III)-Pyr complexes. [Fe(III)-Pyr]<sub>0</sub> = 0.1 mmol.L<sup>-1</sup>, [2,4-D]<sub>0</sub> = 0.1 mmol.L<sup>-1</sup>. 167
- Figure IV-D-19: UV-visible spectrum as a function of the irradiation time. [Fe(III)-Pyr] = 0.3 mmol.L<sup>-1</sup>/0.9 mmol.L<sup>-1</sup>, pH = 3.84. 167
- Figure IV-D-20: Degradation of 2,4-D as a function of Fe(III)-Tar concentration with an initial pH = 3.0. [2,4-D]<sub>0</sub> = 0.1 mmol.L<sup>-1</sup>. 168
- Figure IV-D-21: Photogeneration of Fe(II) as a function of Fe-Tar concentration in solution with an initial pH = 3.0. [2,4-D]<sub>0</sub> = 0.1 mmol.L<sup>-1</sup>. 169
- Figure IV-D-22: UV-visible spectra of the solutions as a function of the irradiation time. [Fe(III)-Tar] = 0.3 mmol.L<sup>-1</sup>/0.6 mmol.L<sup>-1</sup>, pH = 3.0. 170
- Figure IV-D-23: Influence of pH on the photodegradation of 2,4-D in the presence of Fe-Tar complexes. [Fe(III)-Tar]<sub>0</sub> = 0.1 mmol.L<sup>-1</sup>, [2,4-D]<sub>0</sub> = 0.1 mmol.L<sup>-1</sup>. 170
- Figure IV-D-24: Influence of pH on the photogeneration of Fe(II) in the presence of Fe(III)-Tar complexes. [Fe(III)-Tar]<sub>0</sub> = 0.1 mmol.L<sup>-1</sup>, [2,4-D]<sub>0</sub> = 0.1 mmol.L<sup>-1</sup>. 171
- Figure IV-D-25: UV-visible spectrum of the solutions according to the time. [Fe(III)-Tar] = 0.1 mmol.L<sup>-1</sup>/0.2 mmol.L<sup>-1</sup>, pH = 3.5 172
- Figure IV-D-26: Photodegradation of 2,4-D with different complexes. [2,4-D] = 0.1 mmol.L<sup>-1</sup>, pH = 3.0 173
- Figure IV-D-27: Photogeneration of Fe(II) with different iron-complexes. [2,4-D] = 0.1 mmol.L<sup>-1</sup>, pH = 3.0 173
- Figure IV-D-28: Evolution of total organic carbon as function of oxygen concentration. (a) Mixture of 0.1 mmol.L<sup>-1</sup> in Fe(III)-Cit and 174

0.1 mmol.L<sup>-1</sup> in 2,4-D, (b) mixture of 0.3 mmol.L<sup>-1</sup> in Fe(III)-Tar and 0.1 mmol.L<sup>-1</sup> in 2,4-D, pH = 3.0.

- Figure IV-D-29: Evolution of total organic carbon in the solution with 0.1 mmol.L<sup>-1</sup> in Fe(III)-Tar and 0.1 mmol.L<sup>-1</sup> in 2,4-D as function of pH. 175
- Figure IV-E-1: ESR spectra of the aqueous solution with 1 mg.mL<sup>-1</sup> DMPO and 0.3 mmol.L<sup>-1</sup> Fe(III)-Cit complex at pH 3.0 after 50min irradiation  $\lambda \geq 280$  nm. Cell quartz has 1 mm path length. 179
- Figure IV-E-2: ESR spectra of the aqueous solution with 1 mg.mL<sup>-1</sup> DMPO and 0.3 mmol.L<sup>-1</sup> Fe(III)-Cit complex at pH 3.0 during irradiation (a)  $\lambda \geq 280$  nm, (b)  $\lambda \geq 350$  nm 180
- Figure IV-E-3: ESR spectra of the aqueous solution with 1 mg.mL<sup>-1</sup> in DMPO and 0.3 mmol.L<sup>-1</sup> in Fe(III)-Tar complex at pH = 3.0 during irradiation (a)  $\lambda \geq 280$  nm, (b)  $\lambda \geq 350$  nm 180
- Figure IV-E-4: ESR spectra of the aqueous solution with 1 mg.mL<sup>-1</sup> in DMPO and 0.3 mmol.L<sup>-1</sup> in Fe(III)-Pyr complex at pH = 3.0 during irradiation (a)  $\lambda \geq 280$  nm, (b)  $\lambda \geq 350$  nm 181
- Figure IV-E-5: ESR spectra of the aqueous solution with 1mg.mL<sup>-1</sup> in DMPO and (a) 0.3 mmol.L<sup>-1</sup> in Fe(III)-Tar complex, (b) 0.3 mmol.L<sup>-1</sup> in Fe(III)-Pyr complex at pH 6.0 under irradiation at  $\lambda \geq 280$  nm. 182
- Figure IV-E-6 Photodegradation of 2,4-D with different complexes in different systems with 0.1 mmol.L<sup>-1</sup> of 2,4-D at pH = 3.0. 184
- Figure IV-E-7: Evolution of HPLC area of product 2,4-DCP in different systems with 0.1 mmol.L<sup>-1</sup> 2,4-D at pH = 3.0. 185
- Figure IV-E-8: Evolution of the HPLC chromatograms of solution as a function of the irradiation time with 0.3 mmol.L<sup>-1</sup> in Fe(III)-Tar and 0.1 mmol.L<sup>-1</sup> in 2,4-DCP at pH = 3.0. 187
- Figure IV-E-9: HPLC chromatogram of solution of 0.3 mmol.L<sup>-1</sup> Fe(III)-Tar and 0.1 mmol.L<sup>-1</sup> 2,4-DCP at pH = 3.9, after 8 h of irradiation. 187
- Figure IV-E-10: Evolution of HPLC spectrum of reaction solution with 0.1 mmol.L<sup>-1</sup> Fe(III)-Pyr and 0.1 mmol.L<sup>-1</sup> 2,4-DCP at pH = 2.5 188

Figure IV-E-11:	Time evolution of HPLC area of photoproducts generated in the solutions of $0.3 \text{ mmol.L}^{-1}$ Fe(III)-Tar and $0.1 \text{ mmol.L}^{-1}$ 2,4-DCP at pH = 3.9	188
Figure IV-E-12:	LC-MS spectra of 2,4-DCP ( $0.1 \text{ mmol.L}^{-1}$ )	190
FigureIV-E-13-a:	Total ion chromatogram	190
FigureIV-E-13-b:	LC-MS spectra of photoproducts	192
Figure IV-E-14:	Proposed photodegradation scheme of 2,4-DCP	193

## **VII**

# **REFERENCES**





## **VIII-REFERENCES**

Abe K.I., Tanaka K., Fe<sup>3+</sup> and UV-enhanced ozonation of chlorophenolic compounds in aqueous medium. *Chemosphere*. 1997 (35) 2837–2847.

Abida O., Impact complexes of iron and the solar light on the fate of pollutants in the aquatic environment. Ph.D.Thesis. University Blaise Pascal. 2005.

Abida O., Mailhot G., Litter M., Bolte M., Impact of iron-complex (Fe(III)-NTA) on photoinduced degradation of 4-chlorophenol in aqueous solution. *Photochemical and Photobiological Sciences*, 2006 (5) 395-402.

Abrahamson H.B., Rezvani A.B., Brushmiller J.G., Photochemical and spectroscopic studies of complexes of iron(III) with citric acid and other carboxylic acids. *Inorganic Chimica Acta*. 1994 (226) 117–127.

Alabdula'aly A.I., Khan M.A., Chemistry of Rain Water in Riyadh, Saudi Arabia. *Arch. Environ. Contam. Toxicol.*, 2000 (39) 66–73.

Al-Momani I.F., Trace elements in atmospheric precipitation at Northern Jordan measured by ICP-MS: acidity and possible sources. *Atmos. Environ.*, 2003 (37) 4507–4515.

Anderson M.A., Morel F.M.M., The influence of aqueous iron chemistry on the uptake of iron by the coastal diatom *Thalassiosira weissflogii*. *Limnol. Oceanogr.* 1982 (27) 789-813.

Androulaki E., Hiskia A., Dimotikali D., Minero C., Calza P., Pelizzetti E., Papaconstantinou E., Light induced elimination of mono and polychlorinated phenols from aqueous solutions by  $PW_{12}O_{40}^{3-}$ . The case of 2,4,6-trichlorophenol. *Environ. Sci. Technol.* 2000 (34) 2024–2028.

Arakaki T., Faust B.C., Sources, sinks, and mechanisms of hydroxyl radical ( $\bullet$ OH) photoproduction and consumption in authentic acidic continental cloud waters from Whiteface Mountain, New York: the role of the Fe(r) (r = II, III) photochemical cycle. *J. Geophys. Res.*, 1998 (103: D3) 3487–3504.

Arakaki T, Miyake T, Hirakawa T, Sakugawa H: pH dependent photoformation of hydroxyl radical and absorbance of aqueous-phase N(III) ( $HNO_2$  and  $NO_2^-$ ).

Environ. Sci. Technol., 1999 (33) 2561–2565.

ATSDR, Toxicological profile for chlorophenols, Agency for Toxic Substances and Disease Registry, US; 1999, Document No. 205-93-0606.

Balls P.W., Trace metal and major ion composition of precipitation at the North Sea coastal site. *Atmosph. Environ.* 1989 (23) 2751–2759.

Bandara J., Mielczarski J.A., Lopez A., Kiwi J., Sensitized degradation of chlorophenols on iron oxides induced by visible light. Comparison with titanium oxide. *Appl. Catal. B.* 2001 (34) 321–333.

Baum G., Oppenlaender T., Vacuum-UV-oxidation of chloroorganic compounds in an excimer flow through photoreactor. *Chemosphere.* 1995, 30 (9) 1781–1790.

Beavington F., Cawse P.A., The deposition of trace elements and major nutrients in dust and rainwater in northern Nigeria. *Sci. Total. Environ.*, 1979 (13) 263-274.

Behra P., Sigg L., Evidence for redox cycling of iron in atmospheric water. *Nature*, 1990 (344) 419-421.

Benítez F.J., Beltrán-Heredia J., Acero J.L., Rubio F.J., Rate constants for the reactions of ozone with chlorophenols in aqueous solutions. *J. Hazard. Mater. B.* 2000 (79) 271–285.

Benítez F.J., Beltrán-Heredia J., Acero J.L., Rubio F.J., Contribution of free radicals to chlorophenols decomposition by several advanced oxidation techniques. *Chemosphere.* 2000 (41) 1271–1277.

Benítez F.J., Beltrán-Heredia J., Acero J.L., Rubio F.J., Oxidation of several chlorophenolic derivatives by UV irradiation and hydroxyl radicals. *J. Chem. Technol. Biotechnol.* 2001 (76) 312–320.

Betz M., Diplomarbeit, Institut für Meteorologie and Geophysik der Universität Frankfurt/Main, Germany, September 1976.

Bielski B.H.J., Cabelli D.E., Arudi R.L., Reactivity of  $\text{OH}_2/\text{O}_2^-$  radicals in aqueous solutions. *J. Phys. Chem. Ref. Data*, 1985 (14) 1041-1051.

Brandt C., Lepentsiotis V., Paul A., Hohmann H., van Eldik R., Investigation of rain and snow water samples by AAS and IC. *GIT Fachz. Lab.*, 1994 (38) 770

Brillas E., Calpe J.C., Cabot P.L., Degradation of the herbicide

2,4-Dichlorophenoxyacetic acid by ozonation catalyzed with  $\text{Fe}^{2+}$  and UV light, *Appl. Catal. B: Environ.*, 2003 (46) 381-391.

Brown K.W., Donnelly K.C., An estimation of the risk associated with the organic constituents of hazardous and municipal waste landfill leachates. *Haz. Wast. Haz. Mater.* 1988 (5) 1-30.

Buchanan D.N.E., Mossbauer spectroscopy of radiolytic and photolytic effects on ferric citrate. *J. Inorg. Nucl. Chem.*, 1970 (32) 3531-3533.

Burkitt M.J., ESR spin trapping studies into the nature of the oxidizing species formed in the Fenton reaction: pitfalls associated with the use of 5, 5-dimethyl-1-pyrroline-N-oxide in the detection of the hydroxyl radical. *Free Radic. Res. Commun.*, 1993 (18) 43-57.

Byrne R.H., Kester, D.R., Solubility of hydrous ferric oxide and iron speciation in sea water. *Mar. Chem.*, 1976 (4) 255-274.

Byrne R.H., Kump, L.R. and Cantrell, K.J., The influence of temperature and pH on trace metal speciation in seawater. *Mar. Chem.*, 1988(25)163-181.

Calvert J.G., Pitts J.N., *J. Photochemistry*, John Wiley & Sons, New York, 1966, p. 783.

Carla B., Christiane A.R., Rodnei B., Oxidation of pesticides by in situ electrogenerated hydrogen peroxide: study for the degradation of 2,4-dichlorophenoxyacetic acid. *Journal of Hazardous Materials*. 2006, B137, 856-864.

Cautreels W., Van Cauwenberghe K., Determination of organic compounds in airborne particulate matter by gas chromatography –mass spectrometry. *Atmos. Environ.*, 1976 (10) 447-457.

Cawse P., Peirson D.H., An analytical study of trace elements in the atmospheric environment. Atmospheric Energy Research Establishment, AERE-R 7134, Harwell England, 1972.

Chan W.H., Tang J.S., Chung H.S. , Lusic M.A., Concentration and deposition of trace metals in Ontario-1982. *Water, Air, and Soil Pollut.* 1986 (29) 373-389.

Chang C., Chen J., Application of a fluorinated solvent to the conventional

ozonation process for the destruction of 2,4-dichlorophenol. *Environ. Int.* 1995 (21) 305-312.

Chebbi A., Carlier P., Carboxylic acids in the troposphere: occurrence, source and sinks. A review. *Atmos. Environ.*, 1996 (30) 4233-4249.

Chen Y., Wu F., Zhang Xu., Deng N.S., Bazhin N., Glebov E., Fe(III)-pyruvate and Fe(III)-citrate induced photodegradation of glyphosate in aqueous solutions. *J. Coord. Chem.*, 2007 (60) 2431-2439.

Chevela V.V., Matveev S.N., Semenov V.E., Bezryadin S.G., Savitskaya T.V., Gromova I.R., Shamov G.A., The structures of dimeric stereoisomeric tartrates of iron(III) as determined by molecular mechanics calculations. *Journal of molecular structure (Theochem)*. 1995 (343) 195-198.

Christensen H., Sehested K., HO<sub>2</sub> and O<sub>2</sub><sup>-</sup> Radicals at Elevated Temperatures. *J. Phys. Chem.*, 1988 (92) 3007-3011.

Church T.M., Tramontano J.M., Scudlark J.R., Jickells T.D., Tokos J.J., Knap A.H., Galloway J.N., The wet deposition of trace metals to the western Atlantic Ocean at the mid-Atlantic coast and on Bermuda'. *Atmos. Environ.*, 1984 (18) 2657-2664.

Copper G.D., DeGraff B.A., The photochemistry of the monoxalato iron(III) ion. *J. Phys. Chem.* 1972 (76) 2618-2625.

Cunningham K.M., Goldberg M.C., Weiner E.R., Photodissolution of iron oxides in the presence of adsorbed alcohols. *Photochem. Photobiol.*, 1985, 41 (4), 409.

Cunningham K.M., Goldberg M.C., Weiner E.R., Mechanisms for aqueous photolysis of adsorbed benzoate, oxalate, and succinate on iron oxyhydroxide (goethite) surfaces. *Environ. Sci. Technol.*, 1988, 22 (9) 1090-1097.

Davison W., Iron and manganese in lakes. *Earth Sci. Rev.*, 1993(34)119-163.

Deister U., Warneck P., Wurzinger C., OH radicals generated by NO<sub>3</sub><sup>-</sup> photolysis in aqueous solution: Competition kinetics and a study of the reaction OH + CH<sub>2</sub>(OH)SO<sub>3</sub><sup>-</sup>. *Ber. Bunsen-Ges. Phys. Chem.*, 1990 (94) 594-599.

Deng N.S., Wu F., Luo F., Xiao M., Ferric citrate induced photodegradation of dyes in aqueous solutions. *Chemosphere*. 1998 (36) 3101-3112.

Deng Y.W., Chen H., Wu T.X., Krzyaniak M., Wellons A., Dawn B., Douglas K., Zuo Y.G., Iron-catalyzed photochemical transformation of benzoic acid in atmospheric liquids: Product identification and reaction mechanisms. *Atmos. Environ.*, 2006 (40) 3665-3676.

Desroches S., Daydé S., Berthon G., Aluminum speciation studies in biological fluids Part 6. Quantitative investigation of aluminum(III)-tartrate complex equilibria and their potential implications for aluminum metabolism and toxicity. *Journal of Inorganic Biochemistry*. 2000 (81) 301-312.

Dhar S. K., Sichak S., Structure of sodium ferric citrate. *J. Inorg. Nucl. Chem.*, 1979 (41) 126-127.

Emmenegger L, King D W, Sigg L, Sulzberger B, Oxidation kinetics of Fe(II) in a eutrophic Swiss lake, *Environ. Sci. Technol.*, 1998 (32) 2990-2996.

Emilio C.A., Jardim W.F., Litter M.L., Mansilla H.D., EDTA destruction using the solar ferrioxalate advanced oxidation technology (AOT) Comparison with solar photo-Fenton treatment. *J. Photochem. Photobiol. A: Chem.*, 2002 (151) 121-127.

Environmental Protection Agency and Occupational Safety and Health Administration. Chemical advisory and notice of potential risk: skin exposure to molten 2,4-dichlorophenol (2,4-DCP) can cause rapid death. Washington, DC: Environmental Protection Agency and Occupational Safety and Health Administration, 2000. Available at <http://www.epa.gov/oppt/24dcp.htm>. Accessed June 13, 2000.

Erel Y., Pehkonen SO., Hoffmann M.R., Redox chemistry of iron in fog and stratus clouds. *J. Geophys. Res.*, 1993 (98) 18423-18434.

Escot M.T., Thèse de doctorat en Pharmacie, Université d'Auvergne, Clermont Ferrand (France) 1973.

Farahataziz D.Z., Ross A.B., Selected specific rates of reactions of transients from water in aqueous solution, III, Hydroxyl radical and perhydroxyl radical and their radical ions. *Natl. Bur. Stand.*, Washington, DC. 1977.

Faust B.C., Hoffmann M.R., Photoinduced reductive dissolution of alpha-iron oxide ( $\alpha\text{-Fe}_2\text{O}_3$ ) by bisulfite. *Environ. Sci. Technol.*, 1986 (20) 943-948.

Faust B.C., Hoigné J., Photolysis of Fe(III)-hydroxy complexes as sources of  $\cdot\text{OH}$  radicals in clouds, fog and rain, *Atmos. Environ.*, 1990, 24A, 79-89.

Faust B.C., Zepp R.G., Photochemistry of Aqueous Iron(III)-Polycarboxylate complexes: Roles in the Chemistry of Atmospheric and Surface Waters. *Environ. Sci. Technol.*, 1993 (27) 2517-2522

Faust B.C., Allen J.M., Aqueous-phase photochemical formation of hydroxyl radical in authentic cloudwaters and fogwaters. *Environ. Sci. Technol.*, 1993 (27), 1221-1224.

Faust B.C., A review of the photochemical redox reactions of iron(III) species in atmospheric, oceanic, and surface waters: influences on geochemical cycles and oxidant formation. In: Helz G.R., Zepp R.G., Crosby D.G. (Editors), *Aquatic and Surface Photochemistry*, CRC Press, Boca Raton, FL, 1994, 3-38.

Finkelstein E., Rosen G.M., Rauckman E.J., Paxton J., Spin trapping of superoxide. *Mol. Pharmacol.* 1979 (16) 676-685.

Fox T.R., Comerford N.B., Low-molecular-weight organic acids in selected forest soils of the southern USA. *Soil. Sci. Am. J.* 1990 (54) 1139-1144.

Flynn Jr. C.M., Hydrolysis of inorganic iron(III) salts. *Chem. Rev.* 1984 (84) 31-41.

Frahn J.L., The photochemical decomposition of the citrate ferric iron complex: A study of the reaction products by paper ionophoresis. *Aust. J. Chem.*, 1958 (11) 399-405.

Francis A.J., Dodge C.J., Influence of complex structure on the biodegradation of iron-citrate complexes. *Applied and Environmental Microbiology.* 1993, 59 (1), 109-113.

Freydier R., Dupre B., Lacaux J.P., Precipitation chemistry in intertropical Africa. *Atmospheric Environment*, 1998 (32) 749-765.

Gallard H., De Laat J., Kinetic modelling of Fe(III)/ $\text{H}_2\text{O}_2$  oxidation reactions in dilute aqueous solution using atrazine as a model organic compound. *Wat. Res.*, 2000

(34) 3107-3116.

Gallet J.P., Paris R.A., Etude thermometrique de la formation des complexes citriques et tartriques des lanthanides. *Anal. Chim. Acta.*, 1968 (40) 321-327.

Gao H.Z., Zepp R.G., Factors Influencing Photoreactions of Dissolved Organic Matter in a Coastal River of the Southeastern United States. *Environ. Sci. Technol.*, 1998 (32) 2940-2946.

Georgii H.W., Perseke C., Rohbock E., Feststellung der deposition von sauren and langzeitwirksamen luftverunreinigungen ans belastungsgebieten. Teil A: depositionsmessungen in der Bundesrepublik Deutschland (Determination of the deposition of acids and long time effective air pollutants from polluting area. Part A: Deposition measurements in the Federal Republic Germany), Umweltbundesamt Berlin, Forschungsbericht 104 02 600 UBA-FB 82-064, Erich Schmidt Verlag, Berlin, 1983.

Giménez J., Curcó D., Qeral M.A., Photocatalytic treatment of phenol and 2,4-dichlorophenol in a solar plant in the way to scaling-up. *Catal. Today*, 1999 (54) 229-243.

Gledhill M., van den Berg, C.M.G., Determination of complexation of iron (III) with natural organic complexing ligands in seawater using cathodic stripping voltammetry. *Mar. Chem.*, 1994 (47) 41-54.

Gledhill M., van den Berg C.M.G., Measurement of the redox speciation of iron in seawater by catalytic stripping voltammetry. *Mar. Chem.*, 1995 (50) 51-61, this volume.

Gravenhorst G., Beilke S., Betz M., Georgii H.W., Effect of Acid Precipitation on Terrestrial Ecosystems, Hutchinson, T.C., Havas, M., Eds., Plenum Publishing Corporation, New York, 1980, 41-55

Grosjenl D., Van Cauwenberghe K., Schmid J., Kelley P., Pitts J.N., Identification of C3-C10 aliphatic dicarboxylic acids in airborne particulate matter. *Environ. Sci. Technol.*, 1978 (12) 313-317.

Grosjean D., Organic acids in southern California air: ambient concentration, mobile source emissions, in situ formation and removal processes. *Environ. Sci.*

Technol., 1989 (23) 1506-1514.

Grosjean D., Formic acid and acetic acid measurements during the southern California air quality study. *Atmospheric Environment*, 1990, 24A, 2699-2702.

Guiang S.F., Krupa S.V., Pratti G.C., Measurements of S (IV) and organic anions in Minnesota rain. *Atmospheric Environment* 1984 (18) 1677-1682.

Guien C., Chester R., Nimmo M., Martin J.M., Guerzoni S., Nicolas E., Mateu J., Keyse S., Atmospheric input of dissolved and particulate metals to the northwestern Mediterranean. *Deep-Sea Research II*, 1997 (44) 655-674.

Gunz D.W., Hoffmann M.R., Field investigation on the snow chemistry in central and southern California II. Carbonyls and carboxylic acids. *Atmospheric Environment* 1990 (16) 969-981.

Halstead M.J.R., Cunninghame R.G., Hunter K.A., Wet deposition of trace metals to a remote site in Fiordland, New Zealand. *Atmos. Environ.*, 2000 (34)665-676.

Hamburg A., Puvanesarajah V., Burnett T.J., Barnekow D.E., Premkumar N.D., Smith G.A., Comparative Degradation of [<sup>14</sup>C]-2,4-Dichlorophenoxyacetic Acid in Wheat and Potato after Foliar Application and in Wheat, Radish, Lettuce, and Apple after Soil Application. *J. Agric. Food Chem.* 2001 (49) 146-155.

Hamm R.E., Shull C.M., Jr., Grant D.M., Citrate complexes with iron(II) and iron(III). *J. Am. Chem. Soc.* 1954 (76) 2111-2114.

Hartmann W.R., Andreae M.O., Helas G., Measurements of organic acids over Central Germany. *Atmospheric Environment*, 1989 (23) 1531-1533.

Hartwick T.J., The rate constant of the reaction between ferrous ions and hydrogen peroxide in acid solution. *Can. J. Chem.*, 1957 (35) 428-436.

Hemmes P., Rich L.D., Cole D.L., Eyring E.M., Kinetics of Hydrolysis of Ferric Ion in Dilute Aqueous Solution. *The Journal of Physical Chemistry*, 1971 76) 929-932.

Herrmann J.M., Disdier J., Pichat P., Malato S., Blanco J., TiO<sub>2</sub>-based solar photocatalytic detoxification of water containing organic pollutants. Case studies of



2,4-dichlorophenoxyacetic acid (2,4-D) and benzofuran. *Appl.Catal. B: Environ.* 1998 (17) 15–23.

Hofmann H., Hoffmann P., Lieser K.H., Transition metals in atmospheric aqueous samples, analytical determination and speciation. *Fresenius J. Anal. Chem.*, 1991 340) 591–597.

Hoffmann P., Dedik A.N., Deutsch F., Sinner T., Weber S., Eichler R., Sterkel S., Sastri C.S., Ortner H.M., Solubility of single chemical compounds from an atmospheric aerosol in pure water. *Atmospheric Environment*, 1997 (31) 777-2785.

Hong H., Kester D.R., Redox state of iron in the offshore waters of Peru. *imnol. Oceanogr.*, 1986 (31) 512-524.

Hosono T., Okochi H., Igawa M., Fog water chemistry at a mountainside in Japan. *Bull. Chem. Soc. Jpn.*, 1994 (67) 368–374.

Hudson R.J.M., Covault D.M., Morel F.M.M., Investigations of iron coordination and redox reactions in seawater using  $^{59}\text{Fe}$  radiometry and ion-pair solvent extraction of amphiphilic iron complexes. *Mar. Chem.*, 1992 (38) 209-235.

Hug S.L., Laubscher H.U., James B.R., Iron(III) catalyzed photochemical reduction of chromium(VI) by oxalate and citrate in aqueous solutions. *Environ. Sci. Technol.*, 1997 (31) 160-170.

Hugül M., Apak R., Demirci S., Modeling kinetics of UV/hydrogen peroxide of some mono-, di- and trichlorophenols. *J. Hazard. Mater.* 2000 (77) 193–208.

Jacob D.J., Waldman J.M., Munger J.W., Hoffmann M.R., A field investigation of physical and chemical mechanisms affecting pollutant concentrations in fog droplets. *Tellus* 1984 (36B) 272–285.

Jardim W.F., Moraes S.G., Takiyama M.M.K., Photocatalytic degradation of aromatic chlorinated compounds using  $\text{TiO}_2$ : toxicity of intermediates. *Water Res.* 1997 (31) 1728–1732.

Johnson K.W., Coale K.H., Elrod V.A., Tindale N.W., Iron photochemistry in seawater from the equatorial Pacific. *Mar. Chem.*, 1994 (46) 319-334.

Joos F., Baltensperger U., A field study on chemistry S(IV) oxidation rates and vertical transport during fog conditions. *Atmos. Environ.*, 1991 (25A) 217–230.

Joseph J.M., Varghese R., Aravindakumar C.T., Photoproduction of hydroxyl radicals from Fe(III)-hydroxy complex: A quantitative assessment. *J. Photochem. Photobiol. A: Chem.*, 2001 (146) 67–73.

Kawamura K., Steinberg S., Kaplan, I.R., Capillary GC determination of short-chain dicarboxylic acids in rain, fog, and mist. *International Journal of Environmental Analytical Chemistry*. 1985 (19) 175-88.

Kawamura K., Ikushima K., Seasonal changes in the distribution of dicarboxylic acids in the urban atmosphere. *Environ. Sci. Technol.*, 1994 (27) 2227-2235.

Kawamura K., Gagosian R.B., Atmospheric transport of soil-derived dicarboxylic acids over the North Pacific Ocean. *Naturwissenschaften*, 1990(77)25-27

Kawamura K., Sempere R., Imai Y., Water soluble dicarboxylic acids and related compounds in Antarctic aerosols. *Journal of Geophysical Research*, 1996 (101) 18721-18728.

Keating E.J., Brown R.A., Greenberg E.S., Phenolic problems solved with hydrogen peroxide oxidation, *Ind. Water Eng.*, 1978 (2) 22-27.

Keene W.C., Galloway J.N., Organic acidity in precipitation of North America. *Atmospheric Environment*, 1984 (18) 2491-2497.

Keene W.C., Galloway J.N., Considerations regarding sources for formic and acetic acids in the troposphere. *Journal of Geophysical Research*, 1986 (91) 14,466-14,474.

Kester D., Marine redox cycle of iron. Workshop on Iron Speciation and its Availability to Phytoplankton in Seawater, Bermuda Biol. Stn., May 1-5, 1994.

Khare P., Satsangi S., Kumar N., Kumari K.M., Srivastava S.S., HCHO, HCOOH and CH<sub>3</sub>COOH in air and rain water at a rural tropical site in north central India. *Atmospheric Environment*, 1997 (31) 3867-3875.

Khare P., Satsangi S., Kumar N., Kumari K.M., Srivastava S.S., Surface measurements of formaldehyde and formic and acetic acids at a subtropical semiarid site in India. *Journal of Geophysical Research*, 1997,102 D15, 18,997-19,005.

Khwaja A.H., Brudnoy S., Husain L., Chemical characterization of three summer cloud episodes at whiteface mountain. *Chemosphere*, 1995 (31) 3357-3381

Khawaja A.H., Atmospheric concentration of carboxylic acids and related compounds at a semiurban site. *Atmospheric Environment*, 1995 (29) 127-139.

King D.W., Aldrich R.A., Charnecki S E, Photochemical redox cycling of iron in NaCl solutions. *Mar. Chem.*, 1993 (44)105-120.

King D.W., Spectrophotometric Determination of pH and Iron in Seawater: Equilibria and Kinetics. Ph.D. thesis. Univ. Rhode Island, Kingston, RI, 1988, 240 pp.

King D.W., Lin J., Kester D.R., Determination of Fe(II) in seawater at nanomolar concentrations. *Anal. Chim. Acta*, 1991 (247) 125-132.

Knight R.J., Sylva R.N., Spectrophotometric investigation of iron(III) hydrolysis in light and heavy water at 25°C. *J. Inorg. Nucl. Chem.*, 1975 (37) 779-783.

Kochany J., Bolton J.R., Mechanism of photodegradation of aqueous organic pollutants. 2. Measurement of the primary rate constants for reaction of •OH radicals with benzene and some halobenzenes using an EPR spin-trapping method following the photolysis of H<sub>2</sub>O<sub>2</sub>. *Environ Sci Technol.*, 1992 (26) 262–265.

Kostromina N.A., Trunova E.K., Tananaeva N.N., Complex formation of Fe(III) with tartartic acid by the method of the nuclear magnetic relaxation. Institute of General and Inorganic Chemistry, Academy of Sciences of the Ukrainian SSR, Kiev. Translated from *Teoreticheskaya i Eksperimental'naya Khimiya*, Vol. 23, No. 4, pp. 492-497, July-August, 1987.

Kotronarou A., Sigg L., SO<sub>2</sub> Oxidation in Atmospheric Water: Role of Fe(II) and Effect of Ligands. *Environ. Sci. Technol.* 1993 (27) 2725- 2735.

Kuma K., Nakabayashi S., Suzuki Y., Kudo I., Matsunaga K., Photo-reduction of Fe(B) by dissolved organic substances and existence of Fe(B) in seawater during spring blooms. *Mar. Chem.*, 1992 (37) 15-27.

Kumar N., Kulshreshta U.C., Saxena A., Kumari K.M., Srivastava S.S., Effect of antropogenic activity on formate and acetate levels in precipitation at four sites in Agra, India. *Atmospheric Environment*, 1993, 27B, 87-91.

Kumar N., Kulshreshta U.C., Khare P., Saxena A., Kumari K.M., Srivastava, S.S., Measurements of formic and acetic acid levels in the vapor phase at Dayalbagh, Agra, India. *Atmospheric Environment*, 1996 (30) 3545-3550.

Kundu S., Pal A., Dikshit A.K., UV induced degradation of herbicide 2,4-D: kinetics, mechanism and effect of various conditions on the degradation. *Separation and Purification Technology*. 2005 (44) 121–129

Kuo W.S., Synergistic effects of combination of photolysis and ozonation on destruction of chlorophenols in water. *Chemosphere*. 1999, 39 (11) 1853–1860.

Kurbus T., Marechal A.M., Vončina D.B., Comparison of  $\text{H}_2\text{O}_2/\text{UV}$ ,  $\text{H}_2\text{O}_2/\text{O}_3$  and  $\text{H}_2\text{O}_2/\text{Fe}^{2+}$  processes for the decolorisation of vinylsulphone reactive dyes, *Dyes Pigments*. 2003 (58) 245–252.

Kwan C.Y.; Chu W., Photodegradation of 2,4-Dichlorophenoxyacetic Acid in Various Iron-Mediated Oxidation Systems. *Water Res*. 2003, 37 (18), 4405.

Kwan C.Y., Chu W., .Effect of ferrioxalate-exchanged resin on the removal of 2,4-D by a photocatalytic process. *Journal of Molecular Catalysis A: Chemical*. 2006 (255) 236–242

Lamar W.L., Goerlitz D.F., Organic acids in naturally colored surface waters. U.S. Geol. Survey Water-Supply Paper, 1966 (181)7-A, 17.

Landing W.M., Bruland K.W., The contrasting biogeochemistry of iron and manganese in the Pacific Ocean. *Geochim. Cosmochim. Acta*, 1987 (51) 29-43.

Langford C.H., Carey J.H., Can J., The Charge Transfer Photochemistry of the Hexaaquoiron(III) Ion, the Chloropentaaquoiron(III) Ion, and the  $\mu$ -Dihydroxo Dimer Explored with tert-Butyl Alcohol Scavenging. *Can. J. Chem.*, 1975 (53) 2430–2435.

Lee Y., Lee C., Yoon J., High temperature dependence of 2,4-dichlorophenoxyacetic acid degradation by  $\text{Fe}^{3+} / \text{H}_2\text{O}_2$  system. *Chemosphere*. 2003 (51) 963.

Leland J.K., Bard A.J., Photochemistry of colloidal semiconducting iron oxide polymorphs. *J. Phys. Chem.*, 1987 (91) 5076-5083.

Lente G., Fábrián I., A Simple Test to confirm the Ligand Substitution Reactions of the Hydrolytic Iron(III) Dimer. *React. Kinet. Catal. Lett.*, 2001 (73) 117-125.

Likens G.E., Edgerton E.S., Galloway J.N., The composition and deposition of organic carbon in precipitation. *Tellus*, 1983 (35B) 16-24.

Limbeck A., Puxbaum H., Organic acid in continental background aerosols. *Atmos. Environ.*, 1999 (33) 1847-1852.

Liu X.L., Wu F., Deng N.S., Photoproduction of hydroxyl radicals in aqueous solution with algae under high pressure mercury lamp. *Environ. Sci. Technol.*, 2004 (38) 296–299.

Lunar L., Sicilia D., Rubio S., Dolores P.B., Nickel U., Identification of metal degradation products under Fenton's reagent treatment using liquid chromatography–mass spectrometry, *Water Res.* 2000, 34 (13) 3400–3412.

Manoj S.V., Mishra C.D., Sharma M., Rani A., Jain R., Bansal S.P., Gupta K.S., Iron, manganese and copper concentrations in wet precipitations and kinetics of the oxidation of SO<sub>2</sub> in rain water at two urban sites, Jaipur and Kota, in Western India. *Atmos. Environ.*, 2000 (34) 4479-4486.

Marinoni A., Laj P., Abida O., Mailhot G., Iron photochemistry in cloud droplets at the Puy de Dôme. *J. Phys. IV France*, 2003 (107) 823-826.

Marklund E., Öhman L.O., Equilibrium and structural studies of silicon(IV) and aluminium(III) in aqueous solution. Part 22. A potentiometric study of mono- and poly-nuclear aluminium(III) tartrates. *J. Chem. Soc., Dalton Trans.*, 1990, 755-760.

Martin J.H., Fitzwater S.E., Iron deficiency limits phytoplankton growth in the north-east Pacific subarctic. *Nature*, 1988 (331) 341-343.

Martin J.H., Gordon R.M., Fitzwater S.E., Broenkow W.W., VERTEX: phytoplankton/iron studies in the Gulf of Alaska. *Deep-Sea Res.*, 1989 (36) 649-680.

Martin J.H., Fitzwater S.E., Gordon R.M., Iron deficiency limits phytoplankton growth in Antarctic waters. *Global Biogeochem. Cycl.*, 1990 (4) 5-12.

Martin J.H., Gordon R.M., Fitzwater S.E., The case for iron. *Limnol. Oceanogr.*, 1991 (36) 1793-1802.

Martin J.H., Tanner S.J., Barber R.T., Liddicoat M.I., Bidigare R., Zhang J.Z., Greene R., Yungel, Testing the iron hypothesis in ecosystems of the equatorial Pacific Ocean. *Nature*, 1994 (371) 123-129.

Martin J.H., Gordon R.M., Northeast Pacific iron distributions in relation to phytoplankton productivity. *Deep- Sea Res.*, 1988, 35(2) 177-196.

Matsumoto G., Hanya T., Organic constituents in atmospheric fallout in the Tokyo area. *Atmos. Environ.*, 1980 (14) 1409-1419.

Mazellier P., Sulzberger B., Diuron degradation in irradiated, heterogeneous iron/oxalate systems: the rate-determining Step, *Environ. Sci. Technol.*, 2001 (35) 3314-3320.

Mcknight D.M., Kimball B.A., Bencala K.E., Iron photoreduction and oxidation in an acidic mountain stream. *Science*, 1988 (240) 637-640.

Mentasti E., Baiocchi C., The equilibria and kinetics of the complex formation between Fe(III) and tartaric and citric acids. *J. Coord. Chem.*, 1980 (10) 229-237.

Mestanková H., Mailhot G., Pilichowski J.F., Krysa J., Jirkovsky J., Bolte M., Mineralisation of Monuron photoinduced by Fe(III) in aqueous solution. *Chemosphere*, 2004, 57(10), 1307-1315.

Mestanková H., Photodegradation of monuron in homogeneous and heterogeneous systems in the presence of iron and/or TiO<sub>2</sub>: Comparison and complementarity. Ph.D. thesis, 2004.

Milburn R.M., A Spectrophotometric Study of the Hydrolysis of Iron(III) Ion. III. Heats and Entropies of Hydrolysis. *J. Amer. Chem. Soc.*, 1956 (79) 537-540

Miller W.L., King D.W., Lin J., Kester D.R., Photochemical redox cycling of iron in coastal seawater. *Mar. Chem.* 1995 (50) 63-77.

Millero F.J., Yao W.S., Aicher J., The speciation of Fe(II) and Fe(III) in natural waters. *Mar. Chem.*, 1995 (50) 21-39.

Millero F.J., Sotolongo S., The oxidation of Fe(II) with H<sub>2</sub>O<sub>2</sub> in seawater. *Geochim. Cosmochim. Acta*, 1989 (53) 1867-1873.

Millero F.J., Sotolongo S., Izaguirre M., The kinetics of oxidation of Fe(II) in seawater. *Geochim. Cosmochim. Acta*, 1987 (51) 793-801.

Modestov A.D., Lev O., Photocatalytical oxidation of 2,4-dichlorophenoxyacetic acid with titania photocatalyst. Comparison of supported and suspended TiO<sub>2</sub>. *J. Photochem. Photobiol. A: Chem.* 1998 (112) 261-270.

Moffett J.W., Zika R.G., 1987a. Photochemistry of copper complexes in sea water. In: Zika R.G., Cooper W.J. (Editors), *Photochemistry of Environmental*

Aquatic Systems. Am. Chem. Soc. Symp. Ser., Washington, DC, pp. 116-130.

Moffett J.W., Zika R.G., Reaction kinetics of hydrogen peroxide with copper and iron in seawater. Environ. Sci. Technol., 1987b (21) 804-810.

Motekaitis R.J., Martell A.E., Complexes of Aluminum(III) with Hydroxy Carboxylic Acids. Inorg. Chem., 1984 (23) 18-23.

Müller T.S., Sun Z., Kumar G., Itoh K., Murabayashi M., The combination of photocatalysis and ozonolysis as a new approach for cleaning 2,4-dichloroacetic acid polluted water. Chemosphere. 1998 (36) 2043-2055.

Murray K.S., Binuclear oxo-bridged iron(III) complexes. Coord. Chem. Rev., 1974 (12) 1-35.

Nogueira R.F.P., Guimarães J.R., Photodegradation of dichloroacetic acid and 2,4-dichlorophenol by ferrioxalate/H<sub>2</sub>O<sub>2</sub> system. Water Research. 2000 (34) 895-901.

Nogueira R.F.P., Silva M.R.A., Trovo A.G., Influence of the iron source on the solar photo-Fenton degradation of different classes of organic compounds. Solar Energy 2005 (79) 384-392.

Nürnberg H., Valenta P., Nguyen V., Proc. Int. Conf. Heavy Metals in the Environment, Heidelberg, September 1983, CEP consultants, Edinburgh, 1983: 115-123.

Oberg T., Warman K., Bergstrom J., Production of chlorinated aromatics in the post-combustion zone and boiler. Chemosphere, 1989 (19) 317-322.

Ormad M.P., Ovelleiro J.L., Kiwi J., Photocatalytic degradation of concentrated solutions of 2,4-dichlorophenol using low energy light identification of intermediates, Appl. Catal. B Environ. 2001 (32) 157-166.

Othmer D.F., Kirk R.E., Encyclopedia of Chemical Technology. Wiley Interscience, New York, 1979, 5, 325.

O'Sullivan D.W., Hanson A.K., Miller W.L., Kester D.R., Measurement of Fe(B) in equatorial Pacific surface seawater. Limnol. Oceanogr., 1991, 36(8): 1727-1741.

Paasivirta Z., Heinola K., Humppi T., Karjalainen A., Knuutinen J., Mäntykoski K., Paukku R., Piilola T., Surma-Aho K., Tarhanen J., Welling L., Vihonen H.,

Polychlorinated phenols, guaiacols and catechols in environment. *Chemosphere*, 1985 (14) 469-491.

Pan X.M., Schuchmann M.N., von Sonntag C., Oxidation of benzene by the OH radical A product and pulse radiolysis study in oxygenated aqueous solution. *J. Chem. Soc., Perkin Trans.* 1993 (2) 289-297.

Patel K.S., Shukla A., Tripathi A.N., Hoffmann P., Heavy Metal Concentrations of Precipitation in East Madhya Pradesh of India. *Water, Air, and Soil Pollution*, 2001 (130) 463-468.

Pehkonen S.O., Siefert R.L., Webb S., Hoffmann M.R., Photoreduction of iron oxyhydroxides in the presence of important atmospheric organic compounds. *Environ. Sci. Technol.*, 1993 (27) 2056-2062.

Peirson D.H., Cawse P.A., Salmon L., Cambray R.S., Trace Elements in the Atmospheric Environment. *Nature*, 1973 (241) 252-256.

Peller J., Wiest O., Kamat P.V., Hydroxyl Radical's Role in the Remediation of a Common Herbicide, 2,4-Dichlorophenoxyacetic Acid (2,4-D). *J. Phys. Chem. A.*, 2004 (108) 10925-10933.

Perdue E.M., Gjessing E.T., Editors. Life Sciences Research Report 48: Organic Acids in Aquatic Ecosystems. Report on the Dehlem Workshop on Organic Acids in Aquatic Ecosystems Berlin, 1989, May 7-12. 1990, 345.

Piera E., Calpe J.C., Brillas E., Domenech X., Peral J., 2,4-Dichlorophenoxyacetic acid degradation by catalyzed ozonation: TiO<sub>2</sub>/UVA/O<sub>3</sub> and Fe(II)/UVA/O<sub>3</sub> systems. *Appl. Catal. B: Environ.* 2000 (27) 169-177.

Poulain L., Mailhot G., Wong-Wah-Chung P., Bolte M., Photodegradation of chlortoluron: Role of iron(III) aquacomplexes. *J. Photochem. Photobiol. A: Chem.* 2003, 159 (1) 81-88.

Pozdnyakov I.P., Glebov E.M., Plyusnin V.F., Grivin V.P., Ivanov Y.V., Vorobyev D.Y., Bazhin N.M., Mechanism of Fe(OH)<sup>2+</sup>(aq) photolysis in aqueous solution. *Pure Appl. Chem.* 2000 (72) 2187-2197.

Prengle H.W., Ozone/UV oxidation of chlorinated compounds in water, *Proc. Internat. Ozone Inst. Forum on Ozone Disinfection*, International Ozone Institute,



Chicago, 1976, 286-295.

Powell R.T., King D.W., Landing W.M., Iron distributions in surface waters of the south Atlantic. *Mar. Chem.*, 1995 (50) 13-20.

Radojevic M., Clarke A.G., Acid Rain: Scientific and Technical Advances, based on papers presented at the Acid Rain Conference in Lisbon, 1-3 sept. 1987, Perry R., Harrison R.M., Bell J.N.B., Lester J.N. (eds) Publications Division, Selpter Ltd., London, 1987, 67-74.

Ramamoorthy S., Manning P.G., Equilibrium studies of metal ion complexes of interest to natural waters-I simple and mixed complexes of dl- and meso-tartaric acid with Fe(III), La(III) and Nd(III) ions. *J. Inorg. Nucl. Chem.* 1972 (34) 1977-1987.

Rao X., Collett Jr. J.L., The drop size-dependence of iron and manganese concentrations in clouds and fogs: implications for sulfate production. *J. Atmos. Chem.*, 1998 (30) 273-289.

Razdi Bin Abas M., Simoneit B.R.T., Composition of extractable organic matter of air particles from Malaysia: Initial study. *Atmos. Environ.*, 1996 (30) 2779-2793.

Rogge W.F., Mazurek M.A., Hildemann L.M., Cass G.R., Quantification of urban organic aerosols at a molecular level: identification, abundance and seasonal variation. *Atmos. Environ.*, 1993b (27) 1309-1330.

Ross H.B., Trace metal wet deposition in Sweden: insight gained from daily wet only collection. *Atmos. Environ.* 1990 (24A:7) 1929-1938.

Rush J.D., Bielski B.H.J, Pulse radiolysis studies of the reactions of  $\text{HO}_2^- / \text{O}_2^-$  with ferric ions and its implication on the occurrence of the Haber-Weiss reaction. *J. Phys. Chem.*, 1985 (89) 5062-5066.

Rue E.L., Bruland K.W., Complexation of iron(III) by natural organic ligands in the central North Pacific as determined by a new competitive equilibration/adsorptive cathodic stripping voltammetric method. *Mar. Chem.*, 1995 (50) 117-138, this volume.

Sanches L., Peral J., Doménech X., Degradation of 2,4-dichlorophenoxyacetic acid by in situ photogenerated Fenton reagent. *Electrochim. Acta.* 1996, 41 (13) 1981-1985.

Satsumabayashi H., Kurita H., Yokouchi Y., Ueda H., Photochemical formation of particulate dicarboxylic acids under long-range transport in central Japan. *Atmos. Environ.* 1990 (24A) 1443–1450.

Schroeder W.H., Dobson M., Kane D.M., Johnson N.D., Toxic trace elements associated with airborne particulate matter: a review. *J. Air Pollut. Control Assoc.*, 1987 (37) 1267-1285.

Schwanz M., Warneck P., Preiss M., Hoffmann P., Chemical speciation of iron in fog water, *Contr. Atmos. Phys.*, 1998 (70) 131–143.

Sedlak D.L., Hoigne J., The role of copper and oxalate in the redox cycling of iron in atmospheric waters. *Atmos. Environ.*, 1993, 27A: 2173-2185.

Selvam K., Muruganandham M., Swaminathan M., *Solar Energy Materials and Solar Cells.* 2005 (89) 61-74.

Sempéré R., Kawamura K., Comparative distributions of dicarboxylic acids and related polar compounds in snow, rain, and aerosol from urban atmosphere. *Atmos. Environ.*, 1994 (28) 449-459.

Sempéré R., Kawamura K., Low molecular weight dicarboxylic acids and related polar compounds in the remote marine rain sample collected from western pacific. *Atmospheric Environment*, 1996 (30) 1609-1619.

Shul'pin G.B., Bochkova M.M., Nizova G.V., Kozlova N.B., Aerobic photodegradation of phenols in aqueous solutions promoted by metal compounds. *Appl. Catal. B.*, 1997 (12) 1-19.

Siefert R.L., Pehkonen S.O., Erel Y., Hoffmann M.R., Iron photochemistry of aqueous suspensions of ambient aerosol with added organic acids, *Geochim. Cosmochim. Acta*, 1994 (58) 3271-3279.

Siffert C., Sulzberger B., Light-Induced Dissolution of Hematite in the Presence of Oxalate: A Case Study. *Langmuir.* 1991 (7) 1627-1634.

Sigg L., Johnson C.A., Kuhn A., Redox conditions and alkalinity generation in a seasonally anoxic lake. *Mar. Chem.* 1991 (36) 9-26.

Singer Ph C., Stumm W., Acidic mine drainage the rate-determining step. *Science*, 1970 (167) 1121-1123.

Sinner T., Hoffmann P., Ortner H.M., Determination of pH-value, redox-potential, transition metals concentration and Fe(II)- and Fe(III)-content in cloud water samples. *Beitr. Phys. Atmos.*, 1994 (67) 353-357.

Sommer B.A., Margerum D.W., Kinetic study of the hydroxo-iron(III) dimer. *Inorg. Chem.*, 1970 (9) 2517-2521.

Stafford U., Gray K.A., Kamat P.V., Radiolytic and TiO<sub>2</sub>-assisted photocatalytic degradation of 4-chlorophenol. *J. Phys. Chem.* 1994 (98) 6343–6349.

Stover E.L., Kincannon D.F., Biological Treatability of Specific Organic Compounds Found in Chemical Industry Wastewaters. *Journal Water Pollution Control Federation*, 1983 (55) 97-109.

Strouse J., Layten S.W., Strouse C.E., Structural studies of transition metal complexes of triionized and tetraionized citrate. Models for the coordination of the citrate ion to transition metal ions in solution and at the active site of aconitase. *J. Am. Chem. Soc.* 1977 (99) 562-571.

Sulzberger B., Suter D., Siffert C., Banwart S., Stumm W., Dissolution of Fe(III) (hydr)oxides in natural waters, Laboratory assessment on the kinetics controlled by surface coordination. *Mar. Chem.*, 1989 (28) 127-144.

Sulzberger B., Schnoor J.L., Giovanoli R., Hering J.G., Zobrist J., Biogeochemistry of iron in an acidic lake. *Aquat. Sci.* 1990(52) 57-74.

Sulzberger B., Laubscher H., Reactivity of various types of iron(III) (hydr)oxides towards light-induced dissolution. *Mar. Chem.*, 1995 (50) 103-115.

Sun Y., Pignatello J.J., Photochemical reactions involved in the total mineralization of 2,4-D by Fe<sup>3+</sup>/H<sub>2</sub>O<sub>2</sub>/UV. *Environ. Sci. Technol.* 1993 (27) 304-310.

Sun Y., Pignatello J.J., Evidence for a surface dual holeradicalmechanism in the TiO<sub>2</sub> photocatalytic oxidation of 2,4-dichlorophenoxyacetic acid. *Environ. Sci. Technol.* 1995 (29) 2065-2072.

Sunda W.G., Huntsman S.A., Antagonisms between cadmium and zinc toxicity and manganese limitation in a coastal diatom. *Limnol. Oceanogr.* 1996 (41) 373- 387.

Talbot R.W., Beecher K.M., Harriss R.C., Coffey III W.R., Atmospheric

geochemistry of formic and acetic acids at a mid-latitude temperate site. *Journal of Geophysical Research*, 1988 (93) 1638-1652.

Talbot R.W., Bradshaw J.D., Sandholm S.T., Smyth S., Blake D.R., Blake N., Sachse G.W., Collins Jr. J.E., Heikes B.G., Anderson B.E., Gregory G.L., Singh H.B., Lefer B.L., Bachmeier A.S., Chemical characteristics of continental outflow over the tropical south Atlantic Ocean from Brazil and Africa. *Journal of Geophysics*, 1996a (101) 24,187-24,202.

Talbot R.W., Dibb J.E., Klemm K.I., Bradshaw J.D., Sandholm S.T., Blake D.R., Sachse G.W., Collins Jr. J.E., Heikes B.G., Gregory G.L., Anderson B.E., Singh H.B., Thornton D.C., Merrill J.T., Chemical characteristics of continental outflow from Asia to the troposphere over the western Pacific Ocean during September-October 1991: results from PEM-WEST A. *Journal of Geophysical Research*, 1996b (101) 1713-1725.

Talbot R.W., Dibb J.E., Lefer B.L., Bradshaw J.D., Sandholm S.T., Blake D.R., Blake N.J., Sachse G.W., Collins Jr. J.E., Heikes B.G., Merrill J.T., Gregory G.L., Anderson B.E., Sing H.B., Thornton D.C., Bandy A.R., Pueschel R.F., Chemical characteristics of continental outflow from Asia to the troposphere over the western Pacific Ocean during February-March 1994: results from PEM-West B. *Journal of Geophysical Research*, 1997a. (102) 28,255-28,274.

Talbot R.W., Dibb J.E., Lefer B.L., Scheuer E., Bradshaw J.D., Sandholm S.T., Smyth S., Blake D.R., Blake N.J., Sachse G.W., Collins Jr. J.E., Gregory G.L., Large scale distributions of tropospheric nitric, formic, and acetic acids over the western Pacific basin during wintertime. *Journal of Geophysical Research*, 1997b (102) 28,303-28,313.

Talbot R.W., Mosher B.W., Heikes B.G., Jacob D.J., Munger J.W., Daube B.C., Keene W.C., Maben J.R., Artz R.S., Carboxylic acids in the rural continental atmosphere of the eastern United States during SCAPE. *Journal of Geophysical Research*, 1995 (100) 9335-9343.

Tang W.Z., Huang C.P., Effect of chlorine content of chlorinated phenols on their oxidation kinetics by Fenton's reagent. *Chemosphere* 1996, 33 (8) 1621-1635.

Thornton J.D., Eisenreich S.J., Impact of land-use on the acid and trace element composition of precipitation in the north central US. *Atmos. Environ.* 1982 (16) 1945–1955.

Thurman E.M., 1985, *Organic Geochemistry of Natural Waters*: Martinus Nijhoff/ Dr. W. Junk Dordrecht, 1985, 497.

Timberlake C.F., Iron-malate and iron-citrate complexes. *J. Chem. Soc.* 1964, 5078-5085.

Trapido M., Hivronen A., Veressinina Y., Hentunen J., Munter R., Ozonation, ozone/UV and UV/H<sub>2</sub>O<sub>2</sub> degradation of chlorophenols. *Ozone: Sci. Eng.* 1997, 19 (1) 75–96.

Trojanowicz M., Drzewicz P., Pańta P., Gluszewski W., Nalece- Jawecki G., Sawicki J., Radiolytic degradation and toxicity changes in  $\gamma$ -irradiated solutions of 2,4-dichlorophenol, *Radiat. Phys. Chem.* 2002 (65) 357–366.

US EPA. 1981, 118. EPA-440-4-81-008, NTIS PB81-219685.

U.S. Department of Health and Human Services. Hazardous Substances Data Bank ([HSDB, online database](#)). National Toxicology Information Program, National Library of Medicine, Bethesda, MD. 1993.

U.S. Environmental Protection Agency. 2,4-Dichlorophenoxyacetic Acid Health Advisory. Office of Drinking Water, Washington, DC. 1987.

Voelker B M., Sedlak D L., Iron reduction by photoproduct superoxide in seawater. *Mar. Chem.*, 1995 (50) 93-102.

Voelker B.M., Morel F., Sulzberger B., Iron redox cycling in surface waters: Effects of humic substances and light. *Environ. Sci. Technol.* 1997 (31) 1004-1011.

Waite T.D., Morel F.M.M., Photoreductive dissolution of colloidal iron oxides in natural waters. *Environ. Sci. Technol.*, 1984a (18) 860-868.

Waite T.D., Morel F.M.M., Photoreductive dissolution of colloidal iron oxide: effect of citrate. *J. Colloid Interface Sci.*, 1984b, 102 (1) 121-137.

Waite T.D., Torikov A., Photo-assisted dissolution of colloidal iron oxides by thiol-containing compounds. *J. Colloid Interface Sci.*, 1987 (119) 228.

Waite T.D., UV effects on heterogeneous chemical processes. In: N.V. Blough

and R.G. Zepp (Editors), Woods Hole Oceanogr. Inst. Techn. Rep., WHOI-90-09, 1990, 12-15.

Waite T.D., Szymaczak R., Espey Q.I., Furnas M.J., Diel variations in iron speciation in northern Australia. *Mar. Chem.* 1995 (50) 79-91.

Waldman J.M., Münger W.J., Hoffmann D.J., Michael R., Chemical characterization of stratus cloudwater and its role as a vector for pollutant deposition in a Los Angeles pine forest. *Tellus, Series B: Chemical and Physical Meteorology*, 1985 (37B) 91-108.

Wang L., Zhang C.B., Wu F., Deng N.S., Glebov E.M., Bazhin N.M., Determination of Hydroxyl Radicals from Photolysis of Fe(III)-Pyruvate Complexes in Homogeneous Aqueous Solution. *React. Kinet. Catal. Lett.* 2006, 89 (1):183-192.

Welch K.D., Davis T.Z., Aust S.D., Iron autoxidation and free radical generation: effects of buffers, ligands, and chelators. *Archives of Biochemistry and Biophysics*. 2002 (397) 360–369.

Wu F., Deng N.S., Zuo Y., Discoloration of dye solutions induced by solar photolysis of ferric citrate in aqueous solutions. *Chemosphere*. 1999 (39) 2079-2085.

Wu F., Deng N.S., Photochemistry of hydrolytic iron (III) species and photoinduced degradation of organic compounds. A minireview. *Chemosphere*. 2000 (41) 1137-1147

Wu F., Zhang L., Deng N.S., Zuo Y.G., Quantitation for photoinduced formation of hydroxyl radicals in the water containing Fe(III) and oxalate salts. *Fresen. Environ. Bull.*, 2004 (13) 748-752.

Wells M.L., Mayer L.M., The photoconversion of colloidal iron oxyhydroxides in seawater. *Deep-Sea Res.* 1991 (38) 1379-1395.

Wells M.L., Mayer L.M., Guillard R.R.L., A chemical method for estimating the availability of iron to phytoplankton in seawater. *Mar. Chem.*, 1991 (33) 23-40.

Wells M.L., Mayer L.M., Donard O.F.X., de Souza M.M., Ackleson S., The photolysis of colloidal iron in the oceans. *Nature*, 1991 (353) 248-250.

Wells M.L., Price N.M., Bruland K.W., Iron chemistry in seawater and its relationship to phytoplankton: a workshop report. *Mar. Chem.*, 1995 (48) 157-182.

Weschler C.J., Mandich M.L., Graedel T.E., Speciation, photosensitivity, and reactions of transition metal ions in atmospheric water droplets. *J. Geophys. Res.* 1986, 91, D4, 5189-5204.

Wilkinson J., Reynolds B., Neal C., Hill S., Neal M., Harrow M., Major, minor and trace element composition of cloudwater and rainwater at Plynlimon. *Hydrology and Earth System Sciences*, 1997 (1) 557-569

Wobrock W., Schell D., Maser R., Jaeschke W., Georgii H.W., Wieprecht W., Arends B.G., Mols J.J., Kos G.P.A., Fuzzi S., Facchini M.C., Orsi G., Berner A., Solly I., Kruisz C., Svenningsson I.B., Wiedensohler A., Hansson H.C., Ogren J.A., Noone K.J., Hallberg A., Pahl S., Schneider T., Winkler P., Winiwarter W., Colvile R.N., Choularton T.W., Flossmann A.I., Borrmann S., The Kleiner Feldberg Cloud Experiment 1990. An overview. *Journal of Atmospheric Chemistry*, 1994, 19 (1-2) 3-35.

Zafiriou O.C., Chemistry of superoxide ion-radical ( $O_2^-$ ) in seawater. I.  $pK_a$   $sw^*$  (HOO) and uncatalyzed dismutation kinetics studied by pulse radiolysis. *Mar. Chem.*, 1990 (30) 31-43.

Zepp R.G., Wolfe N.L., Gordon N.L., Baughman G.L., Dynamics of 2,4-D Enters in Surface Waters, Hydrolysis, Photolysis and Vaporization. *Environ. Sci. Technol.*, 1975 (9) 1144.

Zepp R.G., Hoigné J., Bader H., Nitrate-induced photooxidation of trace organic chemicals in water. *Environ. Sci. Technol.*, 1987 (21) 443.

Zhang C.B., Wang L., Wu F., Deng N.S., Quantitation of Hydroxyl Radicals from Photolysis of Fe(III)-Citrate Complexes in Aerobic Water. *Environ Sci & Pollut Res.* 2006, 13(3) 156–160

Zheng M., Wan T., Fang M., Wang F., Characterization of non-volatile organic compounds in the aerosols of Hong Kong –Identification, abundance and origin. *Atmos. Environ.*, 1997 (31) 227-237.

Zhuang G., Yi Z., Duce R.A., Brown P.R., Chemistry of iron in marine aerosols. *Global Biogeochem. Cycl.*, 1992a (6) 161-173.

Zhuang G., Yi Z., Duce R.A., Brown P.R., Link between iron and sulphur cycles

suggested by detection of Fe(II) in remote marine aerosols. *Nature*, 1992b (355) 537-539.

Zhu X., Prospero J.M., Millero F.J., Savoie D.L., Brass G.W., The solubility of ferric ion in marine mineral aerosol solutions at ambient relative humidities. *Mar. Chem.*, 1992 (38) 91-107.

Zona R., Schmid S., Solar S., Detoxification of aqueous chlorophenol solutions by ionizing radiation. *Water Res.* 1999, 33 (5), 1314-1319.

Zona R., Solar S., Gehringer P., Degradation of 2,4-dichlorophenoxyacetic acid by ionizing radiation: influence of oxygen concentration. *Water Res.* 2002 (36) 1369-1374.

Zona R., Solar S., Sehested K., Holcman J., Mezyk S.P. OH-Radical Induced Oxidation of Phenoxyacetic Acid and 2,4-Dichlorophenoxyacetic Acid. Primary Radical Steps and Products. *J. Phys. Chem. A.* 2002 (106) 6743-6749.

Zona R., Solar S., Oxidation of 2,4-dichlorophenoxyacetic acid by ionizing radiation: degradation, detoxification and mineralization. *Radiation Physics and Chemistry.* 2003 (66) 137-143.

Zuo Y.G., Hoigné J., Formation of hydrogen peroxide and depletion of oxalic acid in atmospheric water by photolysis of iron(III)-oxalato complexes. *Environ. Sci. Technol.*, 1992 (26) 1014-1022.

Zuo Y.G., Kinetics of photochemical/chemical cycling of iron coupled with organic substances in cloud and fog droplets, *Geochim. Cosmochim. Acta* 1995 (59) 3123-3130.

Zuo Y. G., Light-induced formation of hydroxyl radicals in fog waters determined by an authentic fog constituent, hydroxymethanesulfonate, *Chemosphere* 2003 (51) 175-179.

Zuo Y. G., Zhan J., Effects of Oxalate on Fe-catalyzed photooxidation of Dissolved Sulfur Dioxide in Atmospheric Water. *Atmos. Environ.*, 2005 (39) 27-37.

Zuo Y. G., Zhan J., Wu T.X., Effects of Monochromatic UV-visible light and sunlight on Fe(III)-catalyzed oxidation of dissolved sulfur dioxide. *J. Atmos. Chem.* 2005 (50) 195-210.



## Papers published

Lei Wang, Changbo Zhang, Feng Wu, Nansheng Deng. Photoproduction and determination of hydroxyl radicals in aqueous solution with Fe(III)-Tartrate complexes: a quantitative assessment. *Journal of Coordination Chemistry*. 2006, 59(7): 803-813. (SCI)

Lei Wang, Changbo Zhang, Feng Wu, Nansheng Deng, Evgeni M. Glebov and Nikolai M. Bazhin. Determination of Hydroxyl Radicals from Photolysis of Fe(III)-Pyruvate Complexes in Homogeneous Aqueous Solution. *Reaction Kinetics and Catalysis letter*. 2006, 89(1):183-192. (SCI)

Lei Wang, Changbo Zhang, Feng Wu, Nansheng Deng. Photodegradation of aniline in aqueous suspensions of microalgae. *Journal of photochemistry and photobiology: B*. 2007, 87(1):49-57. (SCI)

Changbo Zhang, Lei Wang, Feng Wu, Nansheng Deng. Quantitation of Hydroxyl Radicals from Photolysis of Fe(III)-citrate Complexes in Aerobic Water. *Environmental Science and Pollution Research*. 2006, 13(3):156-160. (SCI)

L. Deng, Y. X. Liu, P. Y. Chen, L. Wang, and N. S. Deng. Determination of Trace Bisphenol A in Leachate by Solid Phase Microextraction Coupled with High Performance Liquid Chromatography. *Analytical letters*. 2006, 39: 395-404. (SCI)

G. Mailhot, L. Wang, H. Mestanková, M. Bolte, F. Wu, N. S. Deng . Degradation of 2, 4-dichlorophenol photoinduced by Fe(III)-polycarboxylate complexes. 8th European Meeting on Environmental Chemistry (EMEC8), Inverness (Scotland), December 5-8 2007.

Lei Wang, Changbo Zhang, Yinzhong Shang, Feng Wu, Nansheng Deng. Photodegradation of Atrazine Induced by The Photolysis of Fe(III)-Pyruvate Complexes. 2nd International Workshop on Sustainable Asia-Sustainable Land Use and Environment, China, November 23-24, 2006.

Changbo Zhang, Lei Wang, Feng Wu, Nansheng Deng, Jiantong Liu, Tao Fang. Dissolved Oxygen and Irradiation Effects on the Concentrations of Nitrogen and Phosphorus Across the Lake Water–Sediment Interface. 2nd International Workshop

on Sustainable Asia-Sustainable Land Use and Environment, China, November 23-24, 2006.

Nansheng Deng, Feng Wu, Changbo Zhang, Lei Wang. Study of energy consumption and atmosphere quality in Wuhan China. ICCS International Symposium, Japan, 2004.

La photodégradation de l'herbicide 2,4-D (acide 2,4-dichlorophénoxyacétique) et de son principal photoproduit (2,4-DCP) en présence de trois complexes Fe(III)-carboxylate (citrate, pyruvate, tartrate) a été étudiée. Les rendements quantiques de disparition du 2,4-D augmentent dans cet ordre : Fe(III)-Tar < Fe(III)-Cit < Fe(OH)<sup>2+</sup> < Fe(III)-Pyr. Le même mécanisme de dégradation du 2,4-D est observé pour les trois complexes de fer et correspond à celui déjà décrit avec des processus générant des radicaux hydroxyle. Le 2,4-D est dégradé sélectivement en 2,4-DCP, qui après formation de différents photoproduits peut être minéralisé complètement en H<sub>2</sub>O, Cl<sup>-</sup> et CO<sub>2</sub>. La formation de radicaux hydroxyles, obtenue sous irradiation des solutions de complexes de Fe(III), a été confirmée par spectroscopie RPE. Ce travail montre que la présence de complexes Fe(III)-carboxylate peut avoir un impact considérable sur le devenir de polluants organiques présents dans les compartiments aquatiques naturels.

In this study the photodegradation of the herbicide 2,4-D (2,4-dichlorophenoxyacetic acid) and its main photoproduct (2,4-DCP) in the presence of three Fe(III)-carboxylate complexes (citrate, pyruvate and tartrate) have been investigated. The quantum yields of 2,4-D disappearance increases in the following order of Fe(III)-complexes: Fe(III)-Tar < Fe(III)-Cit < Fe(OH)<sup>2+</sup> < Fe(III)-Pyr. We observe the same mechanism of 2,4-D degradation for all complexes corresponding to the mechanism described in the previous work on the degradation of 2,4-D by processes (generating ·OH radicals). 2,4-D is selectively degraded to 2,4-DCP, which through different photodegradation products could be mineralized into H<sub>2</sub>O, Cl<sup>-</sup> and CO<sub>2</sub>. The formation of hydroxyl radicals in the solutions of Fe(III) complexes is confirmed by ESR spectroscopy measurements. Our work shows that the presence of Fe(III)-carboxylate complexes could have a considerable impact on the fate of organic pollutant in aquatic environment.